Development of composite and hybrid materials based on bioactive glass for bone bioengineering

Amel Houaoui

Doctoral thesis

To obtain the Title of PhD in Life and Health Sciences

Delivered by CY Cergy Paris Université

Prepared within the Doctoral School n ° 417 Sciences and Engineering and the Equipe de Recherche sur les Relations Matrice Extracellulaire – Cellule Laboratory

Development of composite and hybrid materials based on bioactive glass for bone bioengineering

By Amel HOUAOUI

Supervised by Pr Emmanuel PAUTHE

Presented and publicly defended on February 19th, 2021 at Neuville-Sur-Oise before a jury composed of

Pr Olivier GALLET	CY Cergy Paris Université	President of the jury
Pr Jérôme CHEVALIER	INSA Lyon, France	Reviewer
Pr Peter DUBRUEL	Ghent University, Belgium	Reviewer
Pr Elzbieta PAMULA	AGH University, Poland	Reviewer
Pr Olivier GALLET	CY Cergy Paris Université	Examiner
Pr Emmanuel PAUTHE	CY Cergy Paris Université	Supervisor
Dr Michel BOISSIERE	CY Cergy Paris Université	Co-supervisor
Pr Jonathan MASSERA	Tampere University, Finland	Invited

Foreword

This work was funded by CY Initiative of Excellence and was carried out through a scientific collaboration between ERRMECe Laboratory (Equipe de Recherche sur les Relations Matrice Extracellulaire – Cellules), CY Cergy Paris Université, France and the Laboratory of Biomaterials and Tissue Engineering, Tampere University, Finland.

This collaboration allowed a 7-month research stay in the Finnish laboratory. In order to recognize the European dimension of this research, this doctoral project aims to be rewarded with the European doctorate label.

Acknowledgements

First, I would like to thank the members of the jury for agreeing to evaluate this PhD thesis. Thanks to **Professor Jérôme Chevalier** (INSA Lyon, France**), Professor Peter Dubruel** (Ghent University, Belgium), and **Professor Elzbieta Pamula** (AGH University, Poland) for agreeing to be reviewers of this thesis. I would also like to thank **Professor Olivier Gallet** (CY Cergy Paris University, France) for having accepted to be examiner of this work. I thank each member of the jury for their consideration for my work.

I would like to deeply thank my thesis supervisor, **Emmanuel Pauthe**. Manu, thank you for the trust you have placed in me since my first internship in ERRMECe laboratory. Thank you for everything you have given me, for believing in me from the beginning, as well as for all the good times spent together, in the lab or at congresses, and our crazy laughs. You have always been there for me, despite your busy schedule. Thank you for all the exchanges, all the long discussions, not just scientific. Thank you again for everything "sahbi", I will never forget. I also thank **Raphaëlle** for her kind words when I was at my lowest, and for her encouragement, which gave me strength.

My thanks also to my thesis co-supervisor, **Michel Boissière**. Michel, you too believed in me from the beginning. You trusted me right away and accepted me for the internship in collaboration with Finland, a great opportunity for me. At that time, I had no idea that it would lead to a PhD position and that we would work together for another three and a half years, much to my great happiness. Thank you for making me a "warrior" as you say so well. I thank you for everything you have given me during this thesis, for your confidence, for having always been present. Thank you for all the short meetings in your office, which often ended in off topic discussion. You are overflowing with ideas, it is incredible. Thank you also for teaching me to relativize, you who do it so well!

I also thank **Jonathan Massera**, my “Finnish” supervisor. Jonathan, you might not have been "officially" my thesis co-supervisor, but it was just like it. You were much more than a collaborator during this thesis. You have always been there for me, always available, despite the distance. Thank you for welcoming me to your laboratory in Finland, for my internship and the PhD. You have always integrated me into your team and allowed me to work in the best conditions. I’m grateful for you and **Laeticia**, for all the times you welcomed me into your home. Thank you for all the exchanges, the discussions, the advice you gave me. And thank

you very much for offering to continue working with you as a Post-Doc. We are off to a good start to continue.

I am infinitely grateful to all three of you for all you have given me. You have made me grow, scientifically, professionally, and personally. All the moments passed remain in my heart, and I will never forget.

I would like to thank our former laboratory director, **Olivier Gallet**. Olivier, thank you for allowing me to do this thesis in ERRMECe laboratory under the best conditions. Thank you for your presence and your dedication to the PhD students. It is thanks to you that we were able to celebrate the 20 years of the laboratory and many other events. Thank you for these evenings spent in the laboratory, for your jokes, and your famous questions, which always give us stress. I thank you for everything.

I would also like to thank the entire **BIOSAN team**, **Violeta Rodriguez**, **Adeline Gand**, **Agnès Mihajlovski** and **Damien Seyer**.

Violeta, in truth, it was with you that it all started during my M1 internship. It was this internship with you that made me want to continue in research. Thank you for everything you taught me, transmitted to me and all our chatter about anything and everything. Thank you for the giggles and all the good times we spent together. At the same time, I would like to thank **Virginie Gueguen** and **Graciela Pavon-Djavid** for also giving me a newfound taste for research during this M1 internship.

Adeline, I cannot thank you enough for everything you have given me during this thesis. Thank you for always being present, available, always listening, whether for rehearsals or for discussions of life in general in your office. You have a gift for appeasing people, and it feels great to discuss with you. I am very happy to know you and I hope to see you again soon in Paris, or in Finland, who knows?

Agnès, I also thank you for being present throughout my thesis. Thank you for having trained me in molecular biology, but also for always listening. Thanks for your availability. You are always there to encourage the PhD students, and to give strength. I also thank you for all the really good honey you provided me, what a delight!!!

Damien, thank you for all the exchanges we've had. Thank you for always being in a good mood and in shape to annoy the PhD students. Your teasing allows us to always keep smiling.

I cannot forget to mention **Professor Véronique Larreta-Garde**, who retired during my thesis, and whom I thank greatly for her presence and her kindness. Thank you for your lessons taught with passion, for the scientific exchanges we have had, for giving me a real taste for research. Your career is incredible, you are a real example for all of us. I hope your well-deserved retirement is going well.

A BIG THANKS also to the **technical STAFF**: **Rémy Agniel**, **Lamia El-Guermah**, **Mathilde Hindié** and **Isabelle Pereira**.

Rémy, thank you for all the time you took with me throughout my thesis under the microscope. Thank you for always being available when needed and for training me in microscopy. I won't forget the good times, the giggles, the gossips at the microscope, and the teasing. I will never forget to put you first in my articles!

Mathilde, thank you for your presence and your availability. Whenever I needed your help and advice for manipulations, protocols, you responded, and I am very grateful to you.

I also thank **all the members of ERRMECe laboratory** for all the exchanges. I especially thank **Sabrina**, for your great kindness, your advice, and your little "coucous" in our office. I would also like to thank **Cédric** for our various discussions on the future, your good humor, and your teasing, in trio with Damien and Rémy.

I thank all the people who contributed to this thesis. I thank **Inari Lyyra** from the Finnish laboratory who helped me with the synthesis of composites; **Sébastien Peralta** from LPPI for AFM studies; **Cédric Vancaeyzeele** from LPPI, **Mathieu Goczkowski** and **Carla Palomino-Durand** for rheology studies; **Isabelle Laurent** for the SEC analysis; **Andres Arciniegas** from SATIE for the characterization of ultrasonic gels. I would like to thank **Susanna Miettinen** and **Arjen Gebraad**, our Finnish collaborators, for training me in stem cells culture. Many thanks to **Annelise Cousture** from L2MGC for sample preparations, initial observations and SEM analysis but also for all the good times spent together in the doctoral school training.

It is with great emotion that I thank **Lamia**. First, thank you for the time you took during my thesis to help me. You are always present and available for the PhD students, a big thank you for that. I would also like you to know that you have been much more than the lab technician to me. You have been like a big sister all these years, always present, in good times and in bad times. You always knew how to find the right words when things were not going too well, and I thank you for all the personal advice you have given me. We met during my M1 internship, it has been 5 years now, and it is going to last.

A VERY BIG THANK YOU to the girls of my office: **Audrey**, **Carine** (**Caro** for close friends), **Mathilde** and **Amel**. Obviously, this thesis would not have been the same without you. Thank you for your support in difficult times, times of sadness, but remember: "This office is made for that!". Thank you so much for the giggles, the great times I will never forget. I really hope that we will continue to have these moments even after the thesis. I miss you already!

I also thank all the PhD students and post-docs: **Maxime**, **Rosa**, **Carla**, **Solène**, **Phuong-Anh**, **Anamar**, **Sahil**, **Clotilde**, **Chahrazed**, **Audrey D.** for the good times spent in the laboratory.

Special thanks to **Maxime**, **Rosa**, **Carla**, **Solène** and **Phuong-Anh** for the great moments spent during conferences, and that even when in remote (ESB 2021)!
Maxime, thank you for your positivity, for always being available to help Caro and I to organize events in the lab, overflowing with ideas and willpower.
Carla, thank you for your precious advice.

Inari, **Sanna**, **Henriikka** and **Mari**, thank you for the great times spent in Finland! I have very good memories of them.

I would like to thank the elders very much: **Hassan**, **Audrey**, **Rony**, **Andrey**, **Mathieu**, **Éléonore**. Thank you for your presence, your unfailing support, and your invaluable advice. This thesis would not have been the same without you. I am very happy to have found you on my way. Thank you for the aperitifs, the giggles, I know it will last for years to come. Thanks also to **Alice** who is obviously part of the team.

I also thank my friends and colleagues, **Hadjer** and **Alexandra**. You have been invaluable support during this thesis. We met on the benches of the university, and we never left each other. I am proud that we have walked this path together, all three of us doctors today, and I wish us the best for the future.

I would like to thank my dear friends: **Inès**, **Kimia**, **Imane**, **Ornella**, **Ahmed**, **Sarah**, **Rihab**. Thank you for your presence and your unfailing support during this thesis. I have always been able to count on you in good times and in bad times. Thank you for the outings, the evenings, the weekends, the trips that took me out of my daily life.
Inès and **Kimia**, you are my sisters from another mother, and I do not intend to let go of you. Prepare to put up with me for a long time to come.

I thank **Kyle** for his presence and support all these years. I have not always been easy to bear, but I know I have always been able to count on you. You are a beautiful person and despite the ups and downs, I only remember the positive.

And as they say, the best for the end ...

My biggest and deepest thanks are for my family. **Dad**, **Mom**, **Hayette**, **Ali**, I cannot thank you enough for everything you have given me all these years. Not only for my PhD but my whole life as well. You believed in me when no one else did. You taught me perseverance, gave me the will and the strength to succeed. If I am successful, it is because of you. If I am a fighter today, it is thanks to you. Thank you for supporting me even when I was unbearable. Thank you for taking care of me and giving me everything so that I can work in the best conditions. This PhD thesis, on which I have worked so hard over the years, is for you and with all my heart I dedicate it to you.

Remerciements

Je remercie tout d'abord les membres du jury d'avoir accepté d'évaluer cette thèse. Merci aux **Professeur Jérôme Chevalier** (INSA Lyon), **Professeur Peter Dubruel** (Ghent University, Belgique), et **Professeur Elzbieta Pamula** (AGH University, Pologne) d'avoir accepté d'être rapporteurs de cette thèse. Je remercie également **Professeur Olivier Gallet** (CY Cergy Paris Université) d'avoir accepté d'être examinateur de ce travail. Je remercie chaque membre du jury pour leur considération pour mon travail.

Je tiens à remercier profondément mon directeur de thèse, **Emmanuel Pauthe**. Manu, je te remercie pour la confiance que tu m'as accordée depuis mon premier stage au sein du laboratoire ERRMECe. Merci pour tout ce que tu m'as apporté, pour avoir cru en moi dès le début, ainsi que pour tous ces bons moments passés, au labo ou en congrès, et nos fous rires. Tu as toujours été présent, malgré ton emploi du temps bien chargé. Je te remercie pour tous les échanges, toutes les longues discussions, pas que scientifiques. Encore merci pour tout « sahbi », je n'oublierai jamais. Je remercie également **Raphaëlle** pour ses mots quand j'étais au plus bas, et pour ses encouragements qui m'ont redonné de la force.

Mes remerciements vont aussi à mon co-encadrant de thèse, **Michel Boissière**. Michel, tu as toi aussi cru en moi dès le début. Tu m'as fait confiance tout de suite et m'a acceptée pour le stage en collaboration avec la Finlande, une grande opportunité pour moi. À ce moment-là je ne me doutais pas du tout que ça déboucherait sur une thèse et qu'on travaillerait ensemble encore trois ans et demi, à mon grand bonheur. Merci à toi de m'avoir rendue « warrior » comme tu le dis si bien. Je te remercie pour tout ce que tu m'as apporté au cours de cette thèse, pour ta confiance, d'avoir toujours été présent. Merci pour toutes les mini réunions dans ton bureau, qui finissaient souvent en discussion hors sujet. Tu es débordant d'idées, c'est incroyable. Merci aussi de m'avoir appris à relativiser, toi qui le fais si bien !

Je remercie également **Jonathan Massera**, mon encadrant « finlandais ». Jonathan, tu n'étais peut-être pas « officiellement » mon co-encadrant de thèse, mais c'était tout comme. Tu as été bien plus qu'un collaborateur au cours de cette thèse. Tu as toujours été présent pour moi, toujours disponible, et ce malgré la distance. Merci de m'avoir accueillie dans ton laboratoire en Finlande, en stage et en thèse. Tu m'as toujours intégrée au sein de ton équipe et m'a permis de travailler dans les meilleures conditions. Je vous remercie, **Laeticia** et toi, pour toutes les fois où vous m'avez accueillie chez vous. Merci pour tous les échanges, les discussions, les

conseils que tu m'as donnés. Et je te remercie infiniment de m'avoir proposé de continuer à travailler avec toi en Post-Doc. On est bien parti pour continuer.

Je vous suis infiniment reconnaissante à tous les trois pour tout ce que vous m'avez apporté. Vous m'avez fait grandir, tant scientifiquement, professionnellement que personnellement. Tous les moments passés restent dans mon cœur, et je n'oublierai jamais.

Je remercie notre ancien directeur de laboratoire, **Olivier Gallet**. Olivier, je te remercie de m'avoir permis de faire cette thèse au sein du laboratoire ERRMECe et ce dans les meilleures conditions. Merci pour ta présence et ton dévouement pour les thésards. C'est grâce à toi que nous avons pu organiser les 20 ans du laboratoire et bien d'autres événements. Merci pour ces soirées passées au laboratoire, pour tes blagues, et tes fameuses questions qui nous font toujours stresser. Je te remercie pour tout.

Je remercie également toute l'**équipe BIOSAN**, **Violeta Rodriguez**, **Adeline Gand**, **Agnès Mihajlovski** et **Damien Seyer**.

Violeta, en réalité c'est avec toi que tout a commencé lors de mon stage de M1. C'est ce stage à tes côtés qui m'a donné l'envie de continuer en recherche. Je te remercie pour tout ce que tu m'as appris, transmis et toutes nos discussions de tout et de rien. Je te remercie pour les fous rires et tous les bons moments passés ensemble. Je remercie dans le même temps **Virginie Gueguen** et **Graciela Pavon-Djavid** pour m'avoir également donné le goût de la recherche pendant ce stage de M1.

Adeline, je ne te remercierai jamais assez pour tout ce que tu m'as apporté au cours de cette thèse. Je te remercie d'avoir toujours été présente, disponible, toujours à l'écoute, que ce soit pour des répétitions ou des discussions de la vie en générale dans ton bureau. Tu as le don d'apaiser les gens et ça fait un grand bien de discuter avec toi. Je suis très heureuse de te connaitre et j'espère te revoir vite à Paris, ou en Finlande, qui sait ?

Agnès, je te remercie également d'avoir été présente tout au long de ma thèse. Merci de m'avoir formée à la BM, mais aussi d'avoir toujours été à l'écoute. Merci pour ta disponibilité. Tu es toujours là pour encourager les thésards, et donner de la force. Je te remercie également pour tout le super bon miel que tu m'as fournie, un délice !!!

Damien, merci à toi pour tous les échanges que nous avons eus. Merci d'être toujours de bonne humeur et en forme pour embêter les thésards. Tes taquineries permettent de toujours garder le sourire.

Sans oublier **Professeur Véronique Larreta-Garde**, partie à la retraite au cours de ma thèse, que je remercie grandement pour sa présence et sa bienveillance à mon égard. Je vous remercie pour vos cours enseignés avec passion, pour les échanges scientifiques que nous avons eus, pour m'avoir donné le goût de la recherche. Votre parcours est incroyable, vous êtes un réel exemple pour nous tous. J'espère que votre retraite tant méritée se passe pour le mieux.

Un GRAND MERCI également au **STAFF technique** : **Rémy Agniel**, **Lamia El-Guermah**, **Mathilde Hindié** et **Isabelle Pereira**.

Rémy, je te remercie pour tout le temps que tu as pris avec moi tout au long de ma thèse au microscope. Merci d'avoir toujours été disponible quand j'en avais besoin et de m'avoir formée en microscopie. Je n'oublie pas les bons moments passés, les fous rires, les commérages au microscope, et les taquineries. Je n'oublierai pas de te mettre en premier auteur dans mes articles !

Mathilde, merci pour ta présence et ta disponibilité. Toutes les fois où j'ai eu besoin de ton aide et tes conseils pour des manips, des protocoles, tu as répondu présente et je te suis très reconnaissante.

Je remercie également **tous les membres du laboratoire ERRMECe** pour tous les échanges. Je remercie tout particulièrement **Sabrina**, pour ta grande bienveillance, tes conseils et tes petits coucous dans notre bureau. Je tiens également à remercier **Cédric** pour nos différentes discussions sur l'avenir, ta bonne humeur et tes taquineries, en trio avec Damien et Rémy.

Je remercie toutes les personnes qui ont contribué dans cette thèse. Je remercie **Inari Lyyra** du laboratoire finlandais qui m'a aidée à la synthèse des composites ; **Sébastien Peralta** du LPPI pour les études en AFM ; **Cédric Vancaeyzeele** du LPPI, **Mathieu Goczkowski** et **Carla Palomino-Durand** pour les études de rhéologie ; **Isabelle Laurent** pour les analyses de GPC ; **Andres Arciniegas** de SATIE pour la caractérisation des gels par ultrasons. Je remercie

Susanna Miettinen et **Arjen Gebraad**, nos collaborateurs finlandais, pour m'avoir formée à la culture des cellules souches. Je remercie grandement **Annelise Cousture** du L2MGC pour les préparations d'échantillons, premières observations et analyses au MEB mais également pour tous les bons moments passés ensemble aux formations de l'école doctorale.

C'est avec beaucoup d'émotion que je remercie **Lamia**. Tout d'abord, je te remercie pour le temps que tu as pris durant ma thèse pour m'aider. Tu es toujours présente et disponible pour les thésards, un grand merci pour ça. Ensuite, je voudrais que tu saches que tu as été bien plus que la technicienne de laboratoire pour moi. Tu as été comme une grande sœur toutes ces années, toujours présente, dans les bons, comme dans les mauvais moments. Tu as toujours su trouver les mots quand ça n'allait pas trop, et je te remercie pour tous les conseils personnels que tu m'as donnés. Nous nous sommes rencontrées durant mon stage de M1, cela fait 5 ans maintenant, et c'est bien partie pour durer.

Un TRÈS GRAND MERCI aux filles du bureau : **Audrey**, **Carine** (**Caro** pour les intimes), **Mathilde** et **Amel**. Il est évident que cette thèse n'aurait pas été la même sans vous. Merci pour votre soutien dans les moments difficiles, moments de tristesse mais n'oubliez pas : « Il est fait pour ça ce bureau ! ». Je vous remercie grandement pour les fous rires, les bons moments passés que je n'oublierai jamais. J'espère bien que nous continuerons à passer ces moments même après la thèse. Vous me manquez déjà !

Je remercie également tous les thésards et post-docs : **Maxime**, **Rosa**, **Carla**, **Solène**, **Phuong-Anh**, **Anamar**, **Sahil**, **Clotilde**, **Chahrazed**, **Audrey D.** pour les bons moments passés au laboratoire.

Un merci spécial pour **Maxime**, **Rosa**, **Carla**, **Solène** et **Phuong-Anh** pour les supers moments passés en congrès, et ça même en distanciel (ESB 2021) !
Maxime, merci à toi pour ta positivité, pour avoir toujours été disponible pour nous aider Caro et moi à l'organisation d'événements au labo, débordant d'idées et de volonté.
Carla, merci à toi pour tes précieux conseils.

Inari, **Sanna**, **Henriikka** et **Mari**, merci pour les bons moments passés en Finlande ! J'en garde de très bons souvenirs.

Je remercie infiniment les anciens : **Hassan**, **Audrey**, **Rony**, **Andrey**, **Mathieu**, **Éléonore**. Merci pour votre présence, votre soutien sans faille et vos précieux conseils. Cette thèse n'aurait pas été la même sans vous. Je suis très heureuse de vous avoir trouvés sur mon chemin. Merci pour les apéros, les fous rires, je sais que cela durera encore des années. Merci aussi à **Alice** qui fait évidemment partie de l'équipe.

Je remercie également mes amies et collègues, **Hadjer** et **Alexandra**. Vous avez été d'un soutien inestimable durant cette thèse. Nous nous sommes croisées sur les bancs de la fac, et nous ne nous sommes plus quittées. Je suis fière que nous ayons parcouru ce chemin ensemble, toutes les trois docteures aujourd'hui et je nous souhaite le meilleur pour la suite.

Je voudrais remercier mes chers amis : **Inès**, **Kimia**, **Imane**, **Ornella**, **Sarah**, **Rihab**, **Ahmed**. Merci pour votre présence et votre soutien sans faille au cours de cette thèse. J'ai toujours pu compter sur vous dans les bons comme dans les mauvais moments. Merci pour les sorties, les soirées, les weekends, les voyages qui m'ont fait sortir de mon quotidien.
Inès et **Kimia**, vous êtes mes sœurettes d'une autre mère et je ne compte pas vous lâcher. Préparez-vous à me supporter encore longtemps.

Je remercie **Kyle** pour sa présence et son soutien toutes ces années. Je n'ai pas toujours été facile à supporter mais je sais que j'ai toujours pu compter sur toi. Tu es une belle personne et malgré les hauts et les bas, je ne retiens que le positif.

Et comme on dit, le meilleur pour la fin…

Mes plus grands et plus profonds remerciements sont pour ma famille. **Papa**, **Maman**, **Hayette**, **Ali**, je ne vous remercierai jamais assez pour tout ce que vous m'avez apporté toutes ces années. Il ne s'agit pas seulement de la thèse mais de toute ma vie. Vous avez cru en moi quand personne ne le faisait. Vous m'avez appris la persévérance, m'avez donné la volonté et la force de réussir. Si j'ai réussi, c'est grâce à vous. Si je suis une battante aujourd'hui, c'est grâce à vous. Merci de m'avoir supportée même quand j'étais insupportable. Merci d'avoir pris soin de moi et de m'avoir tout donné pour que je puisse travailler dans les meilleures conditions. Cette thèse, sur laquelle j'ai tant travaillé ces années, est pour vous et de tout mon cœur, je vous la dédie.

« On n'est pas condamné à l'échec »

Kery James

Table of contents

Table of illustrations

List of tables

Abbreviations

3D	Three-dimensional
ACP	Amorphous Calcium Phosphate
ALP	Alkaline Phosphatase
APTES	3-aminopropyltriethoxysilane
BAG	Bioactive Glass
BCP	Biphasic Calcium Phosphate
BM	Basic Medium
BMP	Bone Morphogenetic Proteins
BMSCs	Bone Marrow Stromal Cells
Ca-P	Calcium-Phosphate
CAD	Computer Aided-Design
CAM	Computer Aided-Manufacturing
Coll I	Collagen I
CSD	Critical Size Defect
CT	Computed Tomography
DBM	Demineralized Bone Matrix
FDA	Food and Drug Administration
FDM	Fused Deposition Modeling
Gla	γ-Carboxy Glutamic Acid-Containing
GPTMS	3-glycidoxypropyltrimethoxysilane
HA	Hydroxyapatite
HCA	Hydroxyl Carbonated Apatite

HSCs	Hematopoietic Stem Cells
ICPTES	3-isocyanatopropyltriethoxysilane
IL	Interleukin
MSCs	Mesenchymal Stem Cells
OC	Osteocalcin
OM	Osteogenic Medium
OP	Osteopontin
PCL	Poly (caprolactone)
PGA	Poly (Glycolic) Acid
PLA	Poly (Lactic Acid)
PLGA	Poly (Lactic-co-Glycolic) Acid
RANK	Receptor Activator of the Nuclear factor κB
RANK-L	Receptor Activator of the Nuclear factor κB Ligand
SF	Silk Fibroin
SBF	Simulated Body Fluid
TCP	Tricalcium Phosphate
TNF	Tumor Necrosis Factor
TGF- β	Transforming Growth Factor β
VEGF	Vascular Endothelial Growth Factor

Abstract

Bone fractures are common traumas usually compensated by the natural repair process called osteogenesis. In the case of complex and critical size defects, due to a traumatic or pathophysiological context, the repair must be assisted by substitutes that can serve as a support and mechanical replacement and/or as bone filling.

The interest of bioactive glass (BAG) lies in their bioactivity. They have the particularity of releasing their calcium and phosphate ions which precipitate and form a reactive hydroxyapatite layer. However, BAG are hard to shape. So, inspired by bone composition, combining them with organic matrices would provide innovative materials for bone bioengineering. It is in this context that this project is focused, on the development of composite and hybrid materials based on bioactive glass for bone bioengineering. In this project, two paths were explored, i) a composite material based on Poly (Lactic Acid) (PLA) and bioactive glass and ii) a hybrid material based on gelatin and bioactive glass. The first system is more dedicated to assist the functions of mechanical support, whereas the second will be more pertinent to address the need of filling bone defects. In this study, the BAG 13-93 was used directly and compared to the 13-93B20, its boron-doped form known to influence its dissolution properties.

The first part of this work, focused on the composites based on PLA and 13-93 or 13-93B20, allowed us to characterize the two composites and to compare the different BAG reactivity. The boron allowed us to modulate the dissolution rate of the BAG in the composites, leading to a faster dissolution. The bioactivity *in vitro* of these composites was more important with the 13-93B20. Preliminary cell experimentations using C2C12 myoblastic cells showed that the materials exhibit osteo-stimulating properties.

The second part of this thesis is focused on the elaboration of hybrids based on gelatin and 13-93 or 13-93B20 using a bifunctional coupling agent, the 3-glycidoxypropyltrimethoxysilane (GPTMS). The GPTMS appeared to form covalent links between the organic and inorganic phases as the gels stay self-supported at biological temperature. The 13-93B20 allowed to accelerate the dissolution and to increase the hybrids bioactivity. The biocompatibility of the hybrids has been demonstrated using MC3T3-E1 pre-osteoblastic cells.

The results of this thesis showed that the composition of the BAG is a key property with respect to its behavior and the cellular response. These tailor-made materials have a real potential for physical support, resorbability properties, and bone regeneration capacities via the induction of suitable cellular behaviors favored by bioactive glasses, bringing an osteo-competent and osteo-stimulating dimension to the implant.

Keywords: Composite, Hybrid, Bioactive Glass, Osteo-competence, Bone tissue engineering

Résumé

Les fractures des os sont des traumatismes courants généralement compensés par un processus naturel de réparation appelé ostéogénèse. Lorsqu'il s'agit de défauts complexes et de taille critique, dus à un contexte traumatique ou physiopathologique, la réparation doit être assistée par le biais de matériaux qui puissent servir de support et suppléance mécanique et/ou de comblement osseux.

L'intérêt du verre bioactif (BAG) réside dans sa bioactivité. Ils ont la particularité de libérer leurs ions calcium et phosphate capables de former une couche réactive d'hydroxyapatite. Cependant, les BAG sont difficiles à mettre en forme. Ainsi, inspiré par la composition de l'os, les combiner avec des matrices organiques fournirait des matériaux innovants pour la bio-ingénierie osseuse. C'est dans ce contexte que s'inscrit ce projet, sur le développement de matériaux composites et hybrides à base de verre bioactif pour la bio-ingénierie de l'os. Dans ce projet, deux voies ont été explorées, i) une association composite à base de Poly (Acide Lactique) (PLA) et de verre bioactif pour répondre aux besoins mécaniques et ii) des matériaux hybrides à base de gélatine et de verre bioactif pouvant servir de matériaux de comblement. Dans cette étude, le BAG 13-93 a été utilisé tel quel et dans sa forme dopée au bore 13-93B20; le bore étant connu pour avoir une influence sur ses propriétés de dissolution.

La première partie de cette thèse, centrée sur les composites à base de PLA et 13-93 ou 13-93B20, a permis de caractériser les deux composites et de comparer les différentes réactivités des BAG. Le bore a permis de moduler la vitesse de dissolution du BAG dans les composites, conduisant à une dissolution plus rapide. Leur bioactivité *in vitro* a été trouvée plus importante avec le 13-93B20. A l'aide de cellules myoblastiques C2C12, il a été montré que les matériaux présentaient des propriétés ostéo-stimulantes.

La seconde partie de cette thèse est centrée sur l'élaboration d'hybrides à base de gélatine et 13-93 ou 13-93B20 utilisant un agent de couplage bifonctionnel, le 3-glycidoxypropyltriméthoxysilane (GPTMS). Le GPTMS semble former des liaisons covalentes entre les phases organique et inorganique car les gels restent autosupportés à température biologique. Le 13-93B20 a permis d'accélérer la dissolution et d'augmenter la bioactivité des hybrides. La biocompatibilité des hybrides a été démontrée à l'aide de cellules pré-ostéoblastiques MC3T3-E1.

Les résultats de ce projet ont montré que la composition du BAG est une propriété clé vis-à-vis de son comportement et de la réponse cellulaire. Ces matériaux sur-mesure présentent un réel potentiel de maintien physique, de résorbabilité et de régénération osseuse via l'induction de comportements cellulaires idoines favorisés par des verres bioactifs, apportant une dimension ostéo-compétente et ostéo-stimulante à l'implant.

Mots clés : Composite, Hybride, Verre bioactif, Ostéo-compétence, Ingénierie tissulaire osseuse

General introduction and Objectives

Context

The human **musculoskeletal system** includes the muscular system and the **bone skeleton**. The adult human skeleton has 206 bones [1]. Bone tissue is a material containing an organic matrix mainly composed of collagen and an inorganic matrix made of hydroxyapatite [2]. It constitutes the framework of the body, on which the muscles and other structures can attach themselves. Its main functions are to support and protect the vital organs and the nervous system, to produce blood cells and to store lipids and minerals. Metabolically active, bone undergoes continuous remodeling throughout life. For adults, the skeleton is remodeled at a rate of 10% per year [3]. Bone is often submitted to stresses, but the remodeling process allows it to keep its properties and gives it the capability to heal small fractures naturally [4].

For complex and/or critical size defects, the bone is no longer able to repair naturally, bone remodeling is compromised, and the repair needs to be guided. Indeed, more than **2 million bone grafts** are performed worldwide annually. Bone is the second most transplanted tissue worldwide after blood [5]. The major causes of these defects are traumatisms and tissue resection due to cancer [6–8]. For the reconstruction, the gold standard is the **autologous graft** from the iliac crest, because it allows to keep the fundamental properties of bone for an optimal repair [9,10]. However, it presents some drawbacks such as the limited availability. **Allografts** and **xenografts** are also used but the disease transmission, their expensive cost and the risk of rejection remain limitations [11]. All these drawbacks have thus lead to an interest in developing biomaterials for the repair of bone tissue.

Biomaterials are materials which interact with the human body, to ensure specific functions, which are: repairing, treating, replacing/substituting a given region of the body by the action of its constituents [12]. Nowadays, with the **tissue engineering** and **regenerative medicine** concepts, the challenge of **bone bioengineering** becomes greater, requiring materials that will not only be used to replace but also to **regenerate** the tissue [13,14]. These materials

need to be biocompatible, biodegradable, and present **osteo-properties** i.e., osteointegration, osteo-conduction, osteo-induction. **Osteointegration** is defined as "*the direct bond between the implant surface and bone tissue, without a fibrous layer in between"*. **Osteo-conduction** is *"passive property of a material allowing the deposition of mineralized tissue on its surface"*. **Osteo-induction** refers to "*the ability of a material to stimulate differentiation of a cell toward an osteoblast lineage which will lay down mineral and is often demonstrated by implantation in soft tissue environments, such as muscle"* [15,16]. These three characteristics are fundamental for an optimal bone repair. In addition, research is currently focusing on bioactive materials. Their **bioactivity** will optimize the biological response due to their reactivity and the formation of strong interactions with the surrounding tissue [17]. The bioactivity is a key property which will promote osteointegration.

Thus, according to these properties and inspired by bone composition, **organic – inorganic materials** are a promising alternative for bone repair [18]. The inorganic phase will bring the osteo-properties to the substitute in particular osteo-conduction and osteointegration. It can be dispersed in the organic phase yielding to a **composite material,** or covalently linked to the organic phase thanks to a coupling agent, resulting in a **hybrid material** [19,20]. These materials can be tailor-made, adapted to the type and size of the defect.

Depending on the clinical situation, the defects can require materials for mechanical support and substitution and/or filling materials.

Substitution and mechanical support materials consist in, temporarily or permanently, holding in place and stabilizing fractured bones using osteosynthesis implants. Their role, by relatively immobilising the bone fragments, is to allow the natural consolidation of the bone in good position, while often allowing early functional rehabilitation, or to replace totally the bone in question [21]. They require high strength and toughness.

Filling materials concern defects which can have a high volume, with a large bone loss, and cannot be repaired with osteosynthesis implants alone. This repair needs to be guided thanks to materials which will be used to fill critical skeletal defect, to maintain bone volume until complete repair, with an adapted resorption according the newly formed bone tissue [4,22].

Research objectives

It is in this context that the thesis is based, focused on the **development of composite and hybrid materials based on bioactive glass for bone tissue engineering**. Two materials were developed: **a composite based on Poly (Lactic Acid) (PLA) and bioactive glass** to provide a support and mechanical replacement function; **a hybrid material based on gelatin and bioactive glass** to ensure a filling function.

Bioactive glass (BAG) was first developed by Hench et al. in 1969 and represents a group of reactive materials that can bond to mineralized bone tissue [23]. It is widely used in the biomedical area. During its dissolution in an aqueous medium, it releases therapeutic ions, specifically, calcium and phosphate ions which precipitate in a hydroxyapatite reactive layer [24]. The Bioglass 45S5 and BonAlive S53P4 are the only BAGs commercialized [25]. However, if used in organic – inorganic materials, their fast dissolution rate can have an influence on the integrity of the organic matrix [26]. To avoid this effect, we decided to use the glass **13-93**, which has a slower reactivity. Doping its composition with boron will allow to tailor its dissolution rate. Boron will increase the dissolution rate of the glass while keeping it lower than the commercialized ones [27,28]. Therefore, the second composition of 13-93 was adapted and 20% of silicate was replaced by borate, resulting in the **13-93B20** BAG.

This work is thereby concentrated on composite materials based on PLA and 13-93 or 13-93B20, and hybrids based on gelatin and 13-93 or 13-93B20. Two BAGs were compared in two different strategies.

The **first chapter** of this thesis presents a bibliographic introduction of the subject divided in two parts. The **first part** aims to understand bone tissue background, its structure, its composition, and its different biological processes. This part will allow us to apprehend the properties of the bone which are fundamental to respect for its repair. The **second part** will allow us to know the different types of bone defects, and the strategies used to repair them.

The **second chapter** of this thesis is focused on the **composites based on PLA and 13-93 or 13-93B20** (**Article 1**) [29]. These composites have interesting mechanical properties and a slow dissolution rate, thus, should be more suitable to act as a **mechanical support and substitution material**. The objective was to characterize the two composites and to compare the different BAGs reactivity and bioactivity *in vitro*. Preliminary cell experimentations were done, using C2C12 myoblastic cells, in order to investigate the biocompatibility of the composites and the ability of the cells to commit to an osteoblastic lineage in presence of the BAG. The results showed that:

i) **The boron allows to tailor the dissolution rate of the BAGs, leading to its faster dissolution and higher reactivity.**
ii) **The bioactivity *in vitro* of the composites was demonstrated and was more important with the 13-93B20.**
iii) **The C2C12 cells seem to be able to commit to an osteoblastic lineage in presence of the BAG.**

The **third chapter** is focused on the **hybrids based on gelatin and 13-93 or 13-93B20** (**Article 2**) [30]. These hybrids are materials which can maintain bone volume until repair and thus will be more adapted for a **filling function**. However, the covalent coupling between the gelatin and BAG is fundamental to have a self-supported material at biological temperatures and mechanical properties adapted to this function. The covalent links between the organic and inorganic phases were obtained thanks to the **3-glycidoxypropyltrimethoxysilane (GPTMS)**. The objective of this study was to develop and characterize two different hybrids and compare the effect of the 13-93 and 13-93B20. The bioactivity *in vitro* of these hybrids was investigated. The biocompatibility of the hybrids was studied using MC3T3-E1 pre-osteoblastic cells. The results showed that:

i) **The GPTMS appear to form covalent links between the organic and inorganic phases as the gelatin gels are still self-supported at 37 °C.**
ii) **The dissolution of the glass can be tailored by modifying its composition.**
iii) **The bioactivity *in vitro* of the hybrids was demonstrated and was more important with the 13-93B20.**
iv) **The hybrids appear to be cytocompatible as the MC3T3-E1 cells can proliferate and spread on their surface.**

The next aim was to study the osteo-stimulation of these hybrids on Bone Marrow Stromal Cells (BMSCs). The results showed that it was difficult for the cells to proliferate on the hybrids. Some investigations are required to explain these outcomes and to find a solution to this issue. Next experimentations will be done using adipose stem cells in order to evaluate their behavior and the osteo-stimulation of this new generation of materials on these stem cells.

These three chapters will be followed by a general conclusion about these results and the perspectives will be presented.

The composition of the BAGs is a key property with respect to its behavior and the cellular response. By adding the boron in the glass composition, its dissolution in aqueous medium is tailored and its bioactivity is more important. Also, it was observed that the effect of BAGs on the organic phase was limited and did not lead to a degradation of the materials. Cells behavior investigations showed that the BAGs can influence the differentiation of the cells. In the two systems studied, the bioactivity of the BAGs is preserved, and the formulation of the 13-93B20 BAG would be a better candidate for applications requiring materials with osteo-properties.

This thesis allowed us to propose combined, innovative materials capable of responding to bone bioengineering challenges. Composite materials - based on PLA and BAG - and hybrid materials - based on gelatin and BAG - respectively exhibiting mechanical support and / or filling potentials have been developed. These tailor-made materials have a real potential for physical support, resorbability properties, and bone regeneration capacities via the induction of suitable cellular behaviors favored by bioactive glasses, bringing an osteo-competent and osteo-stimulative dimension to the implant.

<u>Article 1:</u> Dissolution, bioactivity, and osteogenic properties of composites based on polymer and silicate or borosilicate bioactive glass

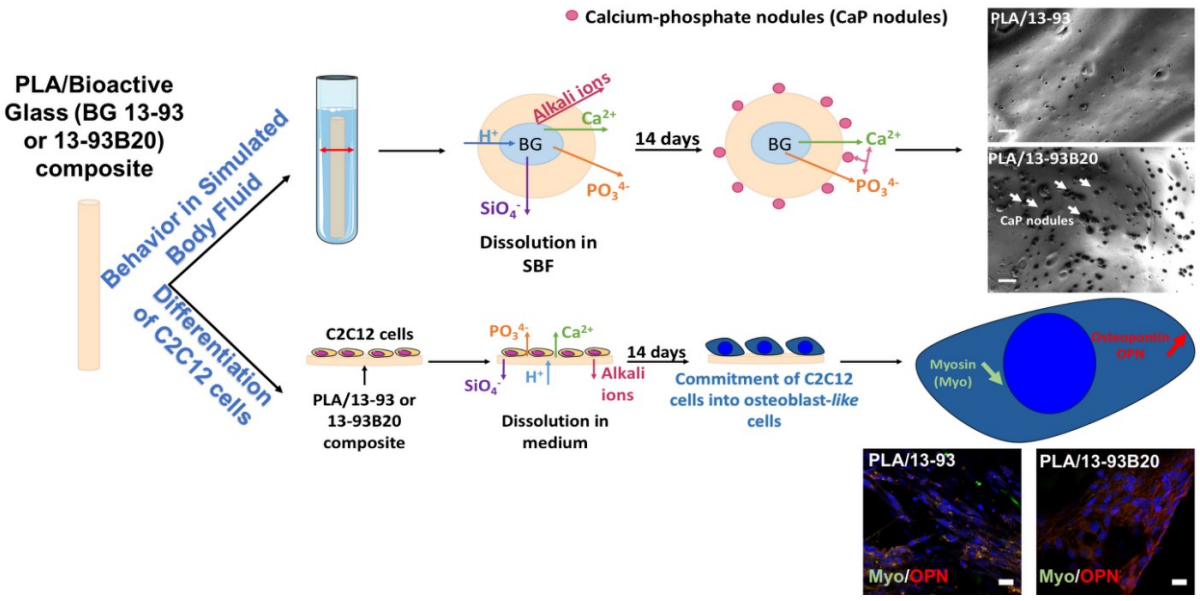

<u>Article 2:</u> New generation of hybrid materials based on gelatin and bioactive glass particles for bone tissue regeneration

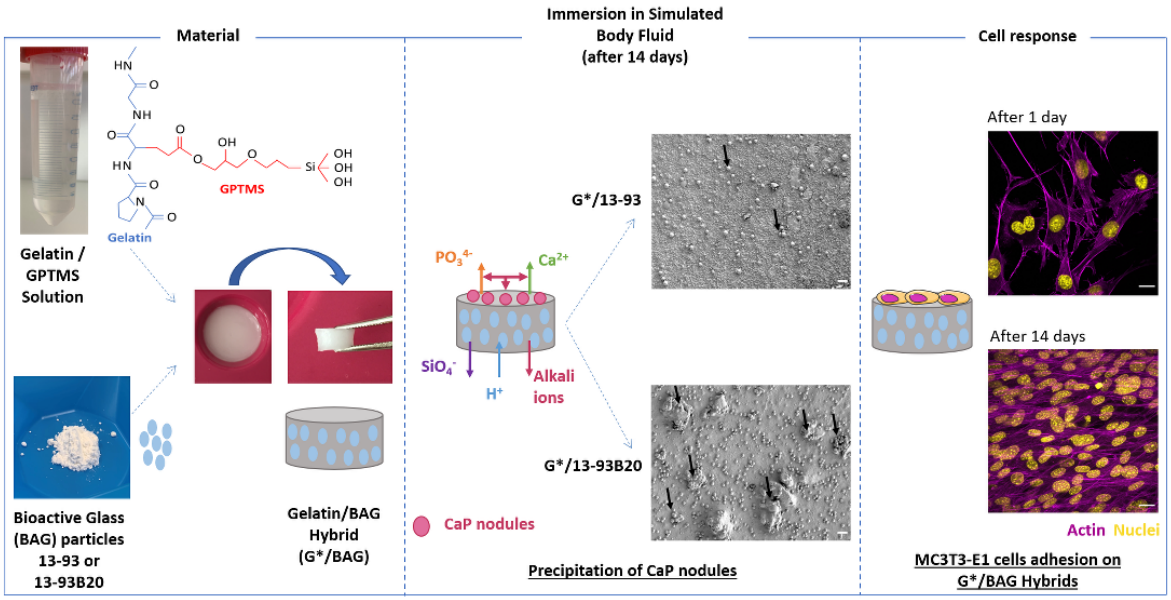

Figure 1: *Schematic summary of the project*

Chapter 1: State of the art

A. BONE TISSUE

The human skeleton is composed of 206 bones. These bones are classified in four categories: long bones, flat bones, short bones and irregular bones. Bone tissue has three main functions [1,31,32]:

1. Mechanical: it supports and protects vital organs as well as the nervous system. Bones allow the transfer of forces from one part of the body to another. The mechanical properties of a bone are a compromise between i) stiffness, low elasticity to reduce stress and ii) ductility, to absorb shocks to reduce the risk of fracture.

2. Metabolic: bone tissue is a dynamic tissue in constant renewal under the effect of mechanical stresses. This remodeling leads to the storage or release of mineral salts. The bone thus participates in the phosphocalcic homeostasis of the body.

3. Hematopoietic: The hematopoietic marrow, enclosed in the medullary space of the bone, is responsible for the production of all three types of blood cell lines.

1. Bone: structure and composition

1.1 Bone structure

Bone is a connective tissue that can be considered as a composite material [2,33]. The inner part is made of cancellous bone, while the outer part is formed by compact bone. The relative mass ratio between these two types of bone varies from 20% to 80% throughout the skeletal system, depending on the bones. The main difference between cancellous and cortical bone lies in their porosity which varies greatly (i.e. highly porous for the cancellous bone and dense for the cortical one) [34]. Cortical bone has a function of support and protection against mechanical stress while cancellous bone allows metabolic functions.

1.1.1 Cortical bone

Compact bone represents up to 80% of the skeleton weight. It is 95% mineralized and presents between 5 and 30% of porosity [34]. This part of the bone consists of bone lamellae and is organized into a basic circular unitary structure called Haversian system or osteons (**Figure 2**). An osteon is a cylindrical structure with a diameter between 100 and 400 μm, containing bone lamellae disposed around Haversian canal. This canal is necessary for the cell survival and contains small vessels, connective tissue cells, and nervous fibers isolated. In the osteon are found the osteocytes. These osteocytes are linked together by the canaliculi, to maintain the nutritional intakes between them. Some transverse canals, the Volkmann canals, cross the osteons perpendicularly to their major axis leading to a porosity of the bone, providing vascularity and nutrition for Haversian systems.

Cortical bone is found at the periphery of the bones and around the medullary cavities containing the bone marrow and trabecular bone. It forms the thick wall of the diaphysis of long bones and the much thinner outer covering of short bones and flat bones, such as in particular the maxillary and mandibular bones [2,34].

1.1.2 Cancellous bone

Trabecular or spongious bone presents between 30 and 95 % of porosity [34]. It has a low density, and it is found in the center of the bone delimited by cortical bone. It is a three-dimensional network of bone spans, branched and anastomosed with a thickness from 100 to 500 μm and a space between trabeculae of 500 – 1000 μm [35]. The trabeculae have a lamellar organization. In this porous structure, there is the bone marrow, constituted of various cell types like for example adipocytes or mesenchymal stem cells, blood vessels, nerves as well as trabeculae osteocytes receiving nutrients through canaliculi network. The bone marrow, involved in hematopoiesis, is the site where blood and immune cells are formed. With age, it becomes the yellow bone marrow, a lipid storage area [31]. Trabecular bone is always

surrounded by cortical bone. It is found in small quantities at the center of the diaphysis of long bones, and forms the major part of the metaphysis and epiphyses of these bones where it serves to absorb mechanical stresses (**Table 1**) [36].

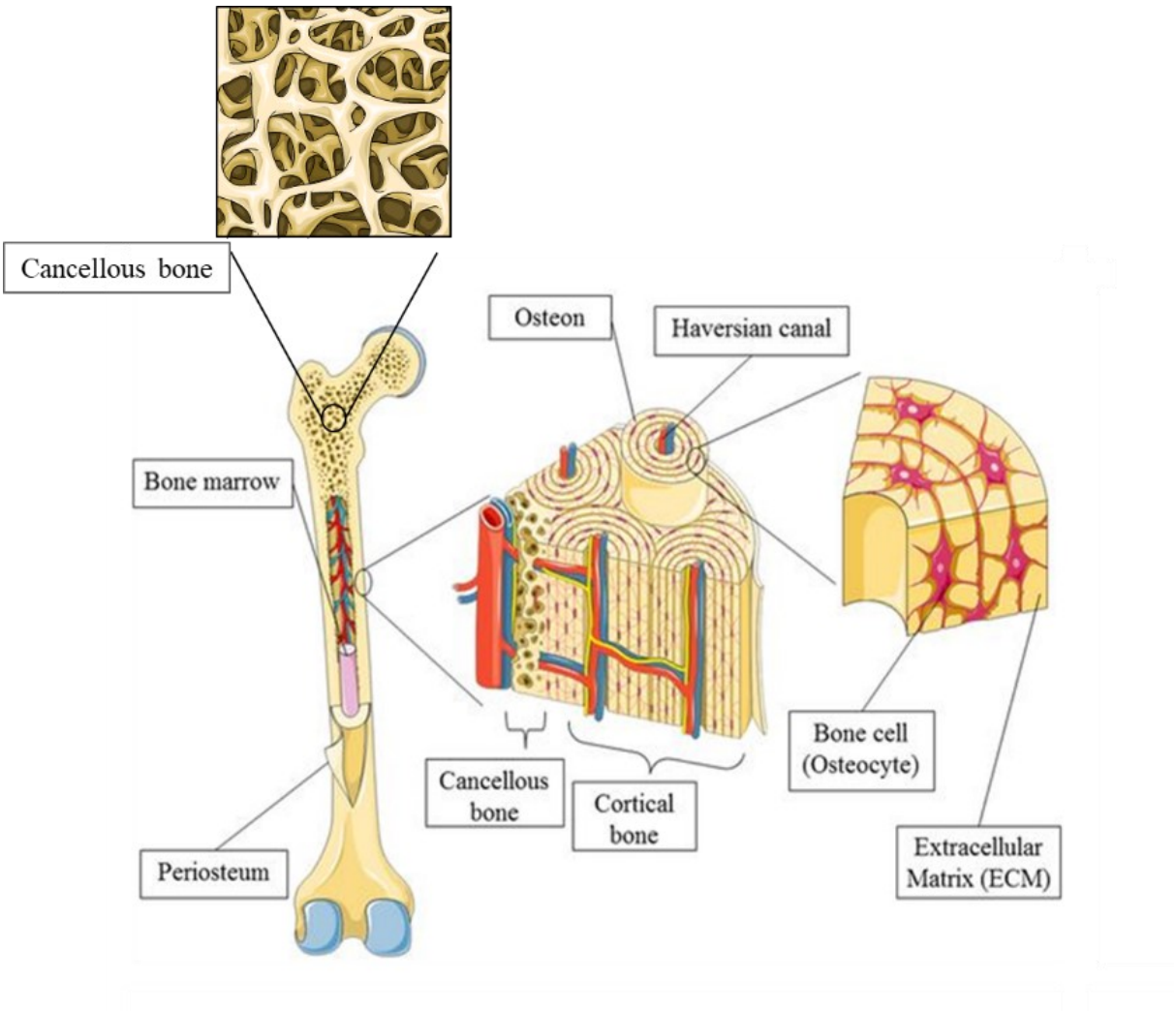

Figure 2: *Structure and composition of bone (from Servier medical art)*

Properties	Cortical Bone	Cancellous Bone
Compressive Strength (MPa)	100 - 230	2 - 12
Flexural, tensile strength (MPa)	50 - 150	10 - 20
Strain to failure (%)	1 - 3	5 - 7
Young modulus (GPa)	7 - 30	0.05 - 0.9

Table 1: *Mechanical properties of cortical and cancellous bone [37,38]*

1.1.3 The periosteum

The periosteum is the connective tissue found on the external surface on almost all bones of the body. It is the transition phase between the cortical bone and soft tissue [31].

It is divided histologically into two distinct layers:

- the outermost layer, called "fibro-elastic", is resistant and composed of collagen, elastic fibers, and many fibroblasts.
- the "cambial" inner layer, in direct contact with the bone, contains numerous blood vessels, fibroblasts and a dense network of collagen fibers, or "Sharpey fibers", which anchor in the bone to bind the periosteum to bone tissue. Finally, it contains mesenchymal stem cells, osteoprogenitor cells and pre-osteoblasts which can activate during bone repair or appositional growth [31].

1.1.4 The endosteum

It is the internal counterpart of the periosteum. It is in the form of a thin membrane that lines the entire inner side of the oscillatory and the walls of the cavities of the cancellous bone. It consists of a single layer of osteoprogenitor cells, giving birth to osteoblasts, and osteoclasts [31].

1.2 Bone composition

Bone is a composite material consisting of mineral and organic phases. It is also composed of many cell types organized and disseminated in an extracellular organic matrix, reinforced by calcium deposits.

1.2.1 Bone matrix

The main function of bone matrix is to bring the biomechanical and biochemical properties to bone tissue. This matrix is based on an organic and an inorganic phase, representing 25% and 65% of the bone tissue (weight%) respectively and the 10% left represents the water [2].

1.2.1.1 Inorganic matrix

Bone tissue has two main roles:

- Endure mechanical stresses exerted on itself, thanks to its hardness and rigidity.
- Also constitute an ions reservoir necessary to the homeostasis.

This matrix represents 65% of dry bone weight. This inorganic phase is mostly constituted of calcium phosphate, forming hydroxyapatite [$Ca_{10}(PO_4)_6(OH)_2$] (HA) crystals. Mineral matrix organization allows the bone to have high stiffness (**Table 2**) [39]. Indeed, the crystals are deposited and incorporated to collagen fibers. They are parallelly arranged to each other and to the collagen fibers. This organization allows a good mechanical resistance for bone tissue [2,31].

In addition to calcium and phosphate, the mineral phase is also constituted of sodium and magnesium ions (**Table 3**). They are released when needed by the organism, to maintain the plasma concentration necessary for functions like nerve conduction or muscle contraction [40].

Density (g/cm^3)	**Elasticity modulus (GPa)**	**Compressive strength (MPa)**	**Tensile strength (MPa)**	**Flexural strength (MPa)**
3.05 – 3.15	80 – 120	300 – 900	40 – 200	100 – 120

Table 2: *Physical properties of hydroxyapatite [39]*

Elements (mass %)	Bone	Dentine	Enamel	Apatite stoichiometric
Ca	34.80	35.10	36.50	39.60
P	15.20	16.90	17.70	18.50
Na	0.90	0.60	0.50	-
Mg	0.72	1.23	0.44	-
K	0.03	0.05	0.08	-
Inorganic C	1.48	1.12	0.7	-
F	0.03	0.06	0.01	-
Cl	0.13	0.01	0.30	-

Table 3: *Comparative composition of inorganic phases of adult human calcified tissue [40–42]*

1.2.1.2 Organic matrix

This matrix represents 25% of dry bone weight. It is mainly composed of collagen (90%), mostly type I collagen, and the 10% left represent the non-collagenous proteins like non-collagenous glycoproteins, proteoglycans, osteopontin, osteocalcin, etc [43].

Collagen is a fibrous protein, insoluble, found in the extracellular matrix of numerous connective tissues. In bone tissue, the organic extracellular matrix proteins are mainly type I collagen (95%) (**Table 4**) [2,44]. Collagen fibers regulate the nucleation and spatial orientation of HA crystals. Indeed, the triple helix of collagen are aligned in collagen fibrils with a shift between the ends of the two consecutive subunits. The shifts are the nucleation site of HA crystals whose size and orientation are controlled by the structure and organization of collagen fibrils (**Figure 3**) [31,45].

The organic extracellular matrix is also constituted of type III and type V collagen in a small quantity which have a role in the fibrillogenic regulation and the diameter fibril modulation [46].

Type of collagens	Function
Type I	Most abundant protein in bone matrix (90%), serves as scaffolding, binds and orients other proteins that nucleate HA deposition
Type III, Type V	Present in bone in small amounts, may regulate collagen fibril diameter, their paucity in bone may explain the large diameter size of bone collagen fibrils

Table 4: *Different types of Collagen found in bone matrix and their function.[44]*

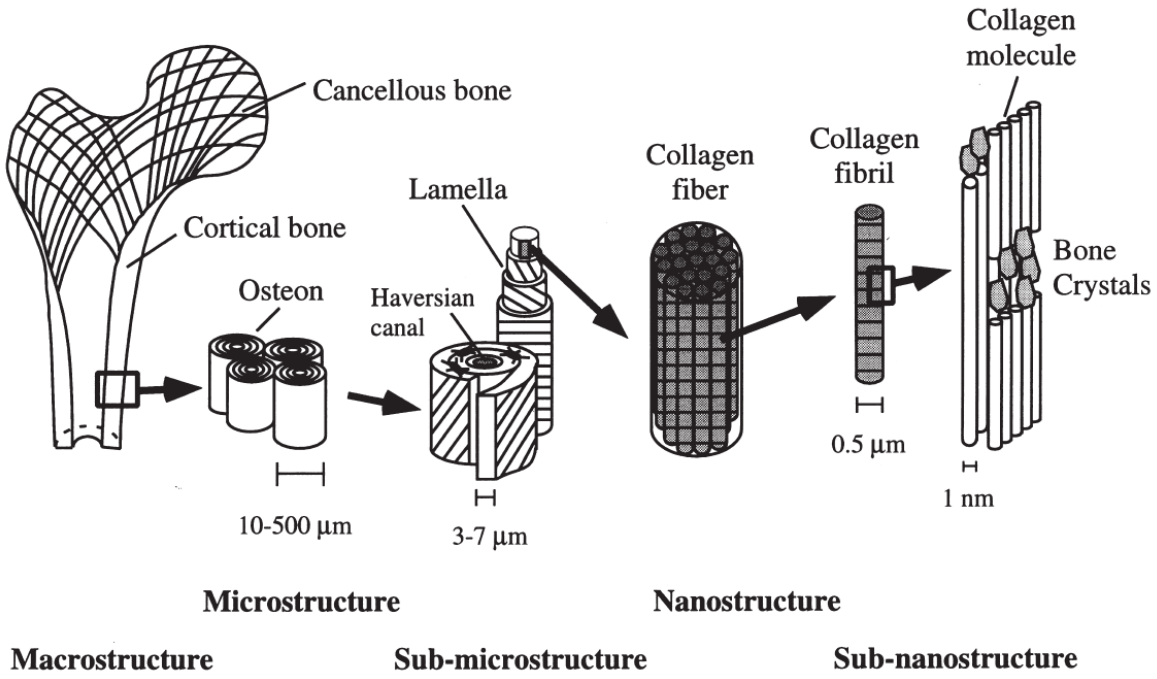

Figure 3: *Hierarchical structural organization of bone: (a) cortical and cancellous bone; (b) osteons with Haversian systems; (c) lamellae; (d) collagen fiber assemblies of collagen fibrils; (e) bone mineral crystals, collagen molecules, and non-collagenous proteins. [45]*

In addition to collagens, the organic matrix is constituted of non-collagenous proteins. These proteins are involved in the organization of the matrix, act as nucleators of the deposition of HA crystals in the matrix during the bone mineralization and modify the behavior of bone cells. Different types of proteins are found in this matrix like proteoglycans, glycoproteins,

serum proteins, Gla proteins (γ-Carboxy Glutamic Acid-Containing Proteins) and the most abundant are presented in **Table 5** [44].

Proteins type	Molecules	Functions
Proteoglycans	Decorin	Involved in the establishment of the collagenous fibrillar network of the bone matrix, in the mineralization by regulating the size, morphology and growth of HA crystals and in the proliferation and differentiation of osteoblasts.
	Biglycan	
Glycoproteins	Osteonectin	Binds to collagen and HA crystals, inhibits crystals nucleation and growth. Involved also in the regulation of bone cells proliferation and the differentiation, maturation, and survival of osteoblasts. It maintains a constant bone remodeling and renewal.
	Osteopontin	Constitutes a receptor of integrin family and promotes bone cells attachments on bone tissue. Inhibits also bone mineralization by stopping HA crystals growth.
	Bone Sialoprotein	Initiates HA crystals formation and act as bone mineralization nucleator.
Gla Proteins	Osteocalcin	Represents 15% to 20% of non-collagenous proteins. Fixes calcium ions and adheres to HA crystals, regulating the nucleation and growth of crystals, and stopping mineralization process. Involved in the resorption phenomenon and bone remodeling by promoting osteoclasts recruitment and differentiation.

Table 5: *Most abundant non-collagenic protein families in the organic matrix and their functions [44]*

This organic matrix has a role in the shape of the bone. It acts as a reservoir of growth factor and cytokines which has a role in bone remodeling. It has also an implication in the overall tissue mechanical resistance.

1.2.2 Bone cells

Four types of cells are responsible for bone remodeling: osteoblasts, osteoclasts, osteocytes and bone-lining cells [32]. The corresponding progenitor cells are Mesenchymal Stem Cells (MSCs) and Hematopoietic Stem Cells (HSCs).

1.2.2.1 Osteoclasts

The osteoclasts are responsible for bone resorption during the bone remodeling process. They come from HSCs. The HSCs, under the influence of a transcription factor, proliferate and differentiate into mononuclear progenitor cells. These cells proliferate also and lead to the monocytic, macrophagic and pre-osteoclastic cell lines which go to bone tissue. This happens in the bone marrow under the control of osteoblasts. The pre-osteoclasts have on their membrane surface a receptor activator of the nuclear factor κB (RANK). This receptor binds to a specific cytokine from the Tumor Necrosis Factor (TNF) superfamily, the ligand of RANK (RANK-L), found on osteoblasts cell membrane. After that, many pre-osteoclasts merge to form one immature osteoclast multinucleated (**Figure 4**) [47,48].

Osteoclasts are responsible for bone resorption by forming resorption lacunae, named Howship lacunae, on the trabecular bone and the periosteum or a resorption tunnel on the cortical bone.

On one hand, bone resorption happens when the mineral phase of the extracellular matrix is degraded thanks to the acidification of the medium. The osteoclasts release H^+ protons and Cl^- ions forming HCl, to obtain a pH of 3 - 4, which will dissolve HA crystals. On the other hand, the organic phase is degraded by enzymes like acidic hydrolases, proteases (cathepsin K), collagenases responsible for type I collagen lysis [48].

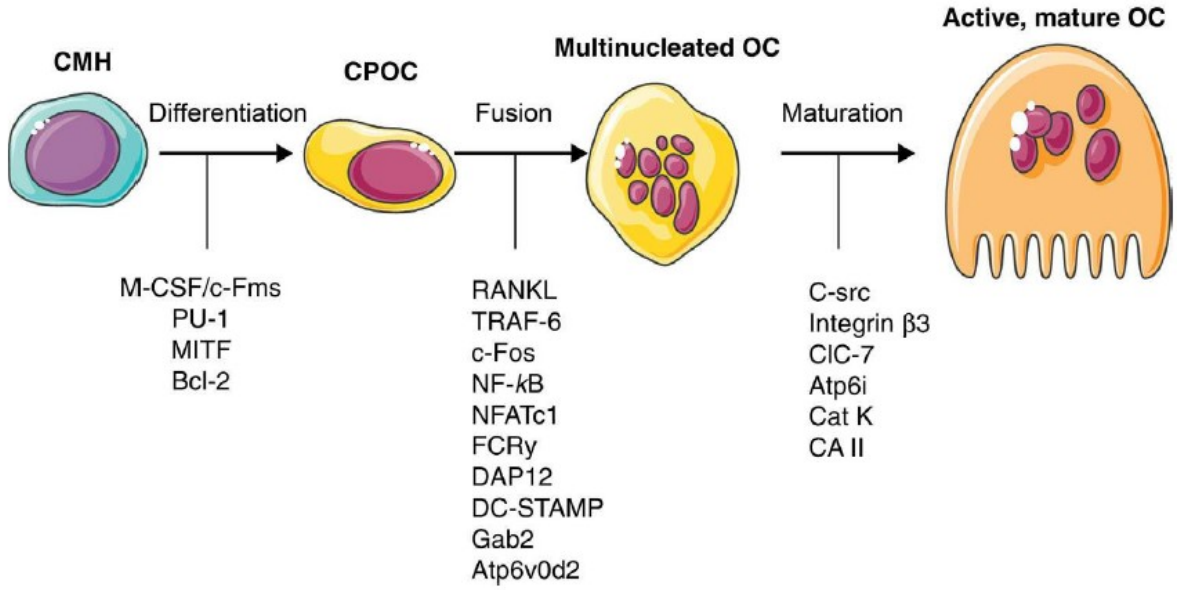

Figure 4: *Differentiation and activation of osteoclast [48].*

1.2.2.2 Osteoblasts

The osteoblasts are responsible for the synthesis and the mineralization of bone matrix. They come from MSCs and are involved in the synthesis of new bone matrix and thus new bone formation. They are also called osteoforming cells. Their differentiation from pre-osteoblasts to osteoblasts is activated by the Transforming Growth Factor β (TGF-β) and Bone Morphogenetic Proteins (BMP) like the BMP2, BMP4 and BMP7 which activate the synthesis of type I collagen and non-collagenous proteins. Then, thanks to transcription factors, the pre-osteoblasts become osteoblasts. After that, the osteoblasts have the capacity to synthesize an important amount of type I collagen called osteoid. It is deposited on the pre-existing bone matrix or surrounds osteoblasts transforming them to osteocytes [31,32,48]. The mineralization is done via the secretion of non-collagenous proteins like the osteopontin, sialoprotein, osteocalcin (**Figure 5**). This induces the formation of HA crystals between type I collagen fibrils by combination of phosphate and calcium, brought by active and passive transfers of constituents from the osteoblasts. This mineralization is progressive, and the extracellular

matrix obtained becomes impermeable to exchanges. The osteoblasts are linked with gap junctions which allow their survival in the mineralized tissue. After the secretion of bone matrix and the mineralization, the osteoblast has three pathways (**Figure 6**) [32,48]:

- To transform itself in an osteocyte surrounded by mineralized matrix,
- To become bone-lining cells,
- To die by apoptosis.

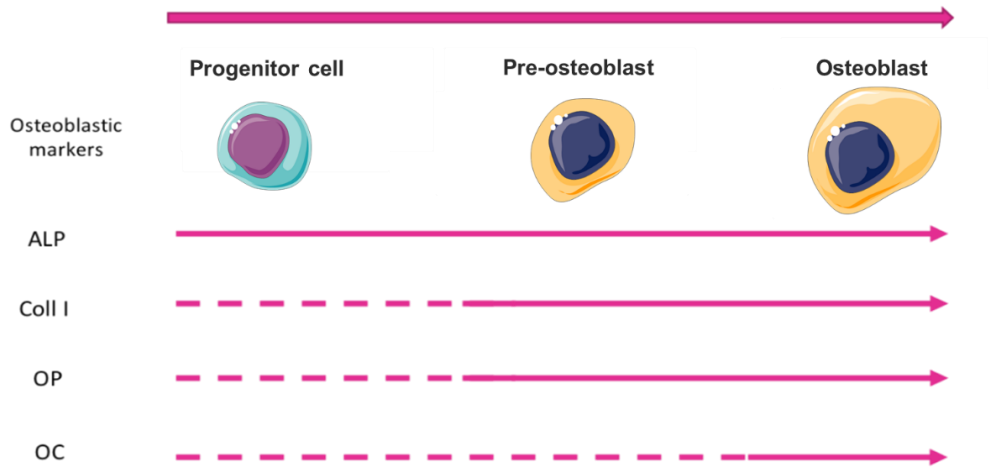

Figure 5: *Main markers expressed during the differentiation of the osteoblast. The progressive differentiation of the osteoblast is characterized by the expression of early osteoblastic genes, Alkaline Phosphatase (ALP), collagen I (Coll I), Osteopontin (OP) or late osteoblastic genes like Osteocalcin (OC).*

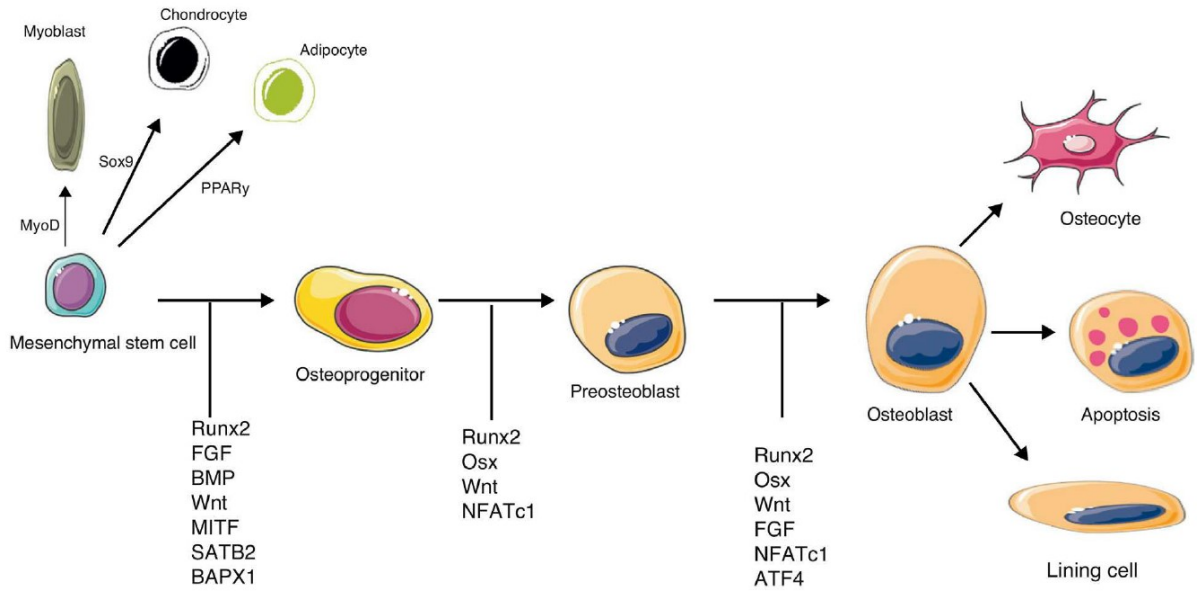

Figure 6: *Pathways of differentiation and activation of osteoblasts [48]*

1.2.2.3 Osteocytes

The osteocytes come from the differentiation of osteoblasts. They are found in the mineralized bone matrix. Their major role is to maintain bone tissue through the bone remodeling process and thus, adapt the tissue to the external mechanical stresses exerted on itself. The osteocytes transform this mechanical stress into a biochemical signal, transmitted to surrounding cells thanks to their cytoplasmic extensions. Dependng on what is needed by the tissue, this signal can:

- Activate the osteoblasts and inhibit the osteoclasts. This anabolic pathway stimulates bone growth,
- Activate the osteoclasts differentiation and stimulate their proliferation. This catabolic pathway activates the osteoclastic bone resorption.

Thus, the osteocytes have a decisive role in the bone tissue remodeling process [32,48].

1.2.2.4 Bone-lining cells

Bone-lining cells are quiescent osteoblasts. They cover bone surface and have no bone formation or resorption activity. Their role is to prevent the osteoclast activity outside the remodeling period. Their metabolic activity is reduced compared to the osteoblasts'. However, it is possible for them to have the capacity to multiply and to differentiate into active osteoblasts, under the influence of stimuli [32].

2. Bone remodeling and healing

2.1 Bone remodeling

Bone remodeling consists in the renewal of bone tissue to maintain its structure, its mechanical properties and its mineral homeostasis [4]. The adult skeleton is renewed by remodeling every 10 years [3]. It allows:

- An adaptation to mechanical stresses,
- A repair of micro-traumatisms or fractures,
- A control of the mineral homeostasis (fast mobilization of calcium and phosphorus) [49]

Bone remodeling starts with the resorption phase initiated by the osteoclasts (**Figure 7**). They dig the lacunae in which the new Volkmann canals and osteons will be placed. After the action of osteoclasts, the osteoblasts migrate in the new placement for the osteons and line it. At this point, the osteoblasts, as described before, secrete the osteoid which is mineralized by the osteocytes. This phenomenon allows to create the new osteons. During bone remodeling process, the bone resorption and apposition need to be balanced. If not, this can result in pathologies such as, for example, the osteoporosis [32].

In the case of a material implanted, this process should be the same. The different bone cells must interact in the same way with the material implanted, that is to be degraded chemically by the osteoclasts and recognized by the osteoblasts for them to migrate and start the remodeling.

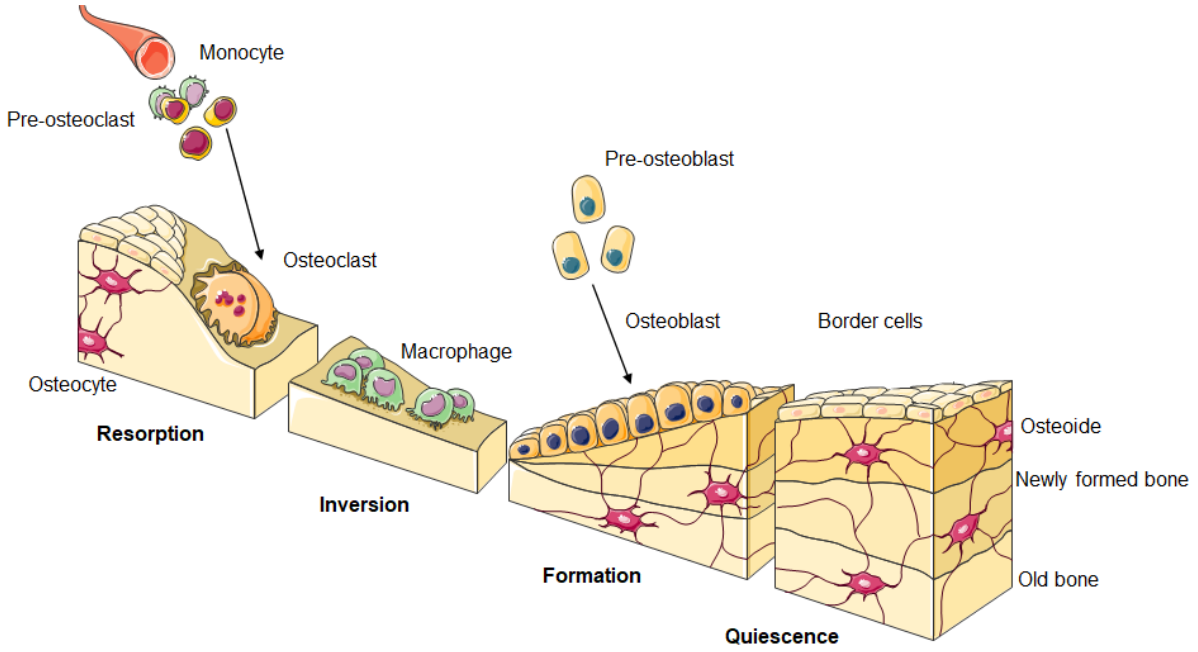

Figure 7: *Bone remodeling process (from Servier medical art)*

2.2 Bone healing

Bone healing is a naturally occurring, complex, process which will take place for small bone defects, for example, fractures which are less than twice the diameter of the injured bone [4]. This process is composed of three different steps (**Figure 8**): the inflammatory phase, the bone repair phase and the bone remodeling phase [4,50,51].

2.2.1 Inflammatory phase

When bone tissue undergoes a small traumatism like a fracture, a hematoma is formed immediately at the lesion site due to the rupture of blood vessels supplying the bone and the periosteum. It is composed of bone marrow cells and peripheral and intramedullary blood cells (**Figure 8**).

The inflammatory reaction starts at the lesion site allowing the degradation of the devitalized tissue to have a favorable area for the tissue repair. The inflammatory reaction causes the coagulation of the hematoma in between and around the fracture ends and, in the medulla, forming a template for the callus.

The proinflammatory response starts with the secretion of the tumor necrosis factor-α (TNF-α), bone morphogenetic proteins (BMPs), interleukin-1 (IL-1) and IL-6. These cytokines allow the recruitment of macrophages, monocytes, and lymphocytes. These cells remove the damaged and necrotic tissue and secrete cytokines like the vascular endothelial growth factor (VEGF).

2.2.2 Bone repair phase

The VEGF allows the angiogenesis at the site while in the hematoma, a fibrin-rich granulation tissue is formed. MSCs are recruited and differentiate to fibroblasts, chondroblasts and osteoblasts for the chondrogenesis. A collagen-rich fibrocartilaginous callus is formed covering the fracture ends. The cartilaginous callus gives a stable structure to the fracture.

After that, the fibrocartilaginous callus starts to undergo an endochondral ossification. The expression of RANK-L stimulates the differentiation of chondroblasts, chondroclasts, osteoblasts, and osteoclasts. These cells are then responsible of the resorption and calcification of the callus. The new blood vessels formed proliferate, allowing the migration of MSCs. Finally, a hard and calcified callus of immature bone is formed.

2.2.3 Bone remodeling phase

Thanks to the osteoblasts and osteoclasts, the hard callus is remodeled repeatedly. This remodeling consists of an equilibrium between the bone resorption by the osteoclasts and the new bone formed by the osteoblasts. The center of the callus is replaced by compact bone while the callus ends are replaced by lamellar bone. The new vascular system appears in parallel

during the remodeling (**Figure 8**). This process takes many months, until the regeneration of the normal bone structure.

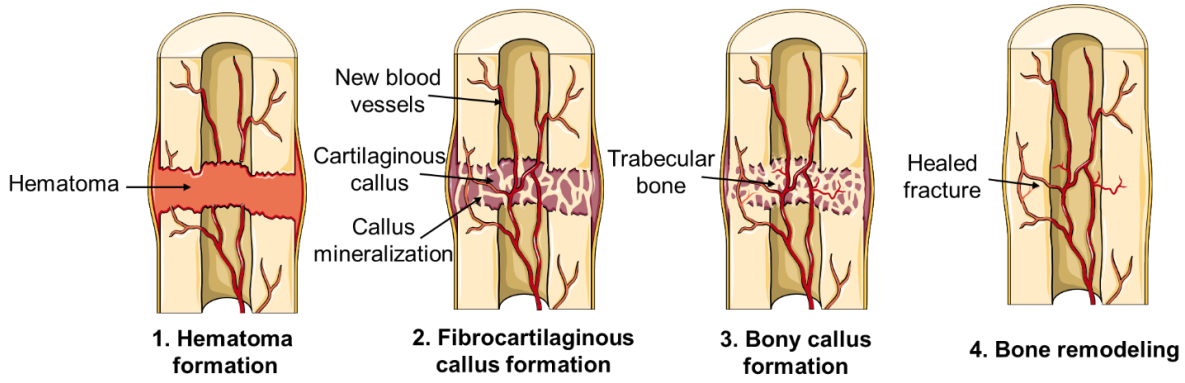

Figure 8: *Bone healing process (from Servier medical art)*

B. BONE SITUATIONS NEEDING REPAIR

Bone tissue has the capacity to heal naturally when the injury has a small volume thanks to the bone remodeling process. However, due to traumatisms or pathologies, bone loss can be important, thus, the natural healing is compromised. From a specific size, the bone tissue is no longer able to regenerate on its own and it is then necessary to proceed to a surgical intervention, this is called the critical bone defect or critical size defect (CSD). According to the Orthopedic Trauma Association, the CSD could be defined by a size around 1 to 2 cm or by a loss in volume of more than 50% of the circumference of the bone. However, this definition depends on the location of the bone defect, its tissue environment, the patient's age and the presence of chronic diseases or comorbidities [52]. Philippe Beaudet, orthopedic surgeon, thinks otherwise. According to him, a bone defect smaller than 6 mm in size does not require surgery. The question arises when the bone defect is between 8 and 12 mm. From 12 mm, the bone defect is considered critical [53]. CSD can be caused by important trauma, pathologies, developmental

deformities, tumor resection [4,54–56]. The bone loss in this defect can affect revascularization and tissue differentiation, and possibly leads to spontaneous bone fracture, which cannot be repaired without interventions [57,58].

1. Bone defect

1.1 Traumatic situations

Bone tissue has a stiffness giving itself the ability to resist to external mechanical stress. When this stress is greater than its resistance capacity, it can cause fractures [8].

A fracture is a breach in the structural continuity of bone cortex, with a degree of injury to the surrounding soft tissues [59]. Different types of fractures exist (**Figure 9**). These fractures can be due to a violent traumatism and the treatment of the injury depends on its severity. Usually, the limb is immobilized by a cast, but for CSD, it is repaired by a surgery.

Another cause of fractures can be the overuse [51]. This results from a repeated stress which can cause microfractures within the bone. If this stress increases, more microfractures will appear until a complete fracture. For that, rest, immobilization, and physical therapy are required. Surgical treatment in this case remain exceptional [60].

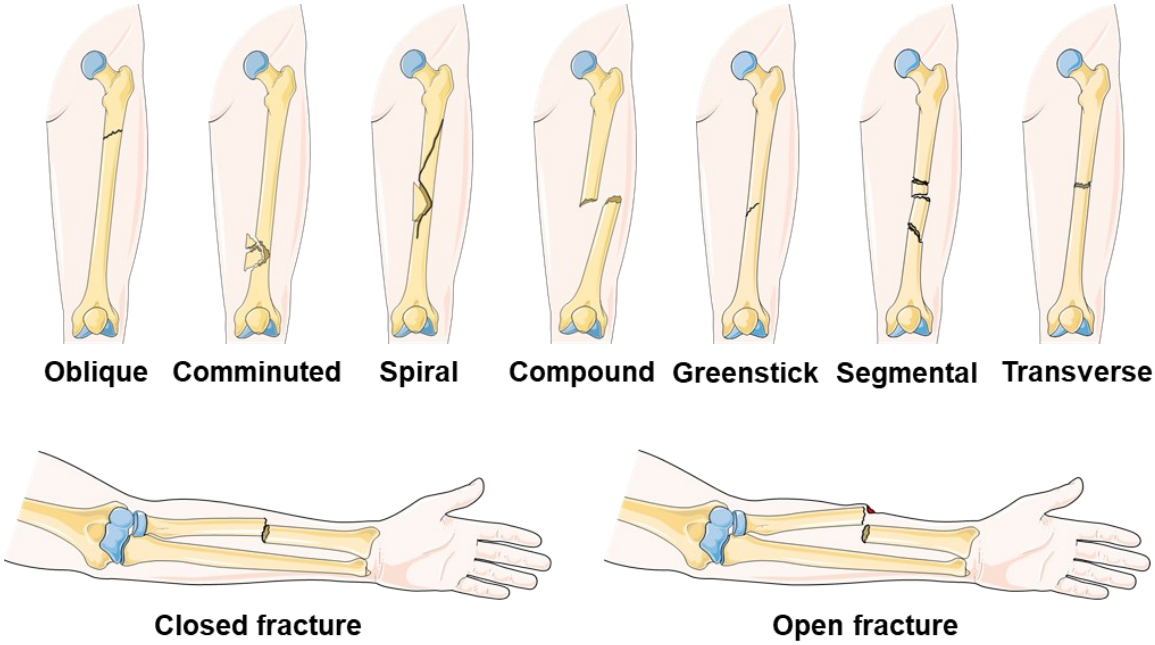

Figure 9: *Different types of bone fractures (from Servier medical art)*

1.2 Defects linked to a pathophysiological context

1.2.1 Population aging

Despite its aspect, bone is alive and constantly remodeling. However, with the aging of the population, this process is more subject to disabling pathologies [61]. During life, the evolution of bone mass is composed of three phases:

- Increase of bone mass until the age of 20 – 30 years old,
- Stabilization of bone mass,
- Decrease of bone mass.

It is difficult to fixe an age at which the stabilization and decrease steps starts because this last step depends on many factors, such as the menopause for women. A woman, at the end of her life, has lost between 35% and 50% of bone mass compared to man for whom it is estimated at 30% [62].

With age, the bone cell activity decreases which becomes a major concern with the aging of the populations. Bone remodeling is dysregulated, which induces pathologies such as, but not limited to, osteoporosis [63]. This pathology represents a public health problem. At 65 years old, almost 39% of women suffer of osteoporosis, and 70% at > 80 years. Osteoporosis corresponds to the decrease in bone density and resistance and disturbances of bone micro-architecture causing its fragility and thus the increase of the risk of fractures. These fractures compromise the patients' quality of life due to the persistent pain they can cause. In the case of severe fractures (humerus, vertebrae, pelvis, femur), complications can be life-threatening for old or fragile patients [64].

1.2.2 Cancer

In bone tissue, benign or malignant tumors exist [6,7]. There are two possibilities:

- Primary tumors found in young adults or adolescents,
- Secondary tumors named also bone metastasis which are the most frequent after 50 years old. These are cancers which have spread from the original site to a bone.

The tumors can be found on different part of the bone:

- Diaphyseal: Ewing tumor, osteoid osteoma
- Metaphyseal: osteosarcoma, chondroma, osteogenic exostosis
- Epiphyseal: Giant cell tumor, chondroblastoma, clear cell sarcoma

To treat these tumors, a surgery with different therapeutic treatments such as chemotherapy or radiotherapy are needed. The surgery is used for a bone resection, to remove the tumor.

1.2.3 Infections

Bone defects can be due to infections named osteitis [65]. These can be bacterial, mycotic, or parasitic. These contaminations can be due to an opened fracture, a bone surgery, an implanted osteosynthesis material. It can also be hematogenous. They are usually treated thanks

to antibiotics but sometimes, it is not enough after a surgery. Thus, it is necessary to extract the infected tissue followed by the antibiotics treatment to eradicate the pathogens.

2. Therapeutic solutions and repair strategies

Bone tissue has the capacity to heal naturally when the injury has a small volume as explained in the previous parts. However, due to traumatisms or pathologies, bone loss can be important, thus, the natural healing is compromised. The healing needs to be supported. For that, natural and synthetic bone substitutes can be used. They are named biomaterials [66–68]. Biomaterials are materials which interact with the human body, to ensure specific functions, which are repairing, treating, replacing, or regenerating a given region of the body by the action of its constituents or for diagnosis. They can be natural or synthetic, alive or lifeless and made of components which interact with biological systems [12].

First, the different repair approaches will be presented. Then, the manufacturing techniques employed for bone substitutes obtention will be introduced. Finally, the materials used for bone applications will be reported also.

2.1 Natural and engineered approaches

For bone repair, different approaches are used, depending on the defect. The materials must have properties adapted to the defect but also to the tissue, so that the result of the repair is as close as possible to the shape and initial properties of the bone.

2.1.1 Bone grafts

2.1.1.1 Autograft

The autograft is the case where the donor and the recipient of the graft are the same patient. This involves removing patient's own bone tissue from a donor site and then placing it on the recipient site. Usually, the graft is taken from the iliac crest and more rarely from the tibia [69].

The graft is composed of a living organic and cellular tissue with intact cells, and a mineral portion. Autologous bone is osteoconductive, osteoinductive, biocompatible and non-immunogenic. This is the gold standard for a bone tissue repair [9,10].

However, autografts present limitations (**Table 6**). Indeed, bone tissue is available in a limited quantity, and the graft may show high morbidity at the site of implantation.

2.1.1.2 Allograft

The allograft is the case where the transplantation is done from one individual to another from the same species [70]. This is used when the human patient has a significant bone loss or is an elderly person. In this case, the autograft is not possible. Thus, with the allograft, the graft will come from another human donor. It will be a human tissue.

Using allograft is convenient because it avoids the complications of donor site morbidity, it has a better availability than the autograft, it can be used in different forms (powder, strips, bone chips …), in a large quantity and in different types (cancellous, cortical, cortico-cancellous). The allograft can be freeze-dried, freeze-dried demineralized, fresh or frozen [22,71,72]. For the fresh ones, they have a low osteogenicity and can be immunogenic. For the frozen and freeze-dried ones, some processes exist to sterilize them like the gamma-irradiation. Even if the osteoblasts and precursors are lost during the process, that allows to decrease the risk of disease transmission and the grafts still provide osteoconductive properties for new bone formation.

However, allografts have drawbacks (**Table 6**) also as the disease transmission, the immune reaction even if the transplant is irradiated, the random osteo-conduction within the graft [68].

2.1.1.3 Xenograft

Xenografts are grafts from a species different than the recipient, such as bovine xenografts used as a calcified matrix implanted in humans. Xenografts preparation requires different steps [22]:

- Pyrolyzation
- Decalcification
- Deproteination
- Delipidation
- Inactivation of viruses and prions
- Sterilization by irradiation.

The structure (porosity) is close to that of human bone, and in this property lie the interest of these xenografts. Their osteointegration depends on the osteogenic potential of the recipient site. Their biomechanical properties are interesting as they are almost identical to that of the human tissue.

The main advantages of these materials are their structure, close to that of the human bone (which gives them, after treatment, good osteo-conduction and sometimes osteo-induction properties), their availability in large quantities and a low risk of infectious and bacterial/viral transmission (**Table 6**). Compared to other types of transplants, they eliminate the need for human donors and provide total absence of morbidity for the patient. These qualities have enabled this class of biomaterials to become the most widely used today.

Grafts	Advantages	Drawbacks
Autograft	Osteogenesis Osteo-conduction Osteo-induction Non-immunogenic No disease transmission	Low availability Limited quantity High morbidity
Allograft	Osteo-conduction Good availability Different forms available	Immunogenic No osteogenic factor Disease transmission Risk of rejection Expensive Alteration of osteo-induction by sterilization Random osteo-conduction within the graft
Xenograft	Osteo-conduction Good availability Large quantity	

Table 6: *Advantages and drawbacks of Auto-, Allo-, Xeno-grafts [11]*

These three different bone grafts have advantages but also and above all disadvantages. To remedy this, it is necessary to develop new methods of repairing bone tissue.

2.1.2 Repair approaches

Depending on the type of defect, its size and the injured bone, different approaches are possible for repair. The substitutes used must be adapted to the different functions needed. Some materials should be suitable for maintaining and substituting the mechanical properties of bone, or, for filling large defects.

2.1.2.1 Materials for maintaining and substituting mechanical properties

This function consists in, temporarily or permanently, holding in place and stabilizing fractured bones. For this, osteosynthesis implants are used as for example plates, screws, nails, pin or metal wires (**Figure 10**) [21,73]:

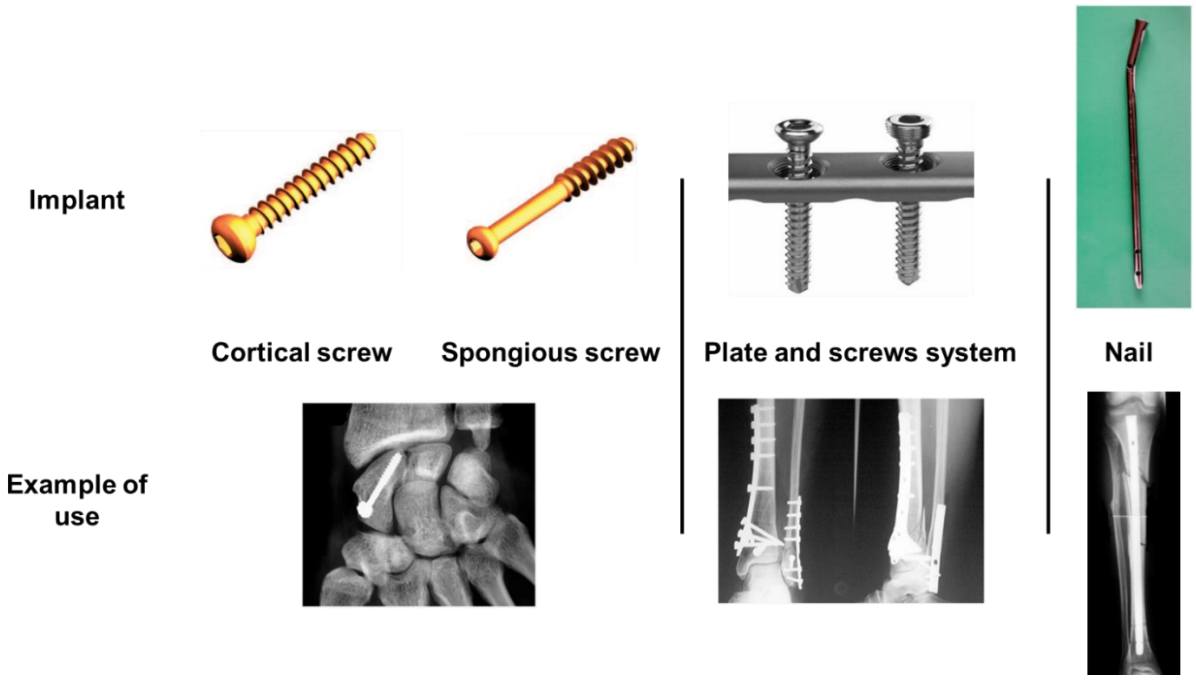

Figure 10: *Example of osteosynthesis implants and their application [21]*

These implants must be biocompatible, non-corrosive and must have high toughness. Nowadays, metals and alloys are the most used, because they present toughness properties adapted for this function. Polymers can be used also, but this is rarer and depends on the bones and mode of repair targeted [74]. Their role, by the relative immobility of the bone fragments obtained, is to allow the natural consolidation of the bone in good position while often allowing early functional rehabilitation [75].

2.1.2.2 Filling materials

Some defects can have a high volume, with a large bone loss, and cannot be repaired with osteosynthesis implants alone. This repair needs to be helped by materials which will be used to fill critical skeletal defect as for example Demineralized Bone Matrix (DBM), bone cement or calcium-phosphates (Ca-P) [4,74,76]. They should be osteoconductive, osteoinductive, have the mechanical properties adapted and be bioresorbable (**Table 7**) [70]. If they do not present these properties, they will need to be suited to allow a bone repair.

Bone substitutes	Osteo-conduction	Osteo-induction	Osteogenic factor	Osteointegration	Disadvantages
DBM	+	++	-	++	Variable osteo-inductivity associated with donors and processing methods
Bone cement	+	-	-	+	Osteoconductive only
Ca-P	+	-/+	-	+	Osteoconductive only

Table 7: *Characteristics of bone grafts [70]*

2.1.2.3 Bone tissue engineering

Tissue engineering was defined in 1993 by Langer and Vacanti as a technique "using principles of life sciences and engineering to develop biological substitutes to restore, maintain or improve tissue function" [13,53].

In response to the urgent need of new treatments to repair bone defects, bone tissue engineering is a promising approach to efficiently regenerate bone and circumvent the limitations associated with conventional treatments [14]. The main applications requiring its use include filling bone loss, filling gaps in spinal fusion, and stabilizing vertebral fractures by compression.

Three parameters can be considered in bone tissue engineering strategies:

- A scaffold biocompatible which mimic the extracellular matrix of natural bones
- Cells which have an osteogenic potential and that will synthesize and deposit bone matrix
- Bioactive components inducing signals which will participate in cell recruitment and differentiation towards the osteogenic phenotype.

Different strategies are possible by combining two or these three parameters (**Figure 11**) [49]:

- **Strategy scaffold/cells (A):** The goal is to bring pluripotent or pre-differentiated cells into an osteogenic lineage to a defined anatomical area. These cells are seeded within a scaffold which can be implanted immediately after its formation or after culturing [5]. The materials selected in order to design the scaffolds must, by their properties, allow cell adhesion, survival and differentiation. When this scaffold-cell complex is implanted, the cells will participate in bone regeneration processes, including synthesizing new bone matrix as material degrades to make space for the newly formed bone tissue [77].

- **Strategy scaffold/bioactive components (B):** The goal is to supply the injured area with bioactive elements which will induce signals stimulating the processes of bone regeneration, recruiting the cells of the host present in the vicinity of the lesion. The release of these molecules (growth factor, or therapeutics ions for example) within the injured site must be perfectly controlled and optimized in order to promote the formation of healthy bone tissue and to avoid complications such as ectopic bone formation [78,79].

- **Strategy scaffold/bioactive components/cells (C):** The scaffold will present the exogenous cells and the bioactive components. The exogenous cells seeded within the scaffold and the cells of the host will be stimulated by the bioactive agents in order to coordinate the process of bone regeneration.

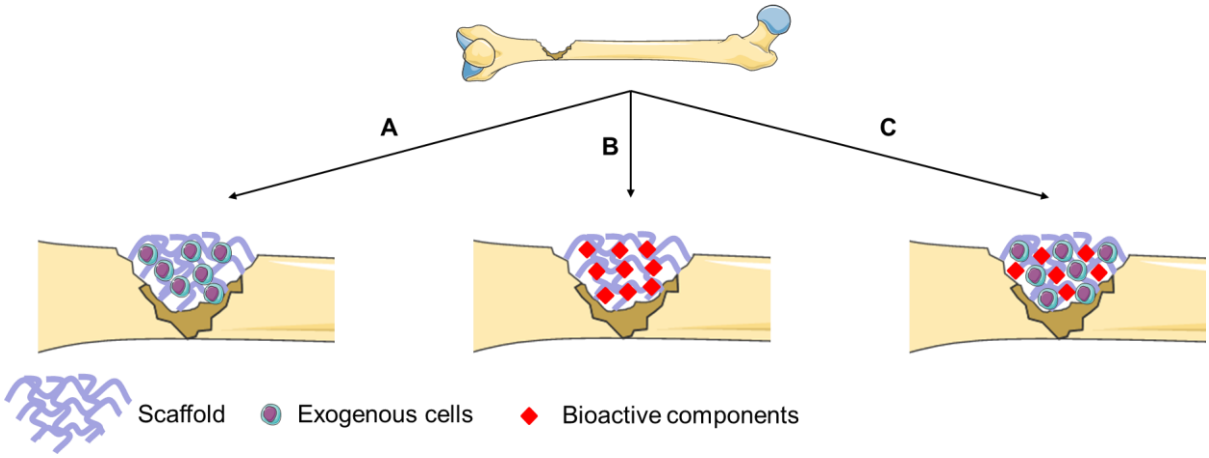

Figure 11: *Different strategies for bone tissue engineering.*

The different components used for bone tissue engineering need to respect different properties to guarantee a complete repair of the bone:

- Biocompatibility:
  - Good integration into the host without toxicity, ability to interact with the environment.
  - Support cellular activity.
- Osteogenic properties:
  - The substitute must be osteoconductive, osteoinductive and osteogenic.
  - The substitute must have a good osteo-integration.
- Biodegradability/Resorbability:
  - The structure must exhibit an adequate rate of degradation so that the formation of new bone tissue with its initial mechanical properties operates at the same time as the degradation of the 3D structure.
  - All residues of the 3D structure must be non-toxic and be able to be excreted by the body without action.

- The 3D structure must have the same mechanical properties of the bone to resist the mechanical stresses imposed on this tissue.

- Porosity:
  - An adequate porosity of the structure will allow the re-vascularization of the new tissue formed in order to optimize the diffusion of nutrients and oxygen from the environment to the 3D structure for cell survival and proliferation.
  - The optimal size for bone tissue growth is between 200 and 350 µm, and a multi-layered structure combining pores of different diameter and interconnected pores is ideal for cell attachment and proliferation.

2.2 Fabrication methods

Many methods have been developed to fabricate scaffold for bone tissue engineering. Depending on the materials used, the techniques should be appropriate to their initial properties and to the scaffold aimed. A distinction is made between conventional and advanced techniques and gelled system synthesis methods [80].

2.2.1 Conventional techniques

- Solvent-casting and particulate-leaching: these techniques involve using a polymer solution uniformly mixed with salt particles of a specific diameter which will leave a porous structure after solvent evaporation and immersion in water [81].

- Gas foaming: Molded biodegradable polymers are pressurized at high pressures with gas-foaming agents, such as CO_2 and nitrogen, water, or fluoroform, until the polymers are saturated resulting in nucleation and growth of gas bubbles with sizes ranging between 100 and 500µm in the polymer [82–84].

- Phase separation: A polymer solution is quenched and undergoes a liquid-liquid phase separation to form two phases; a polymer-rich phase and a polymer-poor phase. The polymer-rich phase solidifies and the polymer poor phase is removed, leaving a highly porous polymer network [85].

- Melt molding: Melt molding involves filling a mold with polymer powder and a porogen component and then heating to above the glass-transition temperature of the polymer while applying pressure to the mixture. During the fabrication process, the raw materials will bind together to form a scaffold with designed specified external shape. Once the mold is removed, the porogen is leached out and the porous scaffold is then dried [86].

- Freeze drying: Polymeric porous scaffolds can be prepared by freeze drying. In the freezing stage, the polymer solution is cooled down to a certain temperature at which point all materials are in a frozen state and the solvent forms ice crystals, forcing the polymer molecules to aggregate into the interstitial spaces. In the second phase, the solvent is removed by applying a pressure lower than the equilibrium vapor pressure of the frozen solvent. When the solvent is completely sublimated, a dry polymer scaffold with an interconnected porous microstructure remains. The porosity of the scaffolds depends on the concentration of the polymer solution; pore size distribution is affected by the freezing temperatures. Apart from fabricating porous scaffolds, this technique is also used to dry biological samples to protect their bioactivities [87,88].

2.2.2 Advanced techniques

- Electrospinning: this is a fabrication technique using electrical charges to draw fine fibers up to the nanometer scale. It has been widely employed to fabricate porous scaffolds with

nanofibrous architectures that can mimic the structure and biological functions of the natural extracellular matrix [26]. This technique is able to generate fibers with diameters ranging from 2 nm to several micrometers using solutions of both natural and synthetic polymers, with small pore sizes and high surface area to volume ratios [80,89].

- 3D printing technologies: 3D printing, through the CAD/CAM technology (Computer-Aided-Design / Computer-Aided-Manufacturing), is a group of methods used to produce scaffolds. It is also an alternative to overcome the limitations of conventional techniques as the use of cytotoxic solvents and the limited control of porosity. This technology allows the production of scaffold with specific shape for patients by images made by Computed Tomography (CT). There are several 3D printing technologies, which are different in the methods of construct creation and materials used for production. Some of them will be described below:
    - Powder-based 3D printing: additive manufacturing method that uses raw material in powder form. The structure is built layer by layer and a liquid binder is sprayed on the surface of each powder layer bonding together the powder granules. The structure is supported throughout the process by the surrounding unprocessed powder [90].
    - Extrusion technology: 3D printers create a model from molten thermoplastic using layer-by-layer method. The main criteria of the materials for this type of printing are the melting temperature and rheology of the molten plastic [89].
    - Stereolithography: based on the photo-polymerization of a resin using a UV laser. The model is emerged in the resin chamber and the process is repeated layer-by-layer until the entire construct is produced [89,91].

- 3D plotting: based on the injection of a solution from a syringe into the liquid collector, the density of which coincides with the density of the solution in the syringe. The collector can also contain polymerizing substances. The process can be performed both at room and elevated temperatures. This method is particularly suitable for obtaining soft matrices from hydrogels [89].
- Selective Laser sintering: based on the sintering of a polymer powder by a CO2 laser beam, while heating it above the transition temperature. The process is repeated layer-by-layer until the entire 3D model is finished. The model should be heated at the end to obtain the final density [91].

2.2.3 Hydrogels synthesis methods

By playing with the method of preparation and with the parameters of the crosslinking reaction it is possible to tailor the final properties of hydrogels. For the preparation of hydrogels, hydrophilic polymers are crosslinked either through covalent bonds or via physical intra- and intermolecular interactions [49].

2.2.3.1 Physical crosslinking

In physically crosslinked hydrogels, the interactions between polymeric chains are non-covalent, as ionic interactions, hydrogen bonds and hydrophobic effects [92]. These processes allow to avoid the addition of cytotoxic initiators and chemical crosslinkers and to employ mild conditions of preparation (e.g., pH and temperature) thus improving the cytocompatibility of the hydrogels and possibly permitting the incorporation of cells prior to gelation [93].

The main drawbacks of physical hydrogels are generally the low stiffness, deriving from the weakness of the secondary forces involved in crosslinking, that limit their application to non-load-bearing sites. In addition, the stability in physiological environments could be an issue given that premature disassembly of the hydrogels can prevent effective cell engraftment.

2.2.3.2 Covalent crosslinking

Covalently crosslinked hydrogels overcome the limitations of physical hydrogels related to stability, dwell time after implantation and, partially, mechanical properties. Generally, these systems are composed of polymeric chains bearing reaction sites for 3D network expansion under specific physical and chemical conditions. There are also composites with covalent grafting particles.

These approaches are suitable for tissue engineering only if the employed possibly toxic reagents (precursors, initiators, crosslinkers) can be completely removed before cell addition or implantation [20,94]. In addition, most of covalently crosslinked hydrogels do not allow direct incorporation of cells inside the hydrogel, making it necessary to seed the cells on the surface and, if there is a suitable open macro porosity, let them migrate inside the scaffold. Moreover, chemical functionalization and crosslinking of the starting polymer chains can thoroughly affect their chemistry and then their biological properties, especially for naturally derived materials.

2.3 Materials used for bone repair

Different type of materials can be used for bone repair. Natural or synthetic, they should be adapted to the targeted application and to the bone properties [67,95].

2.3.1 Natural

2.3.1.1 Organic matrices

Natural polymers are studied to act as organic matrix due to their advantage to constitute a 3D scaffold which will support cells proliferation and differentiation. These polymers are used for bone tissue engineering applications because they have a minimal immunologic response and they present a good biocompatibility, which will promote cell behavior [96,97].

- **Polysaccharides**
  - Chitosan

Chitosan has received great attention because it is biocompatible, biodegradable and osteoconductive. This is a natural polymer, a linear polysaccharide, obtained through the deacetylation process of chitin, which is abundant in nature (found in bacteria and fungi cell walls but also extracted from crustacean exoskeleton). Chitosan can be used in different forms for orthopedic applications for example films, fibers, sponges. Its processability is one of its advantages for bone tissue engineering. Moreover, the Food and Drug Administration (FDA) approved the use of chitosan in wound dressing. However, chitosan scaffolds have low osteo-inductivity and stiffness properties which are not adapted. In addition, other limitations of chitosan use are known, for example, its pH dependent solubility, its rapid *in vivo* degradation [98–100].

  - Alginate

Alginate is an anionic natural polymer known for its biocompatibility, biodegradability, and hydrophilic properties. In physiological conditions, alginate can form porous gels. This porosity is important as it will allow the cells to colonize the network. Moreover, nutrients could easily pass through the biomaterial and ensure a good environment for tissue regeneration. An important disadvantage of using alginate as a biomaterial for tissue engineering is represented by the lack of sites for protein adsorption and cell attachment [101,102].

- **Proteins**
  - Collagen

As explained above, in **Part A 1.2.1.2**, collagen is the most abundant protein found in the body, especially Coll I found in tendon and bone tissues. For that fact, the collagen is the most

used natural polymer in orthopaedics as it is also part of the bone composition, allows the nucleation/deposition of mineral crystals and provides binding sites for osteogenic proteins [103–106]. To ensure the functions necessary for tissue regeneration in scaffold applications, collagen must be treated cross-linked or blended, depending on the specific tissue requirements. They can be used as injectable hydrogels, membranes or films, scaffolds, sponges, microspheres or nanospheres [107] .

- Gelatin

Gelatin is a natural denatured polymer, a derivative of collagen. It is composed of amino acids (hydroxyproline, proline, or sequences such as RGD – arginine-glycine-aspartic acid). Low costs and immunogenicity, aqueous solution solubility, and the different sources of collagen (fish, cattle bone, pig skin) from which it can be extracted are a few examples of the advantages of this protein. Gelatin is used in tissue engineering studies due to its biocompatibility and biodegradability properties. Gelatin is considered a suitable biomaterial to mimic the extracellular matrix due to its functional groups and the possibility to form 3D scaffolds with porous structure [108,109].

- Silk fibroin

Silk fibroin (SF) is a fibrous protein which is produced mainly by silkworms and spiders. Its unique ductility properties, tunable biodegradation rate and the ability to support the differentiation of mesenchymal stem cells along the osteogenic lineage, have made SF a favorable scaffold material for bone tissue engineering. SF can be processed into various scaffold forms, combined synergistically with other biomaterials to form composites, and chemically modified, which provides an impressive toolbox and allows SF scaffolds to be

tailored to specific applications. Moreover, SF has been recognized by the US Food and Drug Administration (FDA) as a biomaterial in 1993 [110].

2.3.1.2 Inorganic matrixes

Natural mineral components are used in a scaffold to mimic the mineral matrix of bone and its properties. These compounds will bring osteo-conduction and osteogenicity.

- **Biological hydroxyapatites**

These types of HA come from xenografts which are ceramized at high temperature (≈ 600 – 1000°C) [111]. It is osteoconductive, biocompatible and has a structure comparable to that of the human bone. All organic components are extracted at high temperature (600 – 1000°C) but the bone maintains its natural architecture. The physical and chemical treatments lead to the disappearance of the antigenic substance (proteins, amino-acids) and a modification of the structure and composition of the inorganic phase [112].

- **Calcium carbonates**

The natural coral is purified (elimination of the organic matrix) and sterilized by X-RAY radiations. This material corresponds to a calcium carbonate, of formula $CaCO_3$, crystallized in the form of aragonite. Different species are used according to their structural characteristics and clinical indications, for example, the *Porites lutea* coral is recommended in odontology. With a porosity of 100 to 200 microns, like that of cancellous bone, calcium carbonate is biocompatible and resorbable. The resorbability kinetics depend on the species, the site of implantation, volume, size and pore volume [113].

2.3.2 Synthetic

2.3.2.1 The main classes of materials

- **Metals**

Metals are the materials the most used in bone repair due to their mechanical properties (toughness, resistance, stiffness) that are the closest to the bone. They are used for osteosynthesis applications or bone replacement.

Many pure metals as iron, silver or gold have been used by surgeons throughout history but only titanium and gold are still used today in France for orthopedic implants and the dental field. In the early stages of its use, titanium was used in a commercially pure form which is essentially a dilute alloy of titanium and oxygen. The higher the oxygen content, the better the metal resistance. Titanium is a highly reactive material, which has the property of oxidizing, whether in air or in water. It then becomes covered with an oxide passivation layer (TiO_2, Ti_2O_3, Ti_3O_4), which makes it not sensitive to corrosion. This oxide layer is the source of its excellent osteointegration. Indeed, it is accepted that pure titanium is extremely well tolerated by tissues and does not induce either toxic effects or inflammatory reactions. Titanium is commonly used in orthopedic and craniomaxillofacial surgery as a screw, plate, nail or pin, but also in the spine as a fusion cage, or in ligamentoplasty as an interference screw [114,115].

- **Alloys**

Different types of alloys for bone repair exist and are presented below. The first materials to have been used for medical applications are stainless steels, cobalt-chromium alloys, nickel-chromium alloys and titanium alloys [114].

- Stainless steel

Even today, stainless steel is the most widely used material for internal fastening. The reasons are a favorable combination of mechanical properties, corrosion resistance and

biocompatibility. All stainless steels used in bone trauma are non-magnetic. Their resistance is obtained by the alloy of selected elements and by the treatment carried out (cold work). Stainless steels contain among others (% by mass):

- 17 to 22% chromium to improve corrosion resistance.
- 9 to 16% nickel which strengthens corrosion resistance.
- 2 to 4.2% of molybdenum.
- 0.03% to 0.08% carbon.

The carbon content, the presence or absence of added elements and the thermal or physicochemical treatments have an influence on the structure and properties of steels. Depending on what is expected of an implant, different types of stainless steel can be used (iron-based alloys, low nickel stainless steel …). 316L steel is currently the most common orthopedic steel.

- Cobalt-based alloys (Co-Cr-Mo alloys)

Cobalt-based alloys are also non-magnetic, resistant to wear, corrosion, heat. They are difficult to produce and machine, but significant progress has been made in recent years. Due to their excellent long-term behavior, these alloys are commonly used for prosthetic surgery. In osteosynthesis, the qualities of these materials are less attractive, when compared to other metals in use, but also have their application (especially for nails).

- Titanium alloys

Titanium-based alloys contain 90% of titanium, 6% of aluminum and 4% of vanadium. They are labeled as Ti6Al4V. Their mechanical properties are lower than the alloys presented before, however superior compared to bone [45].

Metals and alloys	Elastic modulus (GPa)	Tensile strength (MPa)	Density (g/cm^3)
Titanium	110	760	4.5
316L steel	190	590 - 1350	8.8
Co-Cr-Mo	210 - 250	650 - 1900	7.8
Ti6Al4V	116	960 - 1100	4.4

Table 8: *Main characteristics of metals and stainless alloys used in medicine [38]*

Despite their mechanical properties (**Table 8**), metals and alloys present some drawbacks. For example, it happens that, after bone repair, the implant needs to be removed, requiring a second surgery. Also, due to their high mechanical properties, the bone will be less solicited than the implant leading to the implant unsealing.

- **Bioresorbable polymers**

Bone tissue engineering necessitates bioresorbable materials, with the degradation rate adapted to the repair strategy. Therefore, biodegradable polymers are favored. They also need to have good resistance, a good stability and to promote cell adhesion, growth, migration, and differentiation.

Polymer materials can have different characteristics like molecular weight, polydispersity, crystallinity, different degradation rate which would strongly affect polymer scaffold properties [96,116–119]. They can be processed by different fabrication techniques such as extrusion, injection, and compression molding. Their properties and degradation can be affected by the type of processing technique, as they require high temperature, and can induce mechanical stresses.

The most used polymers for bone tissue engineering are (**Figure 12**):

- Poly (glycolic acid) (PGA)

PGA is an aliphatic polyester produced by chain polymerization. PGA has a degradation time of 6 – 12 months *in vivo* which is why it is used in bone tissue engineering and medical applications [117,120].

- Poly (lactic) acid (PLA)

PLA is synthesized by the cyclic dimer of lactic acid which exists as two optical isomers: D & L-lactide is the naturally occurring isomer, and DL-lactide is the synthetic blend of D-lactide and L-lactide. The molar mass of the polymer as well as the degree of crystallinity has a significant influence on the mechanical properties. This polymer is commonly used in biomedical devices because of its excellent biocompatibility with the human body, its biodegradability, thermal plasticity, and suitable mechanical properties. However, the PLA has some drawbacks. For instance, it has an insufficient degradation rate and an inability to fully integrate with the bone [114,117,121–123].

- Poly (lactic-co-glycolic) acid (PLGA)

PLGA is a copolymer synthesized from the two homopolymers PLA and PGA. Synthesizing a copolymer allows to combine the properties of the homopolymer used. For example, the faster biodegradation of the PGA allows to optimize the degradation of the PLA. Their biodegradation is optimized by controlling the amounts of both polymers [114,124].

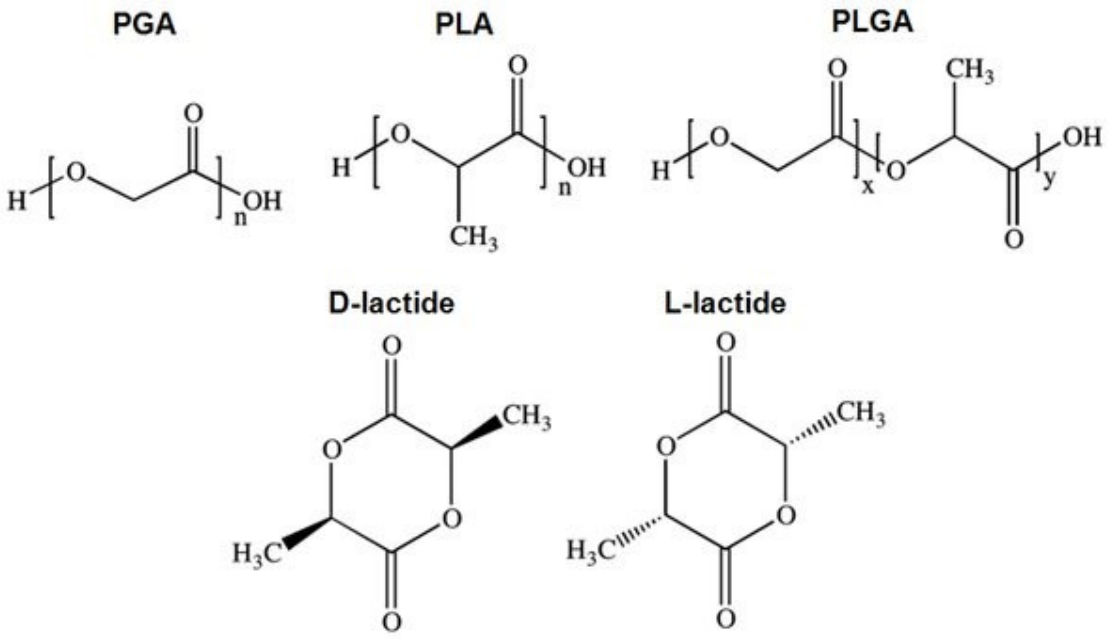

Figure 12: *Chemical structure of PGA, PLA, PLGA and the enantiomers D- and L-lactide [124]*

- Poly (caprolactone) (PCL)

PCL is synthesized by the ring-opening polymerization of cyclic monomer Ɛ-caprolactone in the presence of stannous octoate, serving as a catalyst. Its degradation can take between 2 and 3 years *in vivo* (**Figure 13**) [96,125].

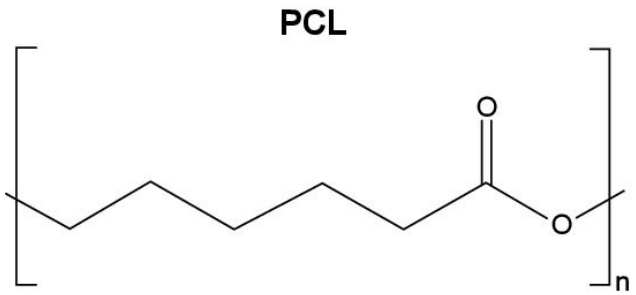

Figure 13: *Structure of poly(e-caprolactone) (PCL) [96]*

- **Ceramics**

About 60% of bone substitutes contain ceramics, whether they are pure or combined with other materials. They are inorganic and non-metallic solids. For the most part, they are made,

like glasses, of mineral raw materials, oxides, or silicates, compacted and treated to varying degrees at more or less high temperatures. This is the sintering process.

Bioactive ceramics are of interest in bone regeneration. The bioactivity of these materials results in the appearance of biological activity in the host organism and the existence of ion exchanges between the material and living tissue [126]. They often have osteoconductive and sometimes osteoinductive properties. However, their very crystalline structure differs from that of the mineral phase of natural bone, which causes a slow absorption. They can be used in different forms as granules, powder, porous blocks, injectable paste… Different ceramics are presented below [127].

- Calcium sulfate ($CaSO_4$):

This is a kind of osteoconductive, and biodegradable ceramics composed of $CaSO_4$ and has been applied in filling void defects since 1892. Although lacking a macroporous structure, calcium sulfate still has a rapid resorption rate and weak internal strength, which implies that it can only be used to fill small bone defects with rigid internal fixation, the ingrowth of vascular and new bone happens in conjunction with the resorption of the graft [128]. Easy preparation and relative low cost have made calcium sulfate resurgent when combined with other synthetic bone substitutes and/or growth factors.

- Calcium phosphate

These materials, based on calcium, are interesting because their chemical composition gets closer to that of the bone. This allows the keep the fundamental properties for bone repair which are osteo-conduction and osteointegration.

Synthetic hydroxyapatite is the major component of bone mineral matrix with the formula $Ca_{10}(PO_4)_6(OH)_2$ [4]. Hydroxyapatite can be available naturally, but also synthesized chemically. Its properties are conserved: biocompatibility, osteointegration and osteo-

conduction [68]. It can be processed in solid blocks, cements, particles. Synthetic hydroxyapatite is not soluble, and its degradation rate *in vivo* is low, but this can depend also on the pH and the form used. Moreover, hydroxyapatite has low toughness properties [128].

Tricalcium phosphate (TCP) with a formula of $Ca_3(PO_4)_2$ has a chemical composition very close to HA and is biocompatible [129]. It is more soluble than HA and has a high degradation rate *in vivo*. TCP has two forms, α and β, but the last one is the most used in bone repair because of its higher biodegradation. Moreover, as the HA, the TCP is fragile and has low stiffness properties [70,129].

Biphasic calcium phosphate (BCP) represents the mixing between HA and TCP (generally 60% and 40% respectively). This allows to combine the properties of both ceramics, HA more stable with a low resorption rate and TCP more soluble and a high resorption rate in vivo. This, in order to control the rapidity of the material degradation [130].

- Bioactive glass

Today, there is an increasing interest for an important group of inorganic and bioactive materials: *i.e.*, bioactive glass (BAG). In 1969, L.L. Hench developed glass compositions which had an excellent biocompatibility and showed the ability to bond bone [23]. Bioactivity describes the characteristic of an implant material to interact with or initiate a specific reaction of living tissue upon exposure. This is a key property that promotes osteointegration for bonding and better stability of bone implants. The glass 45S5, Bioglass®, was the first material found to efficiently bond to hard tissue. BAG forms a carbonated HA layer when exposed to biological fluid, favoring the bonding with hard tissues [24,126,131]. It is osteoconductive, osteoinductive and also able to bond to hard and soft tissue [24,126]. Indeed, it was observed that ionic

dissolution products from the BAG like Silicon, Calcium, Phosphorus, stimulate expression of several genes of osteoblastic cells.

The main advantage of BAG is the ability to control the composition in order to tailor the dissolution rate and/or control the biological response. For instance, some ions are known to promote osteogenesis (Si), antimicrobial activity (Ag), bone density (Sr), angiogenesis (Li) etc (**Figure 14**) [132–139]. Boron has been found to be of high interest since it can promote angiogenesis, a property of paramount importance for successful outcome of a bone implant [140].

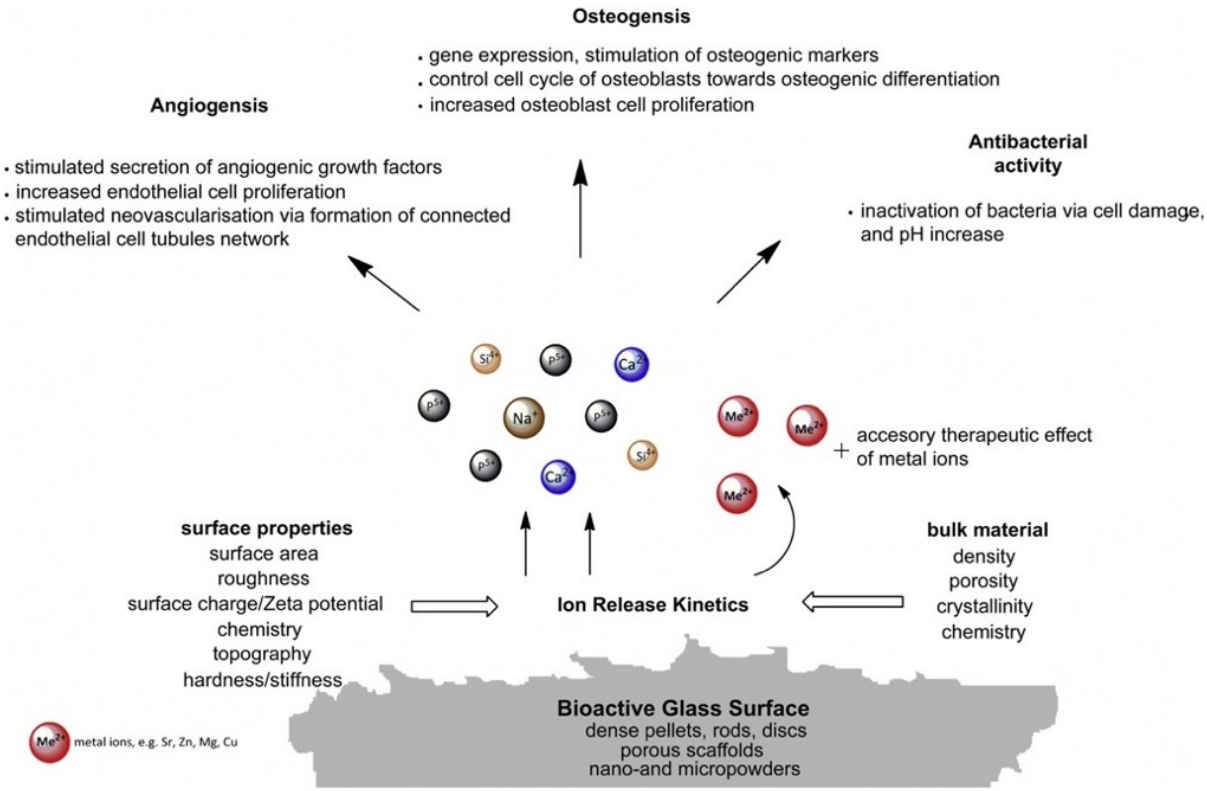

Figure 14: *Overview of biological responses to ionic dissolution products of bioactive glasses [139]*

Silicate BAG is a material containing mostly Silicon in its composition. Silicon plays a significant role in bone mineralization. Intracellular and extracellular response of BAG depends on the Si, Ca, P, and Na release from the glass surface. Silicate BAG like the 45S5, the S53P4

(BonAlive®) or the 13-93 (**Table 9**) are well-known to support the proliferation and differentiation of osteoblastic cells such as murine MC3T3-E1 cells, during conventional *in vitro* cell culture [141].

Glass	SiO_2	Na_2O	CaO	P_2O_5	K_2O	MgO
45S5	45	24.5	24.5	6	--	--
S53P4	53	23	20	4	--	--
13-93	53	6	20	4	12	5

Table 9: *Nominal glass composition (weight %)*

There are five stages governing the reaction of silicate BAG when immersed in a physiological medium [131]:

1. Rapid ion exchange reactions between the glass network modifiers (Na^+ and Ca^{2+}) with H^+ ions from the solution, leads to hydrolysis of the silica groups and the creation of silanol (Si–OH) groups on the glass surface. The pH of the solution increases due to the consumption of H^+ ions.
2. The soluble silica, in the form of silicic acid, Si(OH)4, is then released into the solution, and Si–OH groups form at the glass surface.
3. Condensation and polymerization of an amorphous SiO_2-rich layer on the surface of the glass depleted in Na^+ and Ca^{2+}.
4. Further dissolution of the glass, coupled with migration of Ca^{2+} and $(PO_4)_3$ ions from the glass through the SiO_2-rich layer and from the solution, leading to the formation of an Amorphous Calcium Phosphate (ACP) layer on the surface of the SiO_2-rich layer.

5. The glass continues to dissolve, as the ACP layer incorporates (OH) and $(CO)_2$ from the solution and crystallizes as a Hydroxyl Carbonated Apatite (HCA) layer.

The first five reaction stages that occur on the glass side of the interface can happen in aqueous solutions like TRIS or Simulated Body Fluid (SBF).

TRIS is an aqueous solution which does not contain any mineral ion, so it allows to quantify the dissolution of the glass exclusively. SBF, by Kokubo et Al [142], is a solution allowing to study the bioactivity of the glass and thus the precipitation of calcium-phosphate, resulting from the dissolution of the glass.

Following the glass reaction, the tissue/material interaction takes place as shown in **Figure 15** and **Figure 16** [143].

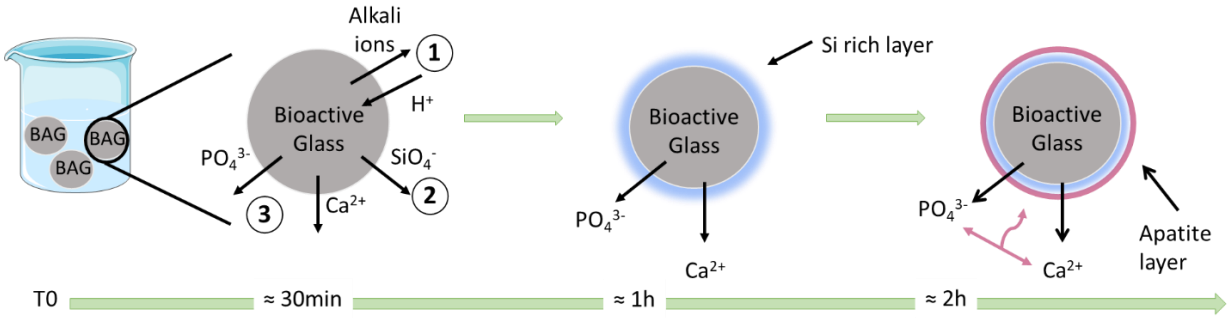

Figure 15: *Dissolution of silicate BAG in an aqueous solution.*

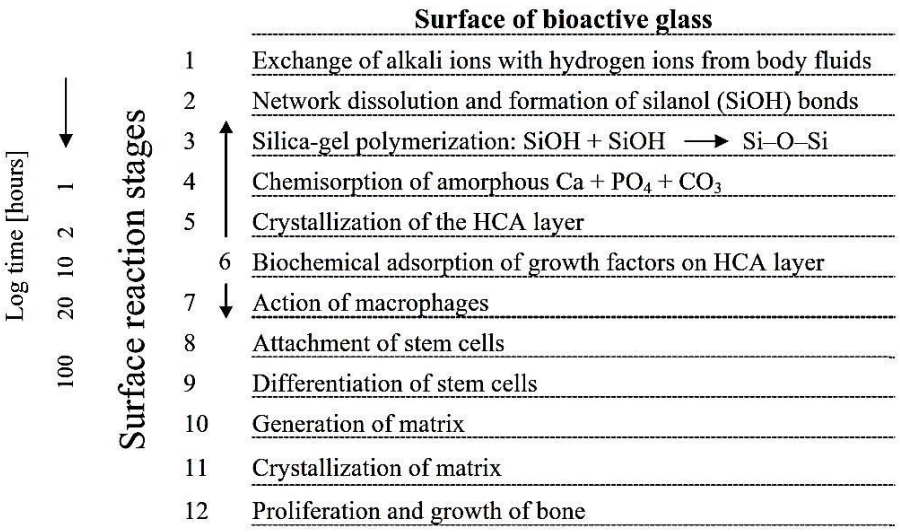

Figure 16: *Sequence of interfacial reactions involved in forming a bond between bone and a bioactive glass [143]*

The reaction layers, formed at the surface, enhance adsorption and desorption of growth factors (Stage 6) and influence the length of time during which macrophages are required to prepare the implant site for tissue repair (Stage 7) and the attachment (Stage 8) and synchronized proliferation and differentiation of osteoblasts (Stage 9). Mineralization of the matrix (Stage 10) follows soon thereafter and mature osteocytes, encased in a collagen-HCA matrix, are the final product by 6–12 days *in vitro* and *in vivo* [144]. The later stages depend on the presence of tissues.

The first Borosilicate glasses were proposed by Brink et al. for biomedical applications in 1990 [145]. In order to get the desirable bioactive properties, the relative proportion of B_2O_3 was tailored. Borate glasses (boron-based BAG) are very reactive; they convert more completely and rapidly to HA than their silica counterparts [146,147]. Huang et al. replaced SiO_2 with B_2O_3 in different proportions and found substantial increase in the conversion of the glass to HA in aqueous phosphate solutions. The increased conversion rate of borosilicate-based glasses lies in the poor mixing between the silica and the borate phase. The silica phase will form a Si-rich layer enabling better cell attachment and proliferation whereas the borate phase

will favor the hydrolysis leading to a faster dissolution rate and therefore a greater amount of ions in solution. The degradation rate and speed of conversion from the glass to HA, can be controlled within a wide range of time periods by replacing silica with boron. Although borate glasses have shown to help in cell differentiation and cell adhesion *in vitro* [147], the toxicity of borate cannot be neglected. But studies done on rats with borate bioactive glass have shown acceptable rates of toxicity [148]. If the composition of these glasses can be tailored, then matching the degradation rate of silicate and borate glasses, *i.e.* borosilicate, with the bone regeneration rate should be possible [149].

Using borosilicate can help to tailor the dissolution properties of the glass. However, a problem remains. Indeed, the BAG is hard and brittle, thus, when using a glass scaffold, its re-shaping is a difficulty. Moreover, as explained in the parts above, the organic natural or synthetic matrices which are biocompatible, biodegradable, do not have osteo-properties. Thereby, the idea is to mix both matrices, organic and inorganic (BAG), in order the obtain a material with their respective properties. The BAG can be used in organic systems that can contain it. This will allow to mix the fundamental properties of the BAG and the organic matrices to have a material which will allow bone repair.

2.3.2.2 Organic-inorganic composites and hybrids for bone bioengineering

Bone is a material consisting of mineral and organic phases. The minerals are deposited in an oriented fashion on a collagen network. For bone regeneration, BAG is pertinent due to its osteo-conduction and osteo-induction, as it would represent the mineral matrix of the tissue. However, this material is brittle and hard to shape. It cannot be used alone as an osteosynthesis system. This is the reason why it is mostly used in composite and hybrid materials.

The use of a bioactive inorganic calcium phosphate filler in composite materials for bone biomaterials was pioneered by Bonfield et al in the early 1980s with the production of particulate HA/polyethylene composites [19].

For bone repair, the implant should have the same properties as the tissue. Polymer/ceramic composite scaffolds represent a convenient alternative due to the possibility to tailor their various properties (e.g., mechanical, and structural behavior, degradation kinetics and bioactivity). Much current research is focused on the fabrication of bioactive composite materials, with the bioactive phase incorporated as filler into the bioresorbable polymer matrix. In particular, composites based on biodegradable polymers are being increasingly studied because this combination does not require a revision surgery for their removal, as newly formed bone gradually substitutes the implanted scaffold during degradation [29,79,150–152]. Effort is devoted to the development of porous, high-strength composite structures for the regeneration of human bone at load-bearing sites. Composites allow the tailoring of the mechanical properties for the specific application to closely match the stiffness of the natural tissue. At the same time, this alternative enables the BAG to be shaped and helps to mimic the bone thanks to its osteo-properties. The bioactivity, here, will allow the osteointegration of the implant in the defect, which will help bone growth and therefore, bone repair. The final properties of the implant depend on the characteristics of the organic phase (such as its chemical composition, molecular weight, and crystallinity) but also on the properties of ceramics (such as their volume fraction, their size, their dispersion, and their agglomeration). Finally, the synthesis conditions could influence the final properties of the implant. Indeed, it is possible for them to influence the mechanical properties of the compounds which can affect the properties of the composite.

Moreover, a drawback with many composites is that the inorganic phase is dispersed in the organic phase and they interact on a micrometer scale, which can result in a gradient of resorption rates during dissolution. This inevitably leads to material instability *in vivo* [20].

Plus, it can be difficult to control properties such as the degradation of the material and surface chemistry characteristics due to different resorption rate of the components and masking of the bioactive component.

The alternative proposed is working with hybrid material [20,153]. Hybrid inorganic–organic materials are made, as composites, of an organic and an inorganic phases, which are mixed homogeneously or heterogeneously.

Different class of hybrids exist depending on the links between the organic and inorganic phases. Class I hybrids present no covalent links between organic and inorganic components, but rather the bonding occurs through van der Waals or hydrogen bonding or by electrostatic forces. Class II hybrids is the category in which the organic and inorganic phases of the material are linked by strong covalent links [153,154]. The Class II hybrids are the most studied for bone repair, as their covalent links cannot be broken by the biological temperature. This is the case of the gelatin, which cannot be dissolved at biological temperatures when cross-linked.

Hybrid materials are increasingly developed as they require soft chemistry processes which allow to preserve the organic phase and to keep its mechanical properties adapted to bone repair [155]. They are commonly formed by sol-gel method which provides low processing temperatures. During this process the constituent phases interact at a molecular level. That allows a better control of material parameters such as degradation rates or mechanical properties [156]. Hybrids obtained can have different forms as gels, thin films, fibres.

The covalent links between the organic and inorganic phases are obtained thanks to bifunctional and hybrid molecules, able to bond inorganic and organic elements such as 3-glycidoxypropyltrimethoxysilane (GPTMS) [157,158], 3-aminopropyltriethoxysilane (APTES) [159], or 3- isocyanatopropyltriethoxysilane (ICPTES) (**Figure 17**) [160]. GPTMS is

a coupling agent which has been shown to be successful for the crosslinking of the gelatin with inorganic phases [20,161].

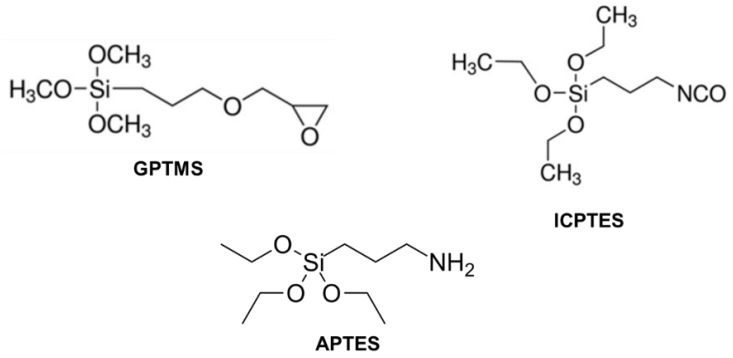

Figure 17: *Structure of different sol–gel precursors used in hybrid materials [162]*

Hybrids scaffold for bone tissue engineering were first studied by Julian R Jones who investigated gelatin/bioactive glass hybrids. The bioactive glass was obtained thanks to a silica precursor, the tetraethyl orthosilicate (TEOS) after its hydrolysis under acidic conditions [20,153,161]. The processed hybrid was composed of a single phase comprising the silica network from TEOS hydrolysis and the gelatin.

In this thesis, a new type of hybrids was developed, comprising two heterogeneous phases but covalently linked, made of bioactive glass particles, and gelatin. It is the hybrid nanocomposites [30,154]. The difference between composites and class II hybrid nanocomposites is schematized on **Figure 18.**

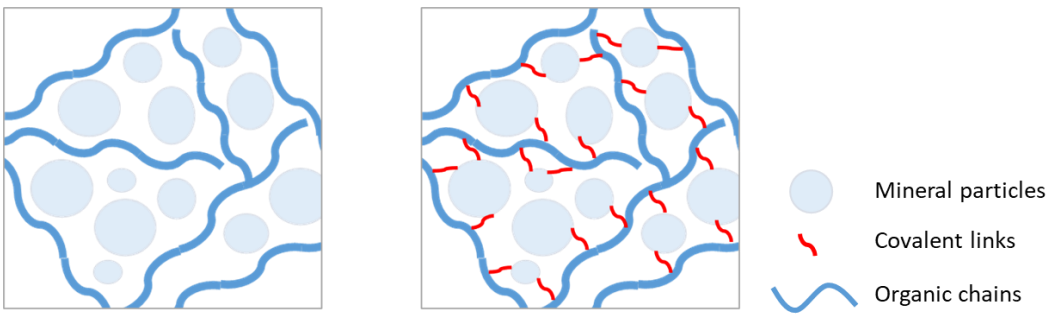

Figure 18: *Schematic representation of a composite material (left) and a class II hybrid nanocomposite material (right).*

Research routes explored

The challenge for bone tissue engineering is to provide a relevant alternative to current clinical solutions whose limitations we have described above. A material for bone tissue engineering must comply with specific and very precise specifications. Ideally, the final material should:

- be biocompatible and bioresorbable with controlled degradation and resorption rates, adapted to that of tissue and cell growth,
- be osteoconductive, osteoinductive, osteogenic and have a good osteointegration,
- have mechanical properties approaching those of the tissues at the implantation site,
- be three-dimensional and porous with a structure of interconnected pores for vascular and cellular growth and the transport of nutrients and metabolic wastes,
- have the appropriate chemistry surface for the attachment, proliferation, and differentiation of host cells.

As presented above, bone repair requires materials resembling bone in its structure but also its composition, for different applications, specifically, the maintenance and substitution of mechanical properties or for filling a critical bone defect. To respond to these challenges, two systems were studied in this thesis: composites and hybrid materials for bone tissue engineering. These systems are part of the **strategy B** presented in **2.1.2.3 in Chapter 1** *i.e.*, to provide a material containing an organic matrix in which bioactive mineral particles are dispersed, covalently or otherwise.

These systems are made of a mixture of an organic and an inorganic matrix allowing to them mimic bone composition. The mineral phase used is the 13-93 BAG or the 13-93B20, the same BAG where 20% of silicate is replaced by borate in order to tailor its dissolution rate, to control its bioactivity and guide the cellular response and differentiation. These compositions of BAGs are of interest because they present a slower dissolution compared to the 45S5 or

S53P4 BAGs. Indeed, these last are highly reactive and this reactivity can have an influence on the organic matrix integrity but also on cell behavior.

The composites will be based on PLA with a (L/DL) ratio of 70/30 and the BAG presented above with a ratio PLA/BAG of 70/30 wgt% corresponding to approximately 83/17 vol%. PLA has interesting resistance properties but an insufficient degradation rate, and an inability to fully integrate with the bone. BAGs have the osteogenic properties and will influence the degradation properties of the polymer. Therefore, adding the BAG will allow to overcome these drawbacks. Combining these properties will allow the composites to be more adapted for a support and mechanical substitution function. The composites PLA/13-93 and PLA/13-93B20 will be characterized. Their dissolution rate *in vitro* and their osteogenic properties using myoblastic cells will be compared.

The hybrids will be made of gelatin and the same BAG with a ratio Gelatin/BAG of 70/30 wgt% corresponding to a ratio of 90/10 vol% when dry. As explained, the difference between a composite and a hybrid lies in the fact that in the hybrid, the organic and inorganic matrices are covalently linked thanks to a bridging agent which here will be the GPTMS. These covalent links will allow to tailor hybrids properties as their stability, their toughness properties and to withstand biological temperatures. Gelatin allows to mimic the organic matrix of the bone. When gelatin is covalently linked to the BAG it has a better stability at high temperatures but also ductility properties which could correspond to those necessary for filling bone defects. Therefore, this material is more adapted for this function. The hybrids Gelatin/13-93 and Gelatin/13-93B20 will be characterized and their biocompatibility *in vitro* investigated with pre-osteoblastic cells.

Chapter 2: Composites strategy

Article 1: Dissolution, bioactivity, and osteogenic properties of composites based on polymer and silicate or borosilicate bioactive glass

A. Houaoui[a], I. Lyyra[b], R. Agniel[a], E. Pauthe[a], J. Massera[b], M. Boissière[a,*]

a. ERRMECe, Equipe de Recherche sur les Relations Matrice Extracellulaire-Cellules (EA1391), Institut des matériaux I-MAT (FD4122), Université de Cergy-Pontoise, Maison Internationale de la Recherche (MIR), rue Descartes, 95001 Neuville sur Oise Cedex, France

b. Laboratory of Biomaterials and Tissue Engineering, Faculty of Medicine and Health Technology and BioMediTech Institute, Tampere University, Korkeakoulunkatu 3, 33720 Tampere, Finland

*Corresponding author: Dr Michel Boissière

Dr Michel Boissière, ERRMECe, Equipe de Recherche sur les Relations Matrice Extracellulaire-Cellules (EA1391), Institut des matériaux I-MAT (FD4122), Université de Cergy-Pontoise, Maison Internationale de la Recherche (MIR), rue Descartes, 95001 Neuville sur Oise Cedex, France

Phone number: +33 (0)1.34.25.75.61, Email: michel.boissiere@cyu.fr

Keywords: Bioactive Glass; Composite material; Osteogenic differentiation

This work has been published in the journal: **Materials Science and Engineering C, Volume 107, February 2020**

Graphical abstract

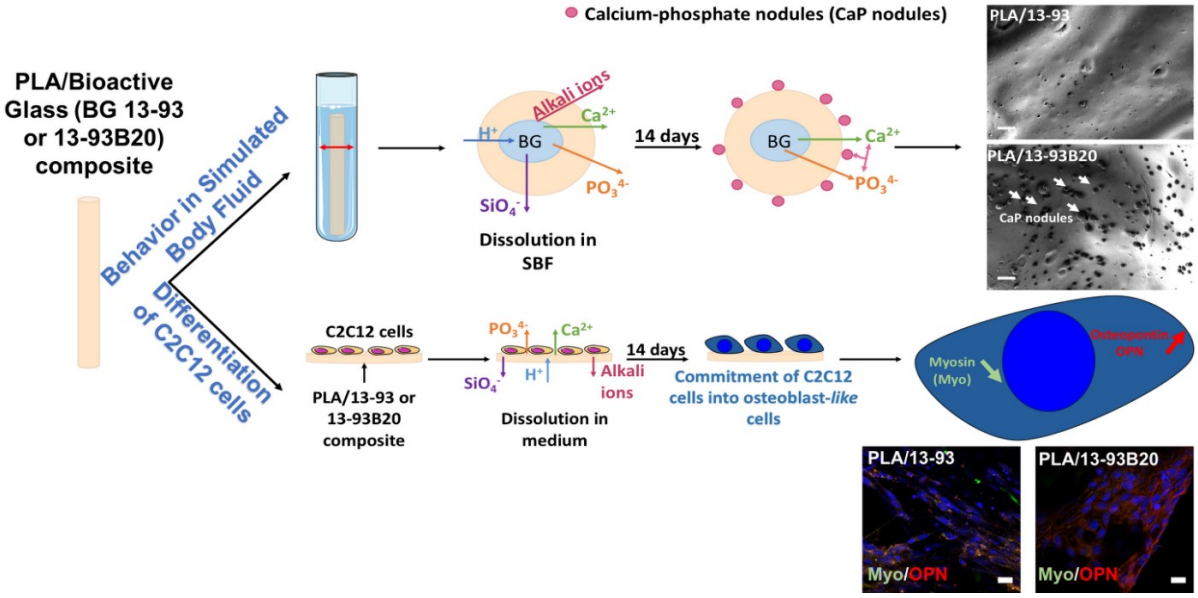

Abstract

Bioactive glass (BAG)/Poly (Lactic Acid) (PLA) composites have great potential for bone tissue engineering. The interest in these materials is to obtain a scaffold with tailorable properties bringing together the advantages of the composites' constituents such as the biodegradability, bioactivity and osteoinduction. The materials studied are PLA/13-93 and PLA/13-93B20 (20% of SiO_2 is replaced with B_2O_3 in the 13-93 composition). To characterize them, they were dissolved in TRIS buffer and Simulated Body Fluid (SBF) *in vitro*. Over the 10 weeks of immersion in TRIS, the ion release from the composites was constant. Following immersion in SBF for 2 weeks, the hydroxyapatite (HA) layer was found to precipitate at the composites surface. By adding Boron, both these reactions were accelerated, as the borosilicate glass dissolves faster than pure silicate glass alone. Polymer degradation was studied and showed that during immersion, the pure PLA rods maintained their molecular weight whereby the composites decreased with time, but despite this the mechanical properties remained stable for at least 10 weeks. Their ability to induce osteogenic differentiation of myoblastic cells was also demonstrated with cell experiments showing that C2C12 cells were able to proliferate and spread on the composites. The Myosin Heavy Chain and Osteopontin were tracked by immunostaining the cells and showed a suppression of the myosin signal and the presence of osteopontin, when seeded onto the composites. This proves osteoinduction occurred. In studying the mineralization of the cells, it was found that BAG presence conditions the synthesizing of mineral matter in the cells. The results show that these composites have a potential for bone tissue engineering.

Keywords: Bioactive Glass, Composite material, Osteogenic differentiation

Introduction

Bioresorbable polymers have been used widely in the past decades as pins, plates and screws in orthopaedic, cranial and oral surgery [1–4]. The bioresorption of the implants enables leaving the fixation in place until it degrades in the body, releasing non-toxic dissolution by-products which are then metabolised [5]. However, the bioresorbable polymers developed thus far clinically, are found to degrade at slow rate and lack osteoconductive properties [1,6]. Bioceramics are a class of materials grouping all traditional nearly inert ceramics such as, Al_2O_3 and ZrO_2, and include calcium phosphate ceramics and silicate bioactive glass (BAG). These demonstrate properties extending from bioresorbable to bioactive class A. Clinically, β-TCP (bioresorbable) and synthetic hydroxyapatite (HA) (bioactive) are the more widely used traditionally [1,7,8], but their slow dissolution rate is a limiting factor [9,10]. Indeed, concerns have been addressed pertaining to the limited resorption of those ceramics, in-vivo, when used in cements [11]. BAG is a sub-category of ceramics showing not only osteoconduction, as in synthetic HA, but also osteoinduction [12]. These glasses are commercialized mainly for hard tissue reconstruction, but they also show significant ability to bond to soft tissue [13]. However, shaping the glass into its final shape is, as for all ceramics, challenging.

The quest for bioresorbable implants which are osteoconductive for use in the treatment of traumas in the skeletal system is still ongoing and presents significant challenges still. To overcome some of the drawbacks of single materials, composites have been developed. Here, the focus will be on polymer/BAG composites, as previous studies have demonstrated that fast release of ions from BAG compensated for the decrease in pH due to the rapid degradation of Poly (Lactic acid-co Glycolic Acid) (PLGA) [14]. By adding BAG to (Poly (D,L-Lactic Acid) (P(D,L)LA) or Poly (Lactide-co-Caprolactone) (PLCL) the mechanical properties increases as well as precipitation of an HA layer at the composite scaffold surface [15,16]. These studies used the solvent-casting method. Vergnol et al. developed composites based on P(L,DL)A/45S5

BAG. In this study, glass particles (3.5µm average diameter) were mixed with polymer dissolved in acetone. The pellets obtained were then injected into molds at 145°C and 150 bars of pressure. The presence of the BAG not only increased the rate of degradation of the polymer, but also significantly promoted new bone formation in this animal study [17]. However, there was a large loss in polymer molecular weight reported over the course of the sample processing. The decrease in molecular weight could not only be assigned to the processing temperature but also to the presence of the BAG particles [18]. The mechanical properties of the scaffold were also found to decrease drastically over the short immersion time *in vitro*. The loss in mechanical properties seemed to be correlated with the loss in the mineral phase, which is assumed to be fast given the rapid dissolution rate of the small BAG particles. Another study by Niemelä et al. presents self-reinforced composites based on P(L,DL)A/13-93 BAG, made by twin-screw extrusion at temperatures varying between 190 and 195°C. In this study, the particle size was between 50 and 125µm. It is noteworthy, that not only 13-93 is slower dissolving than 45S5 (at similar particle size), but also the larger particle size will further slowdown the dissolution rate of the inorganic phase [19,20]. Degradation of the self-reinforced composites was evaluated in PBS and the results supported the effect of glass dissolution on the polymer degradation rate [19]. The 13-93 particles contained in the self-reinforced composite create a porosity which induces a degradation of the polymer due to acidic dissolution products coming from the environment. The use of 13-93 in the composites appeared to retain higher polymer molecular weights than when using faster dissolving glasses such as 45S5 or S53P4. To overcome the slow dissolution rate of 13-93, boron can replace the silica in the structure, yielding a borosilicate glass. The resulting borosilicate and borate glasses, based on the 13-93 composition, show faster in-vitro dissolution and also faster conversion into HA [21,22]. While high boron content was associated with a decrease in the cell proliferation rate, it was also found to stimulate osteogenic commitment and upregulate endothelial markers [22]. In-vivo and in-

vitro studies have shown the promising nature of borosilicate glasses [19,23]. The use of borate and borosilicate glasses as a secondary phase in a polymeric matrix has not yet been widely studied. Taino et al. produced PLCL (Poly(L-lactide-co-ε-caprolactone)/borosilicate glass composites, with varying content of 125-250 µm glass particles using the solvent-casting method. These scaffolds were then foamed by supercritical CO_2. Degradation of the polymer was linked to the dissolution of the glass [15].

Marquardt et al. studied the processing of fibrin / borate glass composites obtained by mixing fibrin with glass microfibers 0.5 – 10 µm diameter, or with rods of 50 – 200 µm diameter which were placed on a fibrin scaffold prior to polymerization. The materials obtained were able to support directed axon growth [24].

However, the effect of boron substitution for silica, in the glass composition, on the composite physico-chemical properties and cell / material interaction has not yet been studied. Added to this, based on previously reported results, the use of glass 13-93 and its boron-containing counterpart might be suitable in maintaining polymer integrity and composite mechanical properties in-vitro while supporting osteogenesis. Therefore, we have developed PLA/BAG composites using 13-93 as control and 13-93B20 with 20% SiO_2 replaced by B_2O_3. To investigate the *in vitro* dissolution behavior of our composites, they were immersed in TRIS buffer solution. Ion release from the glass and change in the polymer molecular weight were quantified. The mechanical properties of the composites were studied during the immersion. The bioactivity, assumed to be related to the precipitation of a HA layer at the surface of the material when immersed in aqueous solution, was assessed in Simulated Body Fluid (SBF), the procedure usually used for testing BAG [25]. Preliminary cell experiments were done to assess cell activity and ability of these two BAG to promote osteogenesis by culturing C2C12 myoblastic cells at the surface of composite discs. Cell proliferation and morphology were studied as well as presence of myosin and/or osteopontin which were tracked by

immunostaining. C2C12 cells capacity to synthesize their mineral matrix was analyzed with Alizarin Red S staining. The aim of this study was to assess if these cells were able to commit to an osteoblastic lineage in presence of the BAG.

Experimental

1. Material preparation and characterization

1.1. Bioactive glass (BAG) preparation

BAG 13-93 and 13-93B20 were prepared from analytical grade K_2CO_3 (Alfa Aesar, Haverhill, USA), (Na_2CO_3, $NH_4H_2PO_4$, $(CaHPO_4)(2(H_2O))$, $CaCO_3$, MgO, H_3BO_3 (Sigma Aldrich, Saint-Louis, MS, USA) and Belgian quartz sand. The 100-gram batches of 13-93 and 13-93B20 were melted for 3 hours in a platinum crucible at 1425°C and 1275°C, respectively. The molten glasses were cast, annealed, crushed and finally sieved into 125-250µm particles. The glasses were dried at 125°C for 2 hours before use. The nominal oxide compositions of the glasses are given in **Table 1**.

Table 1: Nominal glass composition (mol%)

Glass	mol%						
	Na_2O	K_2O	MgO	CaO	P_2O_5	SiO_2	B_2O_3
13-93	6.0	7.9	7.7	22.1	1.7	54.6	--
13-93B20	6.0	7.9	7.7	22.1	1.7	43.7	10.9

1.2. Sample Fabrication

Medical grade Poly(Lactic Acid) (PLA) with a (L/DL) ratio of 70/30, with an inherent viscosity of 4.0dl/g was obtained from Evonik Nutrition & Care GmbH (Essen, Germany). PLA, PLA/13-93 and PLA/13-93B20 rods were produced by melt-extrusion using a co-rotating twin-screw extruder (Mini ZE 20*11.5 D, Neste Oy, Porvoo, Finland) under nitrogen

atmosphere (**Figure 1**). The feed rates for the PLA and the BAG were fixed to 140g.h^{-1} and 60g.h^{-1} respectively to obtain approximately 70wt. % of polymer and 30wt. % of glass in the composite. The processing temperatures and pressures are presented in **Table 2**. The polymer took about 5 minutes to produce in the extruder including melting and producing the final product. The production time is less when the extruder is filled in advance.

Table 2: Materials processing parameters

	Temperature (°C)			Pressure (psi)
	Cylinder	Adapter	Die	
PLA rods	200	230	230	200
PLA/13-93	190	200	220	150
PLA/13-93B20	185	220	215	200

A 4 mm nozzle was used and the rods were pulled using a caterpillar. The speed of the caterpillar was adjusted to obtain 3 mm diameter rods.

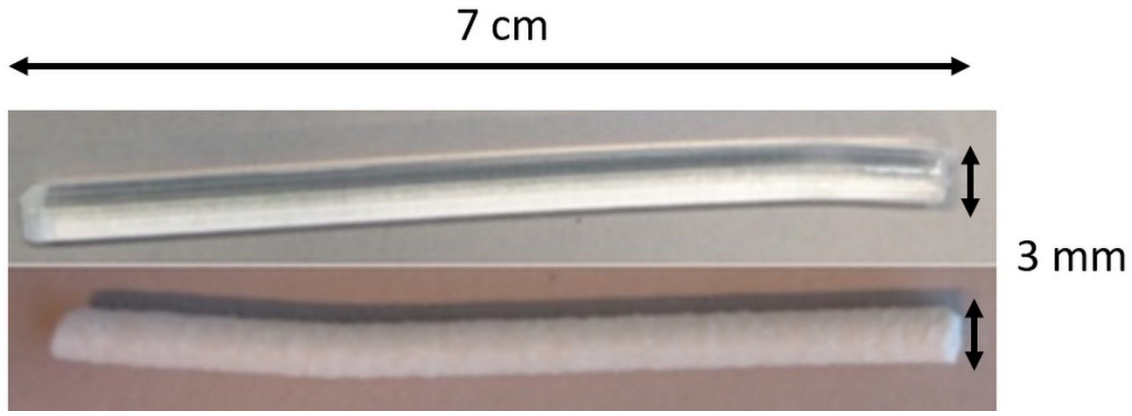

Figure 1: PLA rod (up) and composite rod (down) obtained after extrusion

The rods of each composition (PLA as a control; PLA/13-93; PLA/13-93 B20) were analyzed by Thermogravimetric Analysis (NETZSCH, Leading Thermal Analysis, STA449F1) to measure their glass content. All tests were performed in an Alumina (Al_2O_3) crucible and in a N_2 atmosphere. 10 mg of sample were heated from 25 °C to 1100 °C at a rate of 10 °C/min.

This measurement was repeated on 5 samples for each composite and the average glass content with standard deviation was calculated.

2. Behavior of the PLA/BAG composites

2.1. Physico-chemical properties of the composites

2.1.1 Immersion in TRIS

Tris(hydroxymethyl)aminomethane (TRIS) solution (50mM) was prepared by mixing ultra-pure TRIS (MP Biomedicals) and TRIS-HCl (Sigma Aldrich) in ultra-pure water and the pH was adjusted to 7.4 at 37°C. The rods were cut into lengths of 7cm (≃650 mg) which were immersed in 12mL of TRIS solution for up to 10 weeks at 37°C in a shaking incubator (HT Infors Multitron) at an orbital speed of 100rpm. To avoid saturation of the solution with the ions released from the composite, the TRIS buffer was refreshed each week.

At set times after immersion, the concentration of elements released from the composites was studied by diluting 5mL of the immersion solution in 45mL of ultra-pure water for ion analysis. ICP-OES (Agilent technologies 5110) was employed to quantify P (λ = 253.561 nm), Ca (λ = 422.673 nm), Mg (λ = 279.553 nm), Si (λ = 250.690 nm), B (λ = 249.678nm), K (λ = 766.491 nm) and Na (λ = 589.592 nm) concentrations in the solution after sample immersion. Measurements were made on four separate samples at each set time for each composite and the results presented as mean ± standard deviation (SD). The rods were then rinsed with acetone and dried.

2.1.2 Rod cross section analysis

After immersion in TRIS, the samples were embedded in resin and then polished to observe their cross section using Scanning Electron Microscopy (SEM - GEMINISEM 300 from Zeiss).

2.1.3 Molecular weight of the polymer

Molecular weights of PLA after the samples processing and at various immersion times were determined by Gel Permeation Chromatography (GPC) (Merck Hitachi Lachrom 7000 series) consisting of a pump, a refractive index detector and two Waters Styragel columns (HR5E and HR1). Tetrahydrofuran (THF) was used as eluent at a flow rate of 1 mL/min at 35°C. For each material, an amount of ≃7,5mg of polymer (cross-section of the rod) was weighed and immersed in 5mL of THF until complete dissolution. The solution was then filtered and analyzed. Molecular weights were calibrated using polystyrene standards. The measurements were conducted in four separate samples at each time points for each composition and the results are presented as mean ± SD.

2.1.4 Mechanical properties of the composites

The mechanical properties of the composite rods post-processing and after immersion (wet) were tested on the Instron 4411 (Instron Ltd., High Wycombe, UK) using a 3-point bending and shear test at room temperature. At least four parallel samples of each composite type were tested. For the bending test, the properties were studied with a crosshead speed of 5 $mm.min^{-1}$ and a bending span of 42 mm. For the shear test [26], the crosshead speed was 3 $mm.min^{-1}$. The measurements were conducted in the four samples at each set point for each composite and the results are presented as mean ± SD.

2.2 Composites bioactivity

2.2.1 Immersion in Simulated Body Fluid (SBF)

SBF was prepared following the methodology [27] from the standard ISO/FDIS 23317 as described by Kokubo et al. The samples were cut to obtain rods of 7cm (≃650 mg) which were immersed in 12mL SBF solution for up to 2 weeks at 37°C in a shaking incubator (HT Infors Multitron) with at a speed of 100rpm. During the experiment, the solution was not refreshed so

that calcium phosphate could be measured. The ion concentration in the solution according to immersion time was measured as previously described. Measurements were made on four separate samples at each set time for each composite and the results presented as mean ± SD.

2.2.2 Rod surface analysis

The reactive layer at the rod surface after immersion in SBF was observed by SEM (GEMINISEM 300 from Zeiss) and its composition was analyzed by Energy-Dispersive X-ray spectroscopy (EDX Quantax from BRUKER). The Infrared (IR) absorption spectra of the composites immersed in SBF were also recorded using a Bruker Alpha FTIR in Attenuated Total Reflectance (ATR) mode to see the effect of the dissolution on their structural properties. The measurements were performed on dry samples. All IR spectra were recorded within the range 399–4000 cm^{-1} with a resolution of 2 cm^{-1} and 32 accumulation scans.

2.3 Cell analysis

2.3.1 Disk preparation

PLA, PLA/13-93 and PLA/13-93B20 disks were obtained by compression molding (Nike Hydraulics ZB110, Eskilstuna, Sweden) of a piece of the rods for the cellular tests. The rods were compressed under 10-20 MPa pressure at 140 °C for 1 min, then the mold was cooled down with compressed air and 14mm disks were cut from the plates obtained. These disks were then sterilized by gamma irradiation (25 kGy) at BBF sterilisations service GmbH (Germany). All experiments were performed in 24-well plates and the disks were washed with PBS prior to use.

2.3.2 Cell culture

Myoblastic C2C12 cells were cultured in DMEM Glutamax supplemented with 10 % Fetal Bovine Serum (FBS) and 1 % penicillin/streptomycin, in an humidified atmosphere of 5 % CO_2 at 37 °C.

2.3.3 Cell proliferation and morphology

To compare the behavior of C2C12 cells on the different samples, cell proliferation was studied using CyQUANT Cell Proliferation Assay kit (Invitrogen, Life Technologies). Around 7700 cells/disk were seeded on the 14mm disks in 24-well plate and the medium was changed every 2 days. Cleaned and sterilized microscope glass slides were used as controls. After 1, 2, 4 and 7 days of culture, the cells were lysed with 400 µL 0.1 % Triton-X100 (Sigma–Aldrich) buffer and conserved at -80 °C. After one freeze–thaw-cycle, three 20 µl aliquots of each lysate were pipetted on to a black 96-well plate (Corning) and mixed with 180 µl working solution (CyQUANT GR dye and cell lysis buffer). The fluorescence was then measured at 520nm with a Spectrofluorimeter Xenius XM (SAFAS).

The morphology of the cells on the different samples was observed after 48 h of culture. The same number of cells was seeded on the disks and after 48 h, the cells were fixed with 3 % (w/v) para-formaldehyde solution dissolved in PBS (Sigma Aldrich) for 15 min, then permeabilized with 0.1 % (v/v) Triton X-100 (Sigma Aldrich) for 10 min. Non-specific binding sites were blocked by incubating the disks in PBS containing 1 % Bovine Serum Albumin (BSA) for 1 h. The cytoskeleton and nuclei of the cells were stained respectively with 1:500 FITC-labelled phalloidin (Sigma Aldrich P5282) and 1:1000 4',6-Diamidino-2-phenylindole dihydrochloride (DAPI, Sigma Aldrich D9542) in PBS-BSA 0.5 % for 1 h. Each incubation with antibodies was performed in the dark in a humid atmosphere. Samples were then washed in PBS-BSA 0.5 %, mounted in Prolongold (Invitrogen), and observed under a LSM710 confocal microscope (Carl Zeiss).

2.3.4 Cell differentiation

The expression of a late myoblastic marker (myosin heavy chain) and an early osteoblastic marker (osteopontin) were studied using specific antibodies. Around 600 C2C12 cells were seeded on the disks and cultured for 14 days. Cleaned and sterilized microscope glass slides

were used as controls. Cells were then labelled with mouse anti-myosin heavy chain (MHC, 1:1000, Millipore 05716), and rabbit anti-osteopontin (1:500, Millipore AB10910) diluted in PBS containing 0.5 % BSA. Primary antibodies are revealed using Alexa Fluor 488 or Alexa Fluor 568-conjugated goat anti-mouse or anti-rabbit antibodies both 1:400 in PBS-BSA 0.5 % (Invitrogen) as secondary antibodies. Samples were observed using a LSM710 confocal microscope (Carl Zeiss).

Mineralization was also assessed at 10 days and 14 days using Alizarin Red S stain (the calcium minerals stain red). The staining from a previously described protocol was adjusted [28] in that cells were fixed with paraformaldehyde for 15min at room temperature and stained with 2 % Alizarin red S (pH 4.1–4.3; Sigma–Aldrich) for 20 min at room temperature. The excess color was washed away with three consecutive water washes after which the samples were observed under an optical microscope.

2.3.5 Statistical analysis

Data were analyzed using GraphPad Prism Software. Statistical significance between groups is assessed by one-way analysis of variance (ANOVA). Experimental results are expressed as means ± standard deviation. Statistical significance is taken for values of $p < 0.05$.

Results and discussion

The aim of this study was to develop a polymer-BAG composite able to release ions beneficial for bone regeneration while maintaining, post-processing, the mechanical properties and the molecular weight of the polymer. As it has been reported that it is difficult to produce a polymer-bioglass ® (i.e., 45S5) composite, we decided to incorporate BAG 13-93 into a PLA matrix. As reported by Brink et al. the dissolution rate of the glass 13-93 is much slower than the typical BAG used clinically (*i.e.* 45S5 (Bioglass®) and S53P4 (BonAlive®) [20]). To

control glass dissolution, a second glass composite was tested [23], whereby 20% of the SiO_2 in the 13-93 composition was replaced with B_2O_3.

1. Characterization of the composites after processing

Table 3 presents the glass loading in each composite, with the mechanical properties of the composites and the molecular weight of the polymer included in each composite.

Table 3: Measured glass loading, mechanical properties and average molecular weight of the processed PLA and PLA/BAG composites (for wet samples, the mechanicals properties were measured after 10min of immersion in TRIS).

Materials	Composites glass loading (wt%)	Young modulus (GPa)		Shear stress (MPa)		PLA Mw before extrusion (kDa)	PLA Mw after extrusion (kDa)
		Dry samples	Wet samples	Dry samples	Wet samples		
Bulk PLA	--	--	--	--	--	526 ± 7	--
PLA rods	--	3.5 ± 0.1	3.6 ±0.2	46.6 ± 0.8	50.1 ± 1.4	--	305 ±14
PLA/13-93 rods	38 ± 2	3.6 ± 0.3	3.3 ± 0.3	34.0 ± 2.0	32.3 ± 1.4	--	248 ± 5
PLA/13-93B20 rods	35 ± 4	3.6 ± 0.7	3.1 ± 0.4	32.1 ± 1.5	32.1 ± 1.1	--	251 ± 15

The targeted glass loading was 30 wt%. Thermogravimetric analysis was conducted (**Figure S1**) to assess the true glass loading in the polymer matrix post-processing as well as the homogeneity of the processed rods. Glass loading was 38±2 wt% and 35±4 wt% for the PLA/13-93 and PLA/13-93B20, respectively, demonstrating good control over the process used to produce the composites.

Before extrusion, the molecular weight of the PLA granules was measured to be ~530 kDa. As expected, after extrusion, the molecular weight of the pure PLA decreased about 40 %, while the PLA loaded with BAG decreased by ~50% regardless of the glass composition. The decrease of the molecular weight recorded is not as high as that reported in the literature. For example, Vergnol et al. show a decrease in molecular weight of ~90% when producing PLA-BAG composite processed by injection molding [17]. Moreover, the PLA/S53P4 composites

were tested, but, during the processing the viscosity of the polymer drastically and rapidly decreased, and the materials obtained were amber-like as reported by Vergnol et al. for the PLA/45S5. The reason for this rapid change in viscosity and subsequent thermal degradation of the PLA is not yet well understood. However, this phenomenon appears when processing PLA with fast reacting BAG and does not occur that readily with more stable glasses. Therefore, a hypothesis for the thermal degradation of PLA upon extrusion of composites using 45S5 and/or S53P4 may be due to the high intrinsic water content in the glass structure or the glass degradation/dissolution when in the polymer melts. The combination of PLA and the proposed BAG 13-93 processed by twin-screw reduces loss of molecular weight during melt processing.

The mechanical properties of the PLA and its composites were measured in 3-point bending and shear. Both composites have an almost stable flexural modulus in wet and dry conditions but show a decrease in shear stress in both conditions, when compared to the polymer alone. The changes in the mechanical properties are only a function of the glass loading but not due to the nature of the glass. The decrease in the shear strength was not unexpected, since polymer glass composites are known to become weaker, and tend to become more brittle, as can be seen by an increase in their elastic modulus. Here, the decrease in the flexural modulus indicates an increase in the ductility. Such behavior, was already reported in self-reinforced polymer/BAG filaments [26]. The loss in mechanical properties is probably due to the absence of chemical bonds between the glass and the polymer, leading to a loss of cohesivity.

2. Behavior of the composites in solution

2.1 Dissolution in TRIS

The co-degradation in TRIS of the polymer and glass was assessed by GPC and ICP-OES measurements and compared to that of the dissolution of the pure PLA rods. **Figure 2** presents the concentration in Si **A**), Na **B**), K **C**), B **D**), Mg **E**), Ca **F**) and P **G**) post immersion in TRIS

for various times. As the immersion solution was refreshed every week the results are presented cumulatively and normalized to the sample mass. As expected, the PLA alone does not exhibit any change in ion concentration. Upon immersion of the composites, the concentration in solution of the different elements increases, indicating that the glass particles are being hydrated and dissolve through the polymer. As expected, the addition of boron to the glass structures leads to faster initial ion release (up to ~10 days). However, at longer immersion times all curves seem to plateau for solutions containing the PLA/13-93B20 composites whereas the dissolution of the glass in the PLA/13-93 composite remains almost linear. It should be noted that; especially at longer immersion times, the standard deviation was higher in the case of the polymer containing the glass 13-93B20 than 13-93.

It is a known fact that upon immersion of a silicate glass in aqueous solution, initially ion exchange occurs followed by condensation and re-polymerization of a silica-rich layer [12]. If this layer is not uniformly formed at the surface of all glass particles, variations in ion release can be expected. All ion concentrations were normalized to the element contained in the starting rod to clearly show the extent of ion release.

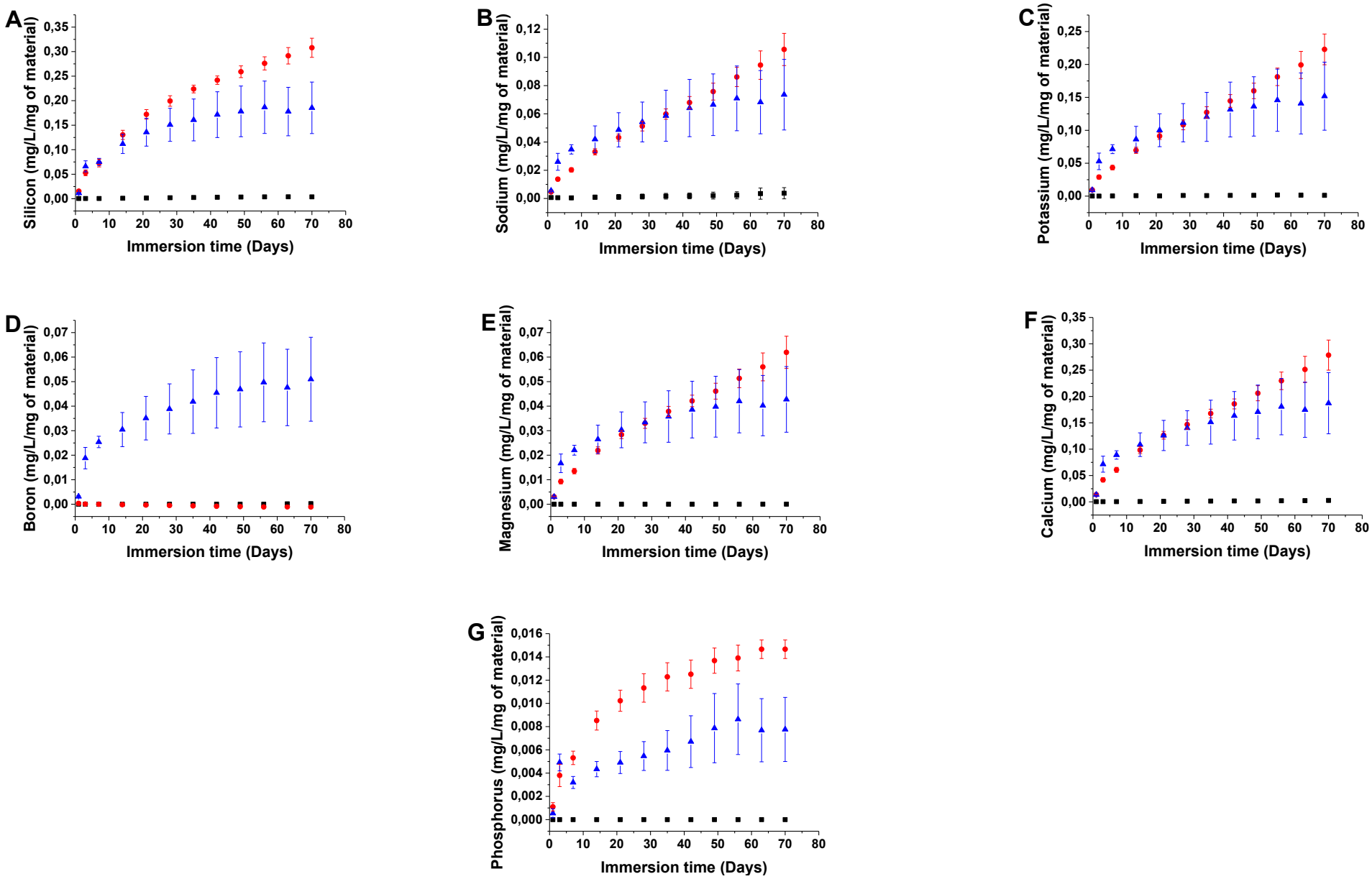

Figure 2: Element concentrations of **A**) Si, **B**) Na, **C**) K, **D**) B, **E**) Mg, **F**) Ca and **G**) P in the dissolution products of PLA (■), PLA/13-93 (●) and PLA/13-93B20 (▲) immersed in TRIS according to time.

Figure 3A) presents the percentage of ion released from glass 13-93 in TRIS solution. It is clear that glass dissolution is limited, whereby at 70 days less than 5% of each element is released into the solution. While the Si and P release seems to level-off at immersion times >20 days, all other constituents, i.e., Na, Ca, Mg and K seemed to be leached-out in an almost linear manner up to 70 days. **Figure 3B**) presents the release of ion from the glass 13-93B20, in % of initial mass of the elements. As seen in the case of the composites containing the glass 13-93, all ions are found to leach out into the solution. However, the difference in the dissolution profile of ions from the composites containing the glass 13-93B20 compared to ion release from composites containing the glass 13-93, is of interest.

1. While in **Figure 3A**) the Ca, K, Mg and Na dissolve, from the glass 13-93, at similar rate, a slower release of Ca was measured during dissolution of composites containing the glass 13-93B20 (**Figure 3B**). Furthermore, Ca release follows a similar dissolution profile to B as shown in **Figure 3B**).
2. The initial release rate for all ions is faster for composites containing the glass 13-93B20. However, at extended immersion time (>15 days) a decrease in the release rate of all ions can be seen; whereas when immersing composites containing the glass 13-93 (**Figure 3A**) only Si and P release rate slows down at extended immersion time, while all other ions show a linear release.
3. The final ion release content in the solution (at 70 days) is slightly lower in the case of the composite containing the glass 13-93B20 than in that containing the glass 13-93.

From the literature many interactions between the B_2O_3 and SiO_2 in the glass were reported to happen. Some are reported below [29–32]:

$$2Si\text{-}O^- + B\text{-}O\text{-}B \rightarrow Si\text{-}O\text{-}Si + 2B\text{-}O^- \quad (1)$$

$$Si\text{-}O^- + B\text{-}O\text{-}B \rightarrow Si\text{-}O\text{-}B + B\text{-}O^- \quad (2)$$

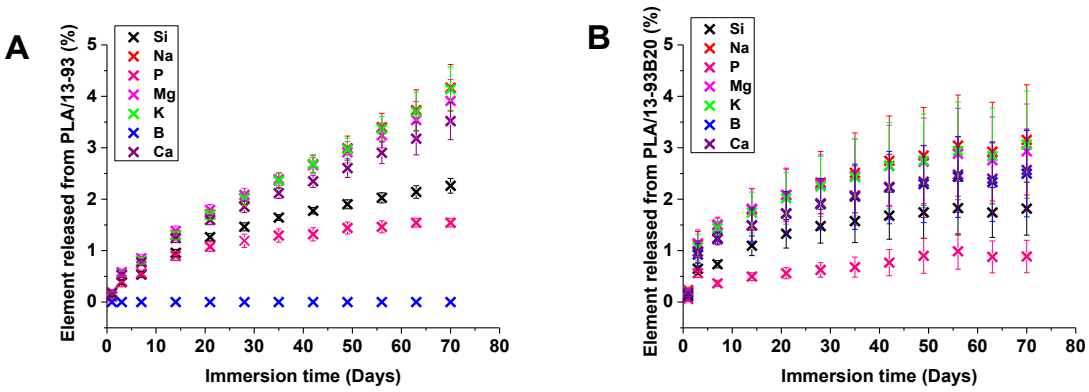

Figure 3: Release of ions from the **A**) PLA/13-93 and **B**) the PLA/13-93B20, immersed in TRIS according to time.

However, those reactions were not sufficient to explain the physical, thermal, and structural changes associated with the substitution of the SiO_2 with B_2O_3. In depth structural analysis showed preferential interaction between CaO and B_2O_3 as follow [33]:

$$BO_3 + CaO \leftrightarrow BO_4 \quad (3)$$

More recently, Yu et al. reported the medium-range structural organization of phosphorus bearing borosilicate glasses and the consequence of B/Si substitution [34]. Their findings support the increase in the polymerization of the silica network with increasing substitution ratio. Furthermore, they demonstrated a higher affinity of the phosphorus to bond with B rather than with Si. Therefore, while in typical silicate glass the majority of the phosphorus is present as Q^0 (zero bridging oxygen atom per PO_4 unit), an increase in Q^1 units, bridging one oxygen atom per PO_4 unit, was evidenced. Overall, the structural modification occurring in the glass network when substituting Si for B is in agreement with the dissolution behavior observed in **Figure 3A**) and **B**), i.e., boron and calcium are released at the same rate (**Figure 3B**) as typically seen in a congruent dissolution. Thus, it appears that the calcium preferentially interacts with the boron sub-network (congruent dissolution) rather than with the silicate sub-network (non-congruent dissolution). The lower, overall release of the ions (at long immersion time) is most likely related to the increase in the degree of polymerization of the silica network as shown in equations 1 and 2, where the number of non-bridging oxygen is expected to decrease with

increasing the boron content. However, such structural analysis does not fit the dissolution behavior reported in the literature, which tend to demonstrate that the addition of B_2O_3 at the expense of SiO_2 should increase the glass dissolution rate [35–38]. It is therefore possible to assume that either the increase in Si-O-Si bridges is associated with a disproportionation of the silicate structure, whereby, $2Q^2 \leftrightarrow Q^1 + Q^3$, and/or Si-O-B bridges form between the borate and silicate units. Both assumptions would be consistent with the increase in the initial dissolution rate of the glass in the composite containing the glass 13-93B20 and a progressive decrease in the ion release rate due to remnants of a more stable silicate. As seen in **Figure 3A**) and **B**), this leads to a higher ion concentration in the solution containing the borosilicate glass at a short immersion time, and saturation occurring at an earlier time than in the case of traditional silicate BAG such as 13-93. Finally, the increased linkages between the phosphorus structural unit and the more stable BO_4 units proposed by Yu et al. [34] is confirmed by the lower phosphorus release profile in the case of the glass 13-93B20 than in 13-93.

Figure 4 shows the cross sections of the composites before and after 10 weeks of immersion in TRIS. Before immersion, the BAG granules are fixed and appear to be maintained by the PLA matrix. After 10 weeks in TRIS, they are seen to be detached from the polymer, regardless of the glass composition, as expected post surface dissolution of the glass particles.

At the same time, the change in the polymer molecular weight was assessed according to time and is presented in **Figure 5**. Although the extrusion process affected the PLA molecular weight (Mw), it does not seem to be impacted by the interaction with the medium after immersion for up to 10 weeks. However, slow but linear molecular weight decrease is apparent during immersion of the composite. The composite containing the BAG 13-93, showed the fastest PLA degradation with a loss of ~45% of its molecular weight post-extrusion at 10 weeks at a rate of 1710 ± 96 Da / day (R^2=0.99).

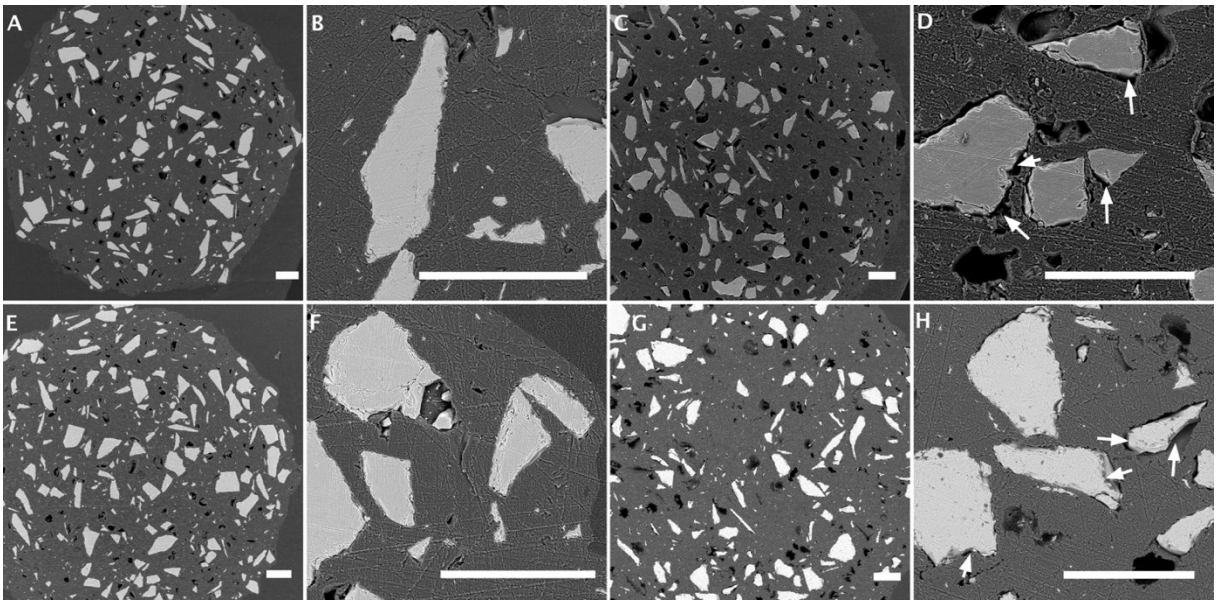

Figure 4: Observations of the cross section of the composites by SEM. **A**) and **B**) show the PLA/13-93 before immersion, **C**) and **D**) show the PLA/13-93 after 10 weeks of immersion in TRIS. **E**) and **F**) present the PLA/13-93B20 before immersion and **G**) and **H**) show the PLA/13-93B20 after 10 weeks of immersion in TRIS. Scale bar 200µm

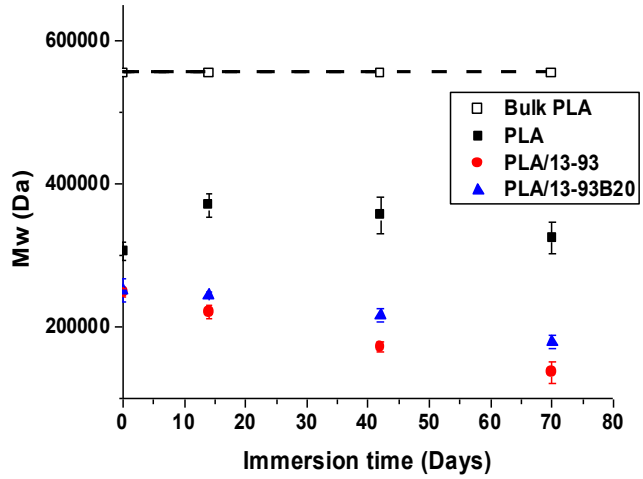

Figure 5: Molecular Weight (Mw) of PLA before extrusion (□) PLA (■), PLA/13-93 (●) and PLA/13-93B20 (▲) rods immersed in TRIS according to time.

The composite containing the BAG 13-93B20 showed a slower decrease, of ~29 % of its original molecular weight after 10 weeks of immersion at a rate of 1133 ± 82 Da / day (R^2=0.98). In both cases, the degradation of the polymer is due to the interaction between glass dissolution by-products and PLA, most likely by alkaline hydrolysis of ester bonds at the glass/PLA interface [39]. Such behavior was, however, not reported by Maquet et al. with the

dissolution of bioglass®-filled polylactic foams but occurred during dissolution of PLA/BAG composite *in vivo* [16,17]. Added to this, the difference in PLA degradation can be related to the more sustained ion release in the case of the composite containing the glass 13-93 as seen in **Figure 3**.

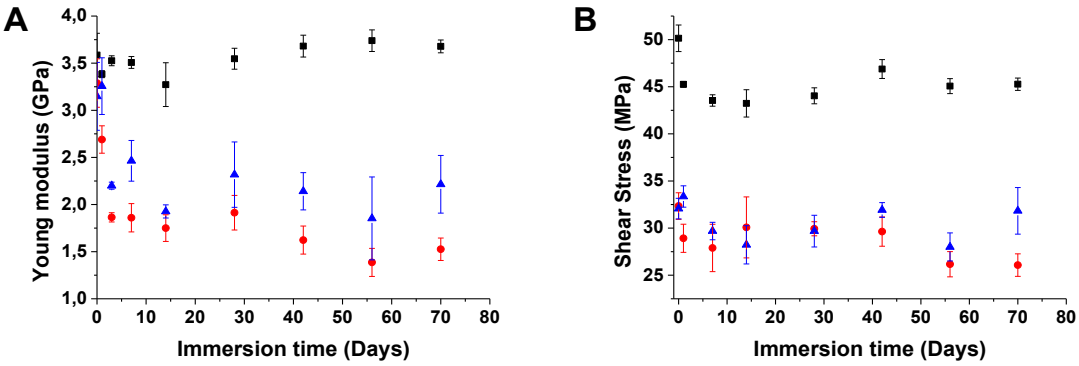

Figure 6: **A**) Young modulus reported from the bending test and **B**) Shear stress of wet PLA (■), PLA/13-93 (●) and PLA/13-93B20 (▲) rods according to immersion time in TRIS.

The mechanical properties (Young modulus and Shear stress) were measured on wet samples as a function of immersion time (**Figure 6**). While no significant changes in shear stress, within the accuracy of the measurement, were recorded, a net fall in the Young modulus can be seen after immersion for up to three days. As all the measurements were corrected to the swelling of the sample, such a drop can be attributed to the diffusion of water within the composite structure, most likely due to pores being formed during the processing. After the initial drop, the Young modulus does not seem to be, drastically, impacted by either the glass or the polymer dissolution/degradation.

Upon immersion of composites in TRIS buffer solution, a decrease in the average molecular weight was measured. However, in this study and in agreement with data reported by Vergnol et al, the decrease of the PLA molecular weight alone could not be correlated to changes in the mechanical properties [17]. Yet, in Vergnol et al., a decrease in mechanical properties was recorded upon immersion of the BAG/PLA composite. The loss in mechanical strength is directly related to the composite mass loss with regards to the immersion time.

Therefore, the dissolution of mineral phase dictated the change in mechanical properties. In our study, the larger particle size of BAG with slower dissolution rate than in Vergnol et al's work were used [17]. The low dissolution rate of the BAG used in this study implies that the composite keeps its integrity for at least 10 weeks.

The immersion of the composites in TRIS helped to understand the dissolution of both composites in solution. The 13- 93B20 dissolves faster initially than the 13-93 and saturates more quickly to the same level as the 13-93 in the end. This dissolution leads to the decrease of the polymer molecular weight, but the mechanical properties stay almost stable.

2.2 Dissolution in SBF

Samples were also immersed in Simulated Body Fluid (SBF). As postulated by L.L. Hench, the ability of a material to induce the precipitation of an hydroxyapatite layer at its surface is considered to be a sign of bioactivity [12].

Immersion in SBF was conducted over a two-week period and the solution was not refreshed. ICP-OES was used to quantify the ion concentration in the solution. The difference between the ion concentration in SBF and ion concentration post composite immersion was calculated (**Figure 7**).

The elements Si, K, Mg and B (for the PLA/13-93B20) show similar trends when immersed in TRIS where the 13-93B20 glass leaches out its ions at a faster rate initially and then stabilizes. However, it is important to point out that i) the dissolution rate starts to slow down at an earlier immersion time in SBF than in TRIS and ii) while limited saturation was noticed, in the case of immersion of the PLA/13-93 in TRIS buffer solution, in SBF, saturation can also be seen for this glass. The Ca concentration seems to increase initially and then decreases with increasing immersion time, whereas the P concentration decreases constantly over dissolution time. Generally, the decrease in Ca and P in SBF is associated with the precipitation of a calcium-

phosphate reactive layer. The decrease in Ca and P is faster and starts at earlier time when the composites containing BAG 13-93B20 are immersed, indicating a faster and more rapid precipitation of the reactive layer in the case of this material. This is most likely due to the faster initial dissolution.

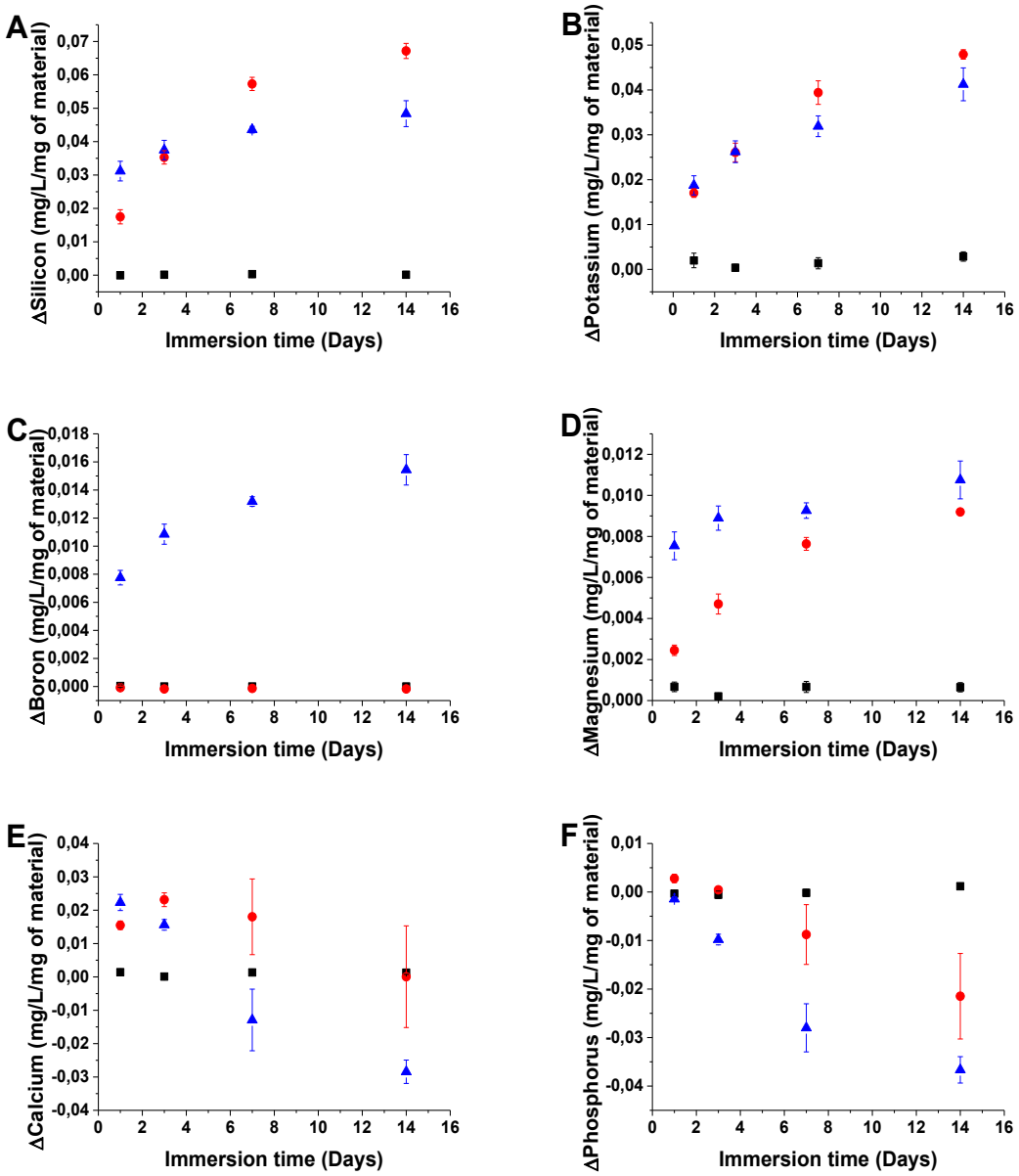

Figure 7: **A**) Si, **B**) K, **C**) B, **D**) Mg, **E**) Ca and **F**) P element concentrations released in SBF from the PLA (■), PLA/13-93 (●) and PLA/13-93B20 (▲) according to immersion time. ΔElement = [Element] in SBF in presence of the sample – [Element] in SBF initial solution.

The precipitation of a reactive layer at the surface of the rods was assessed by SEM/EDX and FTIR. **Figure 8**) presents the SEM images of the PLA (**A** and **B**), PLA/13-93 (**C** and **D**) and PLA/13-93B20 (**E**, **F** and **G**) before and after 14 days of immersion in SBF.

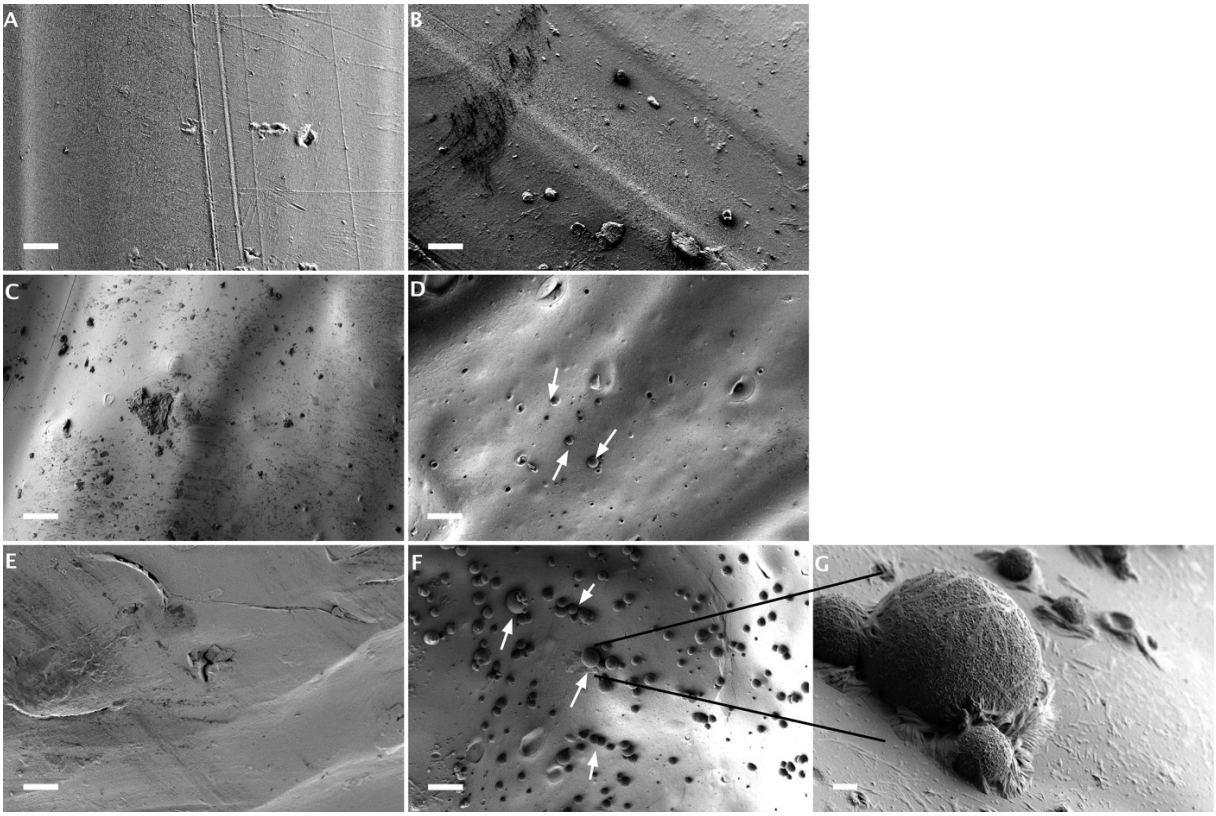

Figure 8: Surface observations and analysis by SEM-EDX and FTIR of the PLA and the composites. **A**) and **B**) show the surface of the PLA before and after 2 weeks of immersion in SBF respectively. **C**) and **D**) represent the PLA/13-93 before and after 2 weeks of immersion in SBF. **E**) and **F**) show the PLA/13-93B20 before and after 2 weeks of immersion in SBF (Scale bar 20µm) and G) represents the nodules found on the PLA/13-93B20 after 2 weeks in SBF (Scale bar 2µm).

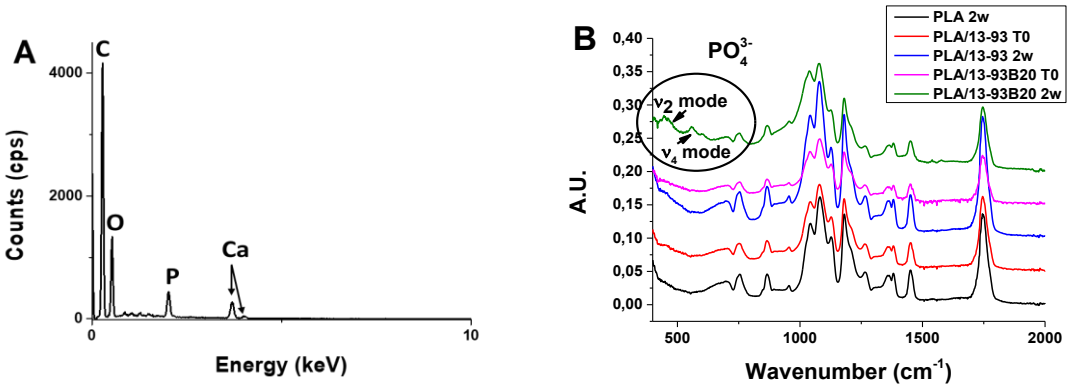

Figure 9: **A**) EDX analysis of the nodules found on PLA/13-93B20 surface and **B**) FTIR analysis of the sample surfaces before and after 2 weeks of immersion.

While no significant change in the surface topography can be seen after immersion of the PLA in SBF, some spheres could be seen at the surface of the composites after 14 days. The spheres were small and sparsely dispersed at the surface of the composites containing the glass 13-93 (**Figure 8D**), while higher density of larger spheres (with a wide size distribution) were covering the composites containing the glass 13-93B20 (**Figure 8F**). This is in agreement with the faster reactive layer formation hypothesized from the ICP analysis for the boron containing composites.

EDX was performed on the spheres showed on **Figure 8G**) and an EDX spectra is presented in **Figure 9A**). The composition of the sphere is mainly Ca and P with a Ca/P ratio of ~1.6. This is a good indication that the calcium phosphate layer precipitating is hydroxyapatite. This was further confirmed by FTIR spectroscopy shown in **Figure 9B**). While only peaks related to the PLA structure were seen in the pure PLA and PLA/13-93 composite, prior and after immersion in SBF, whereas two peaks in the 400-600 cm^{-1} appeared after PLA/13-93B20 immersion in SBF. These peaks are characteristic of the ν_4 (P – O bending) and ν_2 (O – P – O bending) PO_4^{3-} vibration in apatite structure [40,41]. This effect is partially overcome when working with 13-93B20. The particles are mainly embedded in PLA which slows the release rate due to the PLA diffusion barrier. However, one should keep in mind that despite 13-93B20 promoting more effective HA precipitation than 13-93, a similar reactivity to 45S5 or S53P4 has not yet been reached.

We developed PLA/BAG composites using a process that enables limiting the polymer degradation while maintaining mechanical properties which are of interest in bone tissue engineering. Furthermore, the inorganic filler dissolved when immersed in aqueous solution with kinetics function of the glass composition. The PLA/13-93B20 composite was also found to precipitate a hydroxyapatite layer upon immersion in SBF. Therefore, we decided to do

preliminary cell experiments to assess if these composites have potentially osteogenic properties which are of utmost important in bone reconstruction.

3. C2C12 proliferation and morphology

The C2C12 cell system was chosen owing to its known dependence by adhesion to the substrate rigidity, and to the experimental ease in measuring the cellular response to the Bone Morphogenetic Protein 2 (BMP-2). In addition, this cell line is important and relevant in the progenitor cell system for bone tissue engineering [42].

Firstly, the proliferation of C2C12 cells on PLA and both composites was studied for up to 7 days (**Figure 10**).

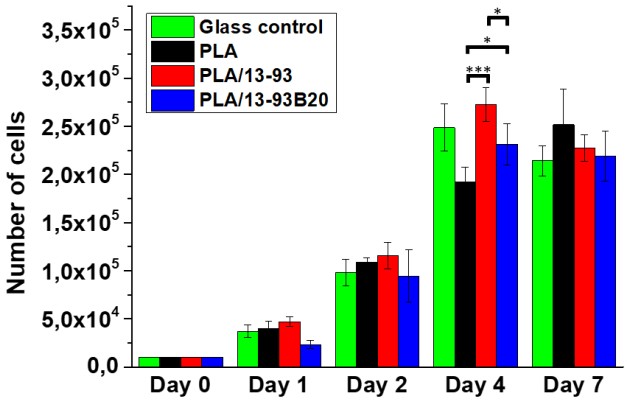

Figure 10: Proliferation of C2C12 cells cultured in DMEM complete medium on glass, PLA, PLA/13-93 and PLA/13-93B20 for 7 days, analyzed with a CyQUANT Cell Proliferation Assay kit, ***p<0.001, *p<0.05.

Glass slides were used as a control. The cells proliferated with the characteristic profile of this cell phenotype on all substrates. At 4 days, the proliferation of C2C12 cells on the composites is significantly higher than on the PLA alone. Fu et al. and Eqtesadi et al. [23,43] have already demonstrated that 13-93 glass alone promotes cell adhesion and proliferation. It is interesting to point out, that at day 4, the cell count is statistically higher at the surface of the PLA/13-93 than on the PLA/13-93B20. This is certainly due to the release of boron from the borosilicate

glass, which is known to decrease cell proliferation while promoting osteogenesis [44]. It can also be seen that the morphology of murine C2C12 myoblasts after 48h of incubation (**Figure 11**), seem to spread more within the cytoskeleton of the cells with PLA/13-93 and PLA/13-93B20, than with PLA alone.

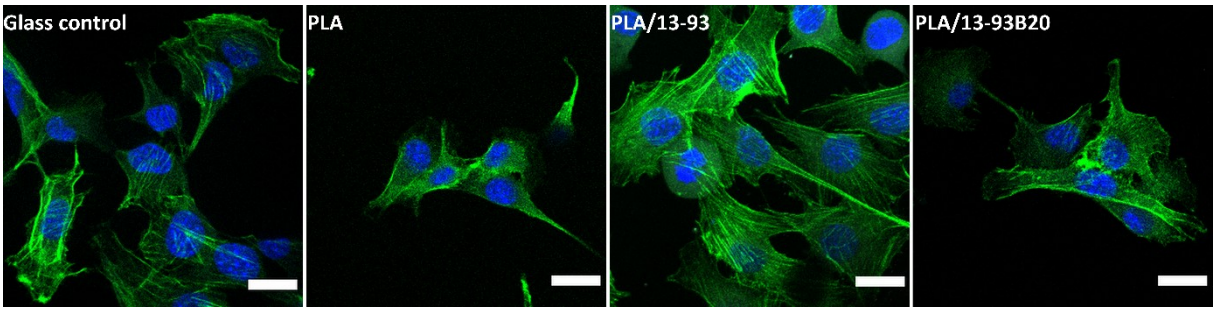

772 ± 212μm² 439 ± 77μm² 1097 ± 358μm² 892 ± 269μm²

Figure 11: Morphology observations of C2C12 cells in DMEM complete medium analyzed by immunostaining, Nuclei (DAPI - blue) and Actin (Phalloidin - green), after 48h of incubation on glass, PLA, PLA/13-93, PLA/13-93B20 (Scale bar 20µm). Under each image the spreading area of the cells is annotated on each sample after 48h of incubation.

This is confirmed by the measurements of the spreading surface of the cells on each material (**Figure 11**). The lower ability of the cells to spread on PLA can be correlated to slightly slower proliferation of cells at day 4 (**Figure 10**), when compared to proliferation on composites. Thereby, both types of BAG do not present cytotoxic effects and when included in the PLA, they promote proliferation and adhesion of C2C12 cells compared to the PLA alone.

4. C2C12 differentiation

In order to study the capacity of C2C12 cells to commit to an osteoblastic lineage in presence of BAG, myosin heavy chain (late marker of myogenic differentiation) and osteopontin (early marker of osteoblastic differentiation) were stained after 14 days of incubation.

In **Figure 12**, it can be seen that the glass control (**Figure 12B** and **C**) and pure PLA (**Figure 12F** and **G**) have a high myosin expression but no osteopontin expression. The

differentiation of C2C12 myoblasts into myotubes can be observed. With a BAG load into the PLA, myosin expression is decreased and osteopontin expression becomes visible (**Figure 12J**, **K**, **N**, **O**). This expression seems higher for the cells seeded on the composite containing 13-93B20 and myosin expression seems completely suppressed. Clearly, the osteopontin, marker of osteoblastic differentiation, is significantly expressed in cells cultured on the composites and this expression seems higher when using the borosilicate glass in PLA. However, the marker needed quantifying to confirm the effect of the boron included in the glass formulation compared to the silicate glass. C2C12 cells are often used to study osteodifferentiation in presence of BMPs [42,45]. Here, their capacity to differentiate into osteoblastic cells is exploited in the presence of BAG showing promising results for osteodifferentiation.

Mineralization was investigated using Alizarin Red Staining after 10 and 14 days of culture. This product stains the mineral calcium. As 10 days appeared to be too short a time to distinguish the mineralization, only images after 14 days of incubation are presented in **Figure 13**. **Figure 13** shows the glass, the PLA, and both composites post staining with Alizarin Red. On the glass control and the PLA without cells (**Figure 13A** and **B**), no red staining could be observed with the cells (**Figure 13E** and **F**), the staining seen is attributed to the high cell density, and therefore gives an indication of background noise. On both composites without cells, a slight red coloration is observed (**Figure 13C** and **D**). As shown in **Figure 7**, the dissolution of the composites leads to a small amount of HA precipitation. This may well occur within the culture medium and, therefore, the slight red coloration may be due to either, Alizarin being trapped at the glass/PLA interface of stained HA mineral. When the PLA/13-93 and the PLA/13-93B20 are seeded with the cells, strong red staining is evident, showing mineral formation (**Figure 13G** and **H**). These results, when compared to the results obtained without cells, suggest that the mineral stained by the Alizarin is not due to the precipitation of HA but

is produced by the cells through their metabolism in presence of the 13-93 or 13-93B20. Therefore, the cells are conditioned by the composites to synthesize their mineral matter.

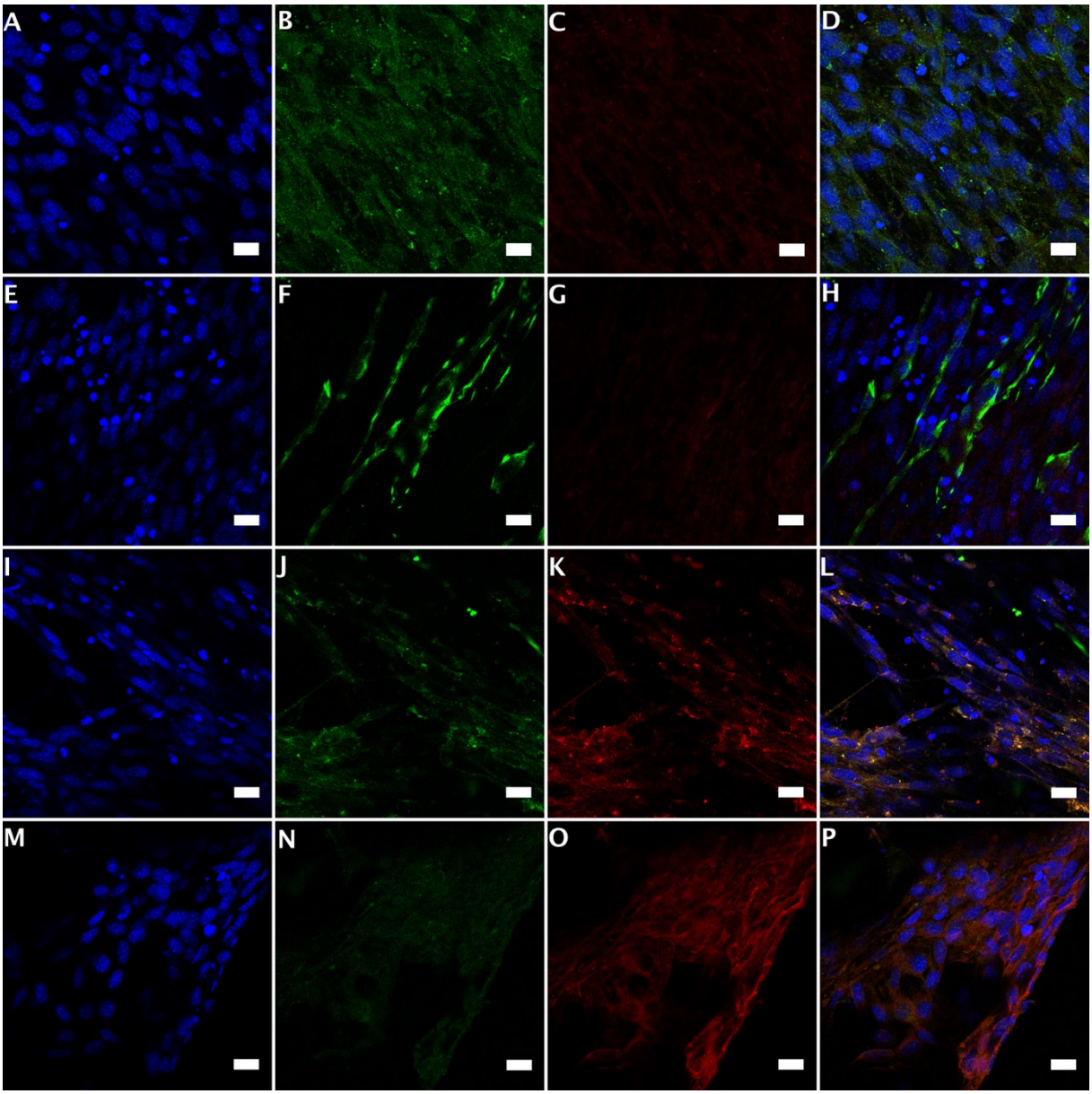

Figure 12: Differentiation of C2C12 cells on glass (**A, B, C, D**), PLA (**E, F, G, H**), PLA/13 - 93 (**I, J, K, L**) and PLA/13-93B20 (**M, N, O, P**) analyzed by Nuclei (DAPI – blue – First column), Myosin (green – Second column), Osteopontin (red – third column) and the merge (fourth column) immunostaining after 14 days of incubation. Scale bar 20µm

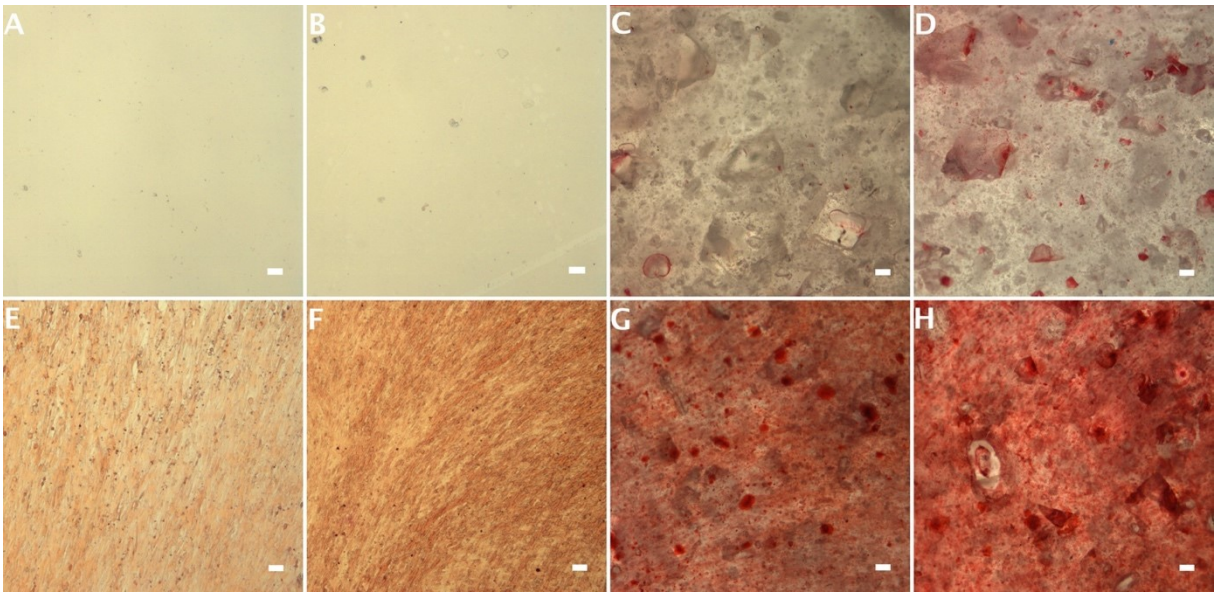

Figure 13: Mineralization of C2C12 cells in DMEM was studied with Alizarin red S staining after 14 days of incubation. The first line shows **A**) the glass, **B**) the PLA, **C**) the PLA/13-93 and **D**) the PLA/13-93B20 without any cells seeded. The second line represents **E**) the glass, **F**) the PLA, **G**) the PLA/13-93 and **H**) the PLA/13-93B20 with C2C12 cells seeded for 14 days. Scale bar 200µm

Conclusion

Composites made of PLA and bioactive glasses (silicate 13-93 and borosilicate 13-93B20) were processed by twin-screw extrusion. This process led to composites with content in the organic phase consistent across the length of the filaments and in agreement with the expected loading. The choice of the glass composition, particle size, glass loading, extrusion temperature as well as pressure for extrusion notably reduced the thermal degradation of the PLA, when compared to previous studies performed with similar or other processing techniques. The presence of BAG particles within the PLA matrix leads to a more ductile, but more fragile material as seen in the case of self-reinforced polymer/BAG composites.

The dissolution of the glass is not impaired by the polymeric matrix. As hypothesized, the substitution of part of the SiO_2 in the 13-93 glass composition with B_2O_3 leads to an increase in the initial dissolution rate. In turns, this leads to a higher level of hydroxyapatite precipitation. However, the dissolution of the BAG leads to an increased degradation rate of the PLA, not

affecting the mechanical properties which remained stable for at least 10 weeks. Finally, the dissolution of the composites in SBF support the hypothesis that the developed composites are bioactive, especially in the case of the composite containing the glass 13-93B20.

The osteogenic response of the C2C12 myoblastic cells to both composites – PLA/13-93 and PLA/13-93B20 – was studied. Cells were grown and spread on the composites and the expression of the myosin and the osteopontin measured after 14 days. When cells were cultured on pure PLA, myosin expression was clearly observed while on composites, only osteopontin was expressed. The mineralization experiment showed that the cells in presence of the 13-93 and the 13-93B20 were able to synthesize their mineral matrix.

These composites are promising for bone application. Nevertheless, we feel that more studies are needed to quantify and confirm the effect of the borosilicate at the cellular level.

Conflict of interest

There are no conflicts to declare.

Acknowledgement

The authors would like to acknowledge the Academy of Finland (Academy Research Fellow grant to JM), TTY-säätiö for IL financial support, the Institute for Advanced Studies (IAE) for enabling researcher mobility, Delphine Logeart-Avramouglou (Laboratory of Bioengineering and Biomechanics for Bone and Articulations, UMR 7052, CNRS, University Paris Diderot) for the kind gift of C2C12 cells and Annette Lane for proofreading this manuscript.

References

1. Schwach, G.; Vert, M. In Vitro and in Vivo Degradation of Lactic Acid-Based Interference Screws Used in Cruciate Ligament Reconstruction. *International Journal of Biological Macromolecules* **1999**, *25*, 283–291, doi:10.1016/S0141-8130(99)00043-4.
2. Claes, L.E.; Ignatius, A.A.; Rehm, K.E.; Scholz, C. New Bioresorbable Pin for the Reduction of Small Gony Fkagm.Ents: Design, Mechanical Properties and in Vitro Degradation. **1996**, *17*, 1621–1626, doi:10.1016/0142-9612(95)00327-4.
3. Suuronen, R. Comparison of Absorbable Self-Reinforced Poly-L-Lactide Screws and Metallic Screws in the Fixation of Mandibular Condyle Osteotomies: An Experimental Study in Sheep. *Journal of Oral and Maxillofacial Surgery* **1991**, *49*, 989–995, doi:10.1016/0278-2391(91)90065-T.
4. Santos Jr., A.R. Bioresorbable Polymers for Tissue Engineering. In *Tissue Engineering*; Eberli, D., Ed.; InTech, 2010 ISBN 978-953-307-079-7.
5. Pietrzak, W.S.; Sarver, D.; Verstynen, M. Bioresorbable Implants — Practical Considerations. *Bone* **1996**, *19*, S109–S119, doi:10.1016/S8756-3282(96)00139-1.
6. Walton, M.; Cotton, N.J. Long-Term *in Vivo* Degradation of Poly- L -Lactide (PLLA) in Bone. *Journal of Biomaterials Applications* **2007**, *21*, 395–411, doi:10.1177/0885328206065125.
7. Shimazaki, K.; Mooney, V. Comparative Study of Porous Hydroxyapatite and Tricalcium Phosphate as Bone Substitute. *Journal of Orthopaedic Research* **1985**, *3*, 301–310, doi:10.1002/jor.1100030306.
8. Ohura, K.; Bohner, M.; Hardouin, P.; Lemaître, J.; Pasquier, G.; Flautre, B. Resorption of, and Bone Formation from, New ?-Tricalcium Phosphate-Monocalcium Phosphate Cements: Anin Vivo Study. *Journal of Biomedical Materials Research* **1996**, *30*, 193–200, doi:10.1002/(SICI)1097-4636(199602)30:2<193::AID-JBM9>3.0.CO;2-M.
9. Hasegawa, S.; Ishii, S.; Tamura, J.; Furukawa, T.; Neo, M.; Matsusue, Y.; Shikinami, Y.; Okuno, M.; Nakamura, T. A 5–7 Year in Vivo Study of High-Strength Hydroxyapatite/Poly(l-Lactide) Composite Rods for the Internal Fixation of Bone Fractures. *Biomaterials* **2006**, *27*, 1327–1332, doi:10.1016/j.biomaterials.2005.09.003.
10. Verheyen, C.C.P.M.; de Wijn, J.R.; van Blitterswijk, C.A.; de Groot, K.; Rozing, P.M. Hydroxylapatite/Poly(L-Lactide) Composites: An Animal Study on Push-out Strengths and Interface Histology. *Journal of Biomedical Materials Research* **1993**, *27*, 433–444, doi:10.1002/jbm.820270404.
11. Ishikawa, K. Calcium Phosphate Cement. In *Advances in Calcium Phosphate Biomaterials*; Ben-Nissan, B., Ed.; Springer Berlin Heidelberg: Berlin, Heidelberg, 2014; pp. 199–227 ISBN 978-3-642-53980-0.
12. Hench, L.L. The Story of Bioglass®. *Journal of Materials Science: Materials in Medicine* **2006**, *17*, 967–978, doi:10.1007/s10856-006-0432-z.
13. Day, R.M.; Boccaccini, A.R.; Shurey, S.; Roether, J.A.; Forbes, A.; Hench, L.L.; Gabe, S.M. Assessment of Polyglycolic Acid Mesh and Bioactive Glass for Soft-Tissue Engineering Scaffolds. *Biomaterials* **2004**, *25*, 5857–5866, doi:10.1016/j.biomaterials.2004.01.043.
14. Li, H.; Chang, J. PH-Compensation Effect of Bioactive Inorganic Fillers on the Degradation of PLGA. *Composites Science and Technology* **2005**, *65*, 2226–2232, doi:10.1016/j.compscitech.2005.04.051.
15. Tainio, J.; Paakinaho, K.; Ahola, N.; Hannula, M.; Hyttinen, J.; Kellomäki, M.; Massera, J. In Vitro Degradation of Borosilicate Bioactive Glass and Poly(l-Lactide-Co-ε-Caprolactone) Composite Scaffolds. *Materials* **2017**, *10*, 1274, doi:10.3390/ma10111274.

16. Maquet, V.; Boccaccini, A.R.; Pravata, L.; Notingher, I.; Jérôme, R. Preparation, Characterization, and *in Vitro* Degradation of Bioresorbable and Bioactive Composites Based on Bioglass®-Filled Polylactide Foams: Porous Polylactide/Bioactive Glass Composites. *Journal of Biomedical Materials Research Part A* **2003**, *66A*, 335–346, doi:10.1002/jbm.a.10587.
17. Vergnol, G.; Ginsac, N.; Rivory, P.; Meille, S.; Chenal, J.-M.; Balvay, S.; Chevalier, J.; Hartmann, D.J. *In Vitro* and *in Vivo* Evaluation of a Polylactic Acid-Bioactive Glass Composite for Bone Fixation Devices: POLYLACTIC ACID-BIOACTIVE GLASS COMPOSITE FOR BONE FIXATION DEVICES. *Journal of Biomedical Materials Research Part B: Applied Biomaterials* **2016**, *104*, 180–191, doi:10.1002/jbm.b.33364.
18. Kometani, H.; Matsumura, T.; Suga, T.; Kanai, T. Quantitative Analysis for Polymer Degradation in the Extrusion Process. *International Polymer Processing* **2006**, *21*, 24–31, doi:10.3139/217.0092.
19. Niemelä, T.; Niiranen, H.; Kellomäki, M. Self-Reinforced Composites of Bioabsorbable Polymer and Bioactive Glass with Different Bioactive Glass Contents. Part II: In Vitro Degradation. *Acta Biomaterialia* **2008**, *4*, 156–164, doi:10.1016/j.actbio.2007.06.007.
20. Brink, M. The Influence of Alkali and Alkaline Earths on the Working Range for Bioactive Glasses. *Journal of Biomedical Materials Research* **1997**, *36*, 109–117, doi:10.1002/(SICI)1097-4636(199707)36:1<109::AID-JBM13>3.0.CO;2-D.
21. Brown, R.F.; Rahaman, M.N.; Dwilewicz, A.B.; Huang, W.; Day, D.E.; Li, Y.; Bal, B.S. Effect of Borate Glass Composition on Its Conversion to Hydroxyapatite and on the Proliferation of MC3T3-E1 Cells. *Journal of Biomedical Materials Research Part A* **2009**, *88A*, 392–400, doi:10.1002/jbm.a.31679.
22. Ojansivu, M.; Mishra, A.; Vanhatupa, S.; Juntunen, M.; Larionova, A.; Massera, J.; Miettinen, S. The Effect of S53P4-Based Borosilicate Glasses and Glass Dissolution Products on the Osteogenic Commitment of Human Adipose Stem Cells. *PLoS ONE* **2018**, *13*, e0202740, doi:10.1371/journal.pone.0202740.
23. Fu, Q.; Rahaman, M.N.; Bal, B.S.; Bonewald, L.F.; Kuroki, K.; Brown, R.F. Silicate, Borosilicate, and Borate Bioactive Glass Scaffolds with Controllable Degradation Rate for Bone Tissue Engineering Applications. II. In Vitro and in Vivo Biological Evaluation. *Journal of Biomedical Materials Research Part A* **2010**, *95A*, 172–179, doi:10.1002/jbm.a.32823.
24. Marquardt, L.M.; Day, D.; Sakiyama-Elbert, S.E.; Harkins, A.B. Effects of Borate-Based Bioactive Glass on Neuron Viability and Neurite Extension: Borate-Based Bioactive Glass. *J. Biomed. Mater. Res.* **2014**, *102*, 2767–2775, doi:10.1002/jbm.a.34944.
25. Maçon, A.L.B.; Kim, T.B.; Valliant, E.M.; Goetschius, K.; Brow, R.K.; Day, D.E.; Hoppe, A.; Boccaccini, A.R.; Kim, I.Y.; Ohtsuki, C.; et al. A Unified in Vitro Evaluation for Apatite-Forming Ability of Bioactive Glasses and Their Variants. *Journal of Materials Science: Materials in Medicine* **2015**, *26*, 115.
26. Niemela, T.; Niiranen, H.; Kellomaki, M.; Tormala, P. Self-Reinforced Composites of Bioabsorbable Polymer and Bioactive Glass with Different Bioactive Glass Contents. Part I: Initial Mechanical Properties and Bioactivity. *Acta Biomaterialia* **2005**, *1*, 235–242, doi:10.1016/j.actbio.2004.11.002.
27. Kokubo, T.; Kushitani, H.; Sakka, S.; Kitsugi, T.; Yamamuro, T. Solutions Able to Reproducein Vivo Surface-Structure Changes in Bioactive Glass-Ceramic A-W3. *Journal of Biomedical Materials Research* **1990**, *24*, 721–734, doi:10.1002/jbm.820240607.
28. Tirkkonen, L.; Halonen, H.; Hyttinen, J.; Kuokkanen, H.; Sievanen, H.; Koivisto, A.-M.; Mannerstrom, B.; Sandor, G.K.B.; Suuronen, R.; Miettinen, S.; et al. The Effects of Vibration Loading on Adipose Stem Cell Number, Viability and Differentiation towards

Bone-Forming Cells. *Journal of The Royal Society Interface* **2011**, *8*, 1736–1747, doi:10.1098/rsif.2011.0211.
29. Wu, X.; Youngman, R.E.; Dieckmann, R. Sodium Tracer Diffusion and 11B NMR Study of Glasses of the Type (Na2O)0.17(B2O3)x(SiO2)0.83−x. *Journal of Non-Crystalline Solids* **2013**, *378*, 168–176, doi:10.1016/j.jnoncrysol.2013.06.012.
30. Du, L.-S.; Stebbins, J.F. Nature of Silicon−Boron Mixing in Sodium Borosilicate Glasses: A High-Resolution ^{11} B and ^{17} O NMR Study. *The Journal of Physical Chemistry B* **2003**, *107*, 10063–10076, doi:10.1021/jp034048l.
31. Du, L.-S.; Stebbins, J.F. Solid-State NMR Study of Metastable Immiscibility in Alkali Borosilicate Glasses. *Journal of Non-Crystalline Solids* **2003**, *315*, 239–255, doi:10.1016/S0022-3093(02)01604-6.
32. Sun, Y.; Zhang, Z. Structural Roles of Boron and Silicon in the CaO-SiO2-B2O3 Glasses Using FTIR, Raman, and NMR Spectroscopy. *Metallurgical and Materials Transactions B* **2015**, *46*, 1549–1554, doi:10.1007/s11663-015-0374-2.
33. Lai, Y.; Zeng, Y.; Tang, X.; Zhang, H.; Han, J.; Su, H. Structural Investigation of Calcium Borosilicate Glasses with Varying Si/Ca Ratios by Infrared and Raman Spectroscopy. *RSC Advances* **2016**, *6*, 93722–93728, doi:10.1039/C6RA20969F.
34. Yu, Y.; Stevensson, B.; Edén, M. Medium-Range Structural Organization of Phosphorus-Bearing Borosilicate Glasses Revealed by Advanced Solid-State NMR Experiments and MD Simulations: Consequences of B/Si Substitutions. *The Journal of Physical Chemistry B* **2017**, *121*, 9737–9752, doi:10.1021/acs.jpcb.7b06654.
35. Huang, W.; Day, D.E.; Kittiratanapiboon, K.; Rahaman, M.N. Kinetics and Mechanisms of the Conversion of Silicate (45S5), Borate, and Borosilicate Glasses to Hydroxyapatite in Dilute Phosphate Solutions. *Journal of Materials Science: Materials in Medicine* **2006**, *17*, 583–596, doi:10.1007/s10856-006-9220-z.
36. Yao, A.; Wang, D.; Huang, W.; Fu, Q.; Rahaman, M.N.; Day, D.E. In Vitro Bioactive Characteristics of Borate-Based Glasses with Controllable Degradation Behavior. *Journal of the American Ceramic Society* **2007**, *90*, 303–306, doi:10.1111/j.1551-2916.2006.01358.x.
37. Liu, X.; Huang, W.; Fu, H.; Yao, A.; Wang, D.; Pan, H.; Lu, W.W.; Jiang, X.; Zhang, X. Bioactive Borosilicate Glass Scaffolds: In Vitro Degradation and Bioactivity Behaviors. *Journal of Materials Science: Materials in Medicine* **2009**, *20*, 1237–1243, doi:10.1007/s10856-009-3691-7.
38. Lepry, W.C.; Nazhat, S.N. Highly Bioactive Sol-Gel-Derived Borate Glasses. *Chemistry of Materials* **2015**, *27*, 4821–4831, doi:10.1021/acs.chemmater.5b01697.
39. de Jong, S.J.; Arias, E.R.; Rijkers, D.T.S.; van Nostrum, C.F.; Kettenes-van den Bosch, J.J.; Hennink, W.E. New Insights into the Hydrolytic Degradation of Poly(Lactic Acid): Participation of the Alcohol Terminus. *Polymer* **2001**, *42*, 2795–2802, doi:10.1016/S0032-3861(00)00646-7.
40. Stanislavov, A.S.; Sukhodub, L.F.; Sukhodub, L.B.; Kuznetsov, V.N.; Bychkov, K.L.; Kravchenko, M.I. Structural Features of Hydroxyapatite and Carbonated Apatite Formed under the Influence of Ultrasound and Microwave Radiation and Their Effect on the Bioactivity of the Nanomaterials. *Ultrasonics Sonochemistry* **2018**, *42*, 84–96, doi:10.1016/j.ultsonch.2017.11.011.
41. Baddiel, C.B.; Berry, E.E. Spectra Structure Correlations in Hydroxy and Fluorapatite. *Spectrochimica Acta* **1966**, *22*, 1407–1416, doi:10.1016/0371-1951(66)80133-9.
42. Gand, A.; Hindié, M.; Chacon, D.; van Tassel, P.R.; Pauthe, E. Nanotemplated Polyelectrolyte Films as Porous Biomolecular Delivery Systems: Application to the Growth Factor BMP-2. *Biomatter* **2014**, *4*, e28823, doi:10.4161/biom.28823.

43. Eqtesadi, S.; Motealleh, A.; Pajares, A.; Miranda, P. Effect of Milling Media on Processing and Performance of 13-93 Bioactive Glass Scaffolds Fabricated by Robocasting. *Ceramics International* **2015**, *41*, 1379–1389, doi:10.1016/j.ceramint.2014.09.071.
44. Ojansivu, M.; Mishra, A.; Vanhatupa, A.; Juntunen, M.; Larionova, A.; Massera, J.; Miettinen, S. The Effect of S53P4-Based Borosilicate Glasses and Glass Dissolution Products on the Osteogenic Commitment of Human Adipose Stem Cells. *PlosOne* 2018.
45. Saito, M.; Karakida, T.; Yamamoto, R.; Nagano, T.; Yamakoshi, Y.; Hayakawa, T.; Oida, S.; Gomi, K. Differentiation Potential of Osteoblast from Cultured C2C12 Cells on Zirconia Disk. *Dental Materials Journal* **2014**, *33*, 275–283, doi:10.4012/dmj.2013-321.

Supplementary data

Figure S1 presents the TGA thermogram of the samples of investigation. As expected, PLA starts decomposing at ~300°C. The decomposition of the PLA ends at ~388°C with a residual mass of ~0.7%. With further heating the mass continues to decrease to reach ~0% at ~670°C.

PLA/BAG composites follow the same pattern with PLA decomposition at ~284 and ~280°C for the PLA/13-93B20 and PLA/13-93 respectively. The slight shift toward lower temperature of the PLA thermal degradation in the composite can be assigned to the lower Mw as seen in **Table 2**. The large mass drop, seen upon heating, ends at ~352°C. The final residual mass is reached and varies with temperature and across samples between 31 and 40%. The average residual mass and standard deviation were measured to be 38±2% and 35±2%, for the PLA/13-93 and PLA/13-93B20, respectively.

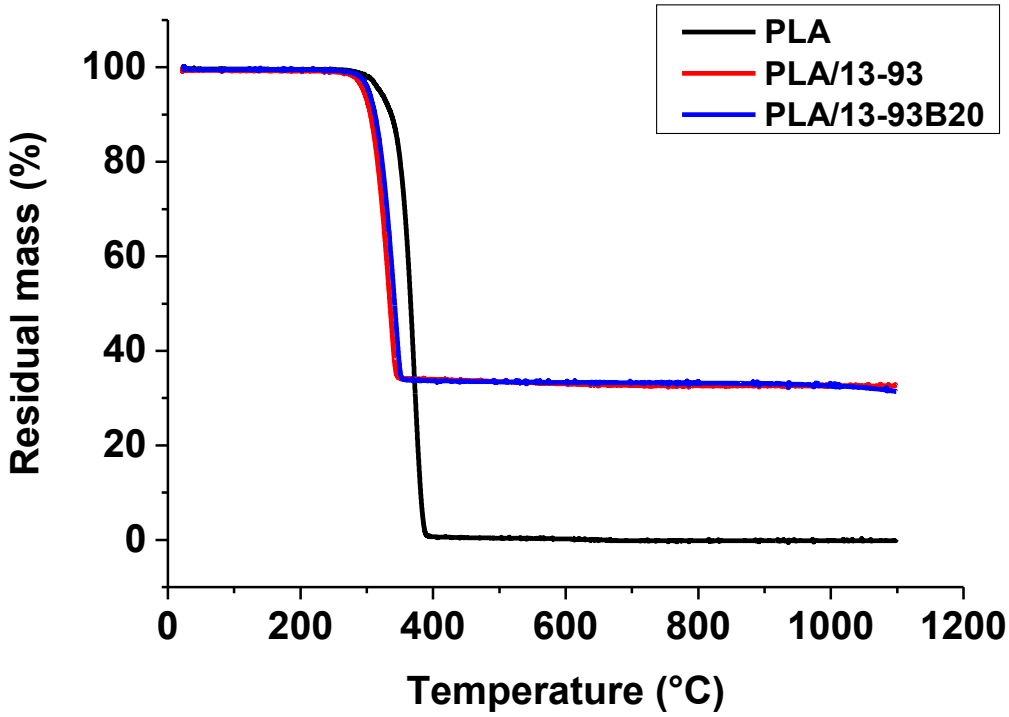

Figure S1: TGA thermogram of the PLA, PLA/13-93 and PLA/13-93B20 obtained at 10°C/min, under N_2 flow, up to 1100°C

From Composites to Hybrid materials

Composites made of PLA and silicate or borosilicate glass have been studied. Their dissolution, bioactivity, and osteogenic properties were tailored with the boron-doped BAG.

These composites made of an inorganic phase which is dispersed in the organic within micrometer scale interactions show interesting glass dissolution behavior and exhibit promising potential for bone application.

This strategy allows to combine the properties of each matrix in the final material. But some drawbacks remain. Indeed, if the organic and inorganic phases have different dissolution rates, this can result in different resorption rates in the material during dissolution. It would inevitably lead to material instability [20]. At the end, it may be difficult to perfectly i) control properties such as the degradation of the material, the surface chemistry due to different resorption rate of the components, and ii) to maintain the bioactivity of the particles while the bioactive component is covered by the polymer. Thereby, a high percentage of the particles do not come into contact with the host bone cells [163]. Moreover, their manufacturing necessitates thermal processes requiring high temperatures which can lead to a partial degradation of the material but also prevent any enrichment of osteogenic biomolecules. In addition, depending on the organic matrix properties, composites usually have mechanical properties that are too high thus limiting the applications in which they could be used.

To remedy these disadvantages, working with materials made of organic and inorganic compounds linked covalently would be an alternative. Indeed, bone is composed of hydroxyapatite organized in the organic matrix. It has been shown that the organic and inorganic phases of the bone interact at the molecular level, and this can have an influence on the properties of the bone. For example, the interactions between anionic groups of the extracellular matrix proteins and the calcium ions from the inorganic matrix gives the bone its high toughness [164]. Thus, to improve the interaction between the organic and inorganic

phases and to stay as close as possible to bone composition, working on hybrid materials appeared obvious to us.

Hybrids are materials where the organic and inorganic phases interact chemically on a nanoscale. That allows a better control of material parameters such as degradation rates or mechanical properties [156]. They are commonly formed by a sol-gel method, in which the constituent phases interact at a molecular level. Contrary to the composites, hybrid materials are made through soft chemistry, which is not offensive to the organic and inorganic components and allow to maintain their integrity. Working with hybrids will allow to obtain materials which can be adaptable and custom-made. Indeed, the inorganic and organic content can vary in order to design the scaffold with specific properties. Also, the amount of covalent coupling can be adapted to the properties needed by the hybrids. All these parameters will allow us to obtain hybrids tailored according to the requirements of the targeted applications. Another positive point of these scaffold is the mode of administration which could be by injectability, avoiding too invasive surgery.

By following this strategy and inspired from other studies, a **new family of materials, hybrids based on gelatin and bioactive glass particles** were proposed [20,156,160,161,163,165]. Biocompatible and biodegradable, the gelatin in this material allowed to mimic the organic matrix of the bone. However, gelatin is not self-supported at biological temperature. Thus, it was necessary to covalently link this organic phase to the BAG particles in order to control the properties of the materials such as, but not limited to, their dissolution. For that, the GPTMS was used as a bridging agent between the gelatin and the BAG [158,163,166,167]. This molecule contains a reactive epoxy-ring, which can undergo an acid catalyzed nucleophilic attack to link itself to the gelatin. Its three methoxy silane groups, which can hydrolyze to obtain Si–OH groups, can form a network through condensation reactions with

the silica-rich layer of the BAG during its dissolution. Thereby, the final scaffold obtained will be made of gelatin covalently linked to the BAG particles.

Hybrid materials were designed, fabricated, and studied with the 13-93 BAG particles and the doped boron-formulation (the 13-93B20) in order to compare their dissolution rate and to verify that the BAG keep its properties in this innovative system.

Chapter 3: Hybrids strategy

Article 2: New generation of hybrid materials based on gelatin and bioactive glass particles for bone tissue regeneration

Amel Houaoui[1], Agata Szczodra[2], Mari Lalluka[2], Lamia El-Guermah[1], Remy Agniel[1], Emmanuel Pauthe[1], Jonathan Massera[2] and Michel Boissiere[1,*]

1. Biomaterials for Health Research Group, ERRMECe, Equipe de recherche sur les Relations Matrice Extracellulaire-Cellules (EA1391), Institut des matériaux I-MAT (FD4122), CY Tech, CY Cergy Paris Université, Maison Internationale de la Recherche (MIR), rue Descartes, 95001 Neuville sur Oise cedex, France

2. Tampere University, Faculty of Medicine and Health Technology, Laboratory of Biomaterials and Tissue Engineering, Korkeakoulunkatu 3, 33720, Tampere, Finland

*Corresponding author: Dr Michel Boissière

Dr Michel Boissière, Biomaterials for Health Research Group, ERRMECe, Equipe de recherche sur les Relations Matrice Extracellulaire-Cellules (EA1391), Institut des matériaux I-MAT (FD4122), CY Tech, CY Cergy Paris Université, Maison Internationale de la Recherche (MIR), rue Descartes, 95001 Neuville sur Oise cedex, France

Phone number: +33 (0)1.34.25.75.61, Email: michel.boissiere@cyu.fr

Keywords: Hybrid scaffold; Bioactive Glass; Gelatin; GPTMS; Bone tissue engineering

This work has been published in the journal: **Biomolecules, Special Issue Bioactive Glasses Applications, Volume 11, March 2021**

Graphical abstract

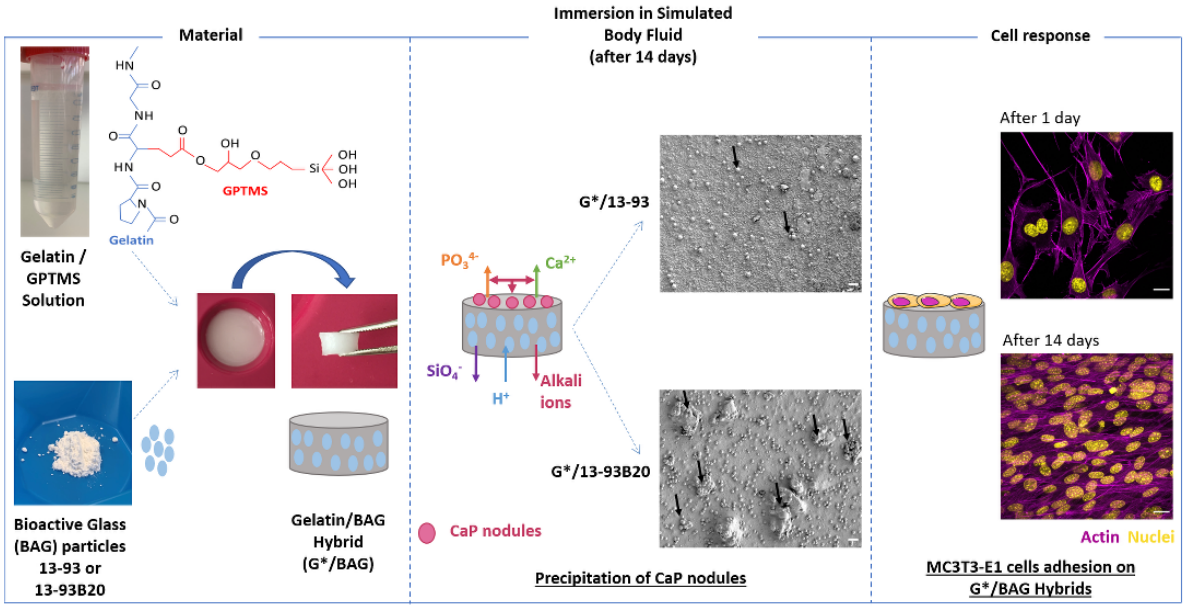

Abstract

Hybrid scaffolds based on bioactive glass (BAG) particles (<38 µm), covalently linked to gelatin (G*) using 3-glycidoxypropyltrimethoxysilane (GPTMS), have been studied for bone bioengineering. In this study, two glass compositions (13-93 and 13-93B20 (where 20% of the SiO_2 was replaced with B_2O_3)) were introduced in the gelatin matrix. The C_{factor} (gelatin/GPTMS molar ratio) was kept constant at 500. The hybrids obtained were found to be stable at 37 °C in solution, the condition in which pure gelatin is liquid. All hybrids were characterized by *in vitro* dissolution in Tris(hydroxymethyl)aminomethane (TRIS) solution (for up to 4 weeks) and Simulated Body Fluid (SBF) (for up to 2 weeks). Samples processed with 13-93B20 exhibited faster initial dissolution and significantly faster precipitation of a hydroxyapatite (HA) layer. The faster ion release and HA precipitation recorded from the G*/13-93B20 samples are attributable to the higher reactivity of borosilicate compared to silicate glass. The MC3T3-E1 cell behavior in direct contact with the hybrids was investigated, showing that the cells were able to proliferate and spread on the developed biomaterials. Tailoring the glass composition allows us to better control the material's dissolution, biodegradability, and bioactivity. Bioactive (especially with 13-93B20 BAG) and biocompatible, the hybrids are promising for bone application.

Introduction

Bone fractures are a common trauma. For a large loss of bone substance (defect greater than 1 cm^3) following a traumatic situation as a pathology or accidental defect, the natural process of self-repair is compromised [1]. Tissue engineering is an innovative approach used for bone repair. Bone reconstruction is assisted with materials that participate in tissue regeneration [2,3]. These materials must have properties adapted to this function.

Bioactive ceramics are of interest in bone regeneration. The bioactivity of these materials results in the appearance of biological activity in the host organism and the existence of ion exchanges between the material and living tissue [4]. Synthetic hydroxyapatite (HA) and β-tricalcium phosphate (β-TCP) are more widely used [5–7]. They often have osteoconductive and sometimes osteoinductive properties. However, their slow resorption limits their clinical relevance [8,9]. Indeed, the limited resorption of those ceramics was demonstrated in-vivo when used in cements [10].

Bioactive Glass (BAG) is a subcategory of ceramics and are not only osteoconductive but also osteoinductive [11]. These glasses are mainly used for hard tissue reconstruction, but they are also able to bond to soft tissue [12]. However, due to their brittleness, shaping the glass into its final shape remains a challenge. Organic/inorganic composite scaffolds represent a convenient alternative to traditional BAGs. They allow for the possibility to tailor the mechanical properties, degradation kinetics, and bioactivity. Current research is focused on the fabrication of bioactive composite materials, with the bioactive phase incorporated as a filler into the bioresorbable polymer matrix [13]. However, a drawback with many conventional composites is that the constituent phases interact on a micrometer scale, which can result in differential resorption rates during dissolution and masking of the bioactive component. This would inevitably lead to material instability *in vivo* [14].

Hybrid scaffolds are materials where the organic and inorganic phases interact chemically on a nanoscale, allowing us to control the properties of the final material, for instance, degradation rates and mechanical properties [14–16]. Moreover, the inorganic and organic contents in addition to the degree of covalent links can be adjusted for precise control of the hybrid properties as stiffness and dissolution rates, leading to material adapted for a specific application [14]. For hybrid formation, covalent links between organic and inorganic matrixes are fundamental. They can be obtained through reaction with organosilanes such as 3-glycidoxypropyltrimethoxysilane (GPTMS) or 3-aminopropyltriethoxysilane (APTES) [17–20].

In our work, we present hybrid materials for bone tissue engineering based on gelatin and BAG (**Figure 1**), where two BAGs, with different compositions (13-93 and 13-93B20), are compared. 13-93 is a Food and Drug Administration (FDA)-approved BAG that exhibits a slower dissolution rate than commercialized BAGs 45S5 or S53P4 [21,22]. The rational for studying 13-93 BAG lies in preventing excessive dissolution of the glass particles during processing, degradation of the organic phase, a decrease in the mechanical properties, and a fast release of ions that could be toxic for the cells. 13-93B20, a similar composition to 13-93 but with 20% of the SiO_2 substituted with B_2O_3, was also included in the study. It has been showed that the borosilicate glasses based on the 13-93 composition have faster *in vitro* dissolution but also faster conversion to HA while maintaining a slower dissolution kinetics than 45S5 and S53P4 [13,23,24].

Here, two hybrid materials were studied, based on gelatin and 13-93 or 13-93B20. The content of the organic and inorganic matrixes was 70/30 (wt%), and a C_{factor} (degree of covalent coupling, molar ratio of GPTMS/gelatin) of 500 was used. To investigate their in-vitro dissolution, the hybrids were immersed in Tris(hydroxymethyl)aminomethane (TRIS) buffer

solution for one month. Ion release from the glass was quantified, and the mineral content was measured.

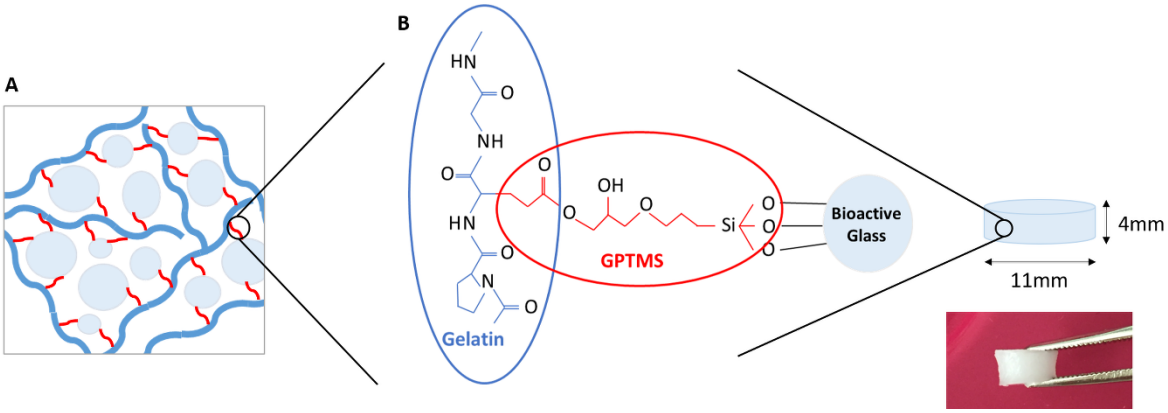

Figure 1: **A**) Schematic representation (inspired from Mahony et Al. [18]) and **B**) chemical structure of the hybrid made of gelatin and BAG covalently linked by the GPTMS.

The compressive properties of the hybrids were studied during the immersion. The bioactivity, assumed to be related to the precipitation of a HA layer at the materials' surface when immersed in aqueous solution, was assessed in Simulated Body Fluid (SBF) [25]. Preliminary cell experiments were performed to assess cell activity by culturing MC3T3-E1 pre-osteoblastic cells at the surface of the hybrids. Cell proliferation and morphology were studied. The aim of this study was to assess the stability of the hybrids, *in vitro*, in aqueous solutions and its biocompatibility.

Materials and Methods

1. Materials preparation and characterization

1.1. Bioactive glass processing

BAGs 13-93 and 13-93B20 were prepared from analytical grade K_2CO_3 (Alfa Aesar, Ward Hill, MA, USA), (Na_2CO_3, $NH_4H_2PO_4$, ($CaHPO_4$)(2(H_2O)), $CaCO_3$, MgO, H_3BO_3 (Sigma Aldrich, St Louis, MO, USA), and Belgian quartz sand. The 100-gram batches of 13-93 and 13-93B20 were melted for 3 hours at 1450 °C in a platinum crucible. The molten

glasses were cast, annealed, crushed, and finally sieved into less than 38 µm particles. The glasses were dried at 200 °C for 2 h prior to be used. The nominal oxide compositions of the glasses are given in **Table 1**.

Table 1: Nominal glass composition (%)

Glass	mol%						
	Na_2O	K_2O	MgO	CaO	P_2O_5	SiO_2	B_2O_3
13-93	6.0	7.9	7.7	22.1	1.7	54.6	-
13-93B20	6.0	7.9	7.7	22.1	1.7	43.7	10.9

1.2. Hybrids synthesis

Gelatin (Porcine, Type A, Bloom 300, Sigma Aldrich, St Louis, MO, USA) was dissolved at 37 °C in 10 mM hydrochloric acid (HCl, Merck Millipore, Burlington, MA, USA) at a concentration of 50 $mg \cdot mL^{-1}$. This solution was functionalized by adding GPTMS (Sigma Aldrich, St Louis, MO, USA) to obtain a C_{factor} (molar ratio of GPTMS/gelatin) of 500. Different C_{factor} have been studied (data not shown), and this parameter was optimized in order to limit the cellular toxicity of GPTMS. The functionalized gelatin (G*) solution was mixed 2 h at 37 °C. The 13-93 or 13-93B20 BAG particles were added and mixed for 1 h at 37 °C for a ratio of G*/BAG of 70/30 wt%. This ratio was optimized (data not shown) to obtain enough covalent links in the structure to obtain a gel self-supported at biological temperature. Finally, sodium fluoride 1% (NaF, Sigma Aldrich, St Louis, MO, USA) was added to catalyze the inorganic condensation reaction. The final solution was mixed for 10 min at 37 °C. The solution was poured in silicon molds and left to gel at room temperature for 24 h.

Hybrid materials with a diameter of 11 mm and height of 4 mm were cut. To measure their glass content, they were freeze-dried and heated for 2 h at 500 °C under air to remove all the

organic phase. The remaining mineral phase was weighed. The measure was repeated on 4 samples per composition, and the average glass content with standard deviation was calculated.

2. Behavior of G*/BAG hybrids

2.1 Physico-chemical properties of the hybrids

- Immersion in TRIS

Tris(hydroxymethyl)aminomethane (TRIS) solution (50 mM) was prepared by mixing ultrapure TRIS (Sigma Aldrich, St Louis, MO, USA) and TRIS-HCl (Sigma Aldrich, St Louis, MO, USA) in ultrapure water, and the pH was adjusted to 7.4 at 37 °C. The samples were punched to obtain small cylinders of 11 mm diameter and 4 mm height (≈380 mg), which were immersed in 30 mL of TRIS solution for up to 28 days at 37 °C on an agitator (Heidolph Instruments, Schwabach, Germany) with an orbital speed of 100 rpm. To avoid saturation of the solution with the ions released from the hybrids, the TRIS buffer was refreshed each week.

At the desired time of immersion, the concentration of elements released from the hybrids was studied by diluting 500 µL of the immersion solution in 4.5 mL of ultrapure water for ion analysis. Inductively Coupled Plasma - Optical Emission Spectroscopy (ICP-OES) (Agilent technologies 5110, Santa Clara, CA, USA) was employed to quantify P (λ = 253.561 nm), Ca (λ = 422.673 nm), Mg (λ = 279.553 nm), Si (λ = 250.690 nm), B (λ = 249.678 nm), K (λ = 766.491 nm), and Na (λ = 589.592 nm) concentrations in the solution after samples immersion. The measurements were conducted in four separate samples at each time points for each composition, and the results are presented as mean ± standard deviation (SD).

- Mineral content in hybrids

Mineral mass after the samples' synthesis and at various immersion times was measured after freeze-drying and burning the samples 2h at 500°C, under air, to remove all the organic phase. The remaining mineral phase was weighed. The measurements were conducted on four

separate samples at each time points for each composition and the results are presented as mean ± SD.

- Mechanical properties of the hybrids

The mechanical properties of the hybrids after synthesis and after immersion (wet) were tested by compression test at room temperature using a texturometer (LS1, Lloyd Instruments, Ametek, Berwyn, PA, USA). The measurements were conducted on four separate samples at each time point for each composition. A 20 N load cell was used for testing, with a compression extension speed of 1 $mm.min^{-1}$. The results are presented as mean ± SD.

2.2 Hybrids bioactivity

- Immersion in Simulated Body Fluid (SBF)

Developed by Kokubo et al., SBF was prepared following the methodology from the standard ISO/FDIS 23317 [27]. The samples were punched to obtain small cylinders of 11 mm diameter and 4 mm height (≃380 mg), which were immersed in 30 mL of SBF for up to 2 weeks at 37 °C on an agitator (Heidolph Instruments, Schwabach, Germany) with an orbital speed of 100 rpm. During the experiment, the solution was not refreshed to study the precipitation of calcium phosphate. The ion concentration in the solution according to immersion time was measured as previously described. The measurements were conducted in four separate samples at each time points for each composition, and the results are presented as mean ± SD.

- Mineral content in hybrids

Mineral mass after various immersion times was measured as explained above. Measurements were conducted on four separate samples at each time points for each composition and the results are presented as mean ± SD.

- Hybrids surface analysis

The reactive layer on the hybrid surface after immersion in SBF was observed by SEM (GEMINISEM 300 from Zeiss, Iena, Germany), and its composition was analyzed by Energy-Dispersive X-ray spectroscopy (EDX Quantax from Bruker, Billerica, MA, USA). The Infrared (IR) absorption spectra of the hybrids immersed in SBF were also recorded using a Bruker Alpha FTIR in Attenuated Total Reflectance (ATR) mode. The measurements were performed on dry samples. All IR spectra were recorded within the range 399–4000 cm^{-1} with a resolution of 2 cm^{-1} and 32 accumulation scans.

2.3 Cell analysis

- Hybrids preparation

G*/13-93 and G*/13-93B20 hybrids were synthesized in sterile conditions. The samples were cut to obtain small cylinders of 11mm of diameter and 4mm of height. Each material of each condition was immersed in sterile TRIS solution during 10 days at 37°C to remove excess components. After that, all cell experiments were performed in 48-well plates.

- Cell culture

Pre-osteoblastic MC3T3-E1 cells subclone four (ATCC, Manassas, VA, USA) were cultured in α-Minimum Essential Media (α-MEM) (Gibco, Life Technologies, Carlsbad, CA, USA) containing glutamine supplemented with 10% Fetal Bovine Serum (FBS, Biosera, Marikina, Philippines) and 1% penicillin/streptomycin (Gibco, Life Technologies, Carlsbad, CA, USA). The cells were cultured with a humidified atmosphere of 5% CO_2 at 37 °C.

- Cell proliferation

To compare the behavior of MC3T3-E1 cells on the different samples, cell proliferation was studied using a CyQUANT Cell Proliferation Assay kit (Invitrogen, Life Technologies, Carlsbad, CA, USA). The control used was the Tissue Culture Polystyrene (TCPS) 48 well-plate. The hybrids were placed in the wells, and 5000 cells/well were seeded. The medium was

changed every 2 days. After 1, 3, 7, 10, and 14 days of culture, the cells were lysed with 700 µL 0.1% Triton-X100 (Fisher Scientific, Hampton, NH, USA) buffer and conserved at −80 °C. After one freeze–thaw cycle, three 20 µl aliquots of each lysate were pipetted to a black 96-well plate (Corning, Corning, NY, USA) and mixed with 180 µl working solution containing CyQUANT GR dye and cell lysis buffer. The fluorescence at 520 nm was measured with a Spectrofluorometer Xenius XM (Safas, Monaco).

- Cell morphology

The morphology of the cells on the different samples was observed after 1, 7, and 14 days of culture. The control used was TCPS coverslips (Nunc Thermanox Coverslips, ThermoFisher Scientific, Waltham, MA, USA) of 13 mm diameter in a 24-well plate. The number of cells was adjusted according to the well area. The same density of cells was seeded on the hybrids and the TCPS coverslips controls, and after each time point, the cells were fixed with 4% (w/v) paraformaldehyde solution for 15 min and then permeabilized with 0.1% (v/v) Triton X-100 (Sigma Aldrich, St Louis, MO, USA) for 10 min. Nonspecific binding sites were blocked by incubating the disks in Phosphate Buffered Saline (PBS) containing 1% Bovine Serum Albumin (BSA, Sigma Aldrich, St Louis, MO, USA) for 1 h. The cytoskeleton and nuclei of the cells were stained, respectively, with 1:500 diluted TRITC-labelled phalloidin (Sigma Aldrich, St Louis, MO, USA P1951) and 1:1000 diluted 4',6-Diamidino-2-phenylindole dihydrochloride (DAPI, Sigma Aldrich, St Louis, MO, USA D9542) in PBS–BSA 0.5% for 1 h. Each incubation with antibodies was performed in wet and dark conditions. The samples were then washed in PBS–BSA 0.5% and pure water and observed using a LSM710 confocal microscope (Zeiss, Iena, Germany).

- Statistical analysis

Data are analyzed using GraphPad Prism Software. Statistical significance between groups is assessed by one-way analysis of variance (ANOVA). Experimental results are expressed as means ± standard deviation. Statistical significance is taken for values of $p < 0.01$.

Results and discussion

The aim of this study is to develop hybrid materials based on gelatin and BAG able to release therapeutic ions for bone regeneration while controlling the dissolution properties of the organic and inorganic phases of the scaffold. The first step was to determine the optimal C_{factor} for targeted applications. Indeed, the higher the C_{factor}, the more covalent links will be formed in the structure. However, an excess of GPTMS can lead to excessive unreacted precursor, leading to cellular toxicity [14,26]. Thus, to avoid this negative effect, studies have led us to use a C_{factor} of 500 for our hybrids (data not shown). Therefore, the BAGs 13-93 and 13-93B20 were covalently linked to gelatin with a C_{factor} of 500. The materials dissolution in aqueous solutions and their bioactivity were compared.

1. Characterization of the hybrids after synthesis

Table 2 presents the glass loading in the hybrids and their young modulus after synthesis. The mineral mass in the hybrids was determined after freeze-drying and burning the inorganic phase at 500 °C under air for 2 h. **Table 2** shows that the glass loading is 34 ± 2 wt% and 33 ± 1 wt% for G*/13-93 and G*/13-93B20, respectively, as expected from the targeted loading.

Table 2: Measured glass loading and Young's modulus of the gelatin alone functionalized (G*) and the G*/13-93 and G*/13-93B20 hybrids (for wet samples, the mechanical properties were measured after 10 min of immersion in TRIS).

Materials	Glass loading in the hybrids (wt%)	Young modulus (MPa)	
		Dry samples	Wet samples
G* alone	--	2.1 ± 0.3	0.8 ± 0.2
G*/13-93	34 ± 2	0.5 ± 0.3	0.5 ± 0.1
G*/13-93B20	33 ± 1	0.7 ± 0.2	0.6 ± 0.2

Young's modulus of G* alone and the hybrids were measured by a compression test. Both hybrids have Young's moduli stable in wet and dry conditions. Young's modulus of the hybrids is lower compared to that for G* alone. This shows that adding the glass in the organic phase influences the mechanical behavior of the scaffolds. This decrease occurs with both BAGs, showing that this is not due to the type of glass. It is interesting to note that, in the case of composite materials, the addition of mineral particles reinforces the mechanical properties [8,9]. However, for our hybrid materials, a decrease in Young's modulus is observed probably because the glass induces defects on the gel structure and adds some heterogeneity. This heterogeneity in turn leads to weak points in the material, which become more friable.

2. Behavior of the hybrids in solution

Resorbable materials needs to present controlled degradation and sufficient mechanical properties until the bone tissue regeneration [27]. Their bioactivity is a fundamental property that will help bone repair. To assess these properties the hybrids were immersed in aqueous solutions and their dissolution was studied.

2.1 Dissolution in TRIS

The hybrids degradation in TRIS was studied by mass measurements, ICP-OES analysis, and compression tests. These tests could not be done on G* without BAG because it was dissolving at 37 °C, contrary to G*/13-93 or 13-93B20. This shows that the materials made of gelatin and BAG, covalently linked by the GPTMS, can be considered as hybrids. Moreover, Mahony et al. worked on hybrids based on gelatin and silica network coming from Tetraethyl orthosilicate (TEOS) hydrolysis and condensation and showed that GPTMS is efficient in creating covalent links between both matrices [14]. **Figure 2** presents the mass loss of the hybrids as a function of the immersion time (**Figure 2A**), the hybrid mass after freeze-drying (**Figure 2B**), and the mineral mass remaining in the materials after immersion (**Figure 2C**).

Figure 2: Mass loss (**A**), dry mass (**B**) and mineral mass (**C**) remained in the hybrid G*/13-93 (●) and G*/13-93B20 (■) as a function of immersion time in TRIS

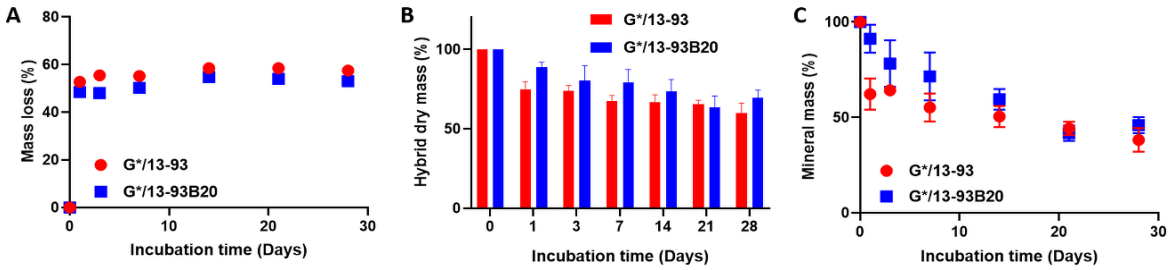

Mass loss graph (**Figure 2A**) shows that, after 24 h, the mass loss reaches 50% and remained stable at longer immersion times. The same results are observed for G*/13-93 and G*/13-93B20, showing that this mass loss is not dependent on the type of glass. In **Figure 2B**, a decrease in the hybrid dry mass is observable. At 24 h, the hybrid dry mass goes from 100% to 75% and 89% for G*/13-93 and G*/13-93B20, respectively, and does not reach 50% during the immersion. This result does not corroborate the mass loss at 24 h in **Figure 2A**. This means that, during the first 24 h, the hybrids lose mostly water. This can be seen from a macroscopic point of view on the hybrids that shrink and lose 2 mm of diameter and 1 mm of height after

24h of immersion, indicating a rearrangement of the hybrids structure, due to a syneresis phenomenon.

In **Figure 2B**, the hybrid dry mass decreases with immersion time, exhibiting a dissolution of the material. In **Figure 2C**, the mineral mass decreases with immersion time. This result shows that 13-93 and 13-93B20 dissolve in TRIS solution during immersion. This is further confirmed by the quantification of ion release in solution (**Figure 3**).

For both hybrids, all ions from the BAG are found to leach out into the solution, showing that the glasses dissolve through the gelatin. The Si release from G*/13-93B20 continuously increases and is slightly lower than that for G*/13-93. Moreover, the initial release of Mg, Na, K, and Ca elements is faster for G*/13-93B20 than for G*/13-93. This can be due to the fact that the borosilicate glass is more reactive with siloxane than G*/13-93, leading to a lower Si release from the hybrids with 13-93B20 than the one with 13-93. The release of the elements coming from G*/13-93B20 directly reaches the plateau from the beginning of the immersion, while it increases for G*/13-93 until it reaches the same plateau (**Figure 3** and **4**). For G*/13-93 (**Figure 4A**), it appears that the glass dissolution is limited for Ca, K, and Mg, with a plateau reached at 14 days and approximately 20% of these elements released in solution. The Si and Na releases seem to be higher than the first ions cited, linear and continuous for 28 days. **Figure 4B** presents the release of ions from the hybrids containing 13-93B20 glass. For Ca, K, Mg, and B, the release of these elements is already at the plateau from the first time point contrary to the hybrid containing 13-93 (results also observed in **Figure 3**). This plateau, reached from the beginning of the immersion at 20% (as for G*/13-93), shows also that the initial dissolution of G*/13-93B20 is faster than for G*/13-93.

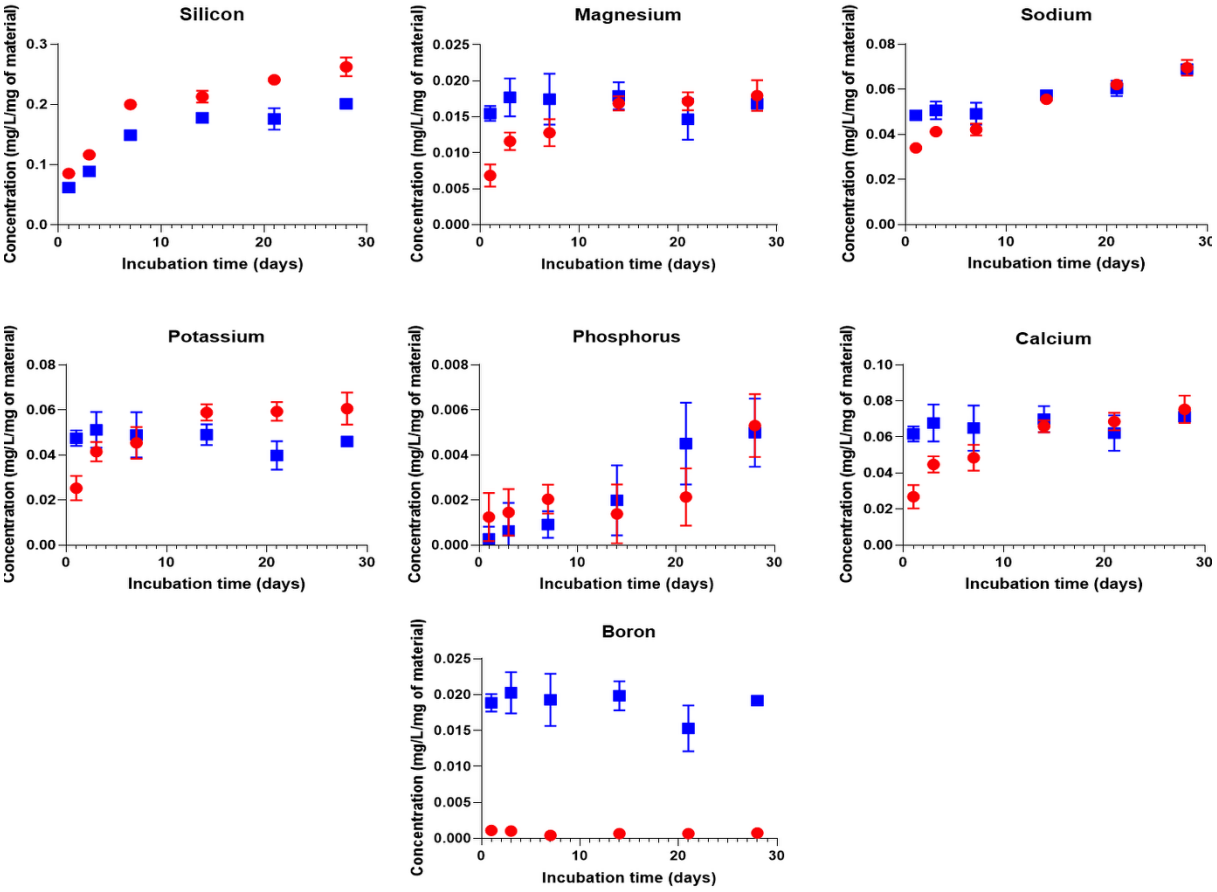

Figure 3: Elements concentrations of Si, Mg, Na, K, P, Ca, and B in the dissolution products of G*/13-93 (●) and G*/13-93B20 (■) immersed in TRIS as a function of time. The concentrations are normalized to the sample mass.

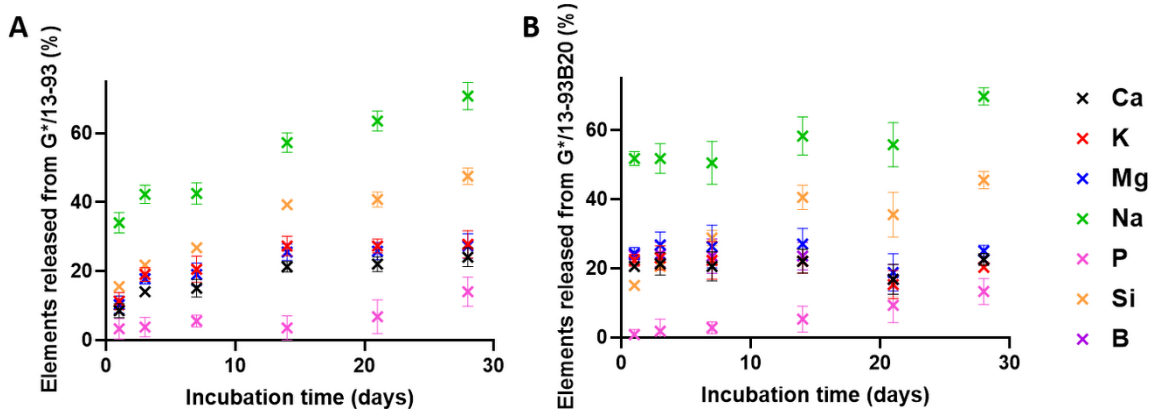

Figure 4: Release of ions from the **A**) G*/13-93 and **B**) G*/13-93B20 hybrids, immersed in TRIS as a function of time

For both hybrids, the Si and Na releases are more important than for the other elements, with a Na release already stable from the first time point for G*/13-93B20. The higher

concentrations of Si and Na are probably because they come not only from the glass but also from the GPTMS and NaF, respectively. The important release of Si in solution is probably followed by condensation and polymerization, forming an amorphous silica-rich layer around the glass [28], slowing down the release of Ca, Mg, K, and B (for G*/13-93).

After analyzing the degradation of the hybrids, their mechanical properties were studied by doing a compression test on wet samples during the immersion (**Figure 5**).

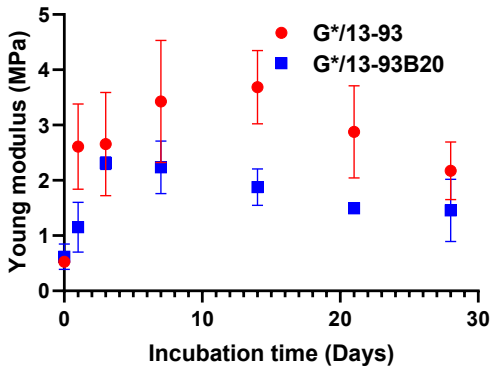

Figure 5: Young modulus measured by a compression test of wet G*/13-93 (●) and G*/13-93B20 (■) hybrids as a function of immersion time in TRIS.

Young's modulus was measured on wet samples as a function of incubation time (**Figure 5**). The evolution of the mechanical properties takes place in two stages. First, an increase in Young modulus for both hybrids can be seen. A maximum is then reached at 3 days for G*/13-93B20 and at 14 days for G*/13-93. At longer immersion times, a decrease in Young's modulus is noticed. The increase in modulus could be due to the syneresis phenomenon, as explained for **Figure 2**. The water loss leads to a reinforcement of the mechanical properties. After that, the decrease in Young's modulus would be due to hybrids erosion, inducing a loss of its mechanical properties. This corroborates the phenomenon showed in **Figure 3** and **4**, showing that this decrease happens when the stabilization of ion release is reached for G*/13-93.

Hybrids immersion in TRIS allowed to understand their dissolution and their ions release in solution. The 13-93B20 dissolves and reaches the saturation faster but finally at the same level than the 13-93. This dissolution has an influence on the mechanical properties but it should be noted that despite these variations, Young's modulus stays close to that of cancellous bone [29–31].

2.2 Dissolution in Simulated Body Fluid (SBF)

The hybrids were immersed in Simulated Body Fluid (SBF) to study their bioactivity. ICP-OES analysis, mass measurements, SEM observations, and EDX and FTIR analysis were conducted to assess the ion release/precipitation and the formation of a reactive layer.

As postulated by L.L. Hench, the ability of a material to induce precipitation of an hydroxyapatite layer at its surface can be considered as a sign of bioactivity [11]. Immersion in SBF was conducted for two weeks, and the solution was not refreshed. The ion concentration in the solution was quantified. The difference between the ion concentration in SBF and ion concentration after hybrid immersion was calculated (**Figure 6**).

The Ca concentration seems to increase initially and then decreases with immersion time, whereas the P concentration decreases from the beginning of the dissolution. This phenomenon was also observed in our previous study on composites based on Poly(Lactic) Acid (PLA) and the same glasses [13]. Generally, the decrease in Ca and P in SBF corresponds to the precipitation of a calcium-phosphate reactive layer. The elements Mg and K show similar trends during immersion in SBF. The 13-93B20 glass leaches out its ions at a faster rate initially than 13-93 and then; for both hybrids, a decrease in Mg and K concentrations appears. It is important to note that the dissolution rate slows down at earlier immersion times in SBF than in TRIS for G*/13-93. This decrease shows the saturation of the solution and probably that Mg and K can be incorporated into the calcium-phosphate reactive layer [32]. Silicon release is linear and continuous, tending towards a plateau, for both hybrids. It is initially higher for G*/13-93,

which can be, as explained above, because the borosilicate glass would be more reactive with the siloxane, leading to a lower Si release from the hybrids with 13-93B20.

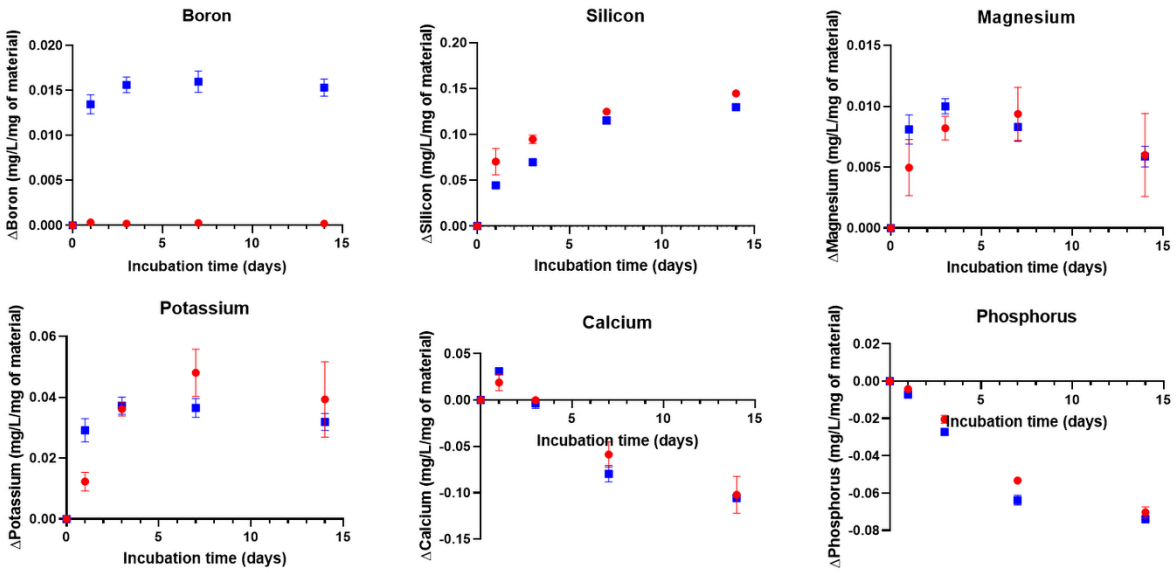

Figure 6: Elements concentrations of Si, Mg, K, P, Ca and B in the dissolution products of G*/13-93 (●) and G*/13-93B20 (■) immersed in SBF as a function of time. The concentrations are normalized to the sample mass. ΔElement = [Element] in SBF in presence of the sample – [Element] in SBF initial solution.

Figure 7 presents the mass loss of the hybrids as a function to immersion time in SBF (**Figure 7A**), the hybrid mass after freeze-drying (**Figure 7B**), and the mineral mass remaining in the materials after immersion (**Figure 7C**).

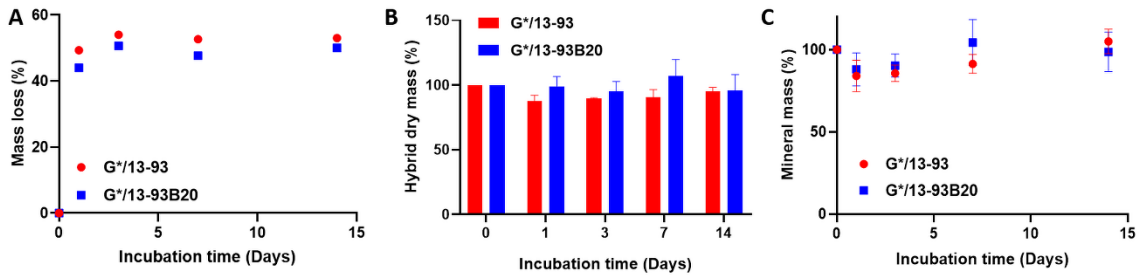

Figure 7: Mass loss (**A**), dry mass (**B**) and mineral mass (**C**) remained in the hybrid G*/13-93 (●) and G*/13-93B20 (■) as a function of immersion time in SBF.

Figure 7A shows that, after 24 h, the mass loss reaches approximately 50%, corresponding to a water loss and thus a shrinking of the materials due to syneresis, as explained for TRIS immersion. Then, the mass loss stays stable during immersion. In **Figure 7B**, the dry mass of hybrids immersed in SBF does not show the same evolution as in TRIS immersion. Indeed, a decrease in the dry mass was observed in TRIS immersion, while in SBF, it appears to stay approximately stable. For the mineral mass (**Figure 7C**), while it decreases during immersion in TRIS, showing the dissolution of the glasses, in SBF, it decreases and then increases. This corresponds to dissolution of the glass followed by the precipitation of the calcium-phosphate layer.

To assess the precipitation of this reactive layer, the hybrids were observed and analyzed using SEM/EDX as well as FTIR (**Figure 8** and **9**).

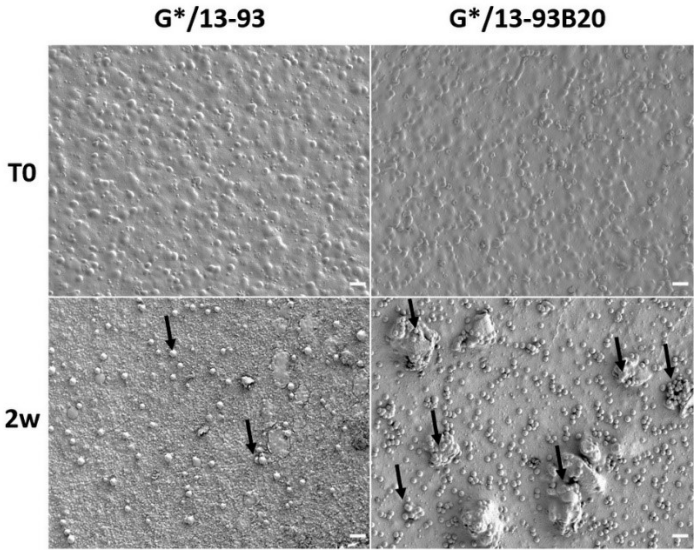

Figure 8: SEM image of the hybrids surface before and after 14 days of immersion in SBF (scale bar 20µm).

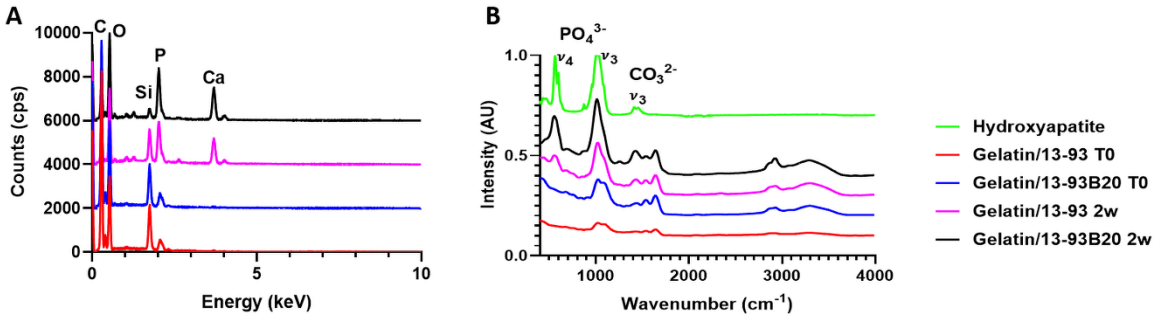

Figure 9: **A**) EDX analysis of the nodules at the hybrids surface and **B**) FTIR analysis of the samples surfaces before and after 14 days of immersion.

After 2 weeks of immersion in SBF, nodules appeared at their surface. The nodules are small and dispersed on the hybrid containing 13-93, while they are more numerous and larger on the G*/13-93B20 hybrid surface. EDX analysis were performed on the nodules shown in **Figure 8**, and the spectra are presented in **Figure 9A**. The composition of the spheres from both hybrids is mainly Ca and P with a ratio of Ca/P of 1.77 ± 0.08, which is close to hydroxyapatite [33]. This corroborates the precipitation of the calcium-phosphate layer hypothesized from the ICP analysis (**Figure 6**) and confirms that these nodules are probably apatite nodules. It is interesting to point out that the materials containing the glass 13-93B20 exhibit a higher

population and bigger nodules than materials processed with the glass 13-93. This is in agreement with Huang et al., who demonstrated that the borosilicate bioactive glasses convert to HA faster and more completely than their silicate counterpart [34].

The nature of the Ca/P precipitate was further analyzed by FTIR spectroscopy (**Figure 9B**). Two peaks at 500–600 cm^{-1} and ≈1000 cm^{-1} appear after G*/13-93B20 (they are also present for G*/13-93 but with a lower intensity) immersion in SBF. These peaks correspond to $\nu 4$ (P–O bending) and $\nu 3$ (P–O stretching) PO_4^{3-} vibrations, respectively, in the apatite structure. The carbonate CO_3^{2-} vibration is also present [35–37]. These peaks are characteristic of a hydroxyapatite structure. This is a good indication that the calcium phosphate layer precipitating on the hybrid surface is a hydroxy-carbonated apatite, indicative of the potential bioactivity of those materials. These results show the difference in reactivity between both glasses. Ion release is slowed down by the organic matrix barrier, but 13-93B20 allows us to remedy this effect compared to 13-93 glass.

We developed gelatin/BAG hybrids using GPTMS as a coupling agent, with a C_{factor} of 500, using a sol-gel method. The target mineral content (70/30 wt%) was guaranteed by careful control of the processing steps. The mineral phase dissolves when immersed in aqueous solution with kinetics depending on the glass composition. The mechanical properties varied per the dissolution of the materials; however, Young's modulus remained close to the value reported for cancellous bone [29–31]. Both hybrids were found to precipitate hydroxy-carbonated apatite during immersion in SBF. The bioactivity seemed significantly higher when using 13-93B20 glass. Therefore, preliminary cell experiments were conducted to assess if the hybrids are biocompatible and, thus, support the growth of pre-osteoblastic cells, which is fundamental for bone application.

2.3 MC3T3-E1 proliferation and morphology

MC3T3-E1 pre-osteoblastic cells were used to study their proliferation and morphology on the hybrids (**Figure 10**).

First, the number of MC3T3-E1 cells on the hybrids was studied for up to 14 days (**Figure 10A**). The hybrids were immersed 10 days in TRIS before cell culture to eliminate unreacted elements, which can prevent cell survival [38]. The hybrids were placed in 48 well plates, and the TCPS was used as a control. However, during their immersion in TRIS, they underwent a shrinking effect due syneresis. Indeed, they went from a diameter of 11 mm to 8 mm in 10 days. Thus, to compare the proliferation on the control and the materials, the cell number was normalized to the area of the respective sample.

For each condition, the cells proliferated with time and reached a plateau indicating the stationary phase (**Figure 10A**). The glass 13-93 alone was already known to promote cell adhesion and proliferation, as demonstrated by Fu et al. and Eqtesadi et al. [39,40]. At 14 days, the proliferation of MC3T3-E1 cells on G*/13-93B20 is significantly lower than on the control. This can be attributed to the release of boron from borosilicate glass, known to decrease cell proliferation while promoting osteogenesis, as observed in previous studies [13,24].

The morphology of the cells was observed at 24 h, 7 days, and 14 days on the control, G*/13-93, and G*/13-93B20 (**Figure 10B**). After 24 h, it can be observed that the cells spread on both hybrid types with their characteristic polygonal morphology. There is no difference noted in the cytoskeleton of cells between the conditions. At 7 days and 14 days, multicellular layers are observed, covering the hybrids. These results show that the cells can spread, attach, and proliferate on the hybrids. Thus, 13-93, 13-93B20, and GPTMS do not present cytotoxic effects and do not prevent the proliferation and adhesion of MC3T3-E1 cells on the hybrids.

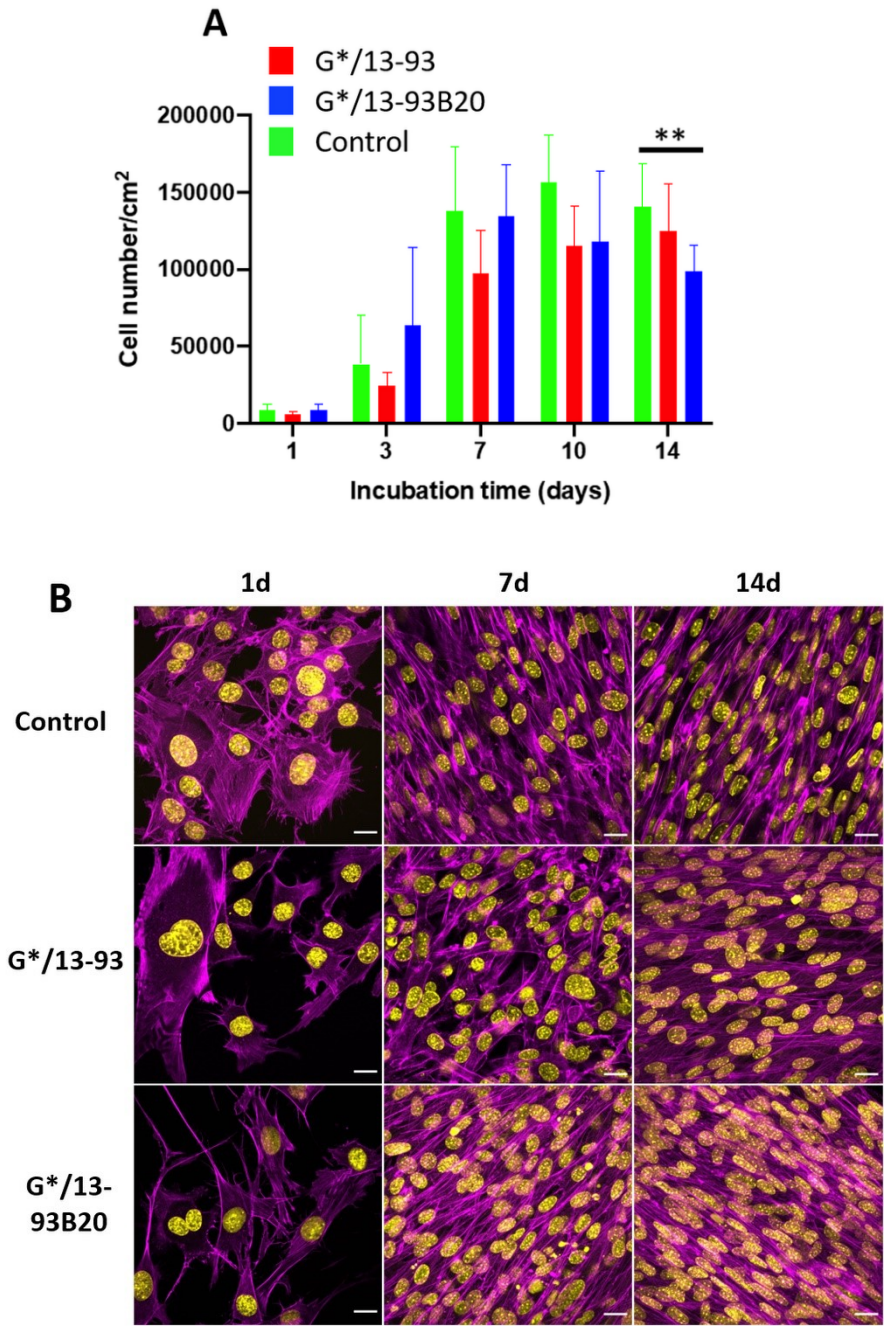

Figure 10. (**A**) Proliferation of MC3T3-E1 cells cultured in α-Minimum Essential Media (α-MEM) complete medium on Tissue Culture Polystyrene (TCPS), G*/13-93, and G*/13-93B20 hybrids for 14 days, analyzed by a CyQUANT Cell Proliferation Assay kit. The number of cells was normalized with the area of the materials surface (** $p < 0.01$). (**B**) Morphology of MC3T3-E1 cells in αMEM complete medium analyzed by nuclei (4',6-Diamidino-2-phenylindole dihydrochloride (DAPI)—yellow) and actin (phalloidin—magenta) immunostaining after 1 day, 7 days, and 14 days of culture. Scale bar 20 µm.

Conclusion

Hybrids made of gelatin and BAG particles (silicate 13-93 and borosilicate 13-93B20) covalently linked with GPTMS were synthesized using the sol-gel method. The process of synthesis was optimized in order to obtain a content of organic/inorganic matter close to that expected and to avoid particle sedimentation and aggregates. These hybrids were stable and self-supported at biological temperature in aqueous medium. When immersed in simulated body fluid, their bioactivity was shown. Cell survival was demonstrated using MC3T3-E1 cells. The substitution of 20% of SiO_2 with B_2O_3 allowed us to tailor the dissolution and bioactivity properties of the hybrids. Once stabilized, the hybrids exhibited mechanical properties which, combined with their ability to precipitate HA and their biocompatible characteristic, make these materials good candidates for bone tissue engineering. Future studies will be conducted to investigate the osteo-stimulation of these materials.

Author Contributions: conceptualization, A.H., M.B., J.M., and E.P.; methodology, R.A. and L.E.-G.; validation, A.H., M.B., J.M., and E.P.; formal analysis, A.H., A.S., and M.L. (ICP analysis); investigation, A.H., M.B., and J.M.; resources, M.B., J.M., and E.P.; data curation, A.H., M.B., and J.M.; writing—original draft preparation, A.H.; writing—review and editing, A.H., M.B., J.M., and E.P.; supervision, M.B, J.M., and E.P.; project administration, M.B., E.P., and J.M.; funding acquisition, M.B. and E.P. All authors have read and agreed to the published version of the manuscript.

Funding: The authors thank Agence Nationale de la Recherche (ANR) INEX Paris Seine Initiative for the doctoral fellowship.

Institutional Review Board Statement: Not applicable

Informed Consent Statement: Not applicable

Acknowledgments: The authors would like to thank the Science and Engineering Doctoral School of CY Cergy Paris Université for the financial support in researcher mobility.

Conflicts of Interest: The authors declare no conflict of interest.

References

1. Schemitsch, E.H. Size Matters: Defining Critical in Bone Defect Size! *J. Orthop. Trauma* **2017**, *31*, S20–S22, doi:10.1097/BOT.0000000000000978.
2. Myon, L.; Ferri, J.; Chai, F.; Blanchemain, N.; Raoul, G. Ingénierie du tissu osseux oro-maxillofacial par combinaison de biomatériaux, cellules souches, thérapie génique. *Rev. De Stomatol. Et De Chir. Maxillo-Faciale* **2011**, *112*, 201–211, doi:10.1016/j.stomax.2011.06.002.
3. Petrovic, V.; Zivkovic, P.; Petrovic, D.; Stefanovic, V. Craniofacial Bone Tissue Engineering. *Oral Surg. Oral Med. Oral Pathol. Oral Radiol.* **2012**, *114*, e1–e9, doi:10.1016/j.oooo.2012.02.030.
4. Kokubo, T. Apatite Formation on Surfaces of Ceramics, Metals and Polymers in Body Environment. *Acta Mater.* **1998**, *46*, 2519–2527, doi:10.1016/S1359-6454(98)80036-0.
5. Shimazaki, K.; Mooney, V. Comparative Study of Porous Hydroxyapatite and Tricalcium Phosphate as Bone Substitute. *J. Orthop. Res.* **1985**, *3*, 301–310, doi:10.1002/jor.1100030306.
6. Ohura, K.; Bohner, M.; Hardouin, P.; Lemaître, J.; Pasquier, G.; Flautre, B. Resorption of, and Bone Formation from, New β-Tricalcium Phosphate-Monocalcium Phosphate Cements: Anin Vivo Study. *J. Biomed. Mater. Res.* **1996**, *30*, 193–200, doi:10.1002/(SICI)1097-4636(199602)30:2<193::AID-JBM9>3.0.CO;2-M.
7. Schwach, G.; Vert, M. In Vitro and in Vivo Degradation of Lactic Acid-Based Interference Screws Used in Cruciate Ligament Reconstruction. *Int. J. Biol. Macromol.* **1999**, *25*, 283–291, doi:10.1016/s0141-8130(99)00043-4.
8. Hasegawa, S.; Ishii, S.; Tamura, J.; Furukawa, T.; Neo, M.; Matsusue, Y.; Shikinami, Y.; Okuno, M.; Nakamura, T. A 5–7 Year in Vivo Study of High-Strength Hydroxyapatite/Poly(l-Lactide) Composite Rods for the Internal Fixation of Bone Fractures. *Biomaterials* **2006**, *27*, 1327–1332, doi:10.1016/j.biomaterials.2005.09.003.
9. Verheyen, C.C.P.M.; de Wijn, J.R.; van Blitterswijk, C.A.; de Groot, K.; Rozing, P.M. Hydroxylapatite/Poly(L-Lactide) Composites: An Animal Study on Push-out Strengths and Interface Histology. *J. Biomed. Mater. Res.* **1993**, *27*, 433–444, doi:10.1002/jbm.820270404.
10. Ishikawa, K. Calcium Phosphate Cement. In *Advances in Calcium Phosphate Biomaterials*; Ben-Nissan, B., Ed.; Springer Berlin Heidelberg: Berlin, Heidelberg, 2014; pp. 199–227, ISBN 978-3-642-53980-0.
11. Hench, L.L. The Story of Bioglass®. *J. Mater. Sci. Mater. Med.* **2006**, *17*, 967–978, doi:10.1007/s10856-006-0432-z.
12. Day, R.M.; Boccaccini, A.R.; Shurey, S.; Roether, J.A.; Forbes, A.; Hench, L.L.; Gabe, S.M. Assessment of Polyglycolic Acid Mesh and Bioactive Glass for Soft-Tissue Engineering Scaffolds. *Biomaterials* **2004**, *25*, 5857–5866, doi:10.1016/j.biomaterials.2004.01.043.
13. Houaoui, A.; Lyyra, I.; Agniel, R.; Pauthe, E.; Massera, J.; Boissière, M. Dissolution, Bioactivity and Osteogenic Properties of Composites Based on Polymer and Silicate or Borosilicate Bioactive Glass. *Mater. Sci. Eng. C* **2020**, *107*, 110340, doi:10.1016/j.msec.2019.110340.
14. Mahony, O.; Tsigkou, O.; Ionescu, C.; Minelli, C.; Ling, L.; Hanly, R.; Smith, M.E.; Stevens, M.M.; Jones, J.R. Silica-Gelatin Hybrids with Tailorable Degradation and

Mechanical Properties for Tissue Regeneration. *Adv. Funct. Mater.* **2010**, *20*, 3835–3845, doi:10.1002/adfm.201000838.
15. Novak, B.M. Hybrid Nanocomposite Materials-between Inorganic Glasses and Organic Polymers. *Adv. Mater.* **1993**, *5*, 422–433, doi:10.1002/adma.19930050603.
16. Nicole, L.; Boissière, C.; Grosso, D.; Quach, A.; Sanchez, C. Mesostructured Hybrid Organic–Inorganic Thin Films. *J. Mater. Chem.* **2005**, *15*, 3598, doi:10.1039/b506072a.
17. Liu, Y.-L.; Su, Y.-H.; Lai, J.-Y. In Situ Crosslinking of Chitosan and Formation of Chitosan–Silica Hybrid Membranes with Using γ-Glycidoxypropyltrimethoxysilane as a Crosslinking Agent. *Polymer* **2004**, *45*, 6831–6837, doi:10.1016/j.polymer.2004.08.006.
18. Mahony, O.; Yue, S.; Turdean-Ionescu, C.; Hanna, J.V.; Smith, M.E.; Lee, P.D.; Jones, J.R. Silica–Gelatin Hybrids for Tissue Regeneration: Inter-Relationships between the Process Variables. *J. Sol.-Gel Sci. Technol.* **2014**, *69*, 288–298, doi:10.1007/s10971-013-3214-3.
19. Vueva, Y.; Connell, L.S.; Chayanun, S.; Wang, D.; McPhail, D.S.; Romer, F.; Hanna, J.V.; Jones, J.R. Silica/Alginate Hybrid Biomaterials and Assessment of Their Covalent Coupling. *Appl. Mater. Today* **2018**, *11*, 1–12, doi:10.1016/j.apmt.2017.12.011.
20. Maeda, H.; Kasuga, T.; Hench, L.L. Preparation of Poly(l-Lactic Acid)-Polysiloxane-Calcium Carbonate Hybrid Membranes for Guided Bone Regeneration. *Biomaterials* **2006**, *27*, 1216–1222, doi:10.1016/j.biomaterials.2005.08.010.
21. Vergnol, G.; Ginsac, N.; Rivory, P.; Meille, S.; Chenal, J.-M.; Balvay, S.; Chevalier, J.; Hartmann, D.J. In Vitro and in Vivo Evaluation of a Polylactic Acid-Bioactive Glass Composite for Bone Fixation Devices: Polylactic acid-bioactive glass composite for bone fixation devices. *J. Biomed. Mater. Res. Part B: Appl. Biomater.* **2016**, *104*, 180–191, doi:10.1002/jbm.b.33364.
22. Brink, M. The Influence of Alkali and Alkaline Earths on the Working Range for Bioactive Glasses. *J. Biomed. Mater. Res.* **1997**, *36*, 109–117, doi:10.1002/(SICI)1097-4636(199707)36:1<109::AID-JBM13>3.0.CO;2-D.
23. Brown, R.F.; Rahaman, M.N.; Dwilewicz, A.B.; Huang, W.; Day, D.E.; Li, Y.; Bal, B.S. Effect of Borate Glass Composition on Its Conversion to Hydroxyapatite and on the Proliferation of MC3T3-E1 Cells. *J. Biomed. Mater. Res. Part. A* **2009**, *88A*, 392–400, doi:10.1002/jbm.a.31679.
24. Ojansivu, M.; Mishra, A.; Vanhatupa, A.; Juntunen, M.; Larionova, A.; Massera, J.; Miettinen, S. The Effect of S53P4-Based Borosilicate Glasses and Glass Dissolution Products on the Osteogenic Commitment of Human Adipose Stem Cells. *PLoS One* **2018,** *13*, 1–20, doi:10.1371/journal.pone.0202740.
25. Maçon, A.L.B.; Kim, T.B.; Valliant, E.M.; Goetschius, K.; Brow, R.K.; Day, D.E.; Hoppe, A.; Boccaccini, A.R.; Kim, I.Y.; Ohtsuki, C.; et al. A Unified in Vitro Evaluation for Apatite-Forming Ability of Bioactive Glasses and Their Variants. *J. Mater. Sci. Mater. Med.* **2015**, *26*, 115, doi:10.1007/s10856-015-5403-9.
26. Connell, L.S.; Gabrielli, L.; Mahony, O.; Russo, L.; Cipolla, L.; Jones, J.R. Functionalizing Natural Polymers with Alkoxysilane Coupling Agents: Reacting 3-Glycidoxypropyl Trimethoxysilane with Poly(γ-Glutamic Acid) and Gelatin. *Polym. Chem.* **2017**, *8*, 1095–1103, doi:10.1039/C6PY01425A.
27. Griffith, L.G.; Naughton, G. Tissue Engineering--Current Challenges and Expanding Opportunities. *Science* **2002**, *295*, 7, doi:10.1126/science.1069210.
28. Hench, L.L. Bioceramics: From Concept to Clinic. *J. Am. Ceram. Soc.* **1991**, *74*, 1487–1510, doi:10.1111/j.1151-2916.1991.tb07132.x.
29. Wu, D.; Isaksson, P.; Ferguson, S.J.; Persson, C. Young's Modulus of Trabecular Bone at the Tissue Level: A Review. *Acta Biomater.* **2018**, *78*, 1–12, doi:10.1016/j.actbio.2018.08.001.
30. Bini, F.; Marinozzi, A.; Marinozzi, F.; Patanè, F. Microtensile Measurements of Single Trabeculae Stiffness in Human Femur. *J. Biomech.* **2002**, *35*, 1515–1519, doi:10.1016/S0021-9290(02)00182-3.

31. Hong, J.; Cha, H.; Park, Y.; Lee, S.; Khang, G.; Kim, Y. Elastic Moduli and Poisson's Ratios of Microscopic Human Femoral Trabeculae. In *11th Mediterranean Conference on Medical and Biomedical Engineering and Computing 2007, Ljubljana, Slovenia, 26–30 June 2007*; Jarm, T., Kramar, P., Zupanic, A., Eds.; IFMBE Proceedings; Springer Berlin Heidelberg: Berlin, Heidelberg, 2007; Volume. 16, pp. 274–277, ISBN 978-3-540-73043-9.
32. Combes, C.; Cazalbou, S.; Rey, C. Apatite Biominerals. *Minerals* **2016**, *6*, doi:10.3390/min6020034.
33. Singh, R.; Tan, C.; Abd Shukor, M.; Sopyan, I.; Teng, W. The Influence of Ca/P Ratio on the Properties of Hydroxyapatite Bioceramics. In *International Conference on Smart Materials and Nanotechnology in Engineering A, Harbin, China, 1–4 July 2007*; Proceedings SPIE; Bellingham, Washington; Volume 6423, doi:10.1117/12.779890.
34. Huang, W.; Day, D.E.; Kittiratanapiboon, K.; Rahaman, M.N. Kinetics and Mechanisms of the Conversion of Silicate (45S5), Borate, and Borosilicate Glasses to Hydroxyapatite in Dilute Phosphate Solutions. *J. Mater. Sci Mater. Med.* **2006**, *17*, 583–596, doi:10.1007/s10856-006-9220-z.
35. Stanislavov, A.S.; Sukhodub, L.F.; Sukhodub, L.B.; Kuznetsov, V.N.; Bychkov, K.L.; Kravchenko, M.I. Structural Features of Hydroxyapatite and Carbonated Apatite Formed under the Influence of Ultrasound and Microwave Radiation and Their Effect on the Bioactivity of the Nanomaterials. *Ultrason. Sonochemistry* **2018**, *42*, 84–96, doi:10.1016/j.ultsonch.2017.11.011.
36. Baddiel, C.B.; Berry, E.E. Spectra Structure Correlations in Hydroxy and Fluorapatite. *Spectrochim. Acta* **1966**, *22*, 1407–1416, doi:10.1016/0371-1951(66)80133-9.
37. Berzina-Cimdina, L.; Borodajenko, N. Research of Calcium Phosphates Using Fourier Transform Infrared Spectroscopy. In *Infrared Spectroscopy-Materials Science, Engineering and Technology*; Theophanides, T., Ed.; InTech, London, United Kingdom; 2012, ISBN 978-953-51-0537-4.
38. Maisani, M.; Pezzoli, D.; Chassande, O.; Mantovani, D. Cellularizing Hydrogel-Based Scaffolds to Repair Bone Tissue: How to Create a Physiologically Relevant Micro-Environment? *J. Tissue Eng.* **2017**, *8*, 1–26, doi:10.1177/2041731417712073.
39. Fu, Q.; Rahaman, M.N.; Bal, B.S.; Bonewald, L.F.; Kuroki, K.; Brown, R.F. Silicate, Borosilicate, and Borate Bioactive Glass Scaffolds with Controllable Degradation Rate for Bone Tissue Engineering Applications. II. In Vitro and in Vivo Biological Evaluation. *J. Biomed. Mater. Res. Part A* **2010**, *95A*, 172–179, doi:10.1002/jbm.a.32823.
40. Eqtesadi, S.; Motealleh, A.; Pajares, A.; Miranda, P. Effect of Milling Media on Processing and Performance of 13-93 Bioactive Glass Scaffolds Fabricated by Robocasting. *Ceram. Int.* **2015**, *41*, 1379–1389, doi:10.1016/j.ceramint.2014.09.071.

General conclusion and perspectives

Bone presents intrinsicly specific and smart properties which allow spontaneous and autonomous healing of small defects. This is the bone remodeling. In the case of large, and sometimes complex and critical defects (which can be due to various physiological traumatic or pathological situations, from natural aging to cancer), this process may be partially or totally compromised. Various medical and chirurgical approaches exist – from auto- to allo- to xeno-grafts – to permit bone substitution and/or restauration. These bone grafts present possibilities to face a lot of chirurgical needed situations. However, these natural bone grafting strategies have limitations, such as sources availability, co-morbidity, safety and risk of rejection, expensive cost… Thus, there is a need to develop innovative and more "sophisticated" materials which will help to promote bone repair and restauration. Such materials will be helpful to face the different and complex situations needing "bone bio-assistance". These materials must be adapted to different clinical situations in particular defects requiring substitution of mechanical properties or defects which must be filled. They have to present specific properties, from mechanical properties to biocompatibility, and to combined bone potentials, from osteo-conduction to osteo-induction. For that, bioactive tailored materials appear as pertinent solutions. Their bioactivity and surface reactivity will promote and induce a biological response, favoring the formation of strong interactions with the surrounding tissue [17].

Bioactive glass (BAG) is a promising material possessing these properties. Indeed, after dissolution in hydrated environment, BAG releases its ions and in particular calcium and phosphate ions, which precipitate and form a hydroxyapatite layer around glass particles. This bioactivity is the key property for its osteointegration. However, BAG is brittle and hard to shape. Its combination with another partner appears as the solution to open the route to efficient and pertinent BAG-based biomaterials.

Organic – inorganic combined materials seem to be the solution to remedy the drawbacks to use BAG as pure material. In such BAG-based materials, BAG will be organized within an

organic matrix. For that, two ways are possible. 1) BAG particles are dispersed in the organic phase yielding to a composite material [19]. 2) BAG is covalently linked to the organic phase, with a coupling agent, resulting in a hybrid material [20]. The inorganic matrix will bring the osteogenic parameter to the final material, whereas the organic matrix will allow to adapt its intrinsic properties.

In this thesis the works developed has focused on **the proposition of composites and hybrid materials based on BAG for bone bioengineering**. The BAG chosen was the 13-93. Compared to the classical 45S5 or the S53P4, this glass presents a slower dissolution rate. This represents an interesting opportunity to better control the stability of the organic matrix phase of our combined biomaterials [26,145]. Moreover, it has been possible to tune its composition to, in one hand increase its dissolution rate, while in another hand maintain it slower than the 45S5 and the S53P4. For that, 20% of silicate was replaced by borate -as the boron is known to increase the dissolution rate-, yielding to the 13-93B20 [28].
So, the effect of the **two formulations** of this pertinent **BAG: 13-93 and 13-93B20, were compared in two different systems, A) a composite and B) a hybrid** BAG-polymer biomaterial.

A. Bio-engineered composites PLA/13-93 and PLA/13-93B20.

In all the composite materials designed and fabricated, a ratio of 70/30 wgt % or 83/17 vol% of polymer vs BAG was defined. The glass particles size was fixed at 125 – 250 µm. These combinations were able to release therapeutical ions which will promote bone repair without degrading the material, while keeping its mechanical properties stable. Their dissolution rates were compared, to assess if bone repair can be optimized by modifying the

composition of the glass. The composites were characterized in different physico-chemical conditions and its biological pertinence was analyzed.

First, the effect of the processing on the composites was studied. The targeted loading of 30% of glass was respected, showing that the extrusion technique allows a good control of the glass loading in the composites. A slight degradation of the polymer due to the high temperature used is showed, however, compared to other similar studies using 45S5 glass, this degradation was contained [26]. The mechanical properties of the composites after processing were studied by 3-point bending and shear. As expected, an increase of the ductility, and some loss of mechanical properties and resistance of the polymer-based composite, was noticed. It is interesting to notice that this increase is only due to the glass loading and not to the glass nature. Indeed, the overall decrease of the composites mechanical properties was linked to the degradation of the polymer, as a loss of its molecular weight was seen. Different hypotheses for this loss are possible. The possible reasons for the drop in the Mw of PLA could be partial glass dissolution in the polymer melt or the high surface energy in some silicate BAG [168], leading to water absorption on their surface to form Si-OH. It appears that with the silicate BAG, the more reactive the glass is, the more readily the excessive thermal degradation of the polymer occurs [169]. This first step thus highlighted the impact of the process on the properties of the composites and the polymer alone, and the fact that the glass degrades the organic matrix.

Second, working with a bioresorbable polymer and bioactive glass allows to obtain a final material biodegradable, and thus avoid a second surgical operation to remove the implant. However, the kinetic of the resorbability needs to be controlled, so that it will be adapted to bone regeneration. If it is too fast, the bone will not have time to regenerate but if it is too slow it will prevent bone repair and can induce an inflammatory reaction. Obtaining a composite with a polymer which keeps its integrity and stable mechanical properties during its implantation is crucial. The dissolution of both composites containing 13-93 or 13-93B20 was

compared, in order to assess if it can be influenced by the presence of boron in the structure. Briefly, the composites were immersed for 3 months in TRIS solution to analyze their dissolution. It was observed that during the first week, the dissolution rate with the glass 13-93B20 starts earlier compared to the non-boron form. This fast dissolution during the first days of immersion, can potentially help to induce the signaling cascade which would allow the cells to commit to an osteoblastic lineage. However, despite this kinetical difference in the first days, the ion release from the materials dissolved reaches the same plateau at 3 months. The molecular weight of the polymer and the mechanical properties of the composites were also studied during these 3 months of dissolution. The molecular weight of the polymer was decreasing with immersion time for both composites. For the PLA alone, the molecular weight was not impacted. Thus, that can confirm that the BAG release has an effect on the polymer. While it is dissolving, the alkali ions catalyze the hydrolysis of polymer chains. About the mechanical properties, they stay roughly stable during immersion, showing that the decrease of the polymer molecular weight in composites does not influence their resistance, which is an important parameter for bone repair. To investigate the bioactivity, the materials were immersed in Simulated Body Fluid, and the precipitation of calcium-phosphate was more important with the composite containing 13-93B20. Thus, the composites loaded with 30% of 13-93B20 will form an HA layer from the first days of immersion in the biological fluid, while the composite containing 13-93 glass will require more time to form this HA layer. This step showed that the behavior of the glass can be adapted through its composition modification, and the effect of the boron was verified.

The third step was to study the biocompatibility of the composites and the osteogenic commitment of C2C12 myoblastic cells. The cells were found to be able to proliferate on the composites even if their proliferation is slowed down by the boron, showing that the 30% of

glass is a proportion allowing a good cell behavior. Finally, they were able to commit to an osteoblastic lineage in presence of the glass and especially the 13-93B20.

> The works done with the PLA/13-93 and PLA/13-93B20 composites allows to understand that the choice of the BAG in the structure is of great importance. Despite its osteogenic properties, the BAG can have an influence on the integrity of the organic matrix. The higher is its reactivity, the higher the negative effects on the polymer. Therefore, the 13-93 and the 13-93B20 glasses were used and the effect on the polymer was limited. The glasses were found bioactive and osteo-stimulative, with a more accentuated action in the presence of boron. The composites containing the glass 13-93B20 are promising for this application. It would be interesting to study their osteo-stimulation with stem cells and to quantify it, before doing experimentations in vivo.

The composites developed are promising for applications where mechanical support and replacement function may be necessary. For instance, formulated as screws, plates, nails…, this kind of material, able to induce osteosynthesis and easy to shape, may be useful for many clinical situations. So, a long term but genuinely nice goal of these composites would be to design 3D structures by 3D printing. This approach would be promising for obtaining a tailor-made osteosynthesis implant with mechanical properties adapted to the grafted site, combining bioresorbable polymers, and mineral matrices with osteo-properties. This will allow to have substitutes with a control of the dissolution, mechanical properties, bioactivity, and osteo-stimulation and osteointegration.

Our study allowed to characterize the properties of the composites and to investigate about the best BAG for this application. In order to challenge the proof of concept, and as preliminary assay, 3D structures were printed using Ultimaker 3D printer. Thereby, these composites can

be used as “ink” for 3D-printing to obtain specific structure, customized to the defect size and shape.

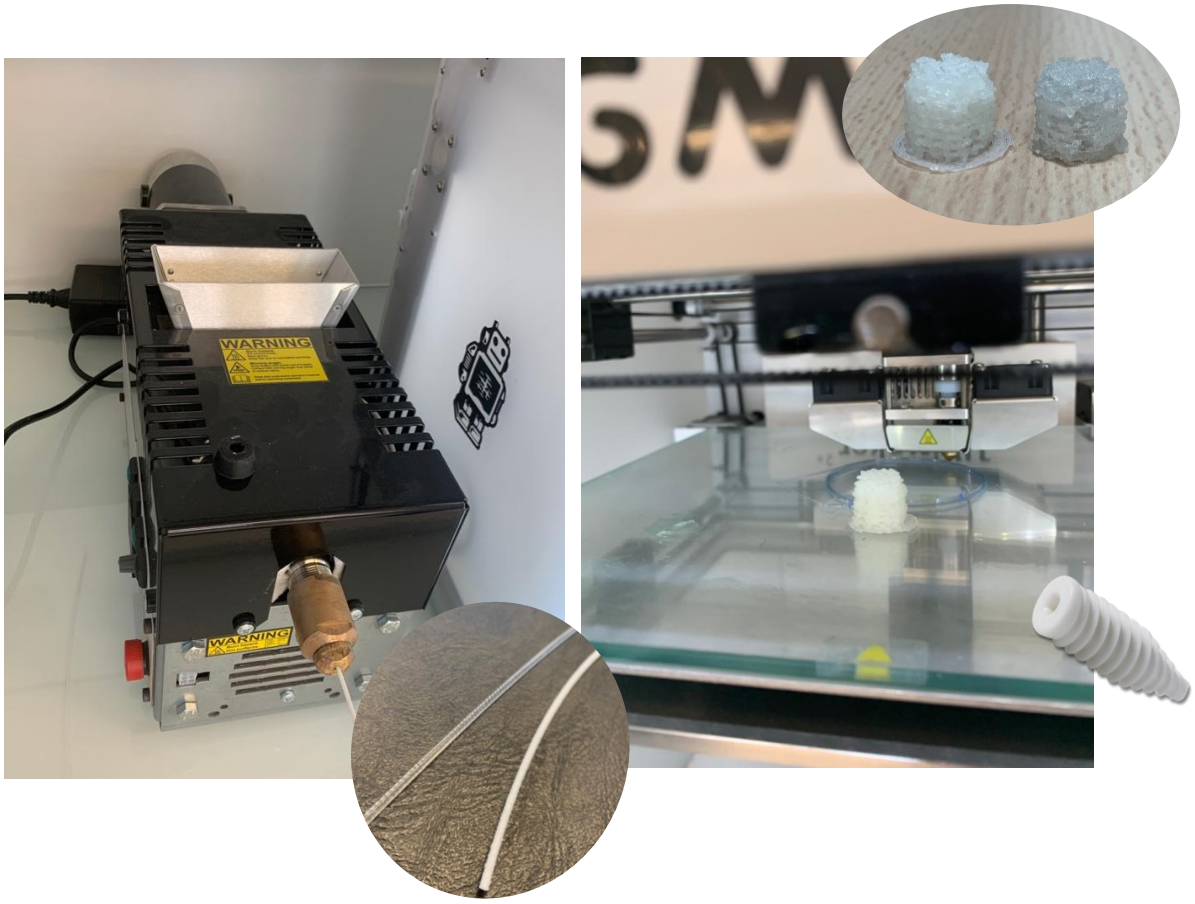

(Left) Rods obtained by extrusion, (Right) Specific structures obtained by 3D-Printing – Fused Deposition Modeling using the rods as “ink”.

However, it should be noted that the 3D printing process can also change the properties of the composites, as this technique is based on the extrusion of the rods, thus requires temperatures above their fusion point. The rods are prepared before printing by heating them, and, this can lead again to a degradation of the polymer. This would be another degradation step added to the one by extrusion to obtain the rods. Thus, after 3D printing, a new study will be needed in order to characterize the new properties of the composite-made substitute.

B. Bio-engineered Hybrids Gelatin/13-93 and Gelatin/13-93B20

For all the hybris materials developed, with glass particles of less than 38 µm, a ratio of 70/30 wgt % (or 90/10 vol% when dry) is defined. This proportion of BAG and the size of the particles are chosen in respect to the idea to use at the end this material for the filling of bone defects. The gelatin and the BAG were covalently linked thanks to the GPTMS. These stable bonds between both matrices are of great importance because they will allow to have a better control of the hybrids' properties, as their mechanical properties, their dissolution. The gelatin alone dissolves at biological temperature, however, thanks to the reticulation between the gelatin and the glass, the gels stay stable at 37°C.

First, extensive characterization was performed in order to study the effect of the synthesis on the composites. The loading of 30% of glass was reached, showing a good control of the synthesis. The mechanical properties of the hybrids after synthesis were studied by compression test. The presence of BAG bonded to the gelatin leads to a decrease of the mechanical properties compared to the gelatin/GPTMS material without BAG. The presence of glass particles dispersed and bonded within the organic phase causes heterogenous reorganisation of the gelatin network that subsequently led to a more brittle material. Moreover, the glass can also release its ions during the hybrid preparation which could in turn contribute to degrade the gelatin.

Second, the dissolution of the hybrids made with the 13-93 is compared with the hybrid made with 13-93B20. The materials were immersed during one month in TRIS solution. As found for the composites, the dissolution starts earlier with the 13-93B20 compared to the 13-93. The 13-93 and 13-93B20 keep the same dissolution behavior in both systems. The mass variations exhibit a decrease of the dry mass and the mineral mass, showing that the hybrids are dissolving. This is an important parameter showing the resorption of the materials. However,

the gelatin degradation is also an important characteristic which needs to be quantified. Hybrids degradability must be controlled in order to have an equilibrium between the materials resorption and bone repair. Here, the covalent links between the BAG and the gelatin prevent the dissolution of the gelatin at 37 °C, so that it keeps its gel form. A fast degradation of the gelatin would release the BAG from the organic matrix in the environment preventing any control of its reactivity on surrounding tissues and thus, will not help bone regeneration. Therefore, an important factor to take also into account is the GPTMS/gelatin molar ratio (C_{factor}). Indeed, this parameter impacts the hybrid structure and organization. Higher is the C_{factor}, more covalent links are present in the structure. This results in increased mechanical properties of the hybrids. However, this parameter needs to be controlled, in one hand in order to avoid excess of covalent links which will slow down or even make impossible the degradation of the material during time, and in other hand because an extensive presence of GPTMS can induce some toxicity for the cells. Indeed, an excessive amount of bridging agent, *i.e.* GPTMS, can result in some unreacted chemical moieties that may be released in the medium and induce cell toxicity. The bioactivity of the materials was investigated by immersing them in Simulated Body Fluid, and the precipitation of calcium-phosphate was more important with the hybrid containing 13-93B20 than for the composite PLA/13-93B20.

The third step was to study the biocompatibility of the hybrids. First experimentations were done with MC3T3-E1 pre-osteoblastic cells showing that they are able to proliferate and spread on the hybrids until 14 days.

> The works with the hybrids (G*/13-93 and G*/13-93B20) showed that the effects of both BAG are conserved in this new system. The hybrids are bioactive and mostly with the 13-93B20. Preliminary cell analysis demonstrates the non-cytotoxicity when using MC3T3-E1 cells. However, complementary experimentations are needed, for example with stem cells, in order to confirm the osteo-stimulation potential. Another important next step with

the hybrids will be to work on the porosity. One of the destinations of these materials will be the filling of bone defect. In such applications, the cell colonization is one of the most important parameters. The porosity of the scaffold is therefore fundamental. The disadvantages of an important porosity are the fact that the mechanical properties will be lower, and the BAG will be more exposed to the cells. However, if necessary, it is still possible to modify the C_{factor} and to adjust it to palliate these effects.

The hybrids obtained are promising for bone filling application. In order to continue their characterization and to estimate their potential for medical applications, the future objectives were to evaluate the osteo-stimulation by these hybrid materials on specific cells, as Bone Marrow Stromal Cells (BMSCs). Preliminary studies were done to investigate their cellular viability in contact with the hybrids.

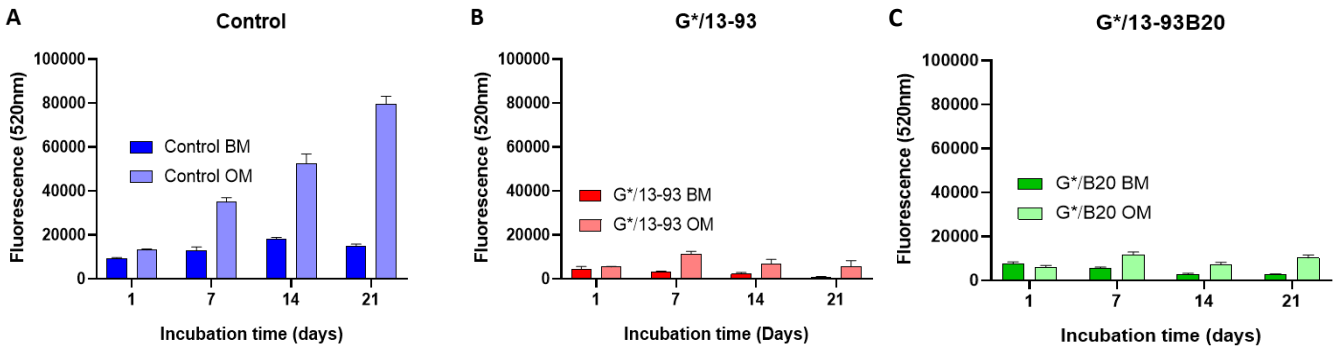

Proliferation of BMSCs cultured in Basic Medium (BM - αMEM supplemented with 1% Penicillin/Streptomycin and 5% Human Serum) or in Osteogenic Medium (OM – BM supplemented with Ascorbic Acid 200µM, β-glycerophosphate 10Mm and Dexamethasone 5nM) on A) TCPS control, B) G/13-93 and C) G*/13-93B20 analyzed by CyQUANT Cell Proliferation Assay kit.*

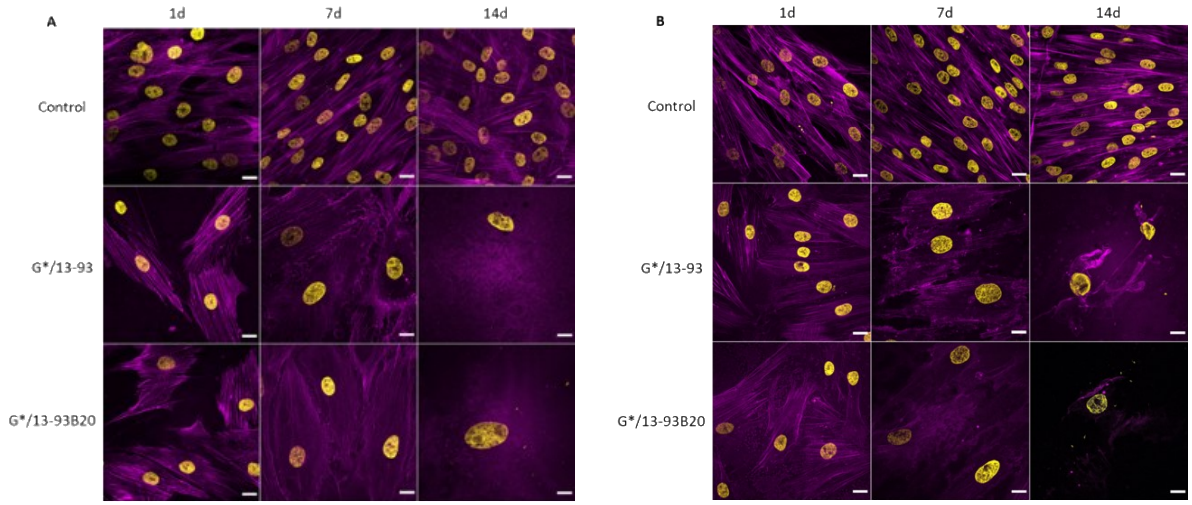

Morphology of BMSCs cultured in A) Basic Medium (BM – αMEM supplemented with 1% Penicillin/Streptomycin and 5% Human Serum) or in B) Osteogenic Medium (OM – BM supplemented with Ascorbic Acid 200µM, β-glycerophosphate 10Mm and Dexamethasone 5nM) on TCPS control, G/13-93 and G*/13-93B20 analyzed by Nuclei (DAPI - yellow) and Actin (Phalloidin - magenta) immunostaining after 1 day, 7 days and 14 days of culture. Scale bar 20µm.*

BMSCs were used as they have been identified as an optimal progenitor cell source to facilitate bone repair. Indeed, they have a higher ability for proliferation and are more easily accessible than mature osteoblastic cells [170].

These first results show that BMSCs were not able to proliferate on the hybrids in both conditions, Basic or Osteogenic medium (BM or OM). It should be noted that they were not proliferating on the control in BM neither.

The morphology staining shows that they are spreading after 24h. At 7 days, they seem to be detaching from the surface of both hybrids and less cells are observed compared to the images after 24h. At 14 days, the cells have become detached from the materials and that in BM and OM. Some hypotheses can explain these results.

During incubation in the medium, it is possible that, during hybrids dissolution, they release some GPTMS. Thus, the first possibility is that the BMSCs are too fragile and do not support the effect of the GPTMS. A second hypothesis is that the BMSCs come from patients, thus it happens that their proliferation is slowed down if they come from old patients for example.

In spite of the potential of BMSCs in bone reconstruction, previous studies showed that the limitations of BMSCs use still remain, including the amount of cells that could be recruited, the compromised bone migration of grafted cells, reduced proliferation and osteoblastic differentiation ability, and likely tumorigenesis [170].

Some investigations are still required to explain these outcomes and to find a solution to this issue. Next experimentations will be done using adipose stem cells in order to evaluate their behavior and the osteo-stimulation of this new generation of materials on these stem cells.

The bone bioengineering challenge consists of proposing different solutions with versatile materials in term of clinical applications, designed to be suitable for clinicians, and, at a physiological and medical point of view, perfectly able to help bone reparation and regeneration processes. Ideally, innovative, and modern bone substitutes will combine mechanical and osteo-properties, volume characteristics and specific adaptable capacities - as the potential to be used as filler for bone defect, to be manufactured as osteosynthesis material, to serve as scaffold for cells. Polymeric-BAG based composite and hybrid bioengineered materials represent one of the pertinent solutions that pave the way to the future generation of combined organic-inorganic solutions for translational research in bone medical surgery.

References

1. Standring, S. *Gray's Anatomy e-Book: The Anatomical Basis of Clinical Practice*; Elsevier Health Sciences, 2015; ISBN 0-7020-6851-9.
2. Tang, S.Y. Natural composites: The structure-function relationships of bone, cartilage, tendon/ligament, and the intervertebral disc. In *Biomedical Composites*; Elsevier, 2017; pp. 1–16 ISBN 978-0-08-100752-5.
3. Langdahl, B.; Ferrari, S.; Dempster, D.W. Bone Modeling and Remodeling: Potential as Therapeutic Targets for the Treatment of Osteoporosis. *Ther. Adv. Musculoskelet. Dis.* **2016**, *8*, 225–235, doi:10.1177/1759720X16670154.
4. Wang, W.; Yeung, K.W.K. Bone Grafts and Biomaterials Substitutes for Bone Defect Repair: A Review. *Bioact. Mater.* **2017**, *2*, 224–247, doi:10.1016/j.bioactmat.2017.05.007.
5. Tevlin, R.; Walmsley, G.G.; Marecic, O.; Hu, M.S.; Wan, D.C.; Longaker, M.T. Stem and Progenitor Cells: Advancing Bone Tissue Engineering. *Drug Deliv. Transl. Res.* **2016**, *6*, 159–173, doi:10.1007/s13346-015-0235-1.
6. Hussain Bukhari, M.; Qamar, S.; Batool, F. Differential Diagnosis of Osteogenic Tumors in the Context of Osteosarcoma. In *Osteosarcoma – Diagnosis, Mechanisms, and Translational Developments*; Gregory Cable, M., Lawrence Randall, R., Eds.; IntechOpen, 2019 ISBN 978-1-83968-014-4.
7. Jm, L. TUMEURS OSSEUSES. 39.
8. Currey, J. The structure and mechanical properties of bone. In *Bioceramics and their Clinical Applications*; Elsevier, 2008; pp. 3–27 ISBN 978-1-84569-204-9.
9. Kinaci, A.; Neuhaus, V.; Ring, D.C. Trends in Bone Graft Use in the United States. *Orthopedics* **2014**, *37*, e783–e788, doi:10.3928/01477447-20140825-54.
10. Rawlinson, J.N. Morbidity after Anterior Cervical Decompression and Fusion. The Influence of the Donor Site on Recovery, and the Results of a Trial of Surgibone Compared to Autologous Bone. *Acta Neurochir. (Wien)* **1994**, *131*, 106–118, doi:10.1007/BF01401460.
11. Tang, D.; Tare, R.S.; Yang, L.-Y.; Williams, D.F.; Ou, K.-L.; Oreffo, R.O.C. Biofabrication of Bone Tissue: Approaches, Challenges and Translation for Bone Regeneration. *Biomaterials* **2016**, *83*, 363–382, doi:10.1016/j.biomaterials.2016.01.024.
12. Detsch, R.; Will, J.; Hum, J.; Roether, J.A.; Boccaccini, A.R. Biomaterials. In *Cell Culture Technology*; Kasper, C., Charwat, V., Lavrentieva, A., Eds.; Learning Materials in Biosciences; Springer International Publishing: Cham, 2018; pp. 91–105 ISBN 978-3-319-74853-5.
13. Myon, L.; Ferri, J.; Chai, F.; Blanchemain, N.; Raoul, G. Ingénierie du tissu osseux oro-maxillofacial par combinaison de biomatériaux, cellules souches, thérapie génique. *Rev. Stomatol. Chir. Maxillofac.* **2011**, *112*, 201–211, doi:10.1016/j.stomax.2011.06.002.
14. Petrovic, V.; Zivkovic, P.; Petrovic, D.; Stefanovic, V. Craniofacial Bone Tissue Engineering. *Oral Surg. Oral Med. Oral Pathol. Oral Radiol.* **2012**, *114*, e1–e9, doi:10.1016/j.oooo.2012.02.030.
15. Pawelec, K.M.; White, A.A.; Best, S.M. Properties and characterization of bone repair materials. In *Bone Repair Biomaterials*; Elsevier, 2019; pp. 65–102 ISBN 978-0-08-102451-5.
16. Albrektsson, T.; Johansson, C. Osteoinduction, Osteoconduction and Osseointegration. 6.
17. Nour, S.; Baheiraei, N.; Imani, R.; Rabiee, N.; Khodaei, M.; Alizadeh, A.; Moazzeni, S.M. Bioactive Materials: A Comprehensive Review on Interactions with Biological Microenvironment Based on the Immune Response. *J. Bionic Eng.* **2019**, *16*, 563–581, doi:10.1007/s42235-019-0046-z.

18. Bonfield, W. Composites for Bone Replacement. *J. Biomed. Eng.* **1988**, *10*, 522–526, doi:10.1016/0141-5425(88)90110-0.
19. Bonfield, W.; Grynpas, M.D.; Tully, A.E.; Bowman, J.; Abram, J. Hydroxyapatite Reinforced Polyethylene — a Mechanically Compatible Implant Material for Bone Replacement. *Biomaterials* **1981**, *2*, 185–186, doi:10.1016/0142-9612(81)90050-8.
20. Mahony, O.; Tsigkou, O.; Ionescu, C.; Minelli, C.; Ling, L.; Hanly, R.; Smith, M.E.; Stevens, M.M.; Jones, J.R. Silica-Gelatin Hybrids with Tailorable Degradation and Mechanical Properties for Tissue Regeneration. *Adv. Funct. Mater.* **2010**, *20*, 3835–3845, doi:10.1002/adfm.201000838.
21. J.-M. Cognet, P.S., M. Altman Matériel d'ostéosynthèse : Vis et Plaques. *Tech. Chir. - Orthopédie-Traumatol.* **2008**, doi:http://dx.doi.org/10.1016/S0246-0467(08)46030-0.
22. Chappard, D.; Zhioua, A.; Grizon, F.; Basle, M.; Rebel, A. Biomaterials for Bone Filling: Comparisons between Autograft, Hydroxyapatite and One Highly Purified Bovine Xenograft. *Bull. Assoc. Anat. (Nancy)* **1994**, *77*, 59–65.
23. Hench, L.L. Biomaterials: A Forecast for the Future. **1998**, 5.
24. Hench, L.L. Bioceramics. *J. Am. Ceram. Soc.* **2005**, *81*, 1705–1728, doi:10.1111/j.1151-2916.1998.tb02540.x.
25. Elisa Fiume; Jacopo Barberi; Enrica Verné; Francesco Baino Bioactive Glasses: From Parent 45S5 Composition to Scaffold-Assisted Tissue-Healing Therapies. *J. Funct. Biomater.* **2018**, *9*, 24, doi:10.3390/jfb9010024.
26. Vergnol, G.; Ginsac, N.; Rivory, P.; Meille, S.; Chenal, J.-M.; Balvay, S.; Chevalier, J.; Hartmann, D.J. *In Vitro* and *in Vivo* Evaluation of a Polylactic Acid-Bioactive Glass Composite for Bone Fixation Devices: POLYLACTIC ACID-BIOACTIVE GLASS COMPOSITE FOR BONE FIXATION DEVICES. *J. Biomed. Mater. Res. B Appl. Biomater.* **2016**, *104*, 180–191, doi:10.1002/jbm.b.33364.
27. Fu, Q.; Rahaman, M.N.; Fu, H.; Liu, X. Silicate, Borosilicate, and Borate Bioactive Glass Scaffolds with Controllable Degradation Rate for Bone Tissue Engineering Applications. I. Preparation and in Vitro Degradation. *J. Biomed. Mater. Res. A* **2010**, *95A*, 164–171, doi:10.1002/jbm.a.32824.
28. Fu, Q.; Rahaman, M.N.; Bal, B.S.; Bonewald, L.F.; Kuroki, K.; Brown, R.F. Silicate, Borosilicate, and Borate Bioactive Glass Scaffolds with Controllable Degradation Rate for Bone Tissue Engineering Applications. II. In Vitro and in Vivo Biological Evaluation. *J. Biomed. Mater. Res. A* **2010**, *95A*, 172–179, doi:10.1002/jbm.a.32823.
29. Houaoui, A.; Lyyra, I.; Agniel, R.; Pauthe, E.; Massera, J.; Boissière, M. Dissolution, Bioactivity and Osteogenic Properties of Composites Based on Polymer and Silicate or Borosilicate Bioactive Glass. *Mater. Sci. Eng. C* **2020**, *107*, 110340, doi:10.1016/j.msec.2019.110340.
30. Houaoui, A.; Szczodra, A.; Lallukka, M.; El-Guermah, L.; Agniel, R.; Pauthe, E.; Massera, J.; Boissiere, M. New Generation of Hybrid Materials Based on Gelatin and Bioactive Glass Particles for Bone Tissue Regeneration. *Biomolecules* **2021**, *11*, doi:10.3390/biom11030444.
31. Fuchs, R.K.; Thompson, W.R.; Warden, S.J. Bone biology. In *Bone Repair Biomaterials*; Elsevier, 2019; pp. 15–52 ISBN 978-0-08-102451-5.
32. Florencio-Silva, R.; Sasso, G.R. da S.; Sasso-Cerri, E.; Simões, M.J.; Cerri, P.S. Biology of Bone Tissue: Structure, Function, and Factors That Influence Bone Cells. *BioMed Res. Int.* **2015**, *2015*, 1–17, doi:10.1155/2015/421746.
33. Piekarski, K. Analysis of Bone as a Composite Material. *Int. J. Eng. Sci.* **1973**, *11*, 557–565, doi:10.1016/0020-7225(73)90018-9.

34. Samuel, S.P.; Baran, G.R.; Wei, Y.; Davis, B.L. Biomechanics - Part II. In *Bone Pathology*; Khurana, J.S., Ed.; Humana Press: Totowa, NJ, 2009; pp. 69–77 ISBN 978-1-58829-766-2.
35. Choël, L.; Last, D.; Duboeuf, F.; Seurin, M.; Lissac, M.; Briguet, A.; Guillot, G. Trabecular Alveolar Bone Microarchitecture in the Human Mandible Using High Resolution Magnetic Resonance Imaging. *Dentomaxillofacial Radiol.* **2004**, *33*, 177–182, doi:10.1259/dmfr/42933309.
36. CURREY, J.D. *Bones*; Princeton University Press, 2002; ISBN 978-0-691-12804-7.
37. Hench, L.L.; Wilson, June. *An Introduction to Bioceramics*; World Scientific: Singapore; River Edge, N.J., 1993; ISBN 981-02-1400-6.
38. Black, J.; Hastings, G.W. *Handbook of Biomaterial Properties*; Chapman & Hall: London; Weinheim; New York, 1998; ISBN 0-412-60330-6.
39. Muster, D. Biomatériaux En Chirurgie Orale et Maxillofaciale (I). *Chir. Orale Maxillo-Faciale* **2014**, doi:http://dx.doi.org/10.1016/S2352-3999(14)69183-4.
40. Dorozhkin, S. Calcium Orthophosphates in Nature, Biology and Medicine. *Materials* **2009**, *2*, 399–498, doi:10.3390/ma2020399.
41. LeGeros, R.Z. Calcium Phosphates in Oral Biology and Medicine. *Monogr. Oral Sci.* **1991**, *15*, 1–201.
42. Daculsi, G.; Bouler, J.-M.; LeGeros, R.Z. Adaptive Crystal Formation in Normal and Pathological Calcifications in Synthetic Calcium Phosphate and Related Biomaterials. In *International Review of Cytology*; Elsevier, 1997; Vol. 172, pp. 129–191 ISBN 978-0-12-364576-0.
43. Feng, X. Chemical and Biochemical Basis of Cell-Bone Matrix Interaction in Health and Disease. *Curr. Chem. Biol.* **2009**, *3*, 189–196, doi:10.2174/187231309788166398.
44. Gehron Robey, P. Noncollagenous Bone Matrix Proteins. In *Principles of Bone Biology*; Elsevier, 2008; pp. 335–349 ISBN 978-0-12-373884-4.
45. Rho, J.-Y.; Kuhn-Spearing, L.; Zioupos, P. Mechanical Properties and the Hierarchical Structure of Bone. *Med. Eng. Phys.* **1998**, *20*, 92–102, doi:10.1016/S1350-4533(98)00007-1.
46. Liu, X.; Wu, H.; Byrne, M.; Krane, S.; Jaenisch, R. Type III Collagen Is Crucial for Collagen I Fibrillogenesis and for Normal Cardiovascular Development. *Proc. Natl. Acad. Sci.* **1997**, *94*, 1852–1856, doi:10.1073/pnas.94.5.1852.
47. Teitelbaum, S.L.; Ross, F.P. Genetic Regulation of Osteoclast Development and Function. *Nat. Rev. Genet.* **2003**, *4*, 638–649, doi:10.1038/nrg1122.
48. Arboleya, L.; Castañeda, S. Osteoimmunology: The Study of the Relationship Between the Immune System and Bone Tissue. *Reumatol. Clínica Engl. Ed.* **2013**, *9*, 303–315, doi:10.1016/j.reumae.2013.02.004.
49. Maisani, M. Conception et développement d'hydrogels pour l'ingénierie tissulaire appliquée au tissu osseux. 192.
50. Marsell, R.; Einhorn, T.A. The Biology of Fracture Healing. *Injury* **2011**, *42*, 551–555, doi:10.1016/j.injury.2011.03.031.
51. Fazzalari, N.L. Bone Fracture and Bone Fracture Repair. *Osteoporos. Int.* **2011**, *22*, 2003–2006, doi:10.1007/s00198-011-1611-4.
52. Schemitsch, E.H. Size Matters: Defining Critical in Bone Defect Size! *J. Orthop. Trauma* **2017**, *31*, S20–S22, doi:10.1097/BOT.0000000000000978.
53. Louise, M. Regeneration osseuse et ingenierie tissulaire Une eponge formee par la reticulation du chitosan avec une adenosine diphosphate est-elle un support adequat pour l encapsulation de cellules osseuses. 94.
54. Laurencin, C.; Khan, Y.; El-Amin, S.F. Bone Graft Substitutes. *Expert Rev. Med. Devices* **2006**, *3*, 49–57, doi:10.1586/17434440.3.1.49.

55. Reichert, J.C.; Saifzadeh, S.; Wullschleger, M.E.; Epari, D.R.; Schütz, M.A.; Duda, G.N.; Schell, H.; van Griensven, M.; Redl, H.; Hutmacher, D.W. The Challenge of Establishing Preclinical Models for Segmental Bone Defect Research. *Biomaterials* **2009**, *30*, 2149–2163, doi:10.1016/j.biomaterials.2008.12.050.
56. Wildemann, B.; Kadow-Romacker, A.; Pruss, A.; Haas, N.P.; Schmidmaier, G. Quantification of Growth Factors in Allogenic Bone Grafts Extracted with Three Different Methods. *Cell Tissue Bank.* **2007**, *8*, 107–114, doi:10.1007/s10561-006-9021-0.
57. Claes, L.; Eckert-Hübner, K.; Augat, P. The Fracture Gap Size Influences the Local Vascularization and Tissue Differentiation in Callus Healing. *Langenbecks Arch. Surg.* **2003**, *388*, 316–322, doi:10.1007/s00423-003-0396-0.
58. Sela, J.J.; Bab, I.A. Healing of Bone Fracture: General Concepts. In *Principles of Bone Regeneration*; Sela, J.J., Bab, I.A., Eds.; Springer US: Boston, MA, 2012; pp. 1–8 ISBN 978-1-4614-2058-3.
59. Sheen, J.R.; Garla, V.V. Fracture Healing Overview. In *StatPearls*; StatPearls Publishing, 2019.
60. Kiel, J.; Kaiser, K. Stress reaction and fractures. In *StatPearls [Internet]*; StatPearls Publishing, 2019.
61. Boskey, A.L.; Coleman, R. Aging and Bone. *J. Dent. Res.* **2010**, *89*, 1333–1348, doi:10.1177/0022034510377791.
62. Ji, M.-X.; Yu, Q. Primary Osteoporosis in Postmenopausal Women. *Chronic Dis. Transl. Med.* **2015**, *1*, 9–13, doi:10.1016/j.cdtm.2015.02.006.
63. Feng, X.; McDonald, J.M. Disorders of Bone Remodeling. *Annu. Rev. Pathol. Mech. Dis.* **2011**, *6*, 121–145, doi:10.1146/annurev-pathol-011110-130203.
64. Nuti, R.; Brandi, M.L.; Checchia, G.; Di Munno, O.; Dominguez, L.; Falaschi, P.; Fiore, C.E.; Iolascon, G.; Maggi, S.; Michieli, R.; et al. Guidelines for the Management of Osteoporosis and Fragility Fractures. *Intern. Emerg. Med.* **2019**, *14*, 85–102, doi:10.1007/s11739-018-1874-2.
65. Tiemann, A.H.; Hofmann, G.O. Principles of the Therapy of Bone Infections in Adult Extremities. *Strateg. Trauma Limb Reconstr.* **2009**, *4*, 57–64, doi:10.1007/s11751-009-0059-y.
66. Khan, S.N.; Cammisa, F.P.; Sandhu, H.S.; Diwan, A.D.; Girardi, F.P.; Lane, J.M. The Biology of Bone Grafting: *J. Am. Acad. Orthop. Surg.* **2005**, *13*, 77–86, doi:10.5435/00124635-200501000-00010.
67. Sheikh, Z.; Sima, C.; Glogauer, M. Bone Replacement Materials and Techniques Used for Achieving Vertical Alveolar Bone Augmentation. *Materials* **2015**, *8*, 2953–2993, doi:10.3390/ma8062953.
68. Roberts, T.T.; Rosenbaum, A.J. Bone Grafts, Bone Substitutes and Orthobiologics: The Bridge between Basic Science and Clinical Advancements in Fracture Healing. *Organogenesis* **2012**, *8*, 114–124, doi:10.4161/org.23306.
69. Canady, J.W.; Zeitler, D.P.; Thompson, S.A.; Nicholas, C.D. Suitability of the Iliac Crest as a Site for Harvest of Autogenous Bone Grafts. *Cleft Palate-Craniofacial J. Off. Publ. Am. Cleft Palate-Craniofacial Assoc.* **1993**, *30*, 579–581, doi:10.1597/1545-1569_1993_030_0579_sotica_2.3.co_2.
70. Bhatt, R.A.; Rozental, T.D. Bone Graft Substitutes. *Hand Clin.* **2012**, *28*, 457–468, doi:10.1016/j.hcl.2012.08.001.
71. Kumar, P.; Fathima, G.; Vinitha, B. Bone Grafts in Dentistry. *J. Pharm. Bioallied Sci.* **2013**, *5*, 125, doi:10.4103/0975-7406.113312.
72. Pelker, R.R.; Friedlaender, G.E.; Markham, T.C. Biomechanical Properties of Bone Allografts. *Clin. Orthop.* **1983**, 54–57.

73. Ilizarov, G.A. [Basic principles of transosseous compression and distraction osteosynthesis]. *Ortop. Travmatol. Protez.* **1971**, *32*, 7–15.
74. Chocholata, P.; Kulda, V.; Babuska, V. Fabrication of Scaffolds for Bone-Tissue Regeneration. *Materials* **2019**, *12*, 568, doi:10.3390/ma12040568.
75. Flores, A.; Marques, A.; Machado, J.; Marta, M.; Vaz, M. Bone Immobilization Devices and Consolidation Mechanisms: Impact on Healing Time. *Procedia Struct. Integr.* **2017**, *5*, 34–39, doi:10.1016/j.prostr.2017.07.058.
76. Finkemeier, C.G. Bone-Grafting and Bone-Graft Substitutes. *VO LU M E* 11.
77. Ma, J.; Both, S.K.; Yang, F.; Cui, F.-Z.; Pan, J.; Meijer, G.J.; Jansen, J.A.; van den Beucken, J.J.J.P. Concise Review: Cell-Based Strategies in Bone Tissue Engineering and Regenerative Medicine. *STEM CELLS Transl. Med.* **2014**, *3*, 98–107, doi:10.5966/sctm.2013-0126.
78. Lee, K.; Silva, E.A.; Mooney, D.J. Growth Factor Delivery-Based Tissue Engineering: General Approaches and a Review of Recent Developments. *J. R. Soc. Interface* **2011**, *8*, 153–170, doi:10.1098/rsif.2010.0223.
79. Niemelä, T.; Kellomäki, M. Bioactive glass and biodegradable polymer composites. In *Bioactive Glasses*; Elsevier, 2011; pp. 227–245 ISBN 978-1-84569-768-6.
80. Zhu, N.; Che, X. Biofabrication of Tissue Scaffolds. In *Advances in Biomaterials Science and Biomedical Applications*; Pignatello, R., Ed.; InTech, 2013 ISBN 978-953-51-1051-4.
81. Mikos, A.G.; Thorsen, A.J.; Czerwonka, L.A.; Bao, Y.; Langer, R.; Winslow, D.N.; Vacanti, J.P. Preparation and Characterization of Poly(l-Lactic Acid) Foams. *Polymer* **1994**, *35*, 1068–1077, doi:10.1016/0032-3861(94)90953-9.
82. Di Maio, E.; Mensitieri, G.; Iannace, S.; Nicolais, L.; Li, W.; Flumerfelt, R.W. Structure Optimization of Polycaprolactone Foams by Using Mixtures of CO2 and N2 as Blowing Agents. *Polym. Eng. Sci.* **2005**, *45*, 432–441, doi:10.1002/pen.20289.
83. Haugen, H.; Ried, V.; Brunner, M.; Will, J.; Wintermantel, E. Water as Foaming Agent for Open Cell Polyurethane Structures. *J. Mater. Sci. Mater. Med.* **2004**, *15*, 343–346, doi:10.1023/B:JMSM.0000021099.33619.ac.
84. Parks, K.L.; Beckman, E.J. Generation of Microcellular Polyurethane Foams via Polymerization in Carbon Dioxide. II: Foam Formation and Characterization. *Polym. Eng. Sci.* **1996**, *36*, 2417–2431, doi:10.1002/pen.10640.
85. Lee, K.-W.D.; Chan, P.K.; Feng, X. Morphology Development and Characterization of the Phase-Separated Structure Resulting from the Thermal-Induced Phase Separation Phenomenon in Polymer Solutions under a Temperature Gradient. *Chem. Eng. Sci.* **2004**, *59*, 1491–1504, doi:10.1016/j.ces.2003.12.025.
86. Thomson, R.C.; Wake, M.C.; Yaszemski, M.J.; Mikos, A.G. Biodegradable Polymer Scaffolds to Regenerate Organs. In Proceedings of the Biopolymers II; Peppas, N.A., Langer, R.S., Eds.; Springer Berlin Heidelberg: Berlin, Heidelberg, 1995; pp. 245–274.
87. Liapis, A.I.; Bruttini, R. A Theory for the Primary and Secondary Drying Stages of the Freeze-Drying of Pharmaceutical Crystalline and Amorphous Solutes: Comparison between Experimental Data and Theory. *Sep. Technol.* **1994**, *4*, 144–155, doi:10.1016/0956-9618(94)80017-0.
88. Pikal, M.; Shah, S.; Roy, M.; Putman, R. The Secondary Drying Stage of Freeze Drying: Drying Kinetics as a Function of Temperature and Chamber Pressure☆. *Int. J. Pharm.* **1990**, *60*, 203–207, doi:10.1016/0378-5173(90)90074-E.
89. Novosibirsk Research Institute of Traumatology and Orthopaedics n.a. Ya.L. Tsivyan, Russia; Tereshchenko, V.; Larionov, P.; Novosibirsk Research Institute of Traumatology and Orthopaedics n.a. Ya.L. Tsivyan, Russia; Kirilova, I.; Novosibirsk Research Institute of Traumatology and Orthopaedics n.a. Ya.L. Tsivyan, Russia; Sadovoy, M.;

Novosibirsk Research Institute of Traumatology and Orthopaedics n.a. Ya.L. Tsivyan, Russia; Mamonova, E.; Innovation Medical Techology Center, Novosibirsk, Russia MATERIALS AND METHODS OF BONE TISSUE ENGINEERING. *Hir. Pozvonočnika* **2016**, 72–81, doi:10.14531/ss2016.1.72-81.

90. Brunello, G.; Sivolella, S.; Meneghello, R.; Ferroni, L.; Gardin, C.; Piattelli, A.; Zavan, B.; Bressan, E. Powder-Based 3D Printing for Bone Tissue Engineering. *Biotechnol. Adv.* **2016**, *34*, 740–753, doi:10.1016/j.biotechadv.2016.03.009.
91. Guduric, V. 3D Printing and Characterization of PLA Scaffolds for Layer-by-Layer BioAssembly in Tissue Engineering. 264.
92. Ahmed, E.M. Hydrogel: Preparation, Characterization, and Applications: A Review. *J. Adv. Res.* **2015**, *6*, 105–121, doi:10.1016/j.jare.2013.07.006.
93. Rajan, N.; Habermehl, J.; Coté, M.-F.; Doillon, C.J.; Mantovani, D. Preparation of Ready-to-Use, Storable and Reconstituted Type I Collagen from Rat Tail Tendon for Tissue Engineering Applications. *Nat. Protoc.* **2006**, *1*, 2753–2758, doi:10.1038/nprot.2006.430.
94. Connell, L.S.; Gabrielli, L.; Mahony, O.; Russo, L.; Cipolla, L.; Jones, J.R. Functionalizing Natural Polymers with Alkoxysilane Coupling Agents: Reacting 3-Glycidoxypropyl Trimethoxysilane with Poly(γ-Glutamic Acid) and Gelatin. *Polym. Chem.* **2017**, *8*, 1095–1103, doi:10.1039/C6PY01425A.
95. Niwa, S.; Perren, S.M.; Hattori, T. *Biomechanics in Orthopedics*; Springer Japan: Tokyo, 1992; ISBN 978-4-431-68216-5.
96. Song, R.; Murphy, M.; Li, C.; Ting, K.; Soo, C.; Zheng, Z. Current Development of Biodegradable Polymeric Materials for Biomedical Applications. *Drug Des. Devel. Ther.* **2018**, *Volume 12*, 3117–3145, doi:10.2147/DDDT.S165440.
97. Zarif, M.-E. A Review of Chitosan-, Alginate-, and Gelatin-Based Biocomposites for Bone Tissue Engineering. *Biomater. Tissue Eng. Bull.* **2018**, *5*, 97–109, doi:10.33263/BTEB534.097109.
98. LogithKumar, R.; KeshavNarayan, A.; Dhivya, S.; Chawla, A.; Saravanan, S.; Selvamurugan, N. A Review of Chitosan and Its Derivatives in Bone Tissue Engineering. *Carbohydr. Polym.* **2016**, *151*, 172–188, doi:10.1016/j.carbpol.2016.05.049.
99. Balagangadharan, K.; Dhivya, S.; Selvamurugan, N. Chitosan Based Nanofibers in Bone Tissue Engineering. *Int. J. Biol. Macromol.* **2017**, *104*, 1372–1382, doi:10.1016/j.ijbiomac.2016.12.046.
100. Preethi Soundarya, S.; Haritha Menon, A.; Viji Chandran, S.; Selvamurugan, N. Bone Tissue Engineering: Scaffold Preparation Using Chitosan and Other Biomaterials with Different Design and Fabrication Techniques. *Int. J. Biol. Macromol.* **2018**, *119*, 1228–1239, doi:10.1016/j.ijbiomac.2018.08.056.
101. Dalheim, M.Ø.; Vanacker, J.; Najmi, M.A.; Aachmann, F.L.; Strand, B.L.; Christensen, B.E. Efficient Functionalization of Alginate Biomaterials. *Biomaterials* **2016**, *80*, 146–156, doi:10.1016/j.biomaterials.2015.11.043.
102. Shaheen, Th.I.; Montaser, A.S.; Li, S. Effect of Cellulose Nanocrystals on Scaffolds Comprising Chitosan, Alginate and Hydroxyapatite for Bone Tissue Engineering. *Int. J. Biol. Macromol.* **2019**, *121*, 814–821, doi:10.1016/j.ijbiomac.2018.10.081.
103. Wahl, D.A.; Sachlos, E.; Liu, C.; Czernuszka, J.T. Controlling the Processing of Collagen-Hydroxyapatite Scaffolds for Bone Tissue Engineering. *J. Mater. Sci. Mater. Med.* **2007**, *18*, 201–209, doi:10.1007/s10856-006-0682-9.
104. Davis, H.; Leach, J. Hybrid and Composite Biomaterials in Tissue Engineering. *Top. Multifunct. Biomater. Devices* **2008**.
105. Salgado, A.J.; Coutinho, O.P.; Reis, R.L. Bone Tissue Engineering: State of the Art and Future Trends. *Macromol. Biosci.* **2004**, *4*, 743–765, doi:10.1002/mabi.200400026.

106. Sachlos, E.; Gotora, D.; Czernuszka, J.T. Collagen Scaffolds Reinforced with Biomimetic Composite Nano-Sized Carbonate-Substituted Hydroxyapatite Crystals and Shaped by Rapid Prototyping to Contain Internal Microchannels. 10.
107. Ferreira, A.M.; Gentile, P.; Chiono, V.; Ciardelli, G. Collagen for Bone Tissue Regeneration. *Acta Biomater.* **2012**, *8*, 3191–3200, doi:10.1016/j.actbio.2012.06.014.
108. Yang, G.; Xiao, Z.; Long, H.; Ma, K.; Zhang, J.; Ren, X.; Zhang, J. Assessment of the Characteristics and Biocompatibility of Gelatin Sponge Scaffolds Prepared by Various Crosslinking Methods. *Sci. Rep.* **2018**, *8*, doi:10.1038/s41598-018-20006-y.
109. Sharifi, E.; Azami, M.; Kajbafzadeh, A.-M.; Moztarzadeh, F.; Faridi-Majidi, R.; Shamousi, A.; Karimi, R.; Ai, J. Preparation of a Biomimetic Composite Scaffold from Gelatin/Collagen and Bioactive Glass Fibers for Bone Tissue Engineering. *Mater. Sci. Eng. C* **2016**, *59*, 533–541, doi:10.1016/j.msec.2015.09.037.
110. Melke, J.; Midha, S.; Ghosh, S.; Ito, K.; Hofmann, S. Silk Fibroin as Biomaterial for Bone Tissue Engineering. *Acta Biomater.* **2016**, *31*, 1–16, doi:10.1016/j.actbio.2015.09.005.
111. Boutinguiza, M.; Pou, J.; Comesaña, R.; Lusquiños, F.; de Carlos, A.; León, B. Biological Hydroxyapatite Obtained from Fish Bones. *Mater. Sci. Eng. C* **2012**, *32*, 478–486, doi:10.1016/j.msec.2011.11.021.
112. Ahmad Fara, A.N.K.; bin Yahya, M.A.; Abdullah, H.Z. Preparation and Characterization of Biological Hydroxyapatite (HAp) Obtained from Tilapia Fish Bone. *Adv. Mater. Res.* **2015**, *1087*, 152–156, doi:10.4028/www.scientific.net/AMR.1087.152.
113. COLAT-PARROS, J.; JORDANA, F. Les substituts osseux. *Univ. Médicale Virtuelle Francoph.* 10.
114. Ginsac, N. Caractérisation de matériaux composite polyacide lactique-bioverre pour application dans la réparation osseuse. 150.
115. Glenske, K.; Donkiewicz, P.; Köwitsch, A.; Milosevic-Oljaca, N.; Rider, P.; Rofall, S.; Franke, J.; Jung, O.; Smeets, R.; Schnettler, R.; et al. Applications of Metals for Bone Regeneration. *Int. J. Mol. Sci.* **2018**, *19*, 826, doi:10.3390/ijms19030826.
116. Ashter, S.A. Types of Biodegradable Polymers. In *Introduction to Bioplastics Engineering*; Elsevier, 2016; pp. 81–151 ISBN 978-0-323-39396-6.
117. Benatti, A.C.B.; Pattaro, A.F.; Rodrigues, A.A.; Xavier, M.V.; Kaasi, A.; Barbosa, M.I.R.; Jardini, A.L.; Filho, R.M.; Kharmandayan, P. Bioreabsorbable polymers for tissue engineering: PLA, PGA, and their copolymers. In *Materials for Biomedical Engineering*; Elsevier, 2019; pp. 83–116 ISBN 978-0-12-816901-8.
118. Sabir, M.I.; Xu, X.; Li, L. A Review on Biodegradable Polymeric Materials for Bone Tissue Engineering Applications. *J. Mater. Sci.* **2009**, *44*, 5713–5724, doi:10.1007/s10853-009-3770-7.
119. Santos Jr., A.R. Bioresorbable Polymers for Tissue Engineering. In *Tissue Engineering*; Eberli, D., Ed.; InTech, 2010 ISBN 978-953-307-079-7.
120. Ikada, Y.; Tsuji, H. Biodegradable Polyesters for Medical and Ecological Applications. 16.
121. Cheng, Y.; Deng, S.; Chen, P.; Ruan, R. Polylactic Acid (PLA) Synthesis and Modifications: A Review. *Front. Chem. China* **2009**, *4*, 259–264, doi:10.1007/s11458-009-0092-x.
122. Schmidmaier, G.; Baehr, K.; Mohr, S.; Kretschmar, M.; Beck, S.; Wildemann, B. Biodegradable Polylactide Membranes for Bone Defect Coverage: Biocompatibility Testing, Radiological and Histological Evaluation in a Sheep Model. *Clin. Oral Implants Res.* **2006**, *17*, 439–444, doi:10.1111/j.1600-0501.2005.01242.x.
123. Gupta, B.; Revagade, N.; Hilborn, J. Poly(Lactic Acid) Fiber: An Overview. *Prog. Polym. Sci.* **2007**, *32*, 455–482, doi:10.1016/j.progpolymsci.2007.01.005.

124. Miranda, C.S.; Ribeiro, A.R.M.; Homem, N.C.; Felgueiras, H.P. Spun Biotextiles in Tissue Engineering and Biomolecules Delivery Systems. *Antibiotics* **2020**, *9*, 174, doi:10.3390/antibiotics9040174.
125. Fang, R.; Zhang, E.; Xu, L.; Wei, S. Electrospun PCL/PLA/HA Based Nanofibers as Scaffold for Osteoblast-Like Cells. *J. Nanosci. Nanotechnol.* **2010**, *10*, 7747–7751, doi:10.1166/jnn.2010.2831.
126. Kokubo, T. Apatite Formation on Surfaces of Ceramics, Metals and Polymers in Body Environment. *Acta Mater.* **1998**, *46*, 2519–2527, doi:10.1016/S1359-6454(98)80036-0.
127. Aubry, P. présentée et soutenue publiquement. 144.
128. Carson, J.S.; Bostrom, M.P.G. Synthetic Bone Scaffolds and Fracture Repair. *Injury* **2007**, *38*, S33–S37, doi:10.1016/j.injury.2007.02.008.
129. Shimazaki, K.; Mooney, V. Comparative Study of Porous Hydroxyapatite and Tricalcium Phosphate as Bone Substitute. *J. Orthop. Res.* **1985**, *3*, 301–310, doi:10.1002/jor.1100030306.
130. Daculsi, G.; Legeros, R.Z.; Nery, E.; Lynch, K.; Kerebel, B. Transformation of Biphasic Calcium Phosphate Ceramicsin Vivo: Ultrastructural and Physicochemical Characterization. *J. Biomed. Mater. Res.* **1989**, *23*, 883–894, doi:10.1002/jbm.820230806.
131. Hench, L.L. Bioceramics: From Concept to Clinic. *J. Am. Ceram. Soc.* **1991**, *74*, 1487–1510, doi:10.1111/j.1151-2916.1991.tb07132.x.
132. Xynos, I.D.; Edgar, A.J.; Buttery, L.D.K.; Hench, L.L.; Polak, J.M. Gene-Expression Profiling of Human Osteoblasts Following Treatment with the Ionic Products of Bioglass® 45S5 Dissolution. 7.
133. Day, R.M. Bioactive Glass Stimulates the Secretion of Angiogenic Growth Factors and Angiogenesis *in Vitro*. *Tissue Eng.* **2005**, *11*, 768–777, doi:10.1089/ten.2005.11.768.
134. Gorustovich, A.A.; Roether, J.A.; Boccaccini, A.R. Effect of Bioactive Glasses on Angiogenesis: A Review of *In Vitro* and *In Vivo* Evidences. *Tissue Eng. Part B Rev.* **2010**, *16*, 199–207, doi:10.1089/ten.teb.2009.0416.
135. Leu, A.; Leach, J.K. Proangiogenic Potential of a Collagen/Bioactive Glass Substrate. *Pharm. Res.* **2008**, *25*, 1222–1229, doi:10.1007/s11095-007-9508-9.
136. Allan, I.; Newman, H.; Wilson, M. Antibacterial Activity of Particulate Bioglass® against Supra- and Subgingival Bacteria. *Biomaterials* **2001**, *22*, 1683–1687, doi:10.1016/S0142-9612(00)00330-6.
137. Gorriti, M.F.; López, J.M.P.; Boccaccini, A.R.; Audisio, C.; Gorustovich, A.A. In Vitro Study of the Antibacterial Activity of Bioactive Glass-Ceramic Scaffolds. *Adv. Eng. Mater.* **2009**, *11*, B67–B70, doi:10.1002/adem.200900081.
138. Hu, S.; Chang, J.; Liu, M.; Ning, C. Study on Antibacterial Effect of 45S5 Bioglass®. *J. Mater. Sci. Mater. Med.* **2009**, *20*, 281–286, doi:10.1007/s10856-008-3564-5.
139. Hoppe, A.; Güldal, N.S.; Boccaccini, A.R. A Review of the Biological Response to Ionic Dissolution Products from Bioactive Glasses and Glass-Ceramics. *Biomaterials* **2011**, *32*, 2757–2774, doi:10.1016/j.biomaterials.2011.01.004.
140. Bi, L.; Rahaman, M.N.; Day, D.E.; Brown, Z.; Samujh, C.; Liu, X.; Mohammadkhah, A.; Dusevich, V.; Eick, J.D.; Bonewald, L.F. Effect of Bioactive Borate Glass Microstructure on Bone Regeneration, Angiogenesis, and Hydroxyapatite Conversion in a Rat Calvarial Defect Model. *Acta Biomater.* **2013**, *9*, 8015–8026, doi:10.1016/j.actbio.2013.04.043.
141. Fu, Q.; Rahaman, M.N.; Sonny Bal, B.; Brown, R.F.; Day, D.E. Mechanical and in Vitro Performance of 13–93 Bioactive Glass Scaffolds Prepared by a Polymer Foam Replication Technique. *Acta Biomater.* **2008**, *4*, 1854–1864, doi:10.1016/j.actbio.2008.04.019.

142. Kokubo, T.; Kushitani, H.; Sakka, S.; Kitsugi, T.; Yamamuro, T. Solutions Able to Reproducein Vivo Surface-Structure Changes in Bioactive Glass-Ceramic A-W3. *J. Biomed. Mater. Res.* **1990**, *24*, 721–734, doi:10.1002/jbm.820240607.
143. Gerhardt, L.-C.; Boccaccini, A.R. Bioactive Glass and Glass-Ceramic Scaffolds for Bone Tissue Engineering. *Materials* **2010**, *3*, 3867–3910, doi:10.3390/ma3073867.
144. Hench, L.L. The Story of Bioglass®. *J. Mater. Sci. Mater. Med.* **2006**, *17*, 967–978, doi:10.1007/s10856-006-0432-z.
145. Brink, M. The Influence of Alkali and Alkaline Earths on the Working Range for Bioactive Glasses. *J. Biomed. Mater. Res.* **1997**, *36*, 109–117, doi:10.1002/(SICI)1097-4636(199707)36:1<109::AID-JBM13>3.0.CO;2-D.
146. Yao, A.; Wang, D.; Huang, W.; Fu, Q.; Rahaman, M.N.; Day, D.E. In Vitro Bioactive Characteristics of Borate-Based Glasses with Controllable Degradation Behavior. *J. Am. Ceram. Soc.* **2007**, *90*, 303–306, doi:10.1111/j.1551-2916.2006.01358.x.
147. Huang, W.; Day, D.E.; Kittiratanapiboon, K.; Rahaman, M.N. Kinetics and Mechanisms of the Conversion of Silicate (45S5), Borate, and Borosilicate Glasses to Hydroxyapatite in Dilute Phosphate Solutions. *J. Mater. Sci. Mater. Med.* **2006**, *17*, 583–596, doi:10.1007/s10856-006-9220-z.
148. Zhang, X.; Jia, W.; Gu, Y.; Xiao, W.; Liu, X.; Wang, D.; Zhang, C.; Huang, W.; Rahaman, M.N.; Day, D.E.; et al. Teicoplanin-Loaded Borate Bioactive Glass Implants for Treating Chronic Bone Infection in a Rabbit Tibia Osteomyelitis Model. *Biomaterials* **2010**, *31*, 5865–5874, doi:10.1016/j.biomaterials.2010.04.005.
149. Rahaman, M.N.; Day, D.E.; Sonny Bal, B.; Fu, Q.; Jung, S.B.; Bonewald, L.F.; Tomsia, A.P. Bioactive Glass in Tissue Engineering. *Acta Biomater.* **2011**, *7*, 2355–2373, doi:10.1016/j.actbio.2011.03.016.
150. Navarro, M.; Aparicio, C.; Charles-Harris, M.; Ginebra, M.P.; Engel, E.; Planell, J.A. Development of a Biodegradable Composite Scaffold for Bone Tissue Engineering: Physicochemical, Topographical, Mechanical, Degradation, and Biological Properties. In *Ordered Polymeric Nanostructures at Surfaces*; Vancso, G.J., Ed.; Springer Berlin Heidelberg: Berlin, Heidelberg, 2006; Vol. 200, pp. 209–231 ISBN 978-3-540-31921-4.
151. Niemela, T.; Niiranen, H.; Kellomaki, M.; Tormala, P. Self-Reinforced Composites of Bioabsorbable Polymer and Bioactive Glass with Different Bioactive Glass Contents. Part I: Initial Mechanical Properties and Bioactivity. *Acta Biomater.* **2005**, *1*, 235–242, doi:10.1016/j.actbio.2004.11.002.
152. Niemelä, T.; Niiranen, H.; Kellomäki, M. Self-Reinforced Composites of Bioabsorbable Polymer and Bioactive Glass with Different Bioactive Glass Contents. Part II: In Vitro Degradation. *Acta Biomater.* **2008**, *4*, 156–164, doi:10.1016/j.actbio.2007.06.007.
153. Jones, J.R. Review of Bioactive Glass: From Hench to Hybrids. *Acta Biomater.* **2013**, *9*, 4457–4486, doi:10.1016/j.actbio.2012.08.023.
154. Sanchez, C.; Julián, B.; Belleville, P.; Popall, M. Applications of Hybrid Organic–Inorganic Nanocomposites. *J. Mater. Chem.* **2005**, *15*, 3559, doi:10.1039/b509097k.
155. Zha, J.; Roggendorf, H. Sol-Gel Science, the Physics and Chemistry of Sol-Gel Processing, Ed. by C. J. Brinker and G. W. Scherer, Academic Press, Boston 1990, Xiv, 908 Pp., Bound?ISBN 0-12-134970-5. *Adv. Mater.* **1991**, *3*, 522–522, doi:10.1002/adma.19910031025.
156. Novak, B.M. Hybrid Nanocomposite Materials - between Inorganic Glasses and Organic Polymers. *Adv. Mater.* **1993**, *5*, 422–433, doi:10.1002/adma.19930050603.
157. Chen, S.; Osaka, A.; Ikoma, T.; Morita, H.; Li, J.; Takeguchi, M.; Hanagata, N. Fabrication, Microstructure, and BMP-2 Delivery of Novel Biodegradable and Biocompatible Silicate–Collagen Hybrid Fibril Sheets. *J. Mater. Chem.* **2011**, *21*, 10942, doi:10.1039/c1jm10829h.

158. Liu, Y.-L.; Su, Y.-H.; Lai, J.-Y. In Situ Crosslinking of Chitosan and Formation of Chitosan–Silica Hybrid Membranes with Using γ-Glycidoxypropyltrimethoxysilane as a Crosslinking Agent. *Polymer* **2004**, *45*, 6831–6837, doi:10.1016/j.polymer.2004.08.006.
159. Maeda, H.; Kasuga, T.; Hench, L.L. Preparation of Poly(l-Lactic Acid)-Polysiloxane-Calcium Carbonate Hybrid Membranes for Guided Bone Regeneration. *Biomaterials* **2006**, *27*, 1216–1222, doi:10.1016/j.biomaterials.2005.08.010.
160. Rhee, S.-H.; Choi, J.-Y.; Kim, H.-M. Preparation of a Bioactive and Degradable Poly(e-Caprolactone)/Silica Hybrid through a Sol–Gel Method. **2002**, 7.
161. Mahony, O.; Yue, S.; Turdean-Ionescu, C.; Hanna, J.V.; Smith, M.E.; Lee, P.D.; Jones, J.R. Silica–Gelatin Hybrids for Tissue Regeneration: Inter-Relationships between the Process Variables. *J. Sol-Gel Sci. Technol.* **2014**, *69*, 288–298, doi:10.1007/s10971-013-3214-3.
162. Gurunathan, T.; Mohanty, S.; Nayak, S.K. Hyperbranched Polymers for Coating Applications: A Review. *Polym.-Plast. Technol. Eng.* **2016**, *55*, 92–117, doi:10.1080/03602559.2015.1021482.
163. Vueva, Y.; Connell, L.S.; Chayanun, S.; Wang, D.; McPhail, D.S.; Romer, F.; Hanna, J.V.; Jones, J.R. Silica/Alginate Hybrid Biomaterials and Assessment of Their Covalent Coupling. *Appl. Mater. Today* **2018**, *11*, 1–12, doi:10.1016/j.apmt.2017.12.011.
164. Farbod, K.; Nejadnik, M.R.; Jansen, J.A.; Leeuwenburgh, S.C.G. Interactions Between Inorganic and Organic Phases in Bone Tissue as a Source of Inspiration for Design of Novel Nanocomposites. *Tissue Eng. Part B Rev.* **2014**, *20*, 173–188, doi:10.1089/ten.teb.2013.0221.
165. Ren, L.; Tsuru, K.; Hayakawa, S.; Osaka, A. Novel Approach to Fabricate Porous Gelatin–Siloxane Hybrids for Bone Tissue Engineering. *Biomaterials* **2002**, *23*, 4765–4773, doi:10.1016/S0142-9612(02)00226-0.
166. Gabrielli, L.; Connell, L.; Russo, L.; Jiménez-Barbero, J.; Nicotra, F.; Cipolla, L.; Jones, J.R. Exploring GPTMS Reactivity against Simple Nucleophiles: Chemistry beyond Hybrid Materials Fabrication. *RSC Adv* **2014**, *4*, 1841–1848, doi:10.1039/C3RA44748K.
167. Negahi Shirazi, A.; Fathi, A.; Suarez, F.G.; Wang, Y.; Maitz, P.K.; Dehghani, F. A Novel Strategy for Softening Gelatin–Bioactive-Glass Hybrids. *ACS Appl. Mater. Interfaces* **2016**, *8*, 1676–1686, doi:10.1021/acsami.5b09006.
168. Blaker, J.J.; Maquet, V.; Boccaccini, A.R.; Jérôme, R.; Bismarck, A. Wetting of Bioactive Glass Surfaces by Poly(α-Hydroxyacid) Melts: Interaction between Bioglass® and Biodegradable Polymers. 13.
169. Backes, E.H. Analysis of the Degradation During Melt Processing of PLA/Biosilicate® Composites. **2019**, 12.
170. Li, J.; Huang, Z.; Li, B.; Zhang, Z.; Liu, L. Mobilization of Transplanted Bone Marrow Mesenchymal Stem Cells by Erythropoietin Facilitates the Reconstruction of Segmental Bone Defect. *Stem Cells Int.* **2019**, *2019*, 1–13, doi:10.1155/2019/5750967.

List of publications and communications

Publications:

- **Houaoui, A.**; Szczodra, A.; Lalluka, M.; El-Guermah L.; Agniel R.; Pauthe E.; Massera J.; and Boissière M. (**2021**). New generation of hybrid materials based on gelatin and bioactive glass particles for bone tissue regeneration. **Biomolecules, Special Issue Bioactive Glasses Applications,** 11(3), 444.

- **Houaoui, A.**; Lyyra, I.; Agniel, R.; Pauthe, E.; Massera, J.; & Boissière, M. (**2020**). Dissolution, bioactivity and osteogenic properties of composites based on polymer and silicate or borosilicate bioactive glass. **Materials Science and Engineering: C**, 107, 110340.

- Nommeots-Nomm, A.; **Houaoui, A.**; Packiyanathar, A. P.; Chen, X.; Hokka, M.; Hill, R.; ... & Massera, J. (**2020**). Phosphate/oxyfluorophosphate glass crystallization and its impact on dissolution and cytotoxicity. **Materials Science and Engineering: C**,117, 111269.

- Rodriguez-Ruiz, V.; Salatti-Dorado, J. Á.; Barzegari, A.; Nicolas-Boluda, A.**; Houaoui, A.**; Caballo, C.; ... & Pavon-Djavid, G. (**2018**). Astaxanthin-loaded nanostructured lipid carriers for preservation of antioxidant activity. **Molecules**, 23(10), 2601.

Book Chapter:

- **Houaoui, A.**; Massera, J. **Bioactive glasses in orthopedics.** Biofabrication for Orthopedics, Wiley-VCH, accepted in september 2021

Oral Communications:

- **Houaoui A.**; Massera J.; Boissière M.; Pauthe E. Composite & hybrid strategies based on Bioactive Glass; toward optimised substitute for bone bioengineering. World Biomaterials Congress, December 2020, Glasgow, Scotland

- **Houaoui A.**; Massera J.; Boissière M.; Pauthe E. Composite & Hybrid (Bio)materials based on bioactive glass: toward optimized substitute for bone bioengineering. 27th Biomaterials

in Medicine and Veterinary Medicine, Polish Society for Biomaterials, Octobre 2019, Rytro, Poland

- **Houaoui A.**; Boissière M.; Massera J.; Pauthe E. Elaboration of a hybrid osteopromotive biomaterial with a hierarchical porosity for bone tissue engineering. Summerschool Tissue Engineering and Regenerative Medicine, june 2018, Bordeaux, France.

- **Houaoui A.**; Boissière M.; Massera J.; Pauthe E. Engineering of an innovative biomaterial based on a polymer/bioactive glass composite for bone tissue application. Congrès BIOMAT, june 2017, Ambleteuse, France.

Poster Presentations:

- **Houaoui A.;** Massera J.; Boissière M.; Pauthe E. Composite and hybrid materials based on bioactive glass, toward optimized substitutes for bone regeneration. 31st Conference of the European Society for Biomaterials, september 5-9 2021, Porto, Portugal.

- **Houaoui A.;** Lukasik K.; Agniel R.; Massera J.; Boissière M.; Pauthe E. Elaboration and characterization of a hybrid material based on gelatin/13-93 bioactive glass for bone tissue engineering. BIOMAT Congress, june 3-7 2019, La Grande Motte, France.

- **Houaoui A.;** Lyyra I.; Boissière M.; Massera J.; Pauthe E. Synthesis and characterization of an innovative composite based on polymer and silicate or borosilicate bioactive glass for bone tissue engineering. Scientific day of the doctoral school, may 14 2018, Neuville-sur-Oise, France.

- **Houaoui A.;** Lyyra I.; Boissière M.; Massera J.; Pauthe E. Elaboration and characterization of an innovative composite based on polymer/bioactive glass for bone tissue engineering. 20th French Days of Biology of Mineralized Tissues, march 21-23 2018, Monaco.

Annexes

Materials Science & Engineering C 107 (2020) 110340

Contents lists available at ScienceDirect

Materials Science & Engineering C

journal homepage: www.elsevier.com/locate/msec

Dissolution, bioactivity and osteogenic properties of composites based on polymer and silicate or borosilicate bioactive glass

A. Houaoui[a], I. Lyyra[b], R. Agniel[a], E. Pauthe[a], J. Massera[b], M. Boissière[a,*]

[a] ERRMECe, Equipe de Recherche sur les Relations Matrice Extracellulaire-Cellules (EA1391), Biomaterials for Health Research Group, Institut des matériaux I-MAT (FD4122), Université de Cergy-Pontoise, Maison Internationale de la Recherche (MIR), rue Descartes, 95001, Neuville sur Oise Cedex, France
[b] Laboratory of Biomaterials and Tissue Engineering, Faculty of Medicine and Health Technology, Tampere University, Korkeakoulunkatu 3, 33720, Tampere, Finland

ARTICLE INFO

Keywords:
Bioactive glass
Composite material
Osteogenic differentiation

ABSTRACT

Bioactive glass (BAG)/Poly (Lactic Acid) (PLA) composites have great potential for bone tissue engineering. The interest in these materials is to obtain a scaffold with tailorable properties bringing together the advantages of the composites' constituents such as the biodegradability, bioactivity and osteoinduction. The materials studied are PLA/13–93 and PLA/13-93B20 (20% of SiO_2 is replaced with B_2O_3 in the 13–93 composition). To characterize them, they were dissolved in TRIS buffer and Simulated Body Fluid (SBF) in vitro. Over the 10 weeks of immersion in TRIS, the ion release from the composites was constant. Following immersion in SBF for 2 weeks, the hydroxyapatite (HA) layer was found to precipitate at the composites surface. By adding Boron, both these reactions were accelerated, as the borosilicate glass dissolves faster than pure silicate glass alone. Polymer degradation was studied and showed that during immersion, the pure PLA rods maintained their molecular weight whereby the composites decreased with time, but despite this the mechanical properties remained stable for at least 10 weeks. Their ability to induce osteogenic differentiation of myoblastic cells was also demonstrated with cell experiments showing that C2C12 cells were able to proliferate and spread on the composites. The Myosin Heavy Chain and Osteopontin were tracked by immunostaining the cells and showed a suppression of the myosin signal and the presence of osteopontin, when seeded onto the composites. This proves osteoinduction occurred. In studying the mineralization of the cells, it was found that BAG presence conditions the synthesizing of mineral matter in the cells. The results show that these composites have a potential for bone tissue engineering.

1. Introduction

Bioresorbable polymers have been used widely in the past decades as pins, plates and screws in orthopaedic, cranial and oral surgery [1–4]. The bioresorption of the implants enables leaving the fixation in place until it degrades in the body, releasing non-toxic dissolution by-products which are then metabolised [5]. However, the bioresorbable polymers developed thus far clinically, are found to degrade at slow rate and lack osteoconductive properties [1,6]. Bioceramics are a class of materials grouping all traditional nearly inert ceramics such as, Al_2O_3 and ZrO_2, and include calcium phosphate ceramics and silicate bioactive glass (BAG). These demonstrate properties extending from bioresorbable to bioactive class A. Clinically, β-TCP (bioresorbable) and synthetic hydroxyapatite (HA) (bioactive) are the more widely used traditionally [1,7,8], but their slow dissolution rate is a limiting factor [9,10]. Indeed, concerns have been addressed pertaining to the limited resorption of those ceramics, in-vivo, when used in cements [11]. BAG is a sub-category of ceramics showing not only osteoconduction, as in synthetic HA, but also osteoinduction [12]. These glasses are commercialized mainly for hard tissue reconstruction, but they also show significant ability to bond to soft tissue [13]. However, shaping the glass into its final shape is, as for all ceramics, challenging.

The quest for bioresorbable implants which are osteoconductive for use in the treatment of traumas in the skeletal system is still ongoing and presents significant challenges still. To overcome some of the drawbacks of single materials, composites have been developed. Here, the focus will be on polymer/BAG composites, as previous studies have demonstrated that fast release of ions from BAG compensated for the decrease in pH due to the rapid degradation of Poly (Lactic acid-co Glycolic Acid) (PLGA) [14]. By adding BAG to (Poly (D,L-Lactic Acid) (P(D,L)LA) or Poly (Lactide-co-Caprolactone) (PLCL)) the mechanical properties increases as well as precipitation of an HA layer at the

* Corresponding author.
E-mail address: michel.boissiere@u-cergy.fr (M. Boissière).

https://doi.org/10.1016/j.msec.2019.110340
Received 29 March 2019; Received in revised form 17 October 2019; Accepted 17 October 2019
Available online 24 October 2019

composite scaffold surface [15,16]. These studies used the solvent-casting method. Vergnol et al. developed composites based on P(L,DL)A/45S5 BAG. In this study, glass particles (3.5 μm average diameter) were mixed with polymer dissolved in acetone. The pellets obtained were then injected into molds at 145 °C and 150 bars of pressure. The presence of the BAG not only increased the rate of degradation of the polymer, but also significantly promoted new bone formation in this animal study [17]. However, there was a large loss in polymer molecular weight reported over the course of the sample processing. The decrease in molecular weight could not only be assigned to the processing temperature but also to the presence of the BAG particles [18]. The mechanical properties of the scaffold were also found to decrease drastically over the short immersion time in vitro. The loss in mechanical properties seemed to be correlated with the loss in the mineral phase, which is assumed to be fast given the rapid dissolution rate of the small BAG particles. Another study by Niemelä et al. presents self-reinforced composites based on P(L,DL)A/13–93 BAG, made by twin-screw extrusion at temperatures varying between 190 and 195 °C. In this study, the particle size was between 50 and 125 μm. It is noteworthy, that not only 13–93 is slower dissolving than 45S5 (at similar particle size), but also the larger particle size will further slowdown the dissolution rate of the inorganic phase [19,20]. Degradation of the self-reinforced composites was evaluated in PBS and the results supported the effect of glass dissolution on the polymer degradation rate [19]. The 13–93 particles contained in the self-reinforced composite create a porosity which induces a degradation of the polymer due to acidic dissolution products coming from the environment. The use of 13–93 in the composites appeared to retain higher polymer molecular weights than when using faster dissolving glasses such as 45S5 or S53P4. To overcome the slow dissolution rate of 13–93, boron can replace the silica in the structure, yielding a borosilicate glass. The resulting borosilicate and borate glasses, based on the 13–93 composition, show faster in-vitro dissolution and also faster conversion into HA [21,22]. While high boron content was associated with a decrease in the cell proliferation rate, it was also found to stimulate osteogenic commitment and upregulate endothelial markers [22]. In-vivo and in-vitro studies have shown the promising nature of borosilicate glasses [19,23]. The use of borate and borosilicate glasses as a secondary phase in a polymeric matrix has not yet been widely studied. Taino et al. produced PLCL (Poly(L-lactide-co-ε-caprolactone)/borosilicate glass composites, with varying content of 125–250 μm glass particles using the solvent-casting method. These scaffolds were then foamed by supercritical CO_2. Degradation of the polymer was linked to the dissolution of the glass [15].

Marquardt et al. studied the processing of fibrin/borate glass composites obtained by mixing fibrin with glass microfibers 0.5–10 μm diameter, or with rods of 50–200 μm diameter which were placed on a fibrin scaffold prior to polymerization. The materials obtained were able to support directed axon growth [24].

However, the effect of boron substitution for silica, in the glass composition, on the composite physico-chemical properties and cell/material interaction has not yet been studied. Added to this, based on previously reported results, the use of glass 13–93 and its boron-containing counterpart might be suitable in maintaining polymer integrity and composite mechanical properties in-vitro while supporting osteogenesis. Therefore, we have developed PLA/BAG composites using 13–93 as control and 13–93B20 with 20% SiO_2 replaced by B_2O_3. To investigate the in vitro dissolution behavior of our composites, they were immersed in TRIS buffer solution. Ion release from the glass and change in the polymer molecular weight were quantified. The mechanical properties of the composites were studied during the immersion. The bioactivity, assumed to be related to the precipitation of a HA layer at the surface of the material when immersed in aqueous solution, was assessed in Simulated Body Fluid (SBF), the procedure usually used for testing BAG [25]. Preliminary cell experiments were done to assess cell activity and ability of these two BAG to promote osteogenesis by culturing C2C12 myoblastic cells at the surface of composite discs. Cell proliferation and morphology were studied as well as presence of myosin and/or osteopontin which were tracked by immunostaining. C2C12 cells capacity to synthesize their mineral matrix was analyzed with Alizarin Red S staining. The aim of this study was to assess if these cells were able to commit to an osteoblastic lineage in presence of the BAG.

2. Experimental

2.1. Material preparation and characterization

2.1.1. Bioactive glass (BAG) preparation

BAG 13–93 and 13–93B20 were prepared from analytical grade K_2CO_3 (Alfa Aesar, Haverhill, USA), (Na_2CO_3, $NH_4H_2PO_4$, ($CaHPO_4$) ($2(H_2O)$), $CaCO_3$, MgO, H_3BO_3 (Sigma Aldrich, Saint-Louis, MS, USA) and Belgian quartz sand. The 100-g batches of 13–93 and 13–93B20 were melted for 3 h in a platinum crucible at 1425 °C and 1275 °C, respectively. The molten glasses were cast, annealed, crushed and finally sieved into 125–250 μm particles. The glasses were dried at 125 °C for 2 h before use. The nominal oxide compositions of the glasses are given in Table 1.

2.1.2. Sample fabrication

Medical grade Poly(Lactic Acid) (PLA) with a (L/DL) ratio of 70/30, with an inherent viscosity of 4.0 dl/g was obtained from Evonik Nutrition & Care GmbH (Essen, Germany). PLA, PLA/13–93 and PLA/13-93B20 rods were produced by melt-extrusion using a co-rotating twin-screw extruder (Mini ZE 20*11.5 D, Neste Oy, Porvoo, Finland) under nitrogen atmosphere (Fig. 1). The feed rates for the PLA and the BAG were fixed to 140 g h^{-1} and 60 g h^{-1} respectively to obtain approximately 70 wt % of polymer and 30 wt % of glass in the composite. The processing temperatures and pressures are presented in Table 2. The polymer took about 5 min to produce in the extruder including melting and producing the final product. The production time is less when the extruder is filled in advance.

A 4 mm nozzle was used and the rods were pulled using a caterpillar. The speed of the caterpillar was adjusted to obtain 3 mm diameter rods.

The rods of each composition (PLA as a control; PLA/13–93; PLA/13–93 B20) were analyzed by Thermogravimetric Analysis (NETZSCH, Leading Thermal Analysis, STA449F1) to measure their glass content. All tests were performed in an Alumina (Al_2O_3) crucible and in a N_2 atmosphere. 10 mg of sample were heated from 25 °C to 1100 °C at a rate of 10 °C/min. This measurement was repeated on 5 samples for each composite and the average glass content with standard deviation was calculated.

2.2. Behavior of the PLA/BAG composites

2.2.1. Physico-chemical properties of the composites

2.2.1.1. Immersion in TRIS. Tris(hydroxymethyl)aminomethane (TRIS) solution (50 mM) was prepared by mixing ultra-pure TRIS (MP Biomedicals) and TRIS-HCl (Sigma Aldrich) in ultra-pure water and the pH was adjusted to 7.4 at 37 °C. The rods were cut into lengths of 7 cm (≃650 mg) which were immersed in 12 mL of TRIS solution for up

Table 1
Nominal glass composition (mol%).

Glass	mol%						
	Na_2O	K_2O	MgO	CaO	P_2O_5	SiO_2	B_2O_3
13–93	6.0	7.9	7.7	22.1	1.7	54.6	–
13–93B20	6.0	7.9	7.7	22.1	1.7	43.7	10.9

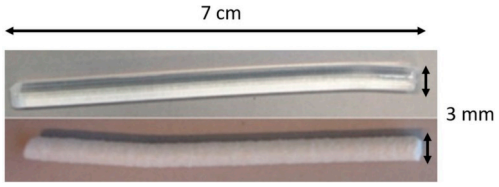

Fig. 1. PLA rod (up) and composite rod (down) obtained after extrusion.

Table 2
Materials processing parameters.

	Temperature (°C)			Pressure (psi)
	Cylinder	Adapter	Die	
PLA rods	200	230	230	200
PLA/13–93	190	200	220	150
PLA/13-93B20	185	220	215	200

to 10 weeks at 37 °C in a shaking incubator (HT Infors Multitron) at an orbital speed of 100 rpm. To avoid saturation of the solution with the ions released from the composite, the TRIS buffer was refreshed each week.

At set times after immersion, the concentration of elements released from the composites was studied by diluting 5 mL of the immersion solution in 45 mL of ultra-pure water for ion analysis. ICP-OES (Agilent technologies 5110) was employed to quantify P (λ = 253.561 nm), Ca (λ = 422.673 nm), Mg (λ = 279.553 nm), Si (λ = 250.690 nm), B (λ = 249.678 nm), K (λ = 766.491 nm) and Na (λ = 589.592 nm) concentrations in the solution after sample immersion. Measurements were made on four separate samples at each set time for each composite and the results presented as mean ± standard deviation (SD). The rods were then rinsed with acetone and dried.

2.2.1.2. Rod cross section analysis. After immersion in TRIS, the samples were embedded in resin and then polished to observe their cross section using Scanning Electron Microscopy (SEM - GEMINISEM 300 from Zeiss).

2.2.1.3. Molecular weight of the polymer. Molecular weights of PLA after the samples processing and at various immersion times were determined by Gel Permeation Chromatography (GPC) (Merck Hitachi Lachrom 7000 series) consisting of a pump, a refractive index detector and two Waters Styragel columns (HR5E and HR1). Tetrahydrofuran (THF) was used as eluent at a flow rate of 1 mL/min at 35 °C. For each material, an amount of ≃7,5 mg of polymer (cross-section of the rod) was weighed and immersed in 5 mL of THF until complete dissolution. The solution was then filtered and analyzed. Molecular weights were calibrated using polystyrene standards. The measurements were conducted in four separate samples at each time points for each composition and the results are presented as mean ± SD.

2.2.1.4. Mechanical properties of the composites. The mechanical properties of the composite rods post-processing and after immersion (wet) were tested on the Instron 4411 (Instron Ltd., High Wycombe, UK) using a 3-point bending and shear test at room temperature. At least four parallel samples of each composite type were tested. For the bending test, the properties were studied with a crosshead speed of 5 mm min^{-1} and a bending span of 42 mm. For the shear test [26], the crosshead speed was 3 mm min^{-1}. The measurements were conducted in the four samples at each set point for each composite and the results are presented as mean ± SD.

2.2.2. Composites bioactivity

2.2.2.1. Immersion in Simulated Body Fluid (SBF). SBF was prepared following the methodology [27] from the standard ISO/FDIS 23317 as described by Kokubo et al. The samples were cut to obtain rods of 7 cm (≃650 mg) which were immersed in 12 mL SBF solution for up to 2 weeks at 37 °C in a shaking incubator (HT Infors Multitron) with at a speed of 100 rpm. During the experiment, the solution was not refreshed so that calcium phosphate could be measured. The ion concentration in the solution according to immersion time was measured as previously described. Measurements were made on four separate samples at each set time for each composite and the results presented as mean ± SD.

2.2.2.2. Rod surface analysis. The reactive layer at the rod surface after immersion in SBF was observed by SEM (GEMINISEM 300 from Zeiss) and its composition was analyzed by Energy-Dispersive X-ray spectroscopy (EDX Quantax from BRUKER). The Infrared (IR) absorption spectra of the composites immersed in SBF were also recorded using a Bruker Alpha FTIR in Attenuated Total Reflectance (ATR) mode to see the effect of the dissolution on their structural properties. The measurements were performed on dry samples. All IR spectra were recorded within the range 399–4000 cm^{-1} with a resolution of 2 cm^{-1} and 32 accumulation scans.

2.2.3. Cell analysis

2.2.3.1. Disk preparation. PLA, PLA/13–93 and PLA/13-93B20 disks were obtained by compression molding (Nike Hydraulics ZB110, Eskilstuna, Sweden) of a piece of the rods for the cellular tests. The rods were compressed under 10–20 MPa pressure at 140 °C for 1 min, then the mold was cooled down with compressed air and 14 mm disks were cut from the plates obtained. These disks were then sterilized by gamma irradiation (25 kGy) at BBF sterilisations service GmbH (Germany). All experiments were performed in 24-well plates and the disks were washed with PBS prior to use.

2.2.3.2. Cell culture. Myoblastic C2C12 cells were cultured in DMEM Glutamax supplemented with 10% Fetal Bovine Serum (FBS) and 1% penicillin/streptomycin, in an humidified atmosphere of 5% CO_2 at 37 °C.

2.2.3.3. Cell proliferation and morphology. To compare the behavior of C2C12 cells on the different samples, cell proliferation was studied using CyQUANT Cell Proliferation Assay kit (Invitrogen, Life Technologies). Around 7700 cells/disk were seeded on the 14 mm disks in 24-well plate and the medium was changed every 2 days. Cleaned and sterilized microscope glass slides were used as controls. After 1, 2, 4 and 7 days of culture, the cells were lysed with 400 µL 0.1% Triton-X100 (Sigma–Aldrich) buffer and conserved at −80 °C. After one freeze–thaw-cycle, three 20 µl aliquots of each lysate were pipetted on to a black 96-well plate (Corning) and mixed with 180 µl working solution (CyQUANT GR dye and cell lysis buffer). The fluorescence was then measured at 520 nm with a Spectrofluorimeter Xenius XM (SAFAS).

The morphology of the cells on the different samples was observed after 48 h of culture. The same number of cells was seeded on the disks and after 48 h, the cells were fixed with 3% (w/v) para-formaldehyde solution dissolved in PBS (Sigma Aldrich) for 15 min, then permeabilized with 0.1% (v/v) Triton X-100 (Sigma Aldrich) for 10 min. Non-specific binding sites were blocked by incubating the disks in PBS containing 1% Bovine Serum Albumin (BSA) for 1 h. The cytoskeleton and nuclei of the cells were stained respectively with 1:500 FITC-labelled phalloidin (Sigma Aldrich P5282) and 1:1000 4′,6-Diamidino-2-phenylindole dihydrochloride (DAPI, Sigma Aldrich D9542) in PBS-BSA 0.5% for 1 h. Each incubation with antibodies was performed in the dark in a humid atmosphere. Samples were then washed in PBS-BSA 0.5%, mounted in Prolongold (Invitrogen), and observed under a LSM710 confocal microscope (Carl Zeiss).

2.2.3.4. Cell differentiation. The expression of a late myoblastic marker (myosin heavy chain) and an early osteoblastic marker (osteopontin) were studied using specific antibodies. Around 600C2C12 cells were seeded on the disks and cultured for 14 days. Cleaned and sterilized microscope glass slides were used as controls. Cells were then labelled with mouse anti-myosin heavy chain (MHC, 1:1000, Millipore 05716), and rabbit anti-osteopontin (1:500, Millipore AB10910) diluted in PBS containing 0.5% BSA. Primary antibodies are revealed using Alexa Fluor 488 or Alexa Fluor 568-conjugated goat anti-mouse or anti-rabbit antibodies both 1:400 in PBS-BSA 0.5% (Invitrogen) as secondary antibodies. Samples were observed using a LSM710 confocal microscope (Carl Zeiss).

Mineralization was also assessed at 10 days and 14 days using Alizarin Red S stain (the calcium minerals stain red). The staining from a previously described protocol was adjusted [28] in that cells were fixed with paraformaldehyde for 15 min at room temperature and stained with 2% Alizarin red S (pH 4.1–4.3; Sigma–Aldrich) for 20 min at room temperature. The excess color was washed away with three consecutive water washes after which the samples were observed under an optical microscope.

2.2.3.5. Statistical analysis. Data were analyzed using GraphPad Prism Software. Statistical significance between groups is assessed by one-way analysis of variance (ANOVA). Experimental results are expressed as means ± standard deviation. Statistical significance is taken for values of $p < 0.05$.

3. Results and discussion

The aim of this study was to develop a polymer-BAG composite able to release ions beneficial for bone regeneration while maintaining, post-processing, the mechanical properties and the molecular weight of the polymer. As it has been reported that it is difficult to produce a polymer-bioglass ® (i.e. 45S5) composite, we decided to incorporate BAG 13–93 into a PLA matrix. As reported by Brink et al. the dissolution rate of the glass 13–93 is much slower than the typical BAG used clinically (*i.e.* 45S5 (Bioglass®) and S53P4 (BonAlive®) [20]). To control glass dissolution, a second glass composite was tested [23], whereby 20% of the SiO_2 in the 13–93 composition was replaced with B_2O_3.

3.1. Characterization of the composites after processing

Table 3 presents the glass loading in each composite, with the mechanical properties of the composites and the molecular weight of the polymer included in each composite.

The targeted glass loading was 30 wt%. Thermogravimetric analysis was conducted (Fig. S1) to assess the true glass loading in the polymer matrix post-processing as well as the homogeneity of the processed rods. Glass loading was 38 ± 2 wt% and 35 ± 4 wt% for the PLA/13–93 and PLA/13-93B20, respectively, demonstrating good control over the process used to produce the composites.

Before extrusion, the molecular weight of the PLA granules was measured to be ~530 kDa. As expected, after extrusion, the molecular weight of the pure PLA decreased about 40%, while the PLA loaded with BAG decreased by ~50% regardless of the glass composition. The decrease of the molecular weight recorded is not as high as that reported in the literature. For example, Vergnol et al. show a decrease in molecular weight of ~90% when producing PLA-BAG composite processed by injection molding [17]. Moreover, the PLA/S53P4 composites were tested, but, during the processing the viscosity of the polymer drastically and rapidly decreased and the materials obtained were amber-like as reported by Vergnol et al. for the PLA/45S5. The reason for this rapid change in viscosity and subsequent thermal degradation of the PLA is not yet well understood. However, this phenomenon appears when processing PLA with fast reacting BAG and does not occur that readily with more stable glasses. Therefore, a hypothesis for the thermal degradation of PLA upon extrusion of composites using 45S5 and/or S53P4 may be due to the high intrinsic water content in the glass structure or the glass degradation/dissolution when in the polymer melts. The combination of PLA and the proposed BAG 13–93 processed by twin-screw reduces loss of molecular weight during melt processing.

The mechanical properties of the PLA and its composites were measured in 3-point bending and shear. Both composites have an almost stable flexural modulus in wet and dry conditions but show a decrease in shear stress in both conditions, when compared to the polymer alone. The changes in the mechanical properties are only a function of the glass loading but not due to the nature of the glass. The decrease in the shear strength was not unexpected, since polymer glass composites are known to become weaker, and tend to become more brittle, as can be seen by an increase in their elastic modulus. Here, the decrease in the flexural modulus indicates an increase in the ductility. Such behavior, was already reported in self-reinforced polymer/BAG filaments [26]. The loss in mechanical properties is probably due to the absence of chemical bonds between the glass and the polymer, leading to a loss of cohesivity.

3.2. Behavior of the composites in solution

3.2.1. Dissolution in TRIS

The co-degradation in TRIS of the polymer and glass was assessed by GPC and ICP-OES measurements and compared to that of the dissolution of the pure PLA rods. Fig. 2 presents the concentration in Si A), Na B), K C), B D), Mg E), Ca F) and P G) post immersion in TRIS for various times. As the immersion solution was refreshed every week the results are presented cumulatively and normalized to the sample mass. As expected, the PLA alone does not exhibit any change in ion concentration. Upon immersion of the composites, the concentration in solution of the different elements increases, indicating that the glass particles are being hydrated and dissolve through the polymer. As expected, the addition of boron to the glass structures leads to faster initial ion release (up to ~10 days). However, at longer immersion times all curves seem to plateau for solutions containing the PLA/13-93B20 composites whereas the dissolution of the glass in the PLA/13–93 composite remains almost linear. It should be noted that; especially at longer immersion times, the standard deviation was higher in the case of the polymer containing the glass 13–93B20 than 13–93.

Table 3
Measured glass loading, mechanical properties and average molecular weight of the processed PLA and PLA/BAG composites (for wet samples, the mechanicals properties were measured after 10min of immersion in TRIS).

Materials	Composites glass loading (wt %)	Young modulus (GPa)		Shear stress (MPa)		PLA Mw before extrusion (kDa)	PLA Mw after extrusion (kDa)
		Dry samples	Wet samples	Dry samples	Wet samples		
Bulk PLA	–	–	–	–	–	526 ± 7	–
PLA rods	–	3.5 ± 0.1	3.6 ± 0.2	46.6 ± 0.8	50.1 ± 1.4	–	305 ± 14
PLA/13–93 rods	38 ± 2	3.6 ± 0.3	3.3 ± 0.3	34.0 ± 2.0	32.3 ± 1.4	–	248 ± 5
PLA/13-93B20 rods	35 ± 4	3.6 ± 0.7	3.1 ± 0.4	32.1 ± 1.5	32.1 ± 1.1	–	251 ± 15

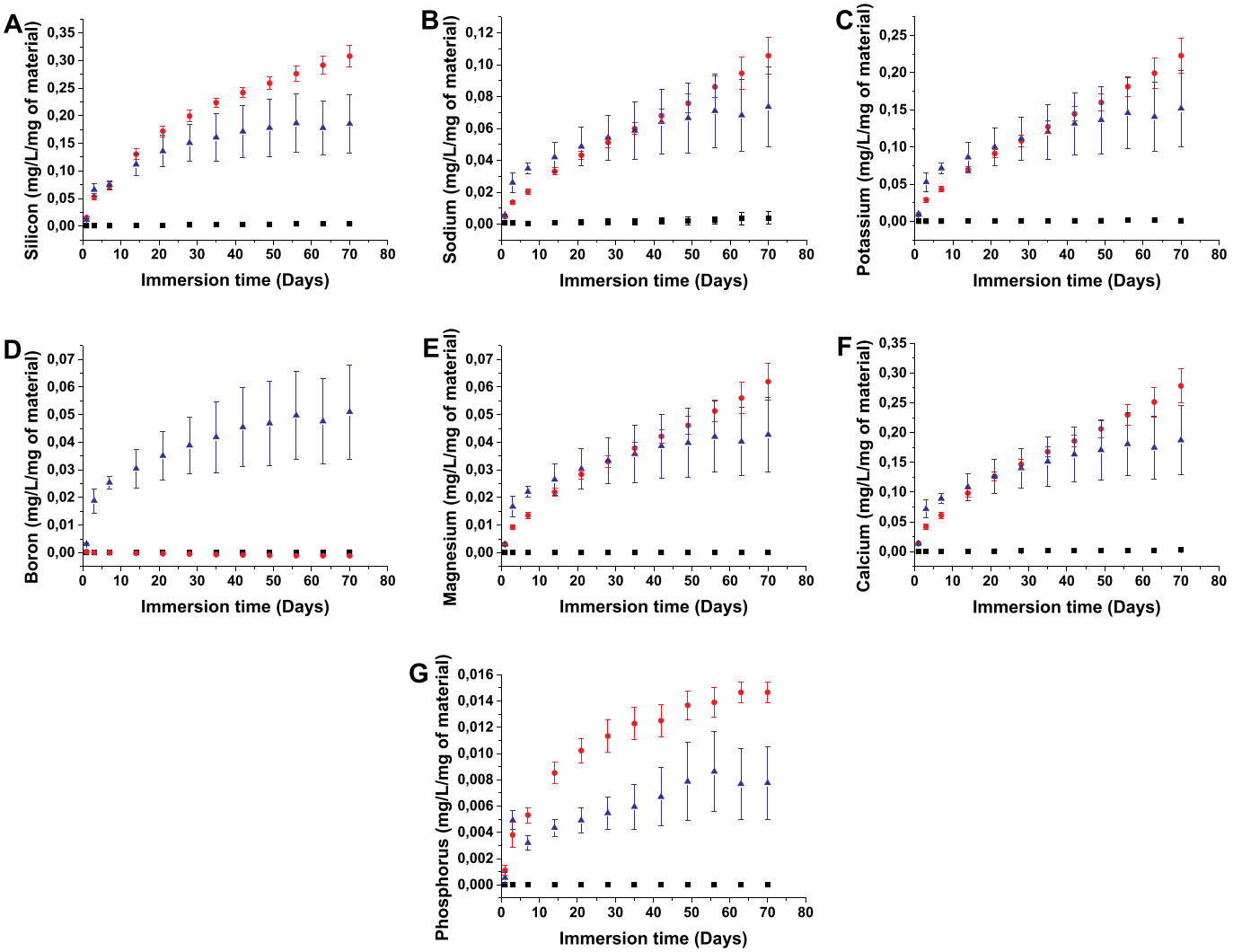

Fig. 2. Element concentrations of A) Si, B) Na, C) K, D) B, E) Mg, F) Ca and G) P in the dissolution products of PLA (■), PLA/13–93 (●) and PLA/13-93B20 (▲) immersed in TRIS according to time.

It is a known fact that upon immersion of a silicate glass in aqueous solution, initially ion exchange occurs followed by condensation and re-polymerization of a silica-rich layer [12]. If this layer is not uniformly formed at the surface of all glass particles, variations in ion release can be expected. All ion concentrations were normalized to the element contained in the starting rod to show clearly the extent of ion release.

Fig. 3A) presents the percentage of ion released from glass 13–93 in TRIS solution. It is clear that glass dissolution is limited, whereby at 70 days less than 5% of each element is released into the solution. While the Si and P release seems to level-off at immersion times > 20 days, all other constituents, *i.e.* Na, Ca, Mg and K seemed to be leached-out in an almost linear manner up to 70 days. Fig. 3B) presents the release of ion from the glass 13–93B20, in % of initial mass of the elements. As seen in the case of the composites containing the glass 13–93, all ions are found

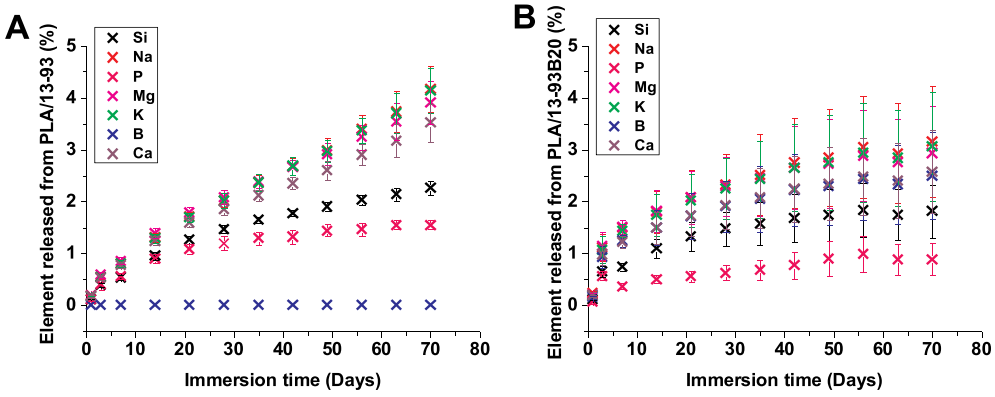

Fig. 3. Release of ions from the A) PLA/13–93 and B) the PLA/13-93B20, immersed in TRIS according to time.

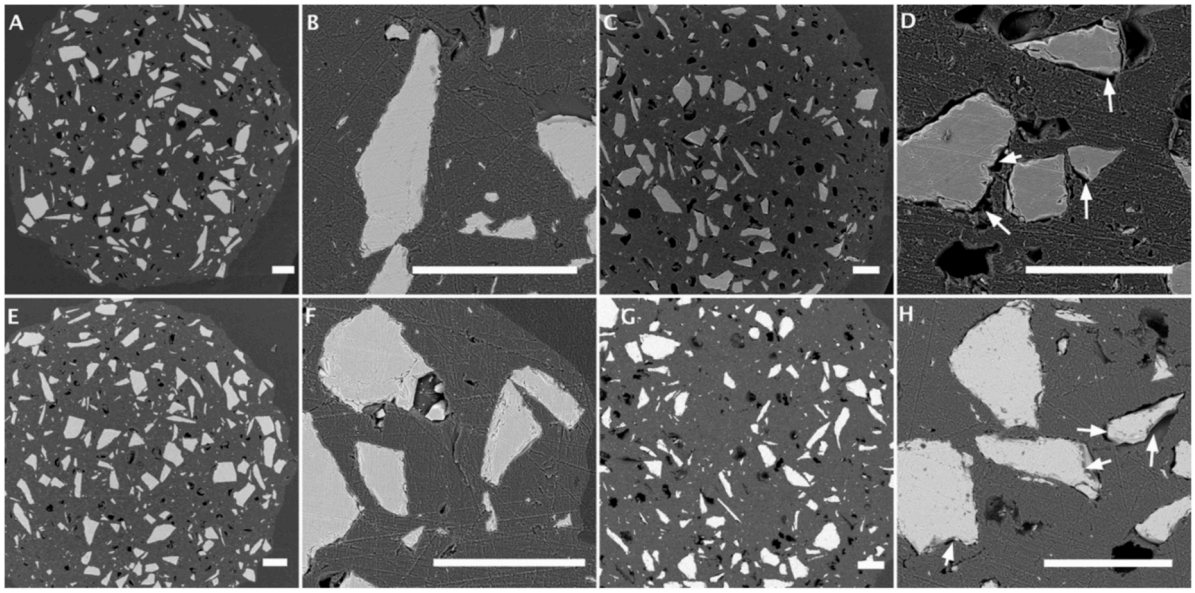

Fig. 4. Observations of the cross section of the composites by SEM. A) and B) show the PLA/13–93 before immersion, C) and D) show the PLA/13–93 after 10 weeks of immersion in TRIS. E) and F) present the PLA/13-93B20 before immersion and G) and H) show the PLA/13-93B20 after 10 weeks of immersion in TRIS. Scale bar 200 μm.

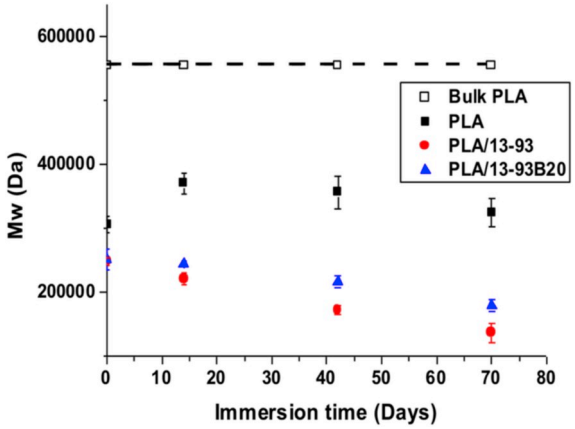

Fig. 5. Molecular Weight (Mw) of PLA before extrusion (□) PLA (▮), PLA/13–93 (●) and PLA/13-93B20 (▲) rods immersed in TRIS according to time.

to leach out into the solution. However, the difference in the dissolution profile of ions from the composites containing the glass 13–93B20 compared to ion release from composites containing the glass 13–93, is of interest.

1. While in Fig. 3A) the Ca, K, Mg and Na dissolve, from the glass 13–93, at similar rate, a slower release of Ca was measured during dissolution of composites containing the glass 13–93B20 (Fig. 3B). Furthermore, Ca release follows a similar dissolution profile to B as shown in Fig. 3B).
2. The initial release rate for all ions is faster for composites containing the glass 13–93B20. However, at extended immersion time (> 15 days) a decrease in the release rate of all ions can be seen; whereas when immersing composites containing the glass 13–93 (Fig. 3A) only Si and P release rate slows down at extended immersion time, while all other ions show a linear release.
3. The final ion release content in the solution (at 70 days) is slightly lower in the case of the composite containing the glass 13–93B20 than in that containing the glass 13–93.

From the literature many interactions between the B_2O_3 and SiO_2 in the glass were reported to happen. Some are reported below [29–32]:

$$2Si–O^- + B–O–B \rightarrow Si–O–Si + 2B–O^- \quad (1)$$

$$Si–O^- + B–O–B \rightarrow Si–O–B + B–O^- \quad (2)$$

However, those reactions were not sufficient to explain the physical, thermal and structural changes associated with the substitution of the SiO_2 with B_2O_3. In depth structural analysis showed preferential interaction between CaO and B_2O_3 as follow [33]:

$$BO_3 + CaO \leftrightarrow BO_4 \quad (3)$$

More recently, Yu et al. reported the medium-range structural organization of phosphorus bearing borosilicate glasses and the consequence of B/Si substitution [34]. Their findings support the increase in the polymerization of the silica network with increasing substitution ratio. Furthermore, they demonstrated a higher affinity of the phosphorus to bond with B rather than with Si. Therefore, while in typical silicate glass the majority of the phosphorus is present as Q^0 (zero bridging oxygen atom per PO_4 unit), an increase in Q^1 units, bridging one oxygen atom per PO_4 unit, was evidenced. Overall, the structural modification occurring in the glass network when substituting Si for B is in agreement with the dissolution behavior observed in Fig. 3A) and B), i.e. boron and calcium are released at the same rate (Fig. 3B) as typically seen in a congruent dissolution. Thus, it appears that the calcium preferentially interacts with the boron sub-network (congruent dissolution) rather than with the silicate sub-network (non-congruent dissolution). The lower, overall release of the ions (at long immersion time) is most likely related to the increase in the degree of polymerization of the silica network as shown in equations (1) and (2), where the number of non-bridging oxygen is expected to decrease with increasing the boron content. However, such structural analysis does not fit the dissolution behavior reported in the literature, which tend to demonstrate that the addition of B_2O_3 at the expense of SiO_2 should increase the glass dissolution rate [35–38]. It is therefore possible to assume that either the increase in Si–O–Si bridges is associated with a disproportionation of the silicate structure, whereby, $2Q^2 \leftrightarrow Q^1 + Q^3$, and/or Si–O–B bridges form between the borate and silicate units. Both assumptions would be consistent with the increase in the initial dissolution rate of the glass in the composite containing the glass 13–93B20 and a progressive decrease in the ion release rate due to

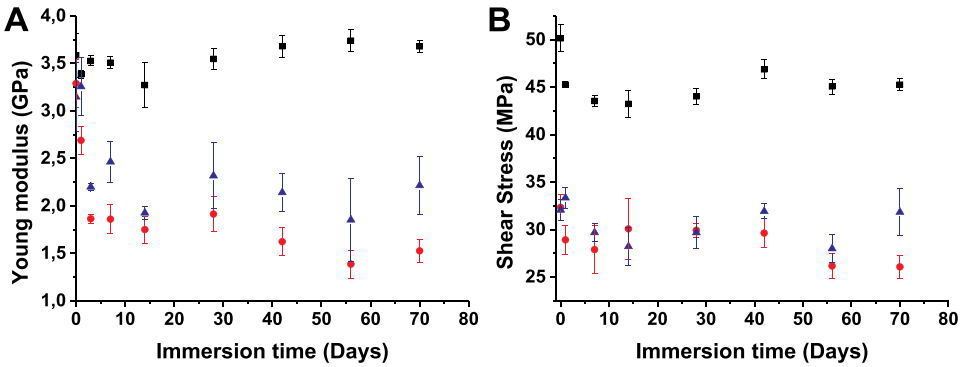

Fig. 6. A) Young modulus reported from the bending test and B) Shear stress of wet PLA (■), PLA/13–93 (●) and PLA/13-93B20 (▲) rods according to immersion time in TRIS.

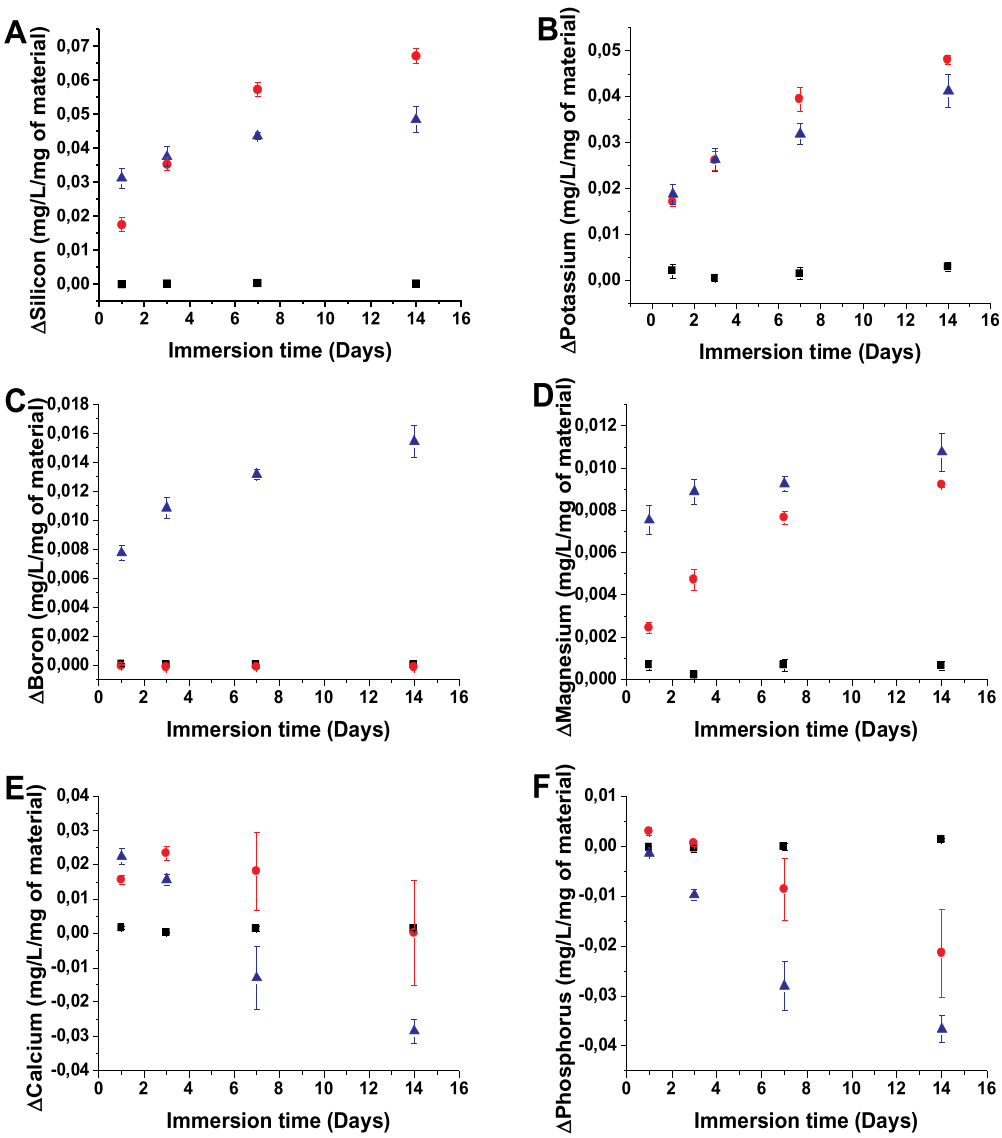

Fig. 7. A) Si, B) K, C) B, D) Mg, E) Ca and F) P element concentrations released in SBF from the PLA (■), PLA/13–93 (●) and PLA/13-93B20 (▲) according to immersion time. ΔElement = [Element] in SBF in presence of the sample – [Element] in SBF initial solution.

remnants of a more stable silicate. As seen in Fig. 3A) and B), this leads to a higher ion concentration in the solution containing the borosilicate glass at a short immersion time, and saturation occurring at an earlier time than in the case of traditional silicate BAG such as 13–93. Finally, the increased linkages between the phosphorus structural unit and the more stable BO_4 units proposed by Yu et al. [34] is confirmed by the lower phosphorus release profile in the case of the glass 13–93B20 than in 13–93.

Fig. 4 shows the cross sections of the composites before and after 10 weeks of immersion in TRIS. Before immersion, the BAG granules are fixed and appear to be maintained by the PLA matrix. After 10 weeks in TRIS, they are seen to be detached from the polymer, regardless of the glass composition, as expected post surface dissolution of the glass particles.

At the same time, the change in the polymer molecular weight was assessed according to time and is presented in Fig. 5. Although the extrusion process affected the PLA molecular weight (Mw), it does not seem to be impacted by the interaction with the medium after

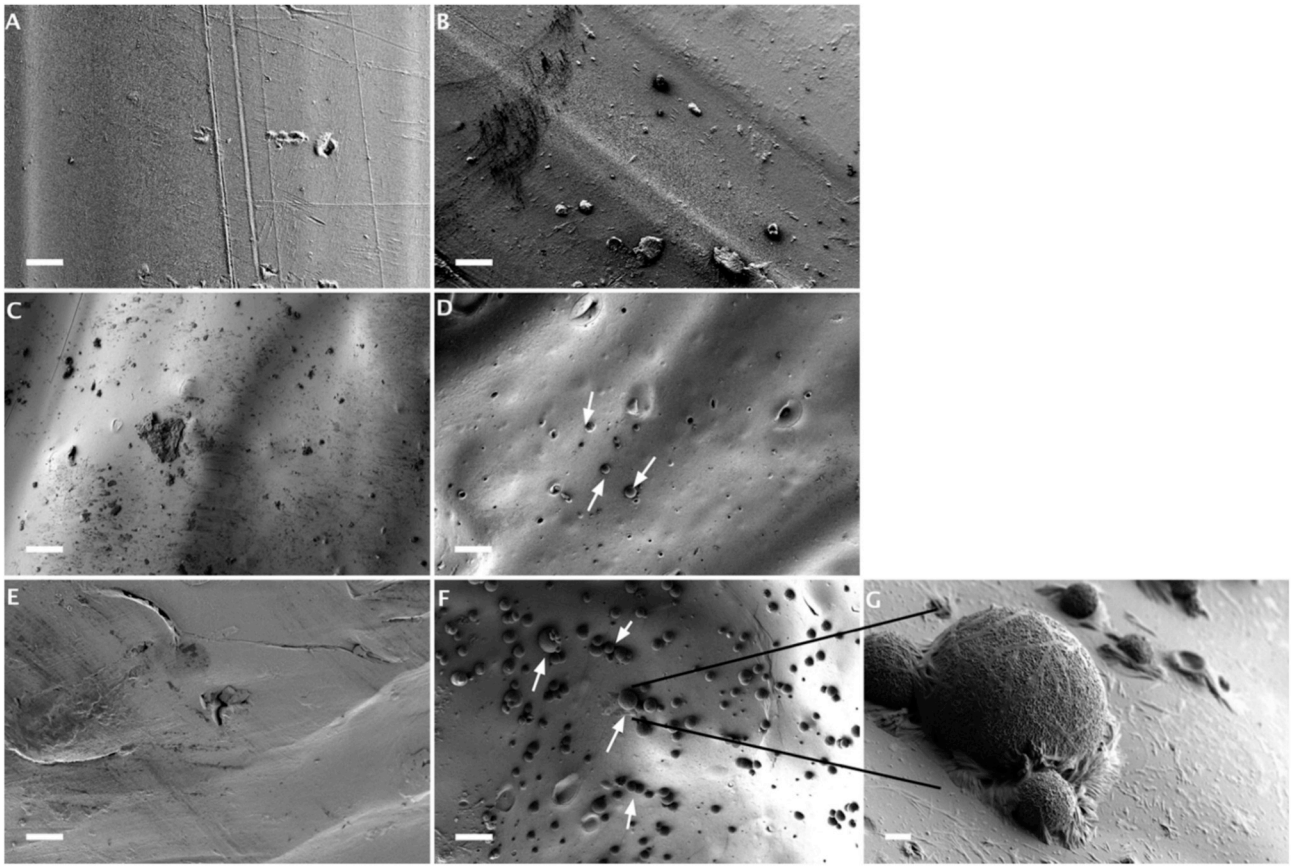

Fig. 8. Surface observations and analysis by SEM-EDX and FTIR of the PLA and the composites. A) and B) show the surface of the PLA before and after 2 weeks of immersion in SBF respectively. C) and D) represent the PLA/13–93 before and after 2 weeks of immersion in SBF. E) and F) show the PLA/13-93B20 before and after 2 weeks of immersion in SBF (Scale bar 20 μm) and G) represents the nodules found on the PLA/13-93B20 after 2 weeks in SBF (Scale bar 2 μm).

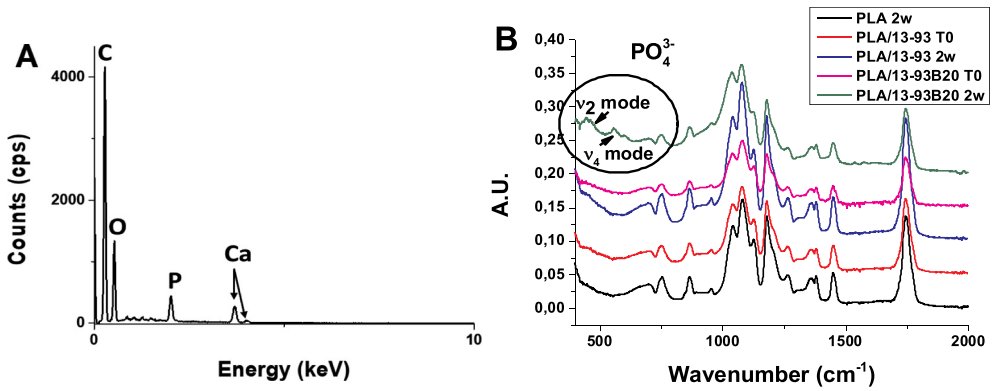

Fig. 9. A) EDX analysis of the nodules found on PLA/13-93B20 surface and B) FTIR analysis of the sample surfaces before and after 2 weeks of immersion.

immersion for up to 10 weeks. However, slow but linear molecular weight decrease is apparent during immersion of the composite. The composite containing the BAG 13–93, showed the fastest PLA degradation with a loss of ~45% of its molecular weight post-extrusion at 10 weeks at a rate of 1710 ± 96 Da/day (R^2 = 0.99).

The composite containing the BAG 13–93B20 showed a slower decrease, of ~29% of its original molecular weight after 10 weeks of immersion at a rate of 1133 ± 82 Da/day (R^2 = 0.98). In both cases, the degradation of the polymer is due to the interaction between glass dissolution by-products and PLA, most likely by alkaline hydrolysis of ester bonds at the glass/PLA interface [39]. Such behavior was, however, not reported by Maquet et al. with the dissolution of bioglass®-filled polylactic foams but occurred during dissolution of PLA/BAG composite in vivo [16,17]. Added to this, the difference in PLA degradation can be related to the more sustained ion release in the case of the composite containing the glass 13–93 as seen in Fig. 3.

The mechanical properties (Young modulus and Shear stress) were measured on wet samples as a function of immersion time (Fig. 6). While no significant changes in shear stress, within the accuracy of the measurement, were recorded, a net fall in the Young modulus can be seen after immersion for up to three days. As all the measurements were corrected to the swelling of the sample, such a drop can be attributed to the diffusion of water within the composite structure, most likely due to pores being formed during the processing. After the initial drop, the Young modulus does not seem to be, drastically, impacted by either the glass or the polymer dissolution/degradation.

Upon immersion of composites in TRIS buffer solution, a decrease in the average molecular weight was measured. However, in this study

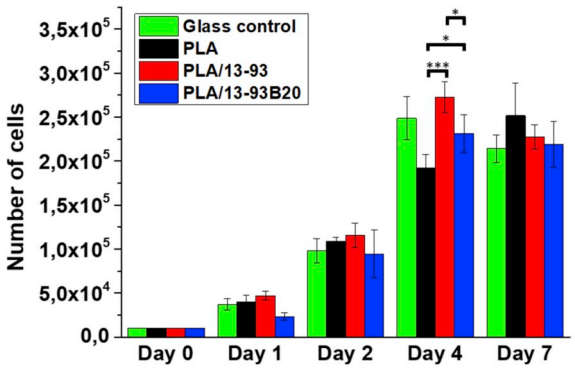

Fig. 10. Proliferation of C2C12 cells cultured in DMEM complete medium on glass, PLA, PLA/13–93 and PLA/13-93B20 for 7 days, analyzed with a CyQUANT Cell Proliferation Assay kit, ***p < 0.001, *p < 0.05.

and in agreement with data reported by Vergnol et al., the decrease of the PLA molecular weight alone could not be correlated to changes in the mechanical properties [17]. Yet, in Vergnol et al., a decrease in mechanical properties was recorded upon immersion of the BAG/PLA composite. The loss in mechanical strength is directly related to the composite mass loss with regards to the immersion time. Therefore, the dissolution of mineral phase dictated the change in mechanical properties. In our study, the larger particle size of BAG with slower dissolution rate than in Vergnol et al.'s work were used [17]. The low dissolution rate of the BAG used in this study implies that the composite keeps its integrity for at least 10 weeks.

The immersion of the composites in TRIS helped to understand the dissolution of both composites in solution. The 13–93B20 dissolves faster initially than the 13–93 and saturates more quickly to the same level as the 13–93 in the end. This dissolution leads to the decrease of the polymer molecular weight, but the mechanical properties stay almost stable.

3.2.2. Dissolution in SBF

Samples were also immersed in Simulated Body Fluid (SBF). As postulated by L.L. Hench, the ability of a material to induce the precipitation of an hydroxyapatite layer at its surface is considered to be a sign of bioactivity [12].

Immersion in SBF was conducted over a two weeks period and the solution was not refreshed. ICP-OES was used to quantify the ion concentration in the solution. The difference between the ion concentration in SBF and ion concentration post composite immersion was calculated (Fig. 7).

The elements Si, K, Mg and B (for the PLA/13-93B20) show similar trends when immersed in TRIS where the 13–93B20 glass leaches out its ions at a faster rate initially and then stabilizes. However, it is important to point out that i) the dissolution rate starts to slow down at an earlier immersion time in SBF than in TRIS and ii) while limited saturation was noticed, in the case of immersion of the PLA/13–93 in TRIS buffer solution, in SBF, saturation can also be seen for this glass. The Ca concentration seems to increase initially and then decreases with increasing immersion time, whereas the P concentration decreases constantly over dissolution time. Generally, the decrease in Ca and P in SBF is associated with the precipitation of a calcium-phosphate reactive layer. The decrease in Ca and P is faster and starts at earlier time when the composites containing BAG 13–93B20 are immersed, indicating a faster and more rapid precipitation of the reactive layer in the case of this material. This is most likely due to the faster initial dissolution.

The precipitation of a reactive layer at the surface of the rods was assessed by SEM/EDX and FTIR. Fig. 8) presents the SEM images of the PLA (A and B), PLA/13–93 (C and D) and PLA/13-93B20 (E, F and G) before and after 14 days of immersion in SBF.

While no significant change in the surface topography can be seen after immersion of the PLA in SBF, some spheres could be seen at the surface of the composites after 14 days. The spheres were small and sparsely dispersed at the surface of the composites containing the glass 13–93 (Fig. 8D), while higher density of larger spheres (with a wide size distribution) were covering the composites containing the glass 13–93B20 (Fig. 8F). This is in agreement with the faster reactive layer formation hypothesized from the ICP analysis for the boron containing composites.

EDX was performed on the spheres showed on Fig. 8G) and an EDX spectra is presented in Fig. 9A). The composition of the sphere is mainly Ca and P with a Ca/P ratio of ~1.6. This is a good indication that the calcium phosphate layer precipitating is hydroxyapatite. This was further confirmed by FTIR spectroscopy shown in Fig. 9B). While only peaks related to the PLA structure where seen in the pure PLA and PLA/13–93 composite, prior and after immersion in SBF, whereas two peaks in the 400-600 cm^{-1} appeared after PLA/13-93B20 immersion in SBF. These peaks are characteristic of the ν_4 (P – O bending) and ν_2 (O – P – O bending) PO_4^{3-} vibration in apatite structure [40,41]. This effect is partially overcome when working with 13–93B20. The particles are mainly embedded in PLA which slows the release rate due to the PLA diffusion barrier. However, one should keep in mind that despite 13–93B20 promoting more effective HA precipitation than 13–93, a similar reactivity to 45S5 or S53P4 has not yet been reached.

We developed PLA/BAG composites using a process that enables limiting the polymer degradation while maintaining mechanical properties which are of interest in bone tissue engineering. Furthermore, the inorganic filler dissolved when immersed in aqueous solution with kinetics function of the glass composition. The PLA/13-93B20 composite was also found to precipitate a hydroxyapatite layer upon immersion in SBF. Therefore, we decided to do preliminary cell experiments to assess if these composites have potentially osteogenic properties which are of utmost important in bone reconstruction.

3.3. C2C12 proliferation and morphology

The C2C12 cell system was chosen owing to its known dependence by adhesion to the substrate rigidity, and to the experimental ease in measuring the cellular response to the Bone Morphogenetic Protein 2 (BMP-2). In addition, this cell line is important and relevant in the progenitor cell system for bone tissue engineering [42].

Firstly, the proliferation of C2C12 cells on PLA and both composites was studied for up to 7 days (Fig. 10).

Glass slides were used as a control. The cells proliferated with the

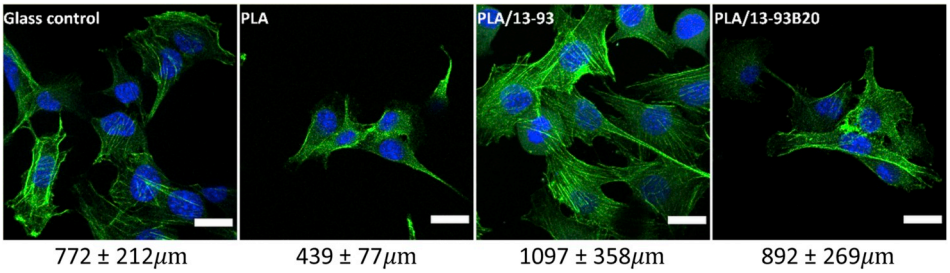

Fig. 11. Morphology observations of C2C12 cells in DMEM complete medium analyzed by immunostaining, Nuclei (DAPI - blue) and Actin (Phalloidin - green), after 48 h of incubation on glass, PLA, PLA/13–93, PLA/13-93B20 (Scale bar 20 μm). Under each image the spreading area of the cells is annotated on each sample after 48 h of incubation. (For interpretation of the references to color in this figure legend, the reader is referred to the Web version of this article.)

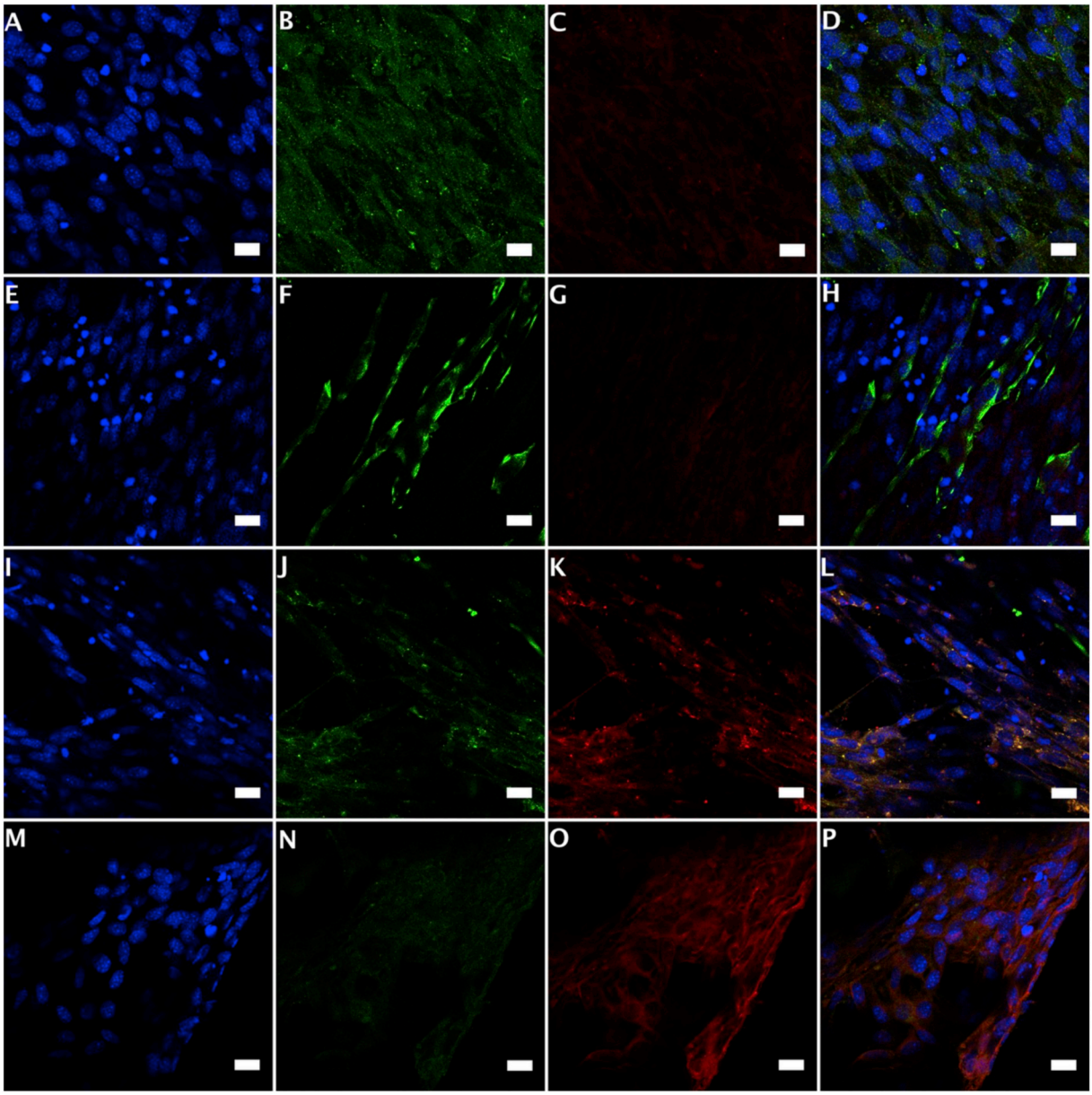

Fig. 12. Differentiation of C2C12 cells on glass (A, B, C, D), PLA (E, F, G, H), PLA/13–93 (I, J, K, L) and PLA/13-93B20 (M, N, O, P) analyzed by Nuclei (DAPI – blue – First column), Myosin (green – Second column), Osteopontin (red – third column) and the merge (fourth column) immunostaining after 14 days of incubation. Scale bar 20 μm. (For interpretation of the references to color in this figure legend, the reader is referred to the Web version of this article.)

characteristic profile of this cell phenotype on all substrates. At 4 days, the proliferation of C2C12 cells on the composites is significantly higher than on the PLA alone. Fu et al. and Eqtesadi et al. [23,43] have already demonstrated that 13–93 glass alone promotes cell adhesion and proliferation. It is interesting to point out, that at day 4, the cell count is statistically higher at the surface of the PLA/13–93 than on the PLA/13-93B20. This is certainly due to the release of boron from the borosilicate glass, which is known to decrease cell proliferation while promoting osteogenesis [44]. It can also be seen that the morphology of murine C2C12 myoblasts after 48 h of incubation (Fig. 11), seem to spread more within the cytoskeleton of the cells with PLA/13–93 and PLA/13-93B20, than with PLA alone.

This is confirmed by the measurements of the spreading surface of the cells on each material (Fig. 11). The lower ability of the cells to spread on PLA can be correlated to slightly slower proliferation of cells at day 4 (Fig. 10), when compared to proliferation on composites. Thereby, both types of BAG do not present cytotoxic effects and when included in the PLA, they promote proliferation and adhesion of C2C12 cells compared to the PLA alone.

3.4. C2C12 differentiation

In order to study the capacity of C2C12 cells to commit to an osteoblastic lineage in presence of BAG, myosin heavy chain (late marker of myogenic differentiation) and osteopontin (early marker of osteoblastic differentiation) were stained after 14 days of incubation.

In Fig. 12, it can be seen that the glass control (Fig. 12B and C) and pure PLA (Fig. 12F and G) have a high myosin expression but no osteopontin expression. The differentiation of C2C12 myoblasts into myotubes can be observed. With a BAG load into the PLA, myosin expression is decreased and osteopontin expression becomes visible (Fig. 12J, K, N, O). This expression seems higher for the cells seeded on the composite containing 13–93B20 and myosin expression seems completely suppressed. Clearly, the osteopontin, marker of osteoblastic

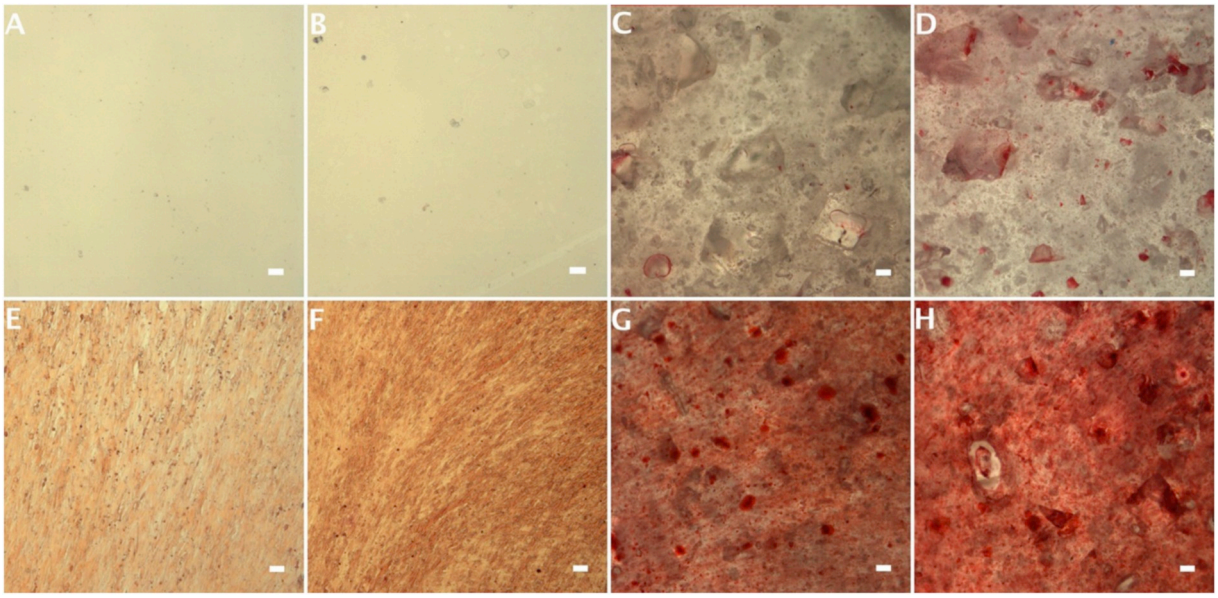

Fig. 13. Mineralization of C2C12 cells in DMEM was studied with Alizarin red S staining after 14 days of incubation. The first line shows A) the glass, B) the PLA, C) the PLA/13–93 and D) the PLA/13-93B20 without any cells seeded. The second line represents E) the glass, F) the PLA, G) the PLA/13–93 and H) the PLA/13-93B20 with C2C12 cells seeded for 14 days. Scale bar 200 μm. (For interpretation of the references to color in this figure legend, the reader is referred to the Web version of this article.)

differentiation, is significantly expressed in cells cultured on the composites and this expression seems higher when using the borosilicate glass in PLA. However, the marker needed quantifying to confirm the effect of the boron included in the glass formulation compared to the silicate glass. C2C12 cells are often used to study osteodifferentiation in presence of BMPs [42,45]. Here, their capacity to differentiate into osteoblastic cells is exploited in the presence of BAG showing promising results for osteodifferentiation.

Mineralization was investigated using Alizarin Red Staining after 10 and 14 days of culture. This product stains the mineral calcium. As 10 days appeared to be too short a time to distinguish the mineralization, only images after 14 days of incubation are presented in Fig. 13. Fig. 13 shows the glass, the PLA, and both composites post staining with Alizarin Red. On the glass control and the PLA without cells (Fig. 13A and B), no red staining could be observed with the cells (Fig. 13E and F), the staining seen is attributed to the high cell density, and therefore gives an indication of background noise. On both composites without cells, a slight red coloration is observed (Fig. 13C and D). As shown in Fig. 7, the dissolution of the composites leads to a small amount of HA precipitation. This may well occur within the culture medium and, therefore, the slight red coloration may be due to either, Alizarin being trapped at the glass/PLA interface of stained HA mineral. When the PLA/13–93 and the PLA/13-93B20 are seeded with the cells, strong red staining is evident, showing mineral formation (Fig. 13G and H). These results, when compared to the results obtained without cells, suggest that the mineral stained by the Alizarin is not due to the precipitation of HA but is produced by the cells through their metabolism in presence of the 13–93 or 13–93B20. Therefore, the cells are conditioned by the composites to synthesize their mineral matter.

4. Conclusion

Composites made of PLA and bioactive glasses (silicate 13–93 and borosilicate 13–93B20) were processed by twin-screw extrusion. This process led to composites with content in the organic phase consistent across the length of the filaments and in agreement with the expected loading. The choice of the glass composition, particle size, glass loading, extrusion temperature as well as pressure for extrusion notably reduced the thermal degradation of the PLA, when compared to previous studies performed with similar or other processing techniques. The presence of BAG particles within the PLA matrix leads to a more ductile, but more fragile material as seen in the case of self-reinforced polymer/BAG composites.

The dissolution of the glass is not impaired by the polymeric matrix. As hypothesized, the substitution of part of the SiO_2 in the 13–93 glass composition with B_2O_3 leads to an increase in the initial dissolution rate. In turns, this leads to a higher level of hydroxyapatite precipitation. However, the dissolution of the BAG leads to an increased degradation rate of the PLA, not affecting the mechanical properties which remained stable for at least 10 weeks. Finally, the dissolution of the composites in SBF support the hypothesis that the developed composites are bioactive, especially in the case of the composite containing the glass 13–93B20.

The osteogenic response of the C2C12 myoblastic cells to both composites – PLA/13–93 and PLA/13-93B20 – was studied. Cells were grown and spread on the composites and the expression of the myosin and the osteopontin measured after 14 days. When cells were cultured on pure PLA, myosin expression was clearly observed while on composites, only osteopontin was expressed. The mineralization experiment showed that the cells in presence of the 13–93 and the 13–93B20 were able to synthesize their mineral matrix.

These composites are promising for bone application. Nevertheless, we feel that more studies are needed to quantify and confirm the effect of the borosilicate at the cellular level.

Declaration of competing interest

There are no conflicts to declare.

Acknowledgement

The authors would like to acknowledge the Academy of Finland (Academy Research Fellow grant to JM), TTY-säätiö for IL financial support, the Institute for Advanced Studies (IAE) for enabling researcher mobility, Delphine Logeart-Avramouglou (Laboratory of Osteoarticular Biology, Bioengineering and Bioimaging UMR CNRS 7052 Inserm U1271, University Paris Diderot) for the kind gift of C2C12 cells and Annette Lane for proofreading this manuscript.

Appendix A. Supplementary data

Supplementary data to this article can be found online at https://doi.org/10.1016/j.msec.2019.110340.

References

[1] G. Schwach, M. Vert, In vitro and in vivo degradation of lactic acid-based interference screws used in cruciate ligament reconstruction, Int. J. Biol. Macromol. 25 (1999) 283–291, https://doi.org/10.1016/S0141-8130(99)00043-4.

[2] L.E. Claes, A.A. Ignatius, K.E. Rehm, C. Scholz, New bioresorbable pin for the reduction of small Gony fkagm.ents: design, mechanical properties and in vitro degradation, 17 (1996) 1621–1626, https://doi.org/10.1016/0142-9612(95)00327-4.

[3] R. Suuronen, Comparison of absorbable self-reinforced poly-L-lactide screws and metallic screws in the fixation of mandibular condyle osteotomies: an experimental study in sheep, J. Oral Maxillofac. Surg. 49 (1991) 989–995, https://doi.org/10.1016/0278-2391(91)90065-T.

[4] A.R. Santos Jr., Bioresorbable polymers for tissue engineering, in: D. Eberli (Ed.), Tissue Engineering, InTech, 2010, , https://doi.org/10.5772/8580.

[5] W.S. Pietrzak, D. Sarver, M. Verstynen, Bioresorbable implants — practical considerations, Bone 19 (1996) S109–S119, https://doi.org/10.1016/S8756-3282(96)00139-1.

[6] M. Walton, N.J. Cotton, Long-term *in vivo* degradation of poly- L -lactide (PLLA) in bone, J. Biomater. Appl. 21 (2007) 395–411, https://doi.org/10.1177/0885328206065125.

[7] K. Shimazaki, V. Mooney, Comparative study of porous hydroxyapatite and tricalcium phosphate as bone substitute, J. Orthop. Res. 3 (1985) 301–310, https://doi.org/10.1002/jor.1100030306.

[8] K. Ohura, M. Bohner, P. Hardouin, J. Lemaître, G. Pasquier, B. Flautre, Resorption of, and bone formation from, new ?-tricalcium phosphate-monocalcium phosphate cements: anin vivo study, J. Biomed. Mater. Res. 30 (1996) 193–200, https://doi.org/10.1002/(SICI)1097-4636(199602)30:2<193::AID-JBM9>3.0.CO;2-M.

[9] S. Hasegawa, S. Ishii, J. Tamura, T. Furukawa, M. Neo, Y. Matsusue, Y. Shikinami, M. Okuno, T. Nakamura, A 5–7 year in vivo study of high-strength hydroxyapatite/poly(l-lactide) composite rods for the internal fixation of bone fractures, Biomaterials 27 (2006) 1327–1332, https://doi.org/10.1016/j.biomaterials.2005.09.003.

[10] C.C.P.M. Verheyen, J.R. de Wijn, C.A. van Blitterswijk, K. de Groot, P.M. Rozing, Hydroxylapatite/poly(L-lactide) composites: an animal study on push-out strengths and interface histology, J. Biomed. Mater. Res. 27 (1993) 433–444, https://doi.org/10.1002/jbm.820270404.

[11] K. Ishikawa, Calcium phosphate cement, in: B. Ben-Nissan (Ed.), Advances in Calcium Phosphate Biomaterials, Springer Berlin Heidelberg, Berlin, Heidelberg, 2014, pp. 199–227, , https://doi.org/10.1007/978-3-642-53980-0_7.

[12] L.L. Hench, The story of Bioglass®, J. Mater. Sci. Mater. Med. 17 (2006) 967–978, https://doi.org/10.1007/s10856-006-0432-z.

[13] R.M. Day, A.R. Boccaccini, S. Shurey, J.A. Roether, A. Forbes, L.L. Hench, S.M. Gabe, Assessment of polyglycolic acid mesh and bioactive glass for soft-tissue engineering scaffolds, Biomaterials 25 (2004) 5857–5866, https://doi.org/10.1016/j.biomaterials.2004.01.043.

[14] H. Li, J. Chang, pH-compensation effect of bioactive inorganic fillers on the degradation of PLGA, Compos. Sci. Technol. 65 (2005) 2226–2232, https://doi.org/10.1016/j.compscitech.2005.04.051.

[15] J. Tainio, K. Paakinaho, N. Ahola, M. Hannula, J. Hyttinen, M. Kellomäki, J. Massera, Vitro degradation of borosilicate bioactive glass and poly(l-lactide-co-ε-caprolactone) composite scaffolds, Materials 10 (2017) 1274, https://doi.org/10.3390/ma10111274.

[16] V. Maquet, A.R. Boccaccini, L. Pravata, I. Notingher, R. Jérôme, Preparation, characterization, and *in vitro* degradation of bioresorbable and bioactive composites based on Bioglass®-filled polylactide foams: porous Polylactide/Bioactive Glass Composites, J. Biomed. Mater. Res. A 66A (2003) 335–346, https://doi.org/10.1002/jbm.a.10587.

[17] G. Vergnol, N. Ginsac, P. Rivory, S. Meille, J.-M. Chenal, S. Balvay, J. Chevalier, D.J. Hartmann, *In vitro* and *in vivo* evaluation of a polylactic acid-bioactive glass composite for bone fixation devices: polylactic acid-bioactive glass composite for bone fixation devices, J. Biomed. Mater. Res. B Appl. Biomater. 104 (2016) 180–191, https://doi.org/10.1002/jbm.b.33364.

[18] H. Kometani, T. Matsumura, T. Suga, T. Kanai, Quantitative analysis for polymer degradation in the extrusion process, Int. Polym. Process. 21 (2006) 24–31, https://doi.org/10.3139/217.0092.

[19] T. Niemelä, H. Niiranen, M. Kellomäki, Self-reinforced composites of bioabsorbable polymer and bioactive glass with different bioactive glass contents. Part II: in vitro degradation, Acta Biomater. 4 (2008) 156–164, https://doi.org/10.1016/j.actbio.2007.06.007.

[20] M. Brink, The influence of alkali and alkaline earths on the working range for bioactive glasses, J. Biomed. Mater. Res. 36 (1997) 109–117, https://doi.org/10.1002/(SICI)1097-4636(199707)36:1<109::AID-JBM13>3.0.CO;2-D.

[21] R.F. Brown, M.N. Rahaman, A.B. Dwilewicz, W. Huang, D.E. Day, Y. Li, B.S. Bal, Effect of borate glass composition on its conversion to hydroxyapatite and on the proliferation of MC3T3-E1 cells, J. Biomed. Mater. Res. A 88A (2009) 392–400, https://doi.org/10.1002/jbm.a.31679.

[22] M. Ojansivu, A. Mishra, S. Vanhatupa, M. Juntunen, A. Larionova, J. Massera, S. Miettinen, The effect of S53P4-based borosilicate glasses and glass dissolution products on the osteogenic commitment of human adipose stem cells, PLoS One 13 (2018) e0202740, https://doi.org/10.1371/journal.pone.0202740.

[23] Q. Fu, M.N. Rahaman, B.S. Bal, L.F. Bonewald, K. Kuroki, R.F. Brown, Silicate, borosilicate, and borate bioactive glass scaffolds with controllable degradation rate for bone tissue engineering applications. II. In vitro and in vivo biological evaluation, J. Biomed. Mater. Res. A 95A (2010) 172–179, https://doi.org/10.1002/jbm.a.32823.

[24] L.M. Marquardt, D. Day, S.E. Sakiyama-Elbert, A.B. Harkins, Effects of borate-based bioactive glass on neuron viability and neurite extension: borate-based Bioactive Glass, J. Biomed. Mater. Res. 102 (2014) 2767–2775, https://doi.org/10.1002/jbm.a.34944.

[25] A.L.B. Maçon, T.B. Kim, E.M. Valliant, K. Goetschius, R.K. Brow, D.E. Day, A. Hoppe, A.R. Boccaccini, I.Y. Kim, C. Ohtsuki, T. Kokubo, A. Osaka, M. Vallet-Regí, D. Arcos, L. Fraile, A.J. Salinas, A.V. Teixeira, Y. Vueva, R.M. Almeida, M. Miola, C. Vitale-Brovarone, E. Verné, W. Höland, J.R. Jones, A unified in vitro evaluation for apatite-forming ability of bioactive glasses and their variants, J. Mater. Sci. Mater. Med. 26 (2015) 115.

[26] T. Niemela, H. Niiranen, M. Kellomaki, P. Tormala, Self-reinforced composites of bioabsorbable polymer and bioactive glass with different bioactive glass contents. Part I: initial mechanical properties and bioactivity, Acta Biomater. 1 (2005) 235–242, https://doi.org/10.1016/j.actbio.2004.11.002.

[27] T. Kokubo, H. Kushitani, S. Sakka, T. Kitsugi, T. Yamamuro, Solutions able to reproducein vivo surface-structure changes in bioactive glass-ceramic A-W3, J. Biomed. Mater. Res. 24 (1990) 721–734, https://doi.org/10.1002/jbm.820240607.

[28] L. Tirkkonen, H. Halonen, J. Hyttinen, H. Kuokkanen, H. Sievanen, A.-M. Koivisto, B. Mannerstrom, G.K.B. Sandor, R. Suuronen, S. Miettinen, S. Haimi, The effects of vibration loading on adipose stem cell number, viability and differentiation towards bone-forming cells, J. R. Soc. Interface 8 (2011) 1736–1747, https://doi.org/10.1098/rsif.2011.0211.

[29] X. Wu, R.E. Youngman, R. Dieckmann, Sodium tracer diffusion and 11B NMR study of glasses of the type (Na2O)0.17(B2O3)x(SiO2)0.83 − x, J. Non-Cryst. Solids 378 (2013) 168–176, https://doi.org/10.1016/j.jnoncrysol.2013.06.012.

[30] L.-S. Du, J.F. Stebbins, Nature of Silicon − Boron mixing in sodium borosilicate glasses: a high-resolution ^{11} B and ^{17} O NMR study, J. Phys. Chem. B 107 (2003) 10063–10076, https://doi.org/10.1021/jp034048l.

[31] L.-S. Du, J.F. Stebbins, Solid-state NMR study of metastable immiscibility in alkali borosilicate glasses, J. Non-Cryst. Solids 315 (2003) 239–255, https://doi.org/10.1016/S0022-3093(02)01604-6.

[32] Y. Sun, Z. Zhang, Structural roles of boron and silicon in the CaO-SiO2-B2O3 glasses using FTIR, Raman, and NMR spectroscopy, Metall. Mater. Trans. B 46 (2015) 1549–1554, https://doi.org/10.1007/s11663-015-0374-2.

[33] Y. Lai, Y. Zeng, X. Tang, H. Zhang, J. Han, H. Su, Structural investigation of calcium borosilicate glasses with varying Si/Ca ratios by infrared and Raman spectroscopy, RSC Adv. 6 (2016) 93722–93728, https://doi.org/10.1039/C6RA20969F.

[34] Y. Yu, B. Stevensson, M. Edén, Medium-range structural organization of phosphorus-bearing borosilicate glasses revealed by advanced solid-state NMR experiments and MD simulations: consequences of B/Si substitutions, J. Phys. Chem. B 121 (2017) 9737–9752, https://doi.org/10.1021/acs.jpcb.7b06654.

[35] W. Huang, D.E. Day, K. Kittiratanapiboon, M.N. Rahaman, Kinetics and mechanisms of the conversion of silicate (45S5), borate, and borosilicate glasses to hydroxyapatite in dilute phosphate solutions, J. Mater. Sci. Mater. Med. 17 (2006) 583–596, https://doi.org/10.1007/s10856-006-9220-z.

[36] A. Yao, D. Wang, W. Huang, Q. Fu, M.N. Rahaman, D.E. Day, Vitro bioactive characteristics of borate-based glasses with controllable degradation behavior, J. Am. Ceram. Soc. 90 (2007) 303–306, https://doi.org/10.1111/j.1551-2916.2006.01358.x.

[37] X. Liu, W. Huang, H. Fu, A. Yao, D. Wang, H. Pan, W.W. Lu, X. Jiang, X. Zhang, Bioactive borosilicate glass scaffolds: in vitro degradation and bioactivity behaviors, J. Mater. Sci. Mater. Med. 20 (2009) 1237–1243, https://doi.org/10.1007/s10856-009-3691-7.

[38] W.C. Lepry, S.N. Nazhat, Highly bioactive sol-gel-derived borate glasses, Chem. Mater. 27 (2015) 4821–4831, https://doi.org/10.1021/acs.chemmater.5b01697.

[39] S.J. de Jong, E.R. Arias, D.T.S. Rijkers, C.F. van Nostrum, J.J. Kettenes-van den Bosch, W.E. Hennink, New insights into the hydrolytic degradation of poly(lactic acid): participation of the alcohol terminus, Polymer 42 (2001) 2795–2802, https://doi.org/10.1016/S0032-3861(00)00646-7.

[40] A.S. Stanislavov, L.F. Sukhodub, L.B. Sukhodub, V.N. Kuznetsov, K.L. Bychkov, M.I. Kravchenko, Structural features of hydroxyapatite and carbonated apatite formed under the influence of ultrasound and microwave radiation and their effect on the bioactivity of the nanomaterials, Ultrason. Sonochem. 42 (2018) 84–96, https://doi.org/10.1016/j.ultsonch.2017.11.011.

[41] C.B. Baddiel, E.E. Berry, Spectra structure correlations in hydroxy and fluorapatite, Spectrochim. Acta 22 (1966) 1407–1416, https://doi.org/10.1016/0371-1951(66)80133-9.

[42] A. Gand, M. Hindié, D. Chacon, P.R. van Tassel, E. Pauthe, Nanotemplated polyelectrolyte films as porous biomolecular delivery systems: application to the growth factor BMP-2, Biomatter 4 (2014) e28823, https://doi.org/10.4161/biom.28823.

[43] S. Eqtesadi, A. Motealleh, A. Pajares, P. Miranda, Effect of milling media on processing and performance of 13-93 bioactive glass scaffolds fabricated by robocasting, Ceram. Int. 41 (2015) 1379–1389, https://doi.org/10.1016/j.ceramint.2014.09.071.

[44] M. Ojansivu, A. Mishra, A. Vanhatupa, M. Juntunen, A. Larionova, J. Massera, S. Miettinen, The Effect of S53P4-Based Borosilicate Glasses and Glass Dissolution Products on the Osteogenic Commitment of Human Adipose Stem Cells, PlosOne, 2018.

[45] M. Saito, T. Karakida, R. Yamamoto, T. Nagano, Y. Yamakoshi, T. Hayakawa, S. Oida, K. Gomi, Differentiation potential of osteoblast from cultured C2C12 cells on zirconia disk, Dent. Mater. J. 33 (2014) 275–283, https://doi.org/10.4012/dmj.2013-321.

biomolecules

MDPI

Article

New Generation of Hybrid Materials Based on Gelatin and Bioactive Glass Particles for Bone Tissue Regeneration

Amel Houaoui [1], Agata Szczodra [2], Mari Lallukka [2], Lamia El-Guermah [1], Remy Agniel [1], Emmanuel Pauthe [1], Jonathan Massera [2] and Michel Boissiere [1,*]

[1] Biomaterials for Health Research Group, ERRMECe, Equipe de Recherche sur les Relations Matrice Extracellulaire-Cellules (EA1391), Institut des Matériaux I-MAT (FD4122), CY Tech, CY Cergy Paris Université, Maison Internationale de la Recherche (MIR), rue Descartes, 95001 Neuville sur Oise CEDEX, France; amel.houaoui@cyu.fr (A.H.); lamia.el-guermah@cyu.fr (L.E.-G.); remy.agniel@cyu.fr (R.A.); emmanuel.pauthe@cyu.fr (E.P.)

[2] Tampere University, Faculty of Medicine and Health Technology, Laboratory of Biomaterials and Tissue Engineering, Korkeakoulunkatu 3, 33720 Tampere, Finland; agata.szczodra@tuni.fi (A.S.); mari.lallukka@polito.it (M.L.); jonathan.massera@tuni.fi (J.M.)

* Correspondence: michel.boissiere@cyu.fr; Tel.: +33-01-34-25-75-61

Abstract: Hybrid scaffolds based on bioactive glass (BAG) particles (<38 µm), covalently linked to gelatin (G*) using 3-glycidoxypropyltrimethoxysilane (GPTMS), have been studied for bone bioengineering. In this study, two glass compositions (13-93 and 13-93B20 (where 20% of the SiO_2 was replaced with B_2O_3)) were introduced in the gelatin matrix. The C_{factor} (gelatin/GPTMS molar ratio) was kept constant at 500. The hybrids obtained were found to be stable at 37 °C in solution, the condition in which pure gelatin is liquid. All hybrids were characterized by in vitro dissolution in Tris(hydroxymethyl)aminomethane (TRIS) solution (for up to 4 weeks) and Simulated Body Fluid (SBF) (for up to 2 weeks). Samples processed with 13-93B20 exhibited faster initial dissolution and significantly faster precipitation of a hydroxyapatite (HA) layer. The faster ion release and HA precipitation recorded from the G*/13-93B20 samples are attributable to the higher reactivity of borosilicate compared to silicate glass. The MC3T3-E1 cell behavior in direct contact with the hybrids was investigated, showing that the cells were able to proliferate and spread on the developed biomaterials. Tailoring the glass composition allows us to better control the material's dissolution, biodegradability, and bioactivity. Bioactive (especially with 13-93B20 BAG) and biocompatible, the hybrids are promising for bone application.

Keywords: hybrid scaffold; bioactive glass; gelatin; GPTMS; bone tissue engineering

Citation: Houaoui, A.; Szczodra, A.; Lallukka, M.; El-Guermah, L.; Agniel, R.; Pauthe, E.; Massera, J.; Boissiere, M. New Generation of Hybrid Materials Based on Gelatin and Bioactive Glass Particles for Bone Tissue Regeneration. *Biomolecules* **2021**, *11*, 444. https://doi.org/10.3390/biom11030444

Academic Editor: Antonio J. Salinas

Received: 27 January 2021
Accepted: 15 March 2021
Published: 17 March 2021

1. Introduction

Bone fractures are a common trauma. For a large loss of bone substance (defect greater than 1 cm^3) following a traumatic situation as a pathology or accidental defect, the natural process of self-repair is compromised [1]. Tissue engineering is an innovative approach used for bone repair. Bone reconstruction is assisted with materials that participate in tissue regeneration [2,3]. These materials must have properties adapted to this function.

Bioactive ceramics are of interest in bone regeneration. The bioactivity of these materials results in the appearance of biological activity in the host organism and the existence of ion exchanges between the material and living tissue [4]. Synthetic hydroxyapatite (HA) and β-tricalcium phosphate (β-TCP) are more widely used [5–7]. They often have osteoconductive and sometimes osteoinductive properties. However, their slow resorption limits their clinical relevance [8,9]. Indeed, the limited resorption of those ceramics was demonstrated in-vivo when used in cements [10].

Bioactive Glass (BAG) is a subcategory of ceramics and are not only osteoconductive but also osteoinductive [11]. These glasses are mainly used for hard tissue reconstruction,

but they are also able to bond to soft tissue [12]. However, due to their brittleness, shaping the glass into its final shape remains a challenge. Organic/inorganic composite scaffolds represent a convenient alternative to traditional BAGs. They allow for the possibility to tailor the mechanical properties, degradation kinetics, and bioactivity. Current research is focused on the fabrication of bioactive composite materials, with the bioactive phase incorporated as a filler into the bioresorbable polymer matrix [13]. However, a drawback with many conventional composites is that the constituent phases interact on a micrometer scale, which can result in differential resorption rates during dissolution and masking of the bioactive component. This would inevitably lead to material instability in vivo [14].

Hybrid scaffolds are materials where the organic and inorganic phases interact chemically on a nanoscale, allowing us to control the properties of the final material, for instance, degradation rates and mechanical properties [14–16]. Moreover, the inorganic and organic contents in addition to the degree of covalent links can be adjusted for precise control of the hybrid properties as stiffness and dissolution rates, leading to material adapted for a specific application [14]. For hybrid formation, covalent links between organic and inorganic matrixes are fundamental. They can be obtained through reaction with organosilanes such as 3-glycidoxypropyltrimethoxysilane (GPTMS) or 3-aminopropyltriethoxysilane (APTES) [17–20].

In our work, we present hybrid materials for bone tissue engineering based on gelatin and BAG (Figure 1), where two BAGs, with different compositions (13-93 and 13-93B20), are compared. 13-93 is an Food and Drug Administration (FDA)-approved BAG that exhibits a slower dissolution rate than commercialized BAGs 45S5 or S53P4 [21,22]. The rational for studying 13-93 BAG lies in preventing excessive dissolution of the glass particles during processing, degradation of the organic phase, a decrease in the mechanical properties, and a fast release of ions that could be toxic for the cells. 13-93B20, a similar composition to 13-93 but with 20% of the SiO_2 substituted with B_2O_3, was also included in the study. It has been showed that the borosilicate glasses based on the 13-93 composition have faster in vitro dissolution but also faster conversion to HA while maintaining a slower dissolution kinetics than 45S5 and S53P4 [13,23,24].

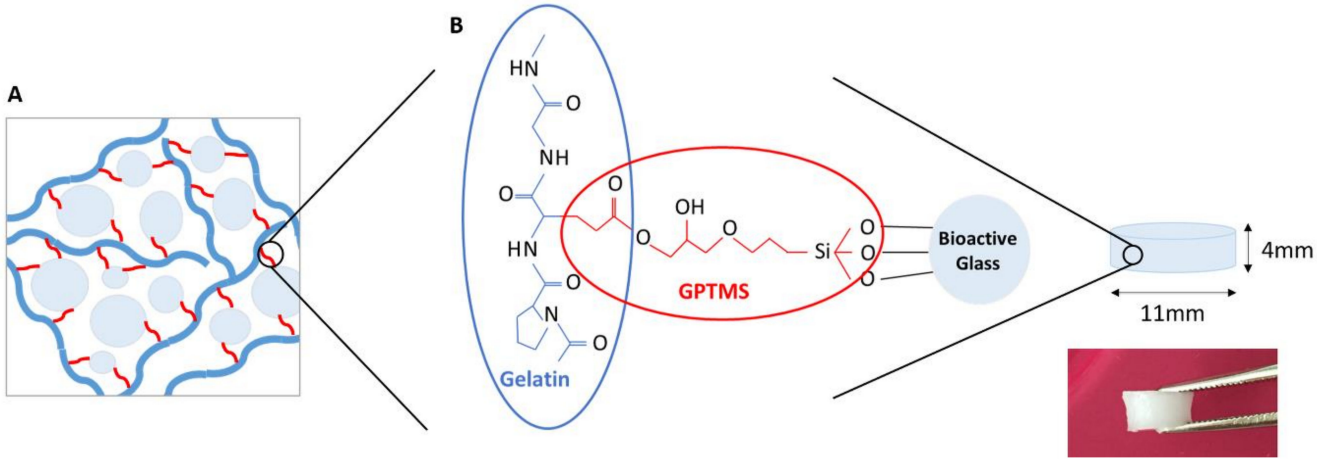

Figure 1. (A) Schematic representation (inspired from Mahony et al. [18]) and (**B**) chemical structure of the hybrid made of gelatin and bioactive glass (BAG) covalently linked by 3-glycidoxypropyltrimethoxysilane (GPTMS).

Here, two hybrid materials were studied, based on gelatin and 13-93 or 13-93B20. The content of the organic and inorganic matrixes was 70/30 (wt%), and a C_{factor} (degree of covalent coupling, molar ratio of GPTMS/gelatin) of 500 was used. To investigate their in-vitro dissolution, the hybrids were immersed in Tris(hydroxymethyl)aminomethane (TRIS) buffer solution for one month. Ion release from the glass was quantified, and the mineral content was measured. The compressive properties of the hybrids were studied during the immersion. The bioactivity, assumed to be related to the precipitation of a

HA layer at the materials' surface when immersed in aqueous solution, was assessed in Simulated Body Fluid (SBF) [25]. Preliminary cell experiments were performed to assess cell activity by culturing MC3T3-E1 pre-osteoblastic cells at the surface of the hybrids. Cell proliferation and morphology were studied. The aim of this study was to assess the stability of the hybrids, in vitro, in aqueous solutions and its biocompatibility.

2. Materials and Methods

2.1. Materials Preparation and Characterization

2.1.1. Bioactive Glass Processing

BAGs 13-93 and 13-93B20 were prepared from analytical grade K_2CO_3 (Alfa Aesar, Ward Hill, MA, USA), (Na_2CO_3, $NH_4H_2PO_4$, ($CaHPO_4$)(2(H_2O)), $CaCO_3$, MgO, H_3BO_3 (Sigma Aldrich, St Louis, MO, USA), and Belgian quartz sand. The 100 g batches of 13-93 and 13-93B20 were melted for 3 h at 1450 °C in a platinum crucible. The molten glasses were cast, annealed, crushed, and finally sieved into less than 38 µm particles. The glasses were dried at 200 °C for 2 h prior to be used. The nominal oxide compositions of the glasses are given in Table 1.

Table 1. Nominal glass composition (%).

Glass	mol%						
	Na_2O	K_2O	MgO	CaO	P_2O_5	SiO_2	B_2O_3
13-93	6.0	7.9	7.7	22.1	1.7	54.6	-
13-93B20	6.0	7.9	7.7	22.1	1.7	43.7	10.9

2.1.2. Hybrids Synthesis

Gelatin (Porcine, Type A, Bloom 300, Sigma Aldrich, St Louis, MO, USA) was dissolved at 37 °C in 10 mM hydrochloric acid (HCl, Merck Millipore, Burlington, MA, USA) at a concentration of 50 mg·mL^{-1}. This solution was functionalized by adding GPTMS (Sigma Aldrich, St Louis, MO, USA) to obtain a C_{factor} (molar ratio of GPTMS/gelatin) of 500. Different C_{factor} have been studied (data not shown), and this parameter was optimized in order to limit the cellular toxicity of GPTMS. The functionalized gelatin (G*) solution was mixed 2 h at 37 °C. The 13-93 or 13-93B20 BAG particles were added and mixed for 1 h at 37 °C for a ratio of G*/BAG of 70/30 wt%. This ratio was optimized (data not shown) to obtain enough covalent links in the structure to obtain a gel self-supported at biological temperature. Finally, sodium fluoride 1% (NaF, Sigma Aldrich, St Louis, MO, USA) was added to catalyze the inorganic condensation reaction. The final solution was mixed for 10 min at 37 °C. The solution was poured in silicon molds and left to gel at room temperature for 24 h.

Hybrid materials with a diameter of 11 mm and height of 4 mm were cut. To measure their glass content, they were freeze-dried and heated for 2 h at 500 °C under air to remove all the organic phase. The remaining mineral phase was weighed. The measure was repeated on 4 samples per composition, and the average glass content with standard deviation was calculated.

2.2. Behavior of G/BAG Hybrids*

2.2.1. Physicochemical Properties of the Hybrids

Immersion in TRIS

Tris(hydroxymethyl)aminomethane (TRIS) solution (50 mM) was prepared by mixing ultrapure TRIS (Sigma Aldrich, St Louis, MO, USA) and TRIS-HCl (Sigma Aldrich, St Louis, MO, USA) in ultrapure water, and the pH was adjusted to 7.4 at 37 °C. The samples were punched to obtain small cylinders of 11 mm diameter and 4 mm height (≈380 mg), which were immersed in 30 mL of TRIS solution for up to 28 days at 37 °C on an agitator (Heidolph Instruments, Schwabach, Germany) with an orbital speed of 100 rpm. To avoid

saturation of the solution with the ions released from the hybrids, the TRIS buffer was refreshed each week.

At the desired time of immersion, the concentration of elements released from the hybrids was studied by diluting 500 µL of the immersion solution in 4.5 mL of ultrapure water for ion analysis. Inductively Coupled Plasma - Optical Emission Spectroscopy (ICP-OES) (Agilent technologies 5110, Santa Clara, CA, USA) was employed to quantify P (λ = 253.561 nm), Ca (λ = 422.673 nm), Mg (λ = 279.553 nm), Si (λ = 250.690 nm), B (λ = 249.678 nm), K (λ = 766.491 nm), and Na (λ = 589.592 nm) concentrations in the solution after samples immersion. The measurements were conducted in four separate samples at each time points for each composition, and the results are presented as mean ± standard deviation (SD).

Mineral Content in Hybrids

Mineral mass after the samples' synthesis and at various immersion times was measured after freeze-drying and burning the samples for 2 h at 500 °C under air to remove all the organic phase. The remaining mineral phase was weighed. The measurements were conducted on four separate samples at each time points for each composition, and the results were presented as mean ± SD.

Mechanical Properties of the Hybrids

The mechanical properties of the hybrids after synthesis and after immersion (wet) were tested by compression test at room temperature using a texturometer (LS1, Lloyd Instruments, Ametek, Berwyn, PA, USA). The measurements were conducted on four separate samples at each time point for each composition. A 20 N load cell was used for testing, with a compression extension speed of 1 mm.min^{-1}. The results are presented as mean ± SD.

2.2.2. Hybrids Bioactivity

Immersion in Simulated Body Fluid (SBF)

Developed by Kokubo et al., SBF was prepared following the methodology from the standard ISO/FDIS 23317 [26]. The samples were punched to obtain small cylinders of 11 mm diameter and 4 mm height (≃380 mg), which were immersed in 30 mL of SBF for up to 2 weeks at 37 °C on an agitator (Heidolph Instruments, Schwabach, Germany) with an orbital speed of 100 rpm. During the experiment, the solution was not refreshed to study the precipitation of calcium phosphate. The ion concentration in the solution according to immersion time was measured as previously described. The measurements were conducted in four separate samples at each time points for each composition, and the results are presented as mean ± SD.

Mineral Content in Hybrids

Mineral mass after various immersion times was measured as explained above. Measurements were conducted on four separate samples at each time point for each composition, and the results are presented as mean ± SD.

Hybrids Surface Analysis

The reactive layer on the hybrid surface after immersion in SBF was observed by SEM (GEMINISEM 300 from Zeiss, Iena, Germany), and its composition was analyzed by Energy-Dispersive X-ray spectroscopy (EDX Quantax from Bruker, Billerica, MA, USA). The Infrared (IR) absorption spectra of the hybrids immersed in SBF were also recorded using a Bruker Alpha FTIR in Attenuated Total Reflectance (ATR) mode. The measurements were performed on dry samples. All IR spectra were recorded within the range 399–4000 cm^{-1} with a resolution of 2 cm^{-1} and 32 accumulation scans.

2.2.3. Cell Analysis

Hybrids Preparation

G*/13-93 and G*/13-93B20 hybrids were synthesized in sterile conditions. The samples were punched to obtain small cylinders of 11 mm diameter and 4 mm height. Each material of each condition was immersed in sterile TRIS solution during 10 days at 37 °C to remove excess components. After that, all cell experiments were performed in 48-well plates.

Cell Culture

Pre-osteoblastic MC3T3-E1 cells subclone four (ATCC, Manassas, VA, USA) were cultured in α-Minimum Essential Media (α-MEM) (Gibco, Life Technologies, Carlsbad, CA, USA) containing glutamine supplemented with 10% Fetal Bovine Serum (FBS, Biosera, Marikina, Philippines) and 1% penicillin/streptomycin (Gibco, Life Technologies, Carlsbad, CA, USA). The cells were cultured with a humidified atmosphere of 5% CO_2 at 37 °C.

Cell Proliferation

To compare the behavior of MC3T3-E1 cells on the different samples, cell proliferation was studied using a CyQUANT Cell Proliferation Assay kit (Invitrogen, Life Technologies, Carlsbad, CA, USA). The control used was the Tissue Culture Polystyrene (TCPS) 48 well-plate. The hybrids were placed in the wells, and 5000 cells/well were seeded. The medium was changed every 2 days. After 1, 3, 7, 10, and 14 days of culture, the cells were lysed with 700 µL 0.1% Triton-X100 (Fisher Scientific, Hampton, NH, USA) buffer and conserved at −80 °C. After one freeze–thaw cycle, three 20 µL aliquots of each lysate were pipetted to a black 96-well plate (Corning, Corning, NY, USA) and mixed with 180 µL working solution containing CyQUANT GR dye and cell lysis buffer. The fluorescence at 520 nm was measured with a Spectrofluorometer Xenius XM (Safas, Monaco).

Cell Morphology

The morphology of the cells on the different samples was observed after 1, 7, and 14 days of culture. The control used was TCPS coverslips (Nunc Thermanox Coverslips, ThermoFisher Scientific, Waltham, MA, USA) of 13 mm diameter in a 24-well plate. The number of cells was adjusted according to the well area. The same density of cells was seeded on the hybrids and the TCPS coverslips controls, and after each time point, the cells were fixed with 4% (w/v) para-formaldehyde solution for 15 min and then permeabilized with 0.1% (v/v) Triton X-100 (Sigma Aldrich, St Louis, MO, USA) for 10 min. Nonspecific binding sites were blocked by incubating the disks in Phosphate Buffered Saline (PBS) containing 1% Bovine Serum Albumin (BSA, Sigma Aldrich, St Louis, MO, USA) for 1 h. The cytoskeleton and nuclei of the cells were stained, respectively, with 1:500 diluted TRITC-labelled phalloidin (Sigma Aldrich, St Louis, MO, USA P1951) and 1:1000 diluted 4′,6-Diamidino-2-phenylindole dihydrochloride (DAPI, Sigma Aldrich, St Louis, MO, USA D9542) in PBS–BSA 0.5% for 1 h. Each incubation with antibodies was performed in wet and dark conditions. The samples were then washed in PBS–BSA 0.5% and pure water and observed using a LSM710 confocal microscope (Zeiss, Iena, Germany).

Statistical Analysis

Data were analyzed using GraphPad Prism 8 Software. Statistical significance between groups was assessed by one-way analysis of variance (ANOVA). The experimental results are expressed as means ± standard deviation. Statistical significance is taken for values of $p < 0.01$.

3. Results and Discussion

The aim of this study is to develop hybrid materials based on gelatin and BAG able to release therapeutic ions for bone regeneration while controlling the dissolution properties of the organic and inorganic phases of the scaffold. The first step was to determine the

optimal C_{factor} for targeted applications. Indeed, the higher the C_{factor}, the more covalent links will be formed in the structure. However, an excess of GPTMS can lead to excessive unreacted precursor, leading to cellular toxicity [14,27]. Thus, to avoid this negative effect, studies have led us to use a C_{factor} of 500 for our hybrids (data not shown). Therefore, the BAGs 13-93 and 13-93B20 were covalently linked to gelatin with a C_{factor} of 500. The materials dissolution in aqueous solutions and their bioactivity were compared.

3.1. Characterization of the Hybrids after Synthesis

Table 2 presents the glass loading in the hybrids and their young modulus after synthesis. The mineral mass in the hybrids was determined after freeze-drying and burning the inorganic phase at 500 °C under air for 2 h. Table 2 shows that the glass loading is 34 ± 2 wt% and 33 ± 1 wt% for G*/13-93 and G*/13-93B20, respectively, as expected from the targeted loading.

Table 2. Measured glass loading and Young's modulus of the gelatin alone functionalized (G*) and the G*/13-93 and G*/13-93B20 hybrids (for wet samples, the mechanical properties were measured after 10 min of immersion in TRIS).

Materials	Glass Loading in the Hybrids (wt%)	Young Modulus (MPa)	
		Dry Samples	Wet Samples
G* alone	-	2.1 ± 0.3	0.8 ± 0.2
G*/13-93	34 ± 2	0.5 ± 0.3	0.5 ± 0.1
G*/13-93B20	33 ± 1	0.7 ± 0.2	0.6 ± 0.2

Young's modulus of G* alone and the hybrids were measured by a compression test. Both hybrids have Young's moduli stable in wet and dry conditions. Young's modulus of the hybrids is lower compared to that for G* alone. This shows that adding the glass in the organic phase influences the mechanical behavior of the scaffolds. This decrease occurs with both BAGs, showing that this is not due to the type of glass. It is interesting to note that, in the case of composite materials, the addition of mineral particles reinforces the mechanical properties [8,9]. However, for our hybrid materials, a decrease in Young's modulus is observed probably because the glass induces defects on the gel structure and adds some heterogeneity. This heterogeneity in turn leads to weak points in the material, which become more friable.

3.2. Behavior of the Hybrids in Solution

Resorbable materials need to present controlled degradation and sufficient mechanical properties until bone tissue regeneration [26]. Their bioactivity is a fundamental property that will help bone repair. To assess these properties, the hybrids were immersed in aqueous solutions and their dissolution was studied.

3.2.1. Dissolution in TRIS

The hybrid degradation in TRIS was studied by mass measurements, ICP-OES analysis, and compression tests. These tests could not be done on G* without BAG because it was dissolving at 37 °C, contrary to G*/13-93 or 13-93B20. This shows that the materials made of gelatin and BAG, covalently linked by the GPTMS, can be considered as hybrids. Moreover, Mahony et al. worked on hybrids based on gelatin and silica network coming from Tetraethyl orthosilicate (TEOS) hydrolysis and condensation and showed that GPTMS is efficient in creating covalent links between both matrices [14]. Figure 2 presents the mass loss of the hybrids as a function of the immersion time (Figure 2A), the hybrid mass after freeze-drying (Figure 2B), and the mineral mass remaining in the materials after immersion (Figure 2C).

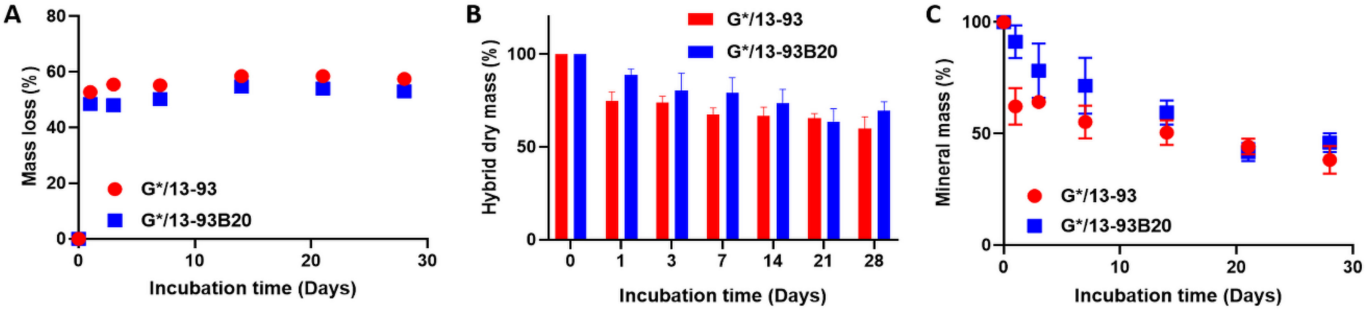

Figure 2. Mass loss (**A**), dry mass (**B**), and mineral mass (**C**) remaining in the hybrid G*/13-93 (●) and G*/13-93B20 (■) as a function of immersion time in TRIS.

Mass loss graph (Figure 2A) shows that, after 24 h, the mass loss reaches 50% and remained stable at longer immersion times. The same results are observed for G*/13-93 and G*/13-93B20, showing that this mass loss is not dependent on the type of glass. In Figure 2B, a decrease in the hybrid dry mass is observable. At 24 h, the hybrid dry mass goes from 100% to 75% and 89% for G*/13-93 and G*/13-93B20, respectively, and does not reach 50% during the immersion. This result does not corroborate the mass loss at 24 h in Figure 2A. This means that, during the first 24 h, the hybrids lose mostly water. This can be seen from a macroscopic point of view on the hybrids that shrink and lose 2 mm of diameter and 1 mm of height after 24 h of immersion, indicating a rearrangement of the hybrids structure due to a syneresis phenomenon.

In Figure 2B, the hybrid dry mass decreases with immersion time, exhibiting a dissolution of the material. In Figure 2C, the mineral mass decreases with immersion time. This result shows that 13-93 and 13-93B20 dissolve in TRIS solution during immersion. This is further confirmed by the quantification of ion release in solution (Figure 3).

For both hybrids, all ions from the BAG are found to leach out into the solution, showing that the glasses dissolve through the gelatin. The Si release from G*/13-93B20 continuously increases and is slightly lower than that for G*/13-93. Moreover, the initial release of Mg, Na, K, and Ca elements is faster for G*/13-93B20 than for G*/13-93. This can be due to the fact that the borosilicate glass is more reactive with siloxane than G*/13-93, leading to a lower Si release from the hybrids with 13-93B20 than the one with 13-93. The release of the elements coming from G*/13-93B20 directly reaches the plateau from the beginning of the immersion, while it increases for G*/13-93 until it reaches the same plateau (Figures 3 and 4). For G*/13-93 (Figure 4A), it appears that the glass dissolution is limited for Ca, K, and Mg, with a plateau reached at 14 days and approximately 20% of these elements released in solution. The Si and Na releases seem to be higher than the first ions cited, linear and continuous for 28 days. Figure 4B presents the release of ions from the hybrids containing 13-93B20 glass. For Ca, K, Mg, and B, the release of these elements is already at the plateau from the first time point contrary to the hybrid containing 13-93 (results also observed in Figure 3). This plateau, reached from the beginning of the immersion at 20% (as for G*/13-93), shows also that the initial dissolution of G*/13-93B20 is faster than for G*/13-93.

For both hybrids, the Si and Na releases are more important than for the other elements, with a Na release already stable from the first time point for G*/13-93B20. The higher concentrations of Si and Na are probably because they come not only from the glass but also from the GPTMS and NaF, respectively. The important release of Si in solution is probably followed by condensation and polymerization, forming an amorphous silica-rich layer around the glass [28], slowing down the release of Ca, Mg, K, and B (for G*/13-93).

After analyzing degradation of the hybrids, their mechanical properties were studied with a compression test on wet samples during the immersion (Figure 5).

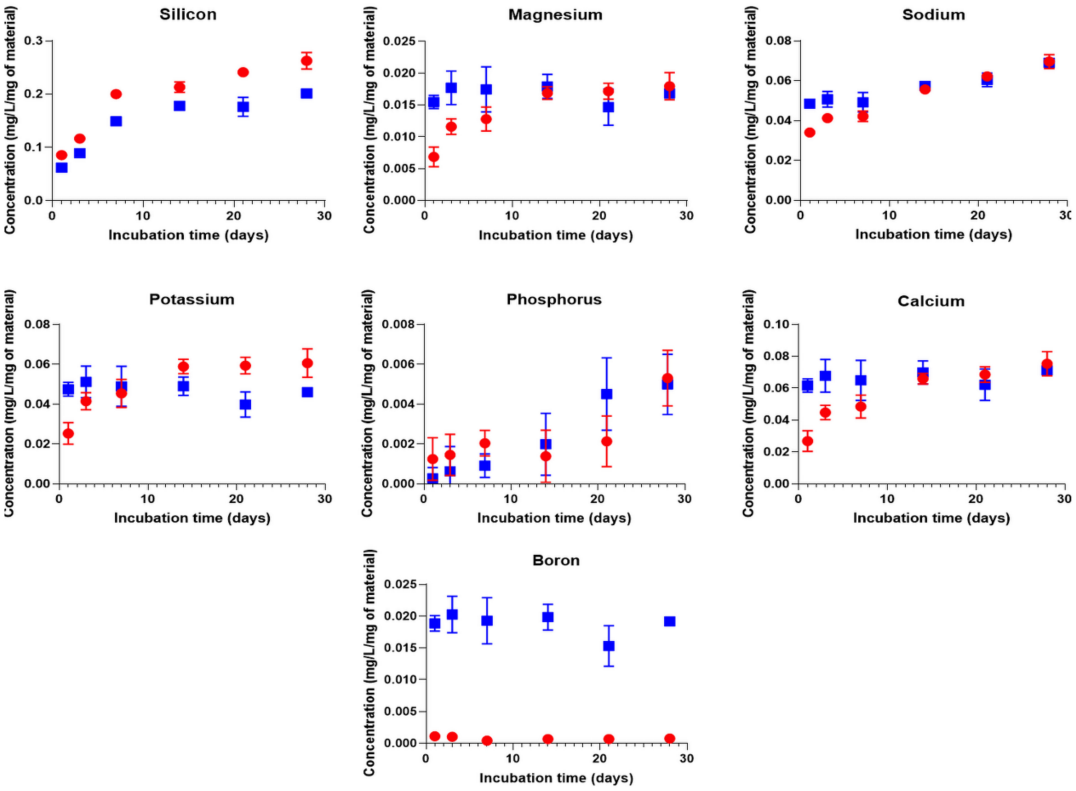

Figure 3. Elements concentrations of Si, Mg, Na, K, P, Ca, and B in the dissolution products of G*/13-93 (●) and G*/13-93B20 (■) immersed in TRIS as a function of time. The concentrations are normalized to the sample mass.

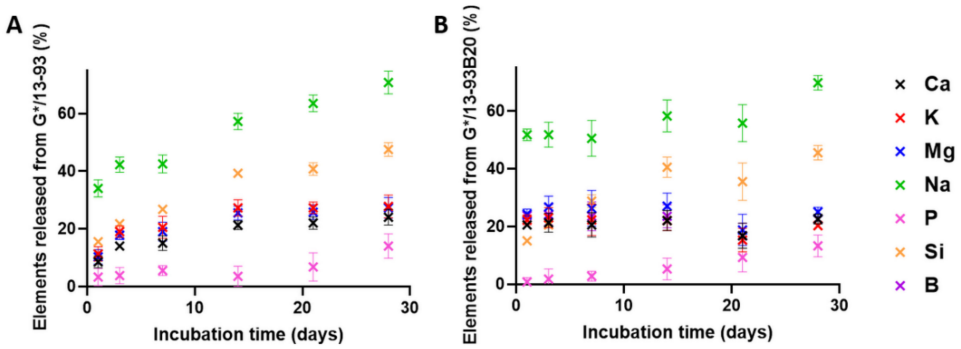

Figure 4. Release of ions from the (**A**) G*/13-93 and (**B**) G*/13-93B20 hybrids, immersed in TRIS as a function of time.

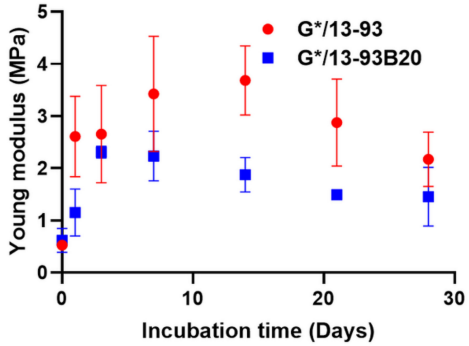

Figure 5. Young's modulus measured by a compression test of wet G*/13-93 (●) and G*/13-93B20 (■) hybrids as a function of immersion time in TRIS.

Young's modulus was measured on wet samples as a function of incubation time (Figure 5). The evolution of the mechanical properties takes place in two stages. First, an increase in Young modulus for both hybrids can be seen. A maximum is then reached at 3 days for G*/13-93B20 and at 14 days for G*/13-93. At longer immersion times, a decrease in Young's modulus is noticed. The increase in modulus could be due to the syneresis phenomenon, as explained for Figure 2. The water loss leads to a reinforcement of the mechanical properties. After that, the decrease in Young's modulus would be due to hybrids erosion, inducing a loss of its mechanical properties. This corroborates the phenomenon showed in Figures 3 and 4, showing that this decrease happens when the stabilization of ion release is reached for G*/13-93.

Hybrids immersion in TRIS allowed to understand their dissolution and their ions release in solution. The 13-93B20 dissolves and reaches the saturation faster but finally at the same level than the 13-93. This dissolution has an influence on the mechanical properties but it should be noted that despite these variations, Young's modulus stays close to that of cancellous bone [29–31].

3.2.2. Dissolution in Simulated Body Fluid (SBF)

The hybrids were immersed in Simulated Body Fluid (SBF) to study their bioactivity. ICP-OES analysis, mass measurements, SEM observations, and EDX and FTIR analysis were conducted to assess the ion release/precipitation and the formation of a reactive layer.

As postulated by L.L. Hench, the ability of a material to induce precipitation of an hydroxyapatite layer at its surface can be considered as a sign of bioactivity [11]. Immersion in SBF was conducted for two weeks, and the solution was not refreshed. The ion concentration in the solution was quantified. The difference between the ion concentration in SBF and ion concentration after hybrid immersion was calculated (Figure 6).

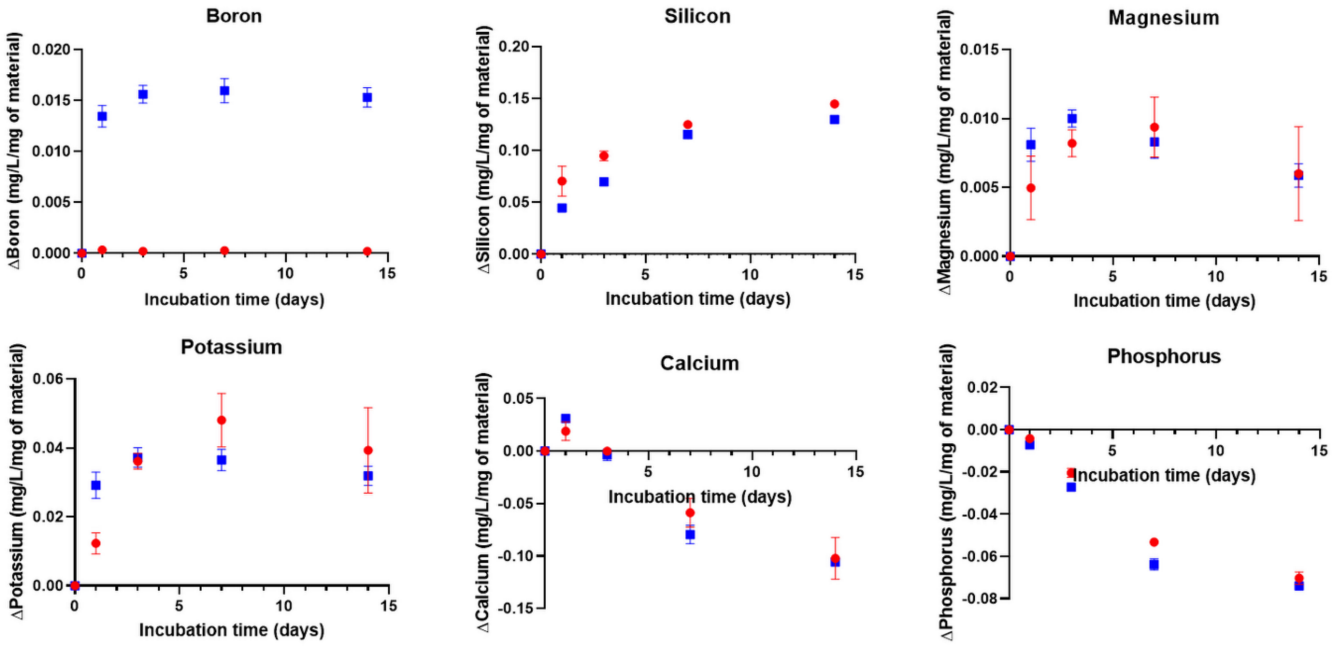

Figure 6. Concentrations of Si, Mg, K, P, Ca, and B in the dissolution products of G*/13-93 (●) and G*/13-93B20 (■) immersed in Simulated Body Fluid (SBF) as a function of time. The concentrations are normalized to the sample mass. ΔElement = [Element] in SBF in the presence of the sample – [Element] in SBF initial solution.

The Ca concentration seems to increase initially and then decreases with immersion time, whereas the P concentration decreases from the beginning of the dissolution. This phenomenon was also observed in our previous study on composites based on Poly(Lactic) Acid (PLA) and the same glasses [13]. Generally, the decrease in Ca and P in SBF corre-

sponds to the precipitation of a calcium-phosphate reactive layer. The elements Mg and K show similar trends during immersion in SBF. The 13-93B20 glass leaches out its ions at a faster rate initially than 13-93 and then; for both hybrids, a decrease in Mg and K concentrations appears. It is important to note that the dissolution rate slows down at earlier immersion times in SBF than in TRIS for G*/13-93. This decrease shows the saturation of the solution and probably that Mg and K can be incorporated into the calcium-phosphate reactive layer [32]. Silicon release is linear and continuous, tending towards a plateau, for both hybrids. It is initially higher for G*/13-93, which can be, as explained above, because the borosilicate glass would be more reactive with the siloxane, leading to a lower Si release from the hybrids with 13-93B20.

Figure 7 presents the mass loss of the hybrids as a function to immersion time in SBF (Figure 7A), the hybrid mass after freeze-drying (Figure 7B), and the mineral mass remaining in the materials after immersion (Figure 7C).

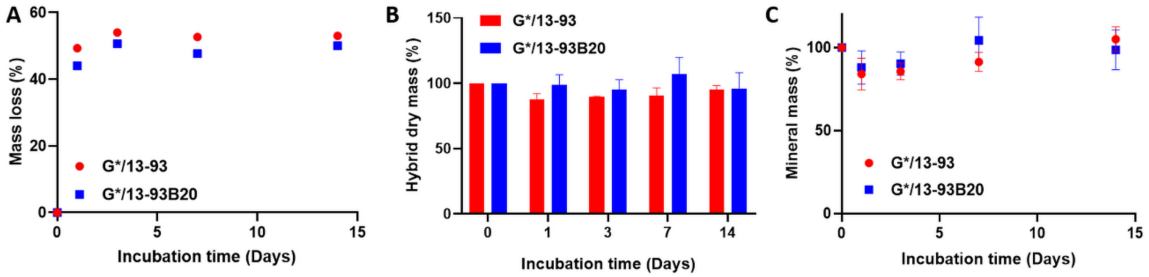

Figure 7. Mass loss (**A**), dry mass (**B**) and mineral mass (**C**) remained in the hybrid G*/13-93 (●) and G*/13-93B20 (■) as a function of immersion time in SBF.

Figure 7A shows that, after 24 h, the mass loss reaches approximately 50%, corresponding to a water loss and thus a shrinking of the materials due to syneresis, as explained for TRIS immersion. Then, the mass loss stays stable during immersion. In Figure 7B, the dry mass of hybrids immersed in SBF does not show the same evolution as in TRIS immersion. Indeed, a decrease in the dry mass was observed in TRIS immersion, while in SBF, it appears to stay approximately stable. For the mineral mass (Figure 7C), while it decreases during immersion in TRIS, showing the dissolution of the glasses, in SBF, it decreases and then increases. This corresponds to dissolution of the glass followed by the precipitation of the calcium-phosphate layer.

To assess the precipitation of this reactive layer, the hybrids were observed and analyzed using SEM/EDX as well as FTIR (Figures 8 and 9).

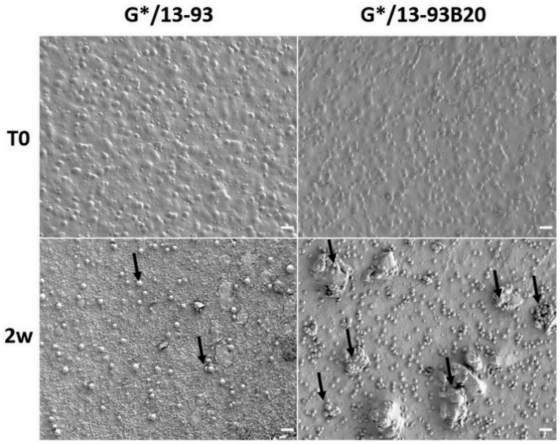

Figure 8. SEM image of the hybrid surface before and after 14 days of immersion in SBF (scale bar 20 μm).

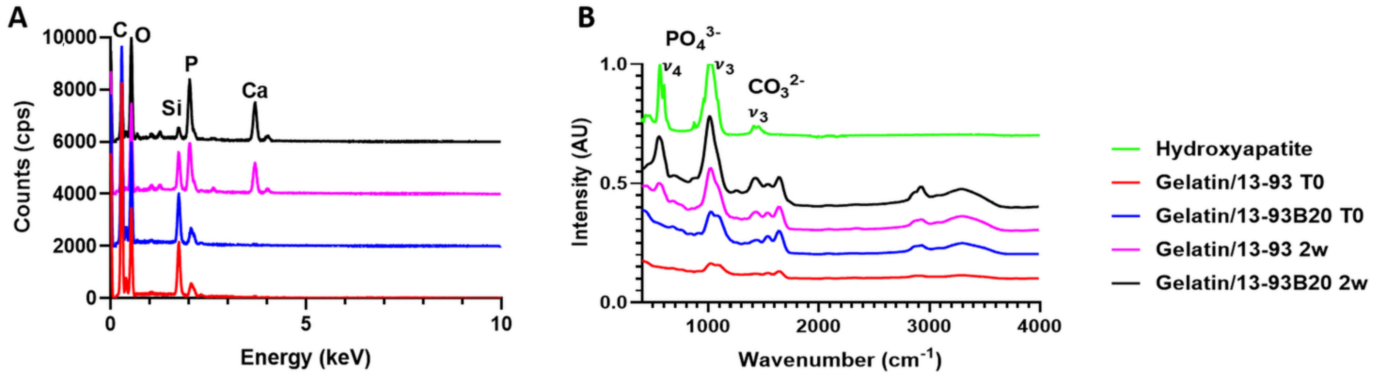

Figure 9. (**A**) EDX analysis of the nodules at the hybrids surface and (**B**) FTIR analysis of the samples surfaces before and after 14 days of immersion.

After 2 weeks of immersion in SBF, nodules appeared at their surface. The nodules are small and dispersed on the hybrid containing 13-93, while they are more numerous and larger on the G*/13-93B20 hybrid surface. EDX analysis were performed on the nodules shown in Figure 8, and the spectra are presented in Figure 9A. The composition of the spheres from both hybrids is mainly Ca and P with a ratio of Ca/P of 1.77 ± 0.08, which is close to hydroxyapatite [33]. This corroborates the precipitation of the calcium-phosphate layer hypothesized from the ICP analysis (Figure 6) and confirms that these nodules are probably apatite nodules. It is interesting to point out that the materials containing the glass 13-93B20 exhibit a higher population and bigger nodules than materials processed with the glass 13-93. This is in agreement with Huang et al., who demonstrated that the borosilicate bioactive glasses convert to HA faster and more completely than their silicate counterpart [34].

The nature of the Ca/P precipitate was further analyzed by FTIR spectroscopy (Figure 9B). Two peaks at 500–600 cm^{-1} and ≈1000 cm^{-1} appear after G*/13-93B20 (they are also present for G*/13-93 but with a lower intensity) immersion in SBF. These peaks correspond to ν_4 (P–O bending) and ν_3 (P–O stretching) PO_4^{3-} vibrations, respectively, in the apatite structure. The carbonate CO_3^{2-} vibration is also present [35–37]. These peaks are characteristic of a hydroxyapatite structure. This is a good indication that the calcium phosphate layer precipitating on the hybrid surface is a hydroxy-carbonated apatite, indicative of the potential bioactivity of those materials. These results show the difference in reactivity between both glasses. Ion release is slowed down by the organic matrix barrier, but 13-93B20 allows us to remedy this effect compared to 13-93 glass.

We developed gelatin/BAG hybrids using GPTMS as a coupling agent, with a C_{factor} of 500, using a sol-gel method. The target mineral content (70/30 wt%) was guaranteed by careful control of the processing steps. The mineral phase dissolves when immersed in aqueous solution with kinetics depending on the glass composition. The mechanical properties varied per the dissolution of the materials; however, Young's modulus remained close to the value reported for cancellous bone [29–31]. Both hybrids were found to precipitate hydroxy-carbonated apatite during immersion in SBF. The bioactivity seemed significantly higher when using 13-93B20 glass. Therefore, preliminary cell experiments were conducted to assess if the hybrids are biocompatible and, thus, support the growth of pre-osteoblastic cells, which is fundamental for bone application.

3.3. MC3T3-E1 Proliferation and Morphology

MC3T3-E1 pre-osteoblastic cells were used to study their proliferation and morphology on the hybrids (Figure 10).

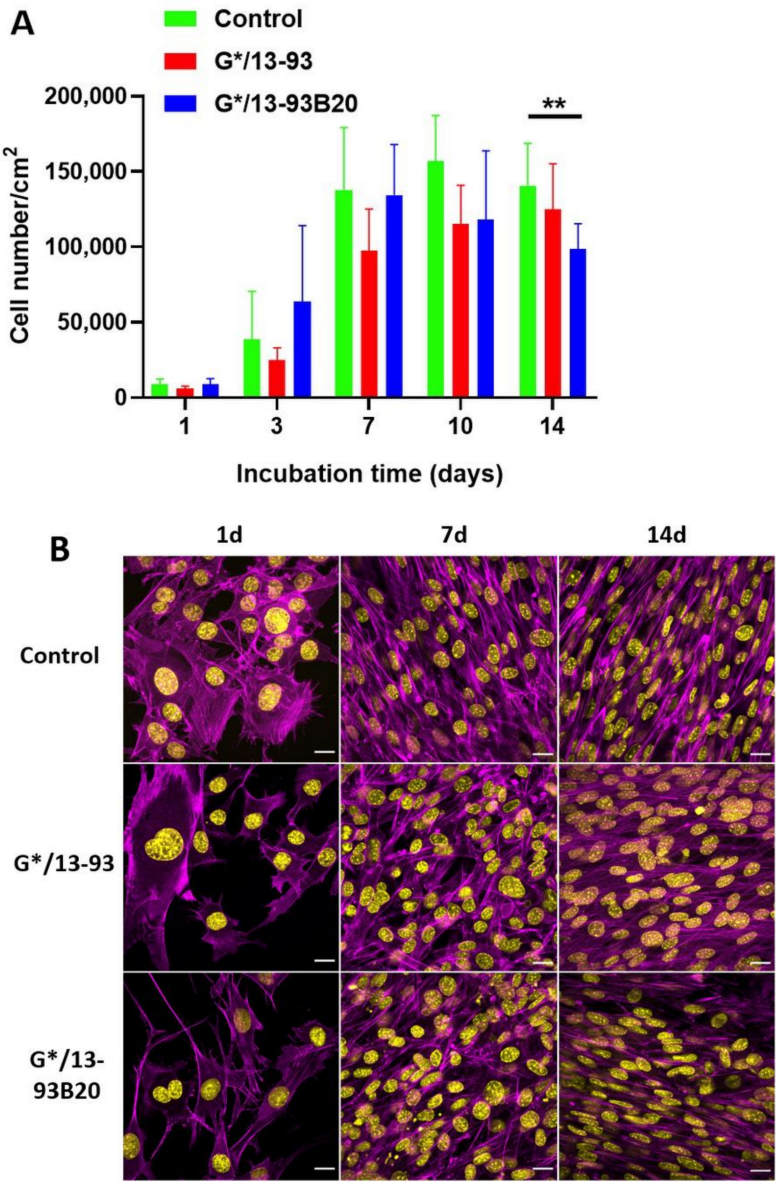

Figure 10. (**A**) Proliferation of MC3T3-E1 cells cultured in α-Minimum Essential Media (α-MEM) complete medium on Tissue Culture Polystyrene (TCPS), G*/13-93, and G*/13-93B20 hybrids for 14 days, analyzed by a CyQUANT Cell Proliferation Assay kit. The number of cells was normalized with the area of the materials surface (** $p < 0.01$). (**B**) Morphology of MC3T3-E1 cells in αMEM complete medium analyzed by nuclei (4',6-Diamidino-2-phenylindole dihydrochloride (DAPI)—yellow) and actin (phalloidin—magenta) immunostaining after 1 day, 7 days, and 14 days of culture. Scale bar 20 μm.

First, the number of MC3T3-E1 cells on the hybrids was studied for up to 14 days (Figure 10A). The hybrids were immersed 10 days in TRIS before cell culture to eliminate unreacted elements, which can prevent cell survival [38]. The hybrids were placed in 48 well plates, and the TCPS was used as a control. However, during their immersion in TRIS, they underwent a shrinking effect due syneresis. Indeed, they went from a diameter of 11 mm to 8 mm in 10 days. Thus, to compare the proliferation on the control and the materials, the cell number was normalized to the area of the respective sample.

For each condition, the cells proliferated with time and reached a plateau indicating the stationary phase (Figure 9A). The glass 13-93 alone was already known to promote cell adhesion and proliferation, as demonstrated by Fu et al. and Eqtesadi et al. [39,40].

At 14 days, the proliferation of MC3T3-E1 cells on G*/13-93B20 is significantly lower than on the control. This can be attributed to the release of boron from borosilicate glass, known to decrease cell proliferation while promoting osteogenesis, as observed in previous studies [13,24].

The morphology of the cells was observed at 24 h, 7 days, and 14 days on the control, G*/13-93, and G*/13-93B20 (Figure 10B). After 24 h, it can be observed that the cells spread on both hybrid types with their characteristic polygonal morphology. There is no difference noted in the cytoskeleton of cells between the conditions. At 7 days and 14 days, multicellular layers are observed, covering the hybrids. These results show that the cells can spread, attach, and proliferate on the hybrids. Thus, 13-93, 13-93B20, and GPTMS do not present cytotoxic effects and do not prevent the proliferation and adhesion of MC3T3-E1 cells on the hybrids.

4. Conclusions

Hybrids made of gelatin and BAG particles (silicate 13-93 and borosilicate 13-93B20) covalently linked with GPTMS were synthesized using the sol-gel method. The process of synthesis was optimized in order to obtain a content of organic/inorganic matter close to that expected and to avoid particle sedimentation and aggregates. These hybrids were stable and self-supported at biological temperature in aqueous medium. When immersed in simulated body fluid, their bioactivity was shown. Cell survival was demonstrated using MC3T3-E1 cells. The substitution of 20% of SiO_2 with B_2O_3 allowed us to tailor the dissolution and bioactivity properties of the hybrids. Once stabilized, the hybrids exhibited mechanical properties which, combined with their ability to precipitate HA and their biocompatible characteristic, make these materials good candidates for bone tissue engineering. Future studies will be conducted to investigate the osteo-stimulation of these materials.

Author Contributions: Conceptualization, A.H., M.B., J.M., and E.P.; methodology, R.A. and L.E.-G.; validation, A.H., M.B., J.M., and E.P.; formal analysis, A.H., A.S., and M.L. (ICP analysis); investigation, A.H., M.B., and J.M.; resources, M.B., J.M., and E.P.; data curation, A.H., M.B., and J.M.; writing—original draft preparation, A.H.; writing—review and editing, A.H., M.B., J.M., and E.P.; supervision, M.B., J.M., and E.P.; project administration, M.B., E.P., and J.M.; funding acquisition, M.B. and E.P. All authors have read and agreed to the published version of the manuscript.

Funding: The authors thank Agence Nationale de la Recherche (ANR) INEX Paris Seine Initiative for the doctoral fellowship.

Institutional Review Board Statement: Not applicable.

Informed Consent Statement: Not applicable.

Acknowledgments: The authors would like to thank the Science and Engineering Doctoral School of CY Cergy Paris Université for the financial support in researcher mobility.

Conflicts of Interest: The authors declare no conflict of interest.

References

1. Schemitsch, E.H. Size Matters: Defining Critical in Bone Defect Size! *J. Orthop. Trauma* **2017**, *31*, S20–S22. [CrossRef] [PubMed]
2. Myon, L.; Ferri, J.; Chai, F.; Blanchemain, N.; Raoul, G. Ingénierie du tissu osseux oro-maxillofacial par combinaison de biomatériaux, cellules souches, thérapie génique. *Rev. De Stomatol. Et De Chir. Maxillo-Faciale* **2011**, *112*, 201–211. [CrossRef] [PubMed]
3. Petrovic, V.; Zivkovic, P.; Petrovic, D.; Stefanovic, V. Craniofacial Bone Tissue Engineering. *Oral Surg. Oral Med. Oral Pathol. Oral Radiol.* **2012**, *114*, e1–e9. [CrossRef] [PubMed]
4. Kokubo, T. Apatite Formation on Surfaces of Ceramics, Metals and Polymers in Body Environment. *Acta Mater.* **1998**, *46*, 2519–2527. [CrossRef]
5. Shimazaki, K.; Mooney, V. Comparative Study of Porous Hydroxyapatite and Tricalcium Phosphate as Bone Substitute. *J. Orthop. Res.* **1985**, *3*, 301–310. [CrossRef]
6. Ohura, K.; Bohner, M.; Hardouin, P.; Lemaître, J.; Pasquier, G.; Flautre, B. Resorption of, and Bone Formation from, New β-Tricalcium Phosphate-Monocalcium Phosphate Cements: Anin Vivo Study. *J. Biomed. Mater. Res.* **1996**, *30*, 193–200. [CrossRef]

7. Schwach, G.; Vert, M. In Vitro and in Vivo Degradation of Lactic Acid-Based Interference Screws Used in Cruciate Ligament Reconstruction. *Int. J. Biol. Macromol.* **1999**, *25*, 283–291. [CrossRef]
8. Hasegawa, S.; Ishii, S.; Tamura, J.; Furukawa, T.; Neo, M.; Matsusue, Y.; Shikinami, Y.; Okuno, M.; Nakamura, T. A 5–7 Year in Vivo Study of High-Strength Hydroxyapatite/Poly(l-Lactide) Composite Rods for the Internal Fixation of Bone Fractures. *Biomaterials* **2006**, *27*, 1327–1332. [CrossRef]
9. Verheyen, C.C.P.M.; de Wijn, J.R.; van Blitterswijk, C.A.; de Groot, K.; Rozing, P.M. Hydroxylapatite/Poly(L-Lactide) Composites: An Animal Study on Push-out Strengths and Interface Histology. *J. Biomed. Mater. Res.* **1993**, *27*, 433–444. [CrossRef]
10. Ishikawa, K. Calcium Phosphate Cement. In *Advances in Calcium Phosphate Biomaterials*; Ben-Nissan, B., Ed.; Springer Berlin Heidelberg: Berlin, Heidelberg, 2014; pp. 199–227. ISBN 978-3-642-53980-0.
11. Hench, L.L. The Story of Bioglass®. *J. Mater. Sci. Mater. Med.* **2006**, *17*, 967–978. [CrossRef]
12. Day, R.M.; Boccaccini, A.R.; Shurey, S.; Roether, J.A.; Forbes, A.; Hench, L.L.; Gabe, S.M. Assessment of Polyglycolic Acid Mesh and Bioactive Glass for Soft-Tissue Engineering Scaffolds. *Biomaterials* **2004**, *25*, 5857–5866. [CrossRef]
13. Houaoui, A.; Lyyra, I.; Agniel, R.; Pauthe, E.; Massera, J.; Boissière, M. Dissolution, Bioactivity and Osteogenic Properties of Composites Based on Polymer and Silicate or Borosilicate Bioactive Glass. *Mater. Sci. Eng. C* **2020**, *107*, 110340. [CrossRef]
14. Mahony, O.; Tsigkou, O.; Ionescu, C.; Minelli, C.; Ling, L.; Hanly, R.; Smith, M.E.; Stevens, M.M.; Jones, J.R. Silica-Gelatin Hybrids with Tailorable Degradation and Mechanical Properties for Tissue Regeneration. *Adv. Funct. Mater.* **2010**, *20*, 3835–3845. [CrossRef]
15. Novak, B.M. Hybrid Nanocomposite Materials-between Inorganic Glasses and Organic Polymers. *Adv. Mater.* **1993**, *5*, 422–433. [CrossRef]
16. Nicole, L.; Boissière, C.; Grosso, D.; Quach, A.; Sanchez, C. Mesostructured Hybrid Organic–Inorganic Thin Films. *J. Mater. Chem.* **2005**, *15*, 3598. [CrossRef]
17. Liu, Y.-L.; Su, Y.-H.; Lai, J.-Y. In Situ Crosslinking of Chitosan and Formation of Chitosan–Silica Hybrid Membranes with Using γ-Glycidoxypropyltrimethoxysilane as a Crosslinking Agent. *Polymer* **2004**, *45*, 6831–6837. [CrossRef]
18. Mahony, O.; Yue, S.; Turdean-Ionescu, C.; Hanna, J.V.; Smith, M.E.; Lee, P.D.; Jones, J.R. Silica–Gelatin Hybrids for Tissue Regeneration: Inter-Relationships between the Process Variables. *J. Sol.-Gel Sci. Technol.* **2014**, *69*, 288–298. [CrossRef]
19. Vueva, Y.; Connell, L.S.; Chayanun, S.; Wang, D.; McPhail, D.S.; Romer, F.; Hanna, J.V.; Jones, J.R. Silica/Alginate Hybrid Biomaterials and Assessment of Their Covalent Coupling. *Appl. Mater. Today* **2018**, *11*, 1–12. [CrossRef]
20. Maeda, H.; Kasuga, T.; Hench, L.L. Preparation of Poly(l-Lactic Acid)-Polysiloxane-Calcium Carbonate Hybrid Membranes for Guided Bone Regeneration. *Biomaterials* **2006**, *27*, 1216–1222. [CrossRef]
21. Vergnol, G.; Ginsac, N.; Rivory, P.; Meille, S.; Chenal, J.-M.; Balvay, S.; Chevalier, J.; Hartmann, D.J. In Vitro and in Vivo Evaluation of a Polylactic Acid-Bioactive Glass Composite for Bone Fixation Devices: Polylactic acid-bioactive glass composite for bone fixation devices. *J. Biomed. Mater. Res. Part B Appl. Biomater.* **2016**, *104*, 180–191. [CrossRef]
22. Brink, M. The Influence of Alkali and Alkaline Earths on the Working Range for Bioactive Glasses. *J. Biomed. Mater. Res.* **1997**, *36*, 109–117. [CrossRef]
23. Brown, R.F.; Rahaman, M.N.; Dwilewicz, A.B.; Huang, W.; Day, D.E.; Li, Y.; Bal, B.S. Effect of Borate Glass Composition on Its Conversion to Hydroxyapatite and on the Proliferation of MC3T3-E1 Cells. *J. Biomed. Mater. Res. Part A* **2009**, *88A*, 392–400. [CrossRef] [PubMed]
24. Ojansivu, M.; Mishra, A.; Vanhatupa, A.; Juntunen, M.; Larionova, A.; Massera, J.; Miettinen, S. The Effect of S53P4-Based Borosilicate Glasses and Glass Dissolution Products on the Osteogenic Commitment of Human Adipose Stem Cells. *PLoS ONE* **2018**, *13*, e0202740. [CrossRef] [PubMed]
25. Maçon, A.L.B.; Kim, T.B.; Valliant, E.M.; Goetschius, K.; Brow, R.K.; Day, D.E.; Hoppe, A.; Boccaccini, A.R.; Kim, I.Y.; Ohtsuki, C.; et al. A Unified in Vitro Evaluation for Apatite-Forming Ability of Bioactive Glasses and Their Variants. *J. Mater. Sci. Mater. Med.* **2015**, *26*, 115. [CrossRef]
26. Griffith, L.G.; Naughton, G. Tissue Engineering–Current Challenges and Expanding Opportunities. *Science* **2002**, *295*, 7. [CrossRef]
27. Connell, L.S.; Gabrielli, L.; Mahony, O.; Russo, L.; Cipolla, L.; Jones, J.R. Functionalizing Natural Polymers with Alkoxysilane Coupling Agents: Reacting 3-Glycidoxypropyl Trimethoxysilane with Poly(γ-Glutamic Acid) and Gelatin. *Polym. Chem.* **2017**, *8*, 1095–1103. [CrossRef]
28. Hench, L.L. Bioceramics: From Concept to Clinic. *J. Am. Ceram. Soc.* **1991**, *74*, 1487–1510. [CrossRef]
29. Wu, D.; Isaksson, P.; Ferguson, S.J.; Persson, C. Young's Modulus of Trabecular Bone at the Tissue Level: A Review. *Acta Biomater.* **2018**, *78*, 1–12. [CrossRef]
30. Bini, F.; Marinozzi, A.; Marinozzi, F.; Patanè, F. Microtensile Measurements of Single Trabeculae Stiffness in Human Femur. *J. Biomech.* **2002**, *35*, 1515–1519. [CrossRef]
31. Hong, J.; Cha, H.; Park, Y.; Lee, S.; Khang, G.; Kim, Y. Elastic Moduli and Poisson's Ratios of Microscopic Human Femoral Trabeculae. In IFMBE Proceedings, Proceedings of the11th Mediterranean Conference on Medical and Biomedical Engineering and Computing 2007, Ljubljana, Slovenia, 26–30 June 2007; Jarm, T., Kramar, P., Zupanic, A., Eds.; Springer: Berlin/Heidelberg, Germany, 2007; Volume 16, pp. 274–277, ISBN 978-3-540-73043-9.
32. Combes, C.; Cazalbou, S.; Rey, C. Apatite Biominerals. *Minerals* **2016**, *6*, 34. [CrossRef]

33. Singh, R.; Tan, C.; Abd Shukor, M.; Sopyan, I.; Teng, W. The Influence of Ca/P Ratio on the Properties of Hydroxyapatite Bioceramics. In Proceedings of the International Conference on Smart Materials and Nanotechnology in Engineering A, Harbin, China, 1–4 July 2007; Proceedings SPIE: Bellingham, WA, USA, 2007; Volume 6423. [CrossRef]
34. Huang, W.; Day, D.E.; Kittiratanapiboon, K.; Rahaman, M.N. Kinetics and Mechanisms of the Conversion of Silicate (45S5), Borate, and Borosilicate Glasses to Hydroxyapatite in Dilute Phosphate Solutions. *J. Mater. Sci. Mater. Med.* **2006**, *17*, 583–596. [CrossRef]
35. Stanislavov, A.S.; Sukhodub, L.F.; Sukhodub, L.B.; Kuznetsov, V.N.; Bychkov, K.L.; Kravchenko, M.I. Structural Features of Hydroxyapatite and Carbonated Apatite Formed under the Influence of Ultrasound and Microwave Radiation and Their Effect on the Bioactivity of the Nanomaterials. *Ultrason. Sonochem.* **2018**, *42*, 84–96. [CrossRef]
36. Baddiel, C.B.; Berry, E.E. Spectra Structure Correlations in Hydroxy and Fluorapatite. *Spectrochim. Acta* **1966**, *22*, 1407–1416. [CrossRef]
37. Berzina-Cimdina, L.; Borodajenko, N. Research of Calcium Phosphates Using Fourier Transform Infrared Spectroscopy. In *Infrared Spectroscopy-Materials Science, Engineering and Technology*; Theophanides, T., Ed.; InTech: London, UK, 2012; ISBN 978-953-51-0537-4.
38. Maisani, M.; Pezzoli, D.; Chassande, O.; Mantovani, D. Cellularizing Hydrogel-Based Scaffolds to Repair Bone Tissue: How to Create a Physiologically Relevant Micro-Environment? *J. Tissue Eng.* **2017**, *8*, 1–26. [CrossRef]
39. Fu, Q.; Rahaman, M.N.; Bal, B.S.; Bonewald, L.F.; Kuroki, K.; Brown, R.F. Silicate, Borosilicate, and Borate Bioactive Glass Scaffolds with Controllable Degradation Rate for Bone Tissue Engineering Applications. II. In Vitro and in Vivo Biological Evaluation. *J. Biomed. Mater. Res. Part A* **2010**, *95A*, 172–179. [CrossRef]
40. Eqtesadi, S.; Motealleh, A.; Pajares, A.; Miranda, P. Effect of Milling Media on Processing and Performance of 13-93 Bioactive Glass Scaffolds Fabricated by Robocasting. *Ceram. Int.* **2015**, *41*, 1379–1389. [CrossRef]

Materials Science & Engineering C 117 (2020) 111269

Contents lists available at ScienceDirect

Materials Science & Engineering C

journal homepage: www.elsevier.com/locate/msec

Phosphate/oxyfluorophosphate glass crystallization and its impact on dissolution and cytotoxicity

A. Nommeots-Nomm[a,1], A. Houaoui[b], A. Pradeepan Packiyanathar[b], X. Chen[f], M. Hokka[d], R. Hill[c], E. Pauthe[b], L. Petit[e], M. Boissière[b], J. Massera[a,*]

[a] Tampere University, Faculty of Medicine and Health Technology, Laboratory of Biomaterials and Tissue Engineering, Korkeakoulunkatu 3, 33720 Tampere, Finland
[b] Biomaterials for Health Research Group, ERRMECe, Equipe de recherche sur les Relations Matrice Extracellulaire-Cellules (EA1391), Institut des matériaux I-MAT (FD4122), CY Tech, CY Cergy Paris University, Maison Internationale de la Recherche (MIR), rue Descartes, 95001 Neuville sur Oise cedex, France
[c] Dental Physical Sciences, Institute of Dentistry, Queen Mary University of London, Mile End Road, London E1 4NS, UK
[d] Tampere University of Technology, Laboratory of Material Sciences, Korkeakoulunkatu 3, 33720 Tampere, Finland
[e] Tampere University of Technology, Laboratory of Photonics, Korkeakoulunkatu 3, 33720 Tampere, Finland
[f] Hunan Key Laboratory of Oral Health Research & Hunan 3D Printing Engineering Research Center of Oral Care Xiangya Stomatological Hospital & Xiangya School of Stomatology, Central South University, Changsha, 410008, Hunan, China

ARTICLE INFO

Keywords:
Oxyfluoride bioactive phosphate glass
MAS-NMR
P-F bonds
Bioactive glass-ceramic
Crystallization
In vitro dissolution
MC3T3 cells
Index of cytotoxicity

ABSTRACT

The role of fluorine in bioactive glasses is of interest due to the potential of precipitating fluorapatite, a phase with higher chemical resistance than the typical hydroxyapatite precipitated from oxide bioactive glasses. However, the introduction of fluorine in silicate bioactive glasses was found deleterious to the bioactivity of the glass. Here, phosphate glasses with the composition $75NaPO_3$-(25-x) CaO-xCaF_2 (in mol%), with x = 0–20 and glass-ceramics were investigated to evaluate their potential as substitutes to the traditional silicate bioactive glass. An increase in CaF_2 substitution for CaO led to an increase in the glass solubility, due to an increase in highly soluble F(*M*)n species (where M is a cation) and to an increased polymerization of the phosphate network. Structural analysis reveals the formation of F—P bonds, in addition to the F(*M*)n species, in the glass with the higher CaF_2 content. Furthermore, with heat treatment, CaF_2 crystals precipitate within the bulk in the newly developed glass, when x = 20. This bulk crystallization reduces the glass dissolution without compromising the precipitation of a reactive layer at the glass surface. Finally, in vitro cell tests were performed using MC3T3 pre-osteoblastic cells. While the substitution of CaF_2 for CaO led to an increased cytotoxicity, the controlled crystallization of the fluorine containing glasses decreased such cytotoxicity to similar values than traditional bioactive phosphate glass (x0). This study reports on new oxyfluorophosphate glass and glass-ceramics able, not only, to precipitate a Ca-P reactive layer but also to be processed into glass-ceramics with controlled crystal size, density and cellular activity.

Statement of significance: Uncontrolled crystallization of bioactive glasses has negative effect on the materials' bioactivity. While in silicate glass the bioactivity is solely reduced, in phosphate glasses it is often completely suppressed. Furthermore, the need for fluorine containing bioactive glasses, not only for use in bone reconstruction but also in toothpaste as emerged. The addition of F in both silicate and phosphate has led to challenges due the lack of Si-F or P-F bonds, generally leading to a decrease in bioactivity. Here, we developed a bioactive invert phosphate glass where up to 20 mol% of CaO was replaced with CaF_2. In the new developed glasses, NMR demonstrated formation of P-F bonds. The content of fluorine was tailored to induce CaF_2 bulk crystallization. Overall an increase in F was associated with an increase network connectivity. In turns it led to an increased dissolution rate which was linked to a higher cytotoxicity. Upon (partial to full) surface crystallization of the F-free glass, the bioactivity (ability to form a reactive layer) was loss and the cytotoxicity again increased due to the rapid dissolution of one crystal phase and of the remaining amorphous phase. On another hand, the controlled bulk precipitation of CaF_2 crystals, in the F-containing glass, was associated with a reduced cytotoxicity. The new oxyfluorophosphate glass-ceramic developed is promising for application in the biomedical field.

* Corresponding author.
E-mail address: jonathan.massera@tuni.fi (J. Massera).
[1] Now at McGill University, Department of Mining and Materials Engineering, Canada.

https://doi.org/10.1016/j.msec.2020.111269
Received 13 February 2020; Received in revised form 3 July 2020; Accepted 4 July 2020
Available online 06 July 2020

1. Introduction

Despite the tremendous progress in large defect bone treatment, challenges remain. As of today, a large variety of grafts, natural or synthetic, can be used, from autograft to synthetic hydroxyapatite, with or without addition of growth factors [1]. A challenge to be considered is the production of porous synthetic substitutes able to support fast bone growth while also supporting wide vascularization within the scaffold structure. The need for bone augmentation/regeneration might also be associated with cancer treatment or high prevalence for infection. In such condition, the clinical outcomes, using traditional biomaterials remain poor [2]. To this respect, bioactive glasses can play a major role. They are known to allow the release of a large variety of ions with therapeutic interest while promoting both osteogenesis and angiogenesis [3–5].

The osteoconductivity and osteoinductivity of traditional silicate bioactive glasses and, therefore, their potential in hard tissue regeneration is nowadays well-known [6–7]. Part of the bioactivity of the glass is attributed to the ability of the glass to precipitate a hydroxyapatite layer, similar to the mineral phase of the bone, at the surface of the glass particles [8]. Today, bioactive glasses have found use in a wide range of clinical application such as bone healing, osteomyelitis treatment and wound healing [9–11]. More recently, the incorporation of glass particles in toothpaste have proven to be successful in reducing teeth hypersensitivity such as in the Sensodyne® Repair and Protect and the newly launched BioMin™ [12–14]. Such effects were attributed to the occlusion of dentinal tubule due to the precipitation of hydroxyapatite upon glass dissolution.

Fluorine containing glasses have become glasses of interest due to the fluorides' ability to enhance their optical [15–17] and bioactive properties [18]. The incorporation of fluorine into silicate and borosilicate glasses reduces the glass transition temperature and facilitates nano-scale crystallization [19–23]. In silicate glasses, the thermal properties, crystallization behaviour, and the precipitated phases are strongly influenced by the interplay of ions within the local glass structure [18,24–25]. In most cases, the fluorine is complexed by metal cations forming F-M(n) species with fluorine having preference for the cations of the highest charge to size ratio [26]. The presence of fluorine in bioactive glass has been found to lead to the precipitation of a fluorapatite layer [1]. Interest in the precipitation of the fluorapatite, from bioactive glasses within sensitive toothpaste has been growing momentum [18,22,27]. It is thought that the precipitation of fluorapatite offers enhanced repair for tooth sensitivity due to its aforementioned higher chemical durability in the acidic environment of the mouth [28]. Fluorapatite is not only of interest in dental applications. The use of a fluorapatite coating, in place of the traditionally use hydroxyapatite, is already in use in implants inserted in the iliac crest of consenting patients [29]. The study suggests that the fluorapatite coating is more stable than the hydroxyapatite coating against resorption by bone marrow. Furthermore, Freeman et al. demonstrated in their study that the larger the proportion of fluorapatite crystal at the specimen surface the better the bone bonding in rat femur [30].

Until now, most of the work on fluorine containing bioactive glasses has been conducted on phosphosilicate glasses. However, these glasses have limitations, especially when fluorine is introduced into the glass network. The replacement of CaF_2 for CaO leads to an increase in the glass network connectivity due to the formation of highly connected silica and the absence of Si—F bonds, which in turn reduces the glass bioactivity [31–33]. The consequence of a lower bioactivity results in the formation of an inhomogeneous hydroxyapatite and silica-rich layer at the glass particle surface [34]. A second challenge arises when developing bioactive glasses for use in orthopaedic applications. In the case of glass particles for toothpaste application, the processing of small particles is not a complex challenge and can be completed in one processing step. However, in orthopaedics applications, the optimal bone graft should be a 3D scaffold with controlled porosity to enable fluid penetration, cell migration and vascularization [35]. The processing of scaffolds from glass particles almost systematically relies upon a two-step process: first the glass is produced and crushed into powder then secondly the glass particles are fused together via a high temperature sintering process. Upon heating, uncontrolled surface crystallization occurs in typical bioactive silicate glasses (such as 45S5 and S53P4), which not only prevents proper glass particle sintering but also significantly alters the glasses bioactivity [36–38].

One alternative to the typical silicate bioactive glasses is phosphate-based glass. The composition of phosphate glasses can be tailored so the glasses are bioactive and possess suitable thermal properties enabling hot forming [39–41]. For example, De Silva Thompson produced titanium doped phosphate glass microsphere to be used as microcarriers [42]. These microparticles were found to support osteoblastic cell responses in dynamic cell culture condition. Thus, they appear to be a perfect platform for expanding bone forming cells while promoting their osteogenic commitment. Not only phosphate-based glasses are suitable for bone regeneration, they are also commercially available (Zincosel® Cattle Bolus, Bimeda) for their ability to release therapeutic ions in a controlled manner [43]. However, it is worth mentioning that while the crystallization of silicate bioactive glasses leads to a decrease in the bioactivity, the surface crystallization of phosphate bioactive glasses suppresses completely the bioactivity and leads to the release of phosphorous in the medium in high concentration [44].

Given some of the benefits of using phosphate bioactive glasses, Christie et al. [32] studied the structure of oxyfluorophosphate glasses using ab initio molecular dynamics simulations. The studied glasses were metaphosphate (with P_2O_5 close to 50 mol%) and CaF_2 was not replaced for CaO but rather doped into the glass. In their glass composition, a large amount of P—F bonds were formed when adding CaF_2, increasing the glass' bioactivity. Therefore, Christie et al. concluded that the fluorinated phosphate glasses are a more suitable alternative than the fluorinated phosphosilicate bioactive glasses. While these results are promising, the phosphate glasses with metaphosphate structures are known to be less bioactive than invert phosphate glasses [45]. This is due to the rapid dissolution of the metaphosphate structure. Shaharyar et al. [46] studied the structure-solubility relationship of fluoride containing glasses having a phosphate content of 45 mol%. In their glasses, little to no P—F bonds were reported as evidenced by the increased network polymerization associated with an increase in the fluorine content.

To the best of our knowledge, Cui et al. published the first study that indicates significant formation of P—F bonds in fluorinated invert phopshate glass [17]. Not only P—F bonds, assumed to be beneficial to bioactivity, were suggested in this glass system, but also bulk crystallization of CaF_2 crystals was reported. This is of particular interest in orthopaedic applications, as bulk crystallization of a bioactive glass helps maintaining the glass bioactivity over the course of the glass degradation. It is also of great potential in dental application as the CaF_2 crystals are known to be cariostatic [47].

Therefore, here we present the in-vitro dissolution of fluorinated invert phosphate glasses with the composition of $75NaPO_3$-(25-x) CaO-$xCaF_2$ (in mol%), with x ranging from 0 to 20. EDX and EPMA characterisation was carried out to quantify the glasses composition. Thermal and structural analyses of the glasses were performed using DSC, FTIR and NMR. Changes in in-vitro dissolution were related to the F-speciation. Finally, the crystallization of the glasses was assessed by defining crystallization kinetics parameters such as the activation

energy of the crystallization and the Johnson-Mehl-Avrami exponent. The impact of the crystallization on the dissolution behaviour of the F-free and F-containing invert phosphate glasses was studied in order to gauge the ability of the glass to remain bioactive upon controlled internal crystallization. The index of cytotoxicity (IC50) and cell spreading was established for the glass and glass-ceramics.

2. Experimental

2.1. Glass and glass-ceramic preparation

Glass compositions of $75NaPO_3$-(25-x) CaO-xCaF_2 (in mol%), with x = 0, 5, 10, 15 and 20 (the glasses are labelled as x0, x5, x10, x15 and x20) were prepared by melt quenching technique. The mol% of each oxide is presented in Table 1.

10 g batches were prepared from analytical grades of $NaPO_3$, CaO, and CaF_2 purchased from Sigma Aldrich. Glasses were melted at 950 °C for 5 min in a platinum/rhodium (95%/5%) crucible covered with a platinum lid, to minimise volatilisation, and then quenched. The glasses were then annealed for 4 h at 40 °C below the glass transition temperature. After annealing, the as-prepared glass was crushed, by hand, using a ceramic pestle and mortar, into powder. The glass particles with a 125–250 μm size range were heat treated in an electrical oven at T_x (onset of crystallization) and T_x + 20 for 3 h in air. Glasses were heated to the target temperature in platinum pans at a rate of 20 K/min, dwelled for the required time and quenched in air. The heat treated glasses are labelled as HTx0, HT5, HTx10, HTx15 and HTx20.

2.2. Thermal analysis

Non-isothermal Differential Thermal Analysis was performed using a Netzsch Jupiter STA 449. Glasses were ground to particles between 125 and 250 μm and 30.00 ± 0.025 mg was weighed into a platinum pan. Samples were analysed under nitrogen flow, using an empty platinum crucible as a reference. The thermograms were recorded from 40 to 600 °C at the heating rates of 5, 10, 15, and 20 K/min. The glass transition temperatures (T_g) were taken as the point of inflection of the first second order transition event, and the crystallization temperature (T_p) was taken at the maximum of the exothermic peak. T_x is the onset of crystallization taken from the thermographs at 20 K/min. The accuracy of the temperature measurement was ± 3 °C.

2.3. Composition analysis

The composition of the glasses was checked using scanning electron microscope (SEM) Leo 1530 Gemini from Zeiss coupled with Energy-dispersive X-ray spectroscopy (EDX) from Vantage by Thermo Electron Corporation. The accuracy of the elemental analysis was ~1.5 mol%. The Electron Probe MicroAnalyzer (EPMA) (CAMECA, SX100) equipped with 5 wavelength dispersive X-ray analyzers (WDX) was used to quantify the fluorine content (± 0.1 at.%). The EPMA was operated at 15 keV and 40 nA. Quantitative analyses were performed using the Cameca QUANTITOOL analytical programme, calibrated with ErF_3 reference standard, applying a PAP matrix correction. The samples were polished and were coated with a carbon layer in the same time than the reference to prevent charging.

2.4. Crystallization kinetics

The activation energy of crystallization (E_c) was calculated using the Kissinger equation [48]:

$$ln\frac{q}{T_p^2} = \frac{-E_c}{RT_p} + constant \quad (1)$$

where R is the gas constant, q is the heating rate and T_p, is the maximum peak of crystallization measured at the heating rate of 5, 10, 15, and 20 °C/min.

The limitations of the Kissinger methodology are discussed in detail elsewhere [49–50]. Therefore, to ensure accurate estimation of the activation energies of crystallization and to evidence any change in crystallization mechanisms during the course of the crystallization, the Friedman equation was also applied [51]:

$$ln\left(\frac{d\alpha_i}{dt}\right) = \frac{-E_{c\alpha}}{RT_i} + constant \quad (2)$$

where α is the proportion of glass converted into crystals and $\frac{d\alpha_i}{dt}$ is the rate of transformation at temperature T_i. The activation energy was taken from the average of the $E_{c\alpha}$ values collected.

2.5. Dissolution study

TRIS buffer solution was prepared at 37 °C, using TRIZMA Base (CAS: 77-86-1) and TRIZMA HCL (CAS: 1185-53-1). The pH was then measured and adjusted to 7.4. The glass mass-to-volume ratio was kept constant using 75 mg of glass to 50 ml of TRIS buffer [52]. Samples were studied in triplicate and kept in an orbital incubator (INFORS Multitron II) at 37 °C and 100 RPM. At 6, 24, 48, 72, 168, and 336 h, the pH was measured using a S47-K SevenMulti™ pH-meter (Mettler-Toledo LLC, Ohio, USA) at 37.0 ± 0.2 °C. 1 ml of solution was then taken and replaced from stock TRIS solution and diluted in 9 ml of (2 M) nitric acid (CAS7697-37-2 Romil LTD). Elemental concentrations in the solution were measured using Agilent technologies 5110 Inductively Coupled Plasma Optical Emission Spectrometer (ICP-OES) equipped with an auto sampler. ICP Standards of the applicable elements were all purchased from Romil LTD; phosphorus (Phosphorus 100 ppm PrimAg, solute: $NH_4H_2PO_4$, matrix HNO_3), calcium (Calcium 100 ppm PrimAg, solute: $CaCO_3$, matrix: HNO_3), and sodium (Sodium 100 ppm PrimAg, solute: Na_2CO_3, matrix: HNO_3) were prepared at 0, 4, 10, 20 and 40 μg ml^{-1} to obtain a calibration curve. The calibration was carried out at the beginning of each sequence. Lines for analysis used: P: 253.561 nm, Ca: 422.673 nm, and Na: 589.592 nm. The glass particles were collected at each time point, rinsed with acetone and dried for surface analysis. The particles were embedded in resin and polished in ethanol up to 4000 grit SiC paper.

2.6. XRD

The analysis was conducted using a Panalytical EMPYREAN multipurpose X-Ray Diffractometer using nickel filtered Copper K-Alpha radiation. Scans were completed between 10 and 90 degrees 2Θ, at 45 mA, 40 kV, with a step size of 0.013 step size, and a scan time of 8.67 s per step.

2.7. FTIR

The samples were analysed between 600 and 4000 cm^{-1} using a PerkinElmer Spectrum One FT-IR in Attenuated Total Reflectance mode. The resolution was 2 cm^{-1} and the results presented are the average of 8 scans.

Table 1
Nominal composition (measured composition through EDX and EPMA).

	P_2O_5 (mol%)	Na_2O (mol%)	CaO (mol%)	CaF_2 (mol%)
x0	37.5 (35)	37.5 (41)	25 (24)	0
x5	37.5 (36)	37.5 (41)	20 (19)	5 (4)
x10	37.5 (34)	37.5 (41)	15 (17)	10 (8)
x15	37.5 (35)	37.5 (42)	10 (11)	15 (12)
x20	37.5 (34)	37.5 (42)	5 (7)	20 (17)

2.8. ^{31}P and ^{19}F MAS-NMR

^{31}P and ^{19}F MAS-NMR experiments were carried out using a Bruker Advance 600 MHz spectrometer at the resonance frequencies of 242.9 MHz and 564.7 MHz. 31P MAS-NMR spectra were acquired in a 4 mm zirconia rotor at a spinning speed of 12 kHz after 16 scans, with a recycle delay of 60 s. ^{19}F MAS-NMR experiments were conducted in a 2.5 mm zirconia rotor at a spinning rate of 25 kHz and 60s relaxation. The spectra were recorded after 80 to 400 scans according to the fluoride concentration. The chemical shifts of ^{31}P and ^{19}F were referenced using 85% H_3PO_4 at 0 ppm and 1 M NaF at −120 ppm, respectively.

2.9. In-vitro cell culture

Each sample, (x0, HTx0, x20 and HTx20) was washed with 5 ml of pure acetone in an ultrasound bath for 25 min and dried at 120 °C for 2 h. Samples were then disinfected with 5 ml of 70% ethanol for 10 min followed by 5 ml of absolute ethanol for 10 min. The samples were dried 2 h at room temperature. Successively, glass powder (43.750 mg/ml), are mixed with culture Medium (α-MEM), supplemented with 1% antibiotics (penicillin and streptomycin), 24 h at 37 °C in a shaking incubator at 50 RPM. After the mixing, 10% foetal bovine serum (FBS) was added to the medium followed by sterile filtration using a vacuum-driven stericup (0.2 μm). Herein, this medium will be referred to as the conditioned medium (CM). The medium was then diluted 1, 10, 20, 50, 10^2, 10^3, 10^4 times.

Pre-osteoblastic MC3T3-E1 cells (subclone IV, ATCC4) were cultured in αMEM supplemented with 10% FBS and 1% antibiotics (penicillin/streptomycin), in a humidified atmosphere of 5% CO_2 at 37 °C. During the experiments, the cells were placed in the presence of the different CM prepared and new CM was given to them every other day.

The half maximal inhibitory concentration (IC50) for each sample was determined using the AlamarBlue assay. 10,000 cells/cm^2 were exposed to each diluted CM for 24 h. After exposure, the CMs were removed and a solution containing 50 μl of AlamarBlue and 450 μl of α-MEM was added and incubated for a further 4 h. The absorbance was measured at 570 nm and 600 nm independently using Spectrofluorimeter Xenius XM (SAFAS).

Cellular morphology was observed using immunocytochemical staining after 48 h of exposure to the CM diluted 10^2 times. Approximately 10,000 cells/cm^2 were seeded for each sample. After 48 h, the cells were fixed using 4% paraformaldehyde for 15 min, at room temperature. The cells were then permeabilized using 0.1% Triton X-100 for 10 min at 4 °C. The non-specific binding sites were blocked by incubating the samples, for 30 min, in 1% Bovine Serum Albumin (BSA). The actin filaments and nucleus were stained using a 1:500 diluted FITC-labelled phalloidin and 1:1000 diluted 4′,6-Diamidino-2-phenylindole (DAPI) respectively in a dark and humid environment. Each antibody was diluted using PBS-BSA 0.5%. After staining, the samples were washed with PBS-BSA 0.5% and mounted to coverslips using 10 μl Prolong Gold. Samples were observed using LSM710 confocal microscope (Carl Zeiss).

The morphology, spread and the cytoplasmic nuclear ratios (C:N) were analysed using the confocal microscope CLSM. For the C:N, images were analysed using ImageJ imaging software. For each sample, ten random cells were chosen and the cytoplasmic and nuclear areas were calculated. The average of these values was used and represented as a ratio (C:N ratio).

3. Results and discussion

3.1. Oxyfluoride glasses structure and their dissolution properties

The composition of the as-prepared glasses was assessed by EDX and found to be in agreement, with the theoretical composition at the exception of fluorine that was found to be deficient. The fluorine content in the glasses is difficult to quantify, due to the volatile nature of the fluorine itself [46]. F was quantified using EPMA and with a fluorine ion probe. From EPMA a loss of ~18% in fluorine was quantified while ~21% loss was measured using the ion probe. Work by Brauer et al. [18] suggests that 5–23% of CaF_2 depending on substitution quantity can be lost during melting of phosphosilicate glasses. Cui et al. [17] reported a loss of ~10 atomic % upon melting of a similar glass system as the one presented here. The as prepared glasses were investigated with X-ray diffraction (Fig. S1), and ^{19}F and ^{31}P MAS-NMR (Fig. 1). The FTIR spectra were already presented and discussed in [17]. The XRD analysis, reveals the presence of a broad halo between 20 and 30 degrees (2Θ), without the presence of any characteristic peaks, indicating that all as produced glasses were amorphous. Fig. 1(a) and (b) show the ^{19}F and ^{31}P MAS-NMR results, respectively. The ^{19}F MAS-NMR spectra exhibit multiple peaks assigned to multiple fluorine environments. The peaks marked with asterisks are indicative of the spinning side bands. All the glasses show a primary chemical shift at −75 ppm assigned to P—F species. A small peak at −225 ppm is assigned to F-Na(6), while its relative intensity decreases with increasing CaF_2 content [53]. The glasses with CaF_2 content lower than 20 mol% exhibit a peak with low intensity at −90 ppm, which appears as a shoulder in the NMR spectra of the glasses x10 and x15; this peaks corresponds to F-Ca(n) species according to [25]. In glass x20 this peak is absent, but a new band appears at −108 ppm. This is attributed to a CaF_2-like environment (F-Ca(4)) as previously hypothesised in [25]. With the exception of these environments, the additional peaks overlap in some cases with spinning side bands from the signal at −75 ppm, indicating the possible presence of mixed F-Ca/Na(n) species [54]. Fig. 1(b) shows the ^{31}P MAS-NMR spectra of the studied glasses. There are two broad phosphate signals, one with chemical shift at −2.6 ppm, corresponding to Q^1 phosphate and the other one with chemical shift at around −16.0 ppm, corresponding to Q^2 phosphate [55]. When CaF_2 is substituted for CaO up to 15 mol%, the intensity and position of the Q^1 phosphate peaks remain similar while the Q^2 phosphate peak at lower field increases in intensity with increasing CaF_2 content. This suggests an increase in the proportion of Q^2 species when x increases. In the case of the glass x20, the phosphate signal at −2.6 ppm broadens on the higher field side, while the maximum of the second peak shifts to −18.0 ppm, indicating a change in the first neighbour of the phosphate units.

In the oxyfluorosilicate glasses with high non-bridging oxygen contents, there has not been any evidence of Si—F bonds. However, the presence of fluorine associating with the network modifier cations to form F-M(n) species has been observed previously [18,25,56]. It is therefore expected to observe F-Ca/Na(n) species in the studied glasses in an analogous fashion to those found by Brauer et al. in fluoride containing silicate bioactive glasses [18]. Kasuga et al. investigated a phosphate glass with the composition of 35CaO–10-CaF_2–30P_2O_5–25TiO_2 (in mol%), and the ^{19}F spectra showed a broad peak at about −90 ppm corresponding to an F-Ca(n) environment while during the heat treatment the glass crystallized and exhibited a peak at −103 ppm corresponding to the F-Ca(3) site in fluorapatite [57]. Shaharyar et al. investigated glasses within the 10Na_2O–(45-x)CaO–45P_2O_5–xCaF_2 system [46]. Their study characterized the glasses in terms of ^{31}P MAS-NMR but did not perform any ^{19}F MAS-NMR. However, their molecular dynamics simulations provided the evidence of F-Ca/Na(n) species. In the present series of glasses, as expected, the multiple fluoride features at −90, −131.5, −139, −146.3 and −225 ppm are found in the ^{19}F MAS-NMR spectra and therefore can be associated to F-Ca/Na(n) species [54]. Additionally, all the glasses also show an intense peak at about −75 ppm, which cannot be attributed to F-Ca(n) species (typically at about −90 ppm) or mixed F-Ca/Na(n) species. This peak can be attributed to P—F as seen in the ^{19}F NMR spectra of monofluorophosphate [58].

The maximum in the ^{19}F chemical shift for fluorophosphosilicate

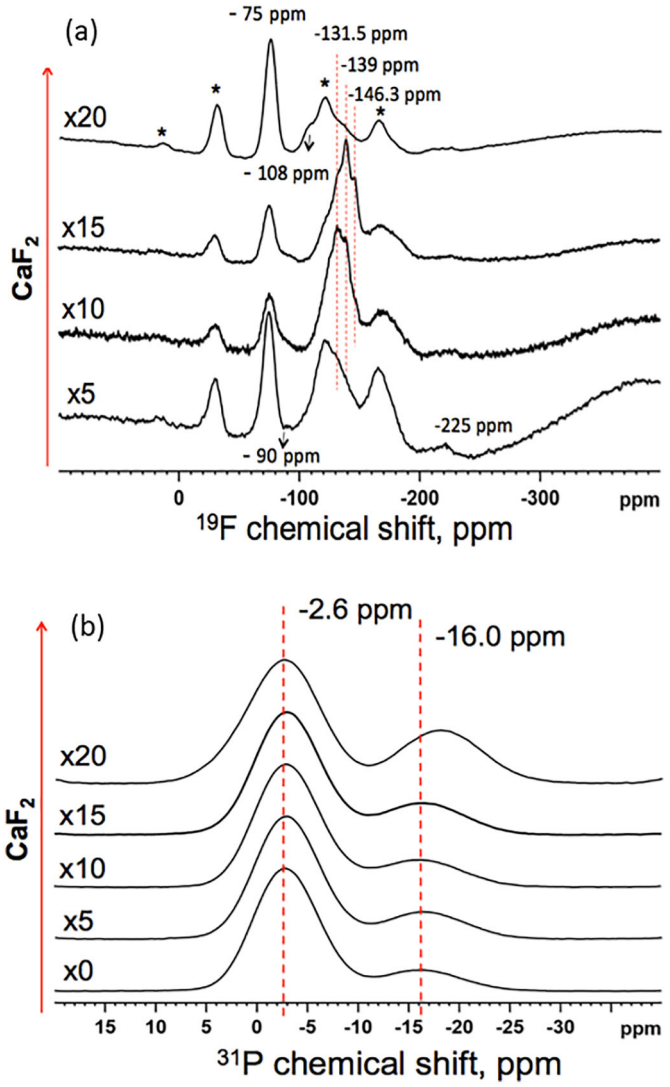

Fig. 1. (a) ^{19}F MAS-NMR spectra (b) ^{31}P MAS-NMR spectra for the ($75NaPO_3$-(25-x) CaO-xCaF_2) glasses.

glasses containing F-Ca/Na(n) species correlates with the Ca/(Ca + 2Na) ratio [53]. In the present glasses, this ratio is 0.67, independently of x. Therefore, a predicted chemical shift of −128 ppm is expected, which correlates with the shoulder to the right of the spinning side band for the x20 and x5 glasses; the shoulder to the left of the principal peak at −139 ppm for the x15 glass, and at the principal peak at −131.5 ppm with a shoulder at −139 ppm for the x10 glass. The more negative chemical shift of the principal peaks may reveal the charge balancing of Q^1 and Q^2 phosphate species, which has a slight preference for the Na^+ as opposed to the Ca^{2+} ions. Another hypothesis is that the x10 and x15 glasses contain nanocrystals which were not detected in the XRD pattern of the as-prepared glasses. The peaks at −139 ppm corresponding to an F-Ca(2)Na(2) species is rather sharp for a glass, and low density of small crystals will appear amorphous in the XRD pattern.

The network connectivity (NC) and the Q speciation assuming a binary Q distribution are shown in Table 2. In one case, only F-Ca/Na (n) species are assumed to be present in the glass network whereas in the other case only P−F species are considered. The presence of F-Ca/Na(n) species increases the NC while the presence of the P−F bonds reduces it as also shown in ref. [32]. From Fig. 1 and Table 2, the proportion of Q^2 increases at the expense of the Q^1 units with increasing CaF_2 content as reported in [59]. It is therefore assumed that F-Ca/Na (n) species are predominant in the glasses network. However, the broadening of the peak assigned to Q^1 units along with the shift of the peak related to the Q^2 species, at the higher CaF_2 content, indicates a change in the Q unit local structure. As supported by the FTIR analysis in [17], an increase in the proportion of P−F bonds along with the combination of a Q^2 and a phosphate bonded to F is the cause for the changes in the NMR spectra and the slower increase in Q^1, at the expense of Q^2, expected if only F-Ca/Na(n) was present in the glass. One can suspect that a terminal Q^1 phosphate is bridged to the end of a Q^2 chain.

In vitro testing in TRIS buffer was conducted over two weeks (336 h) time-period, and the ions released from the glass to the medium are presented in Fig. 2.

The release of all ions from the x0 glass is linear (R^2 = 0.99) with time. As CaF_2 is substituted for CaO, the ion concentration reaches saturation after one week of immersion for the glasses x5, x10 and x15. Dissolution of the glass x20 leads to ion saturation already after 24 h of immersion. The shift in ion saturation towards earlier immersion times indicates an increase in the early dissolution rate of the glass with increasing CaF_2 content [60]. The increase in the dissolution rate with increasing CaF_2 is in agreement with the FTIR and MAS-NMR results. Indeed, fluorine addition increases the Q^2/Q^1 ratio and it is well accepted that the hydration of Q^2 chains occurs at a faster rate than the Q_1 units according to [61].

Fig. 3 presents the FTIR spectra of the x0 a) and x20 glasses b) at various immersion times.

The dissolution of the x0 exhibits the slowest changes in the glass structure with limited changes occurring in the first 24 h. Between 24 h and 2 weeks of immersion, the main band at 880 cm^{-1}, $\nu_{as}(POP)$, shifts to 900 cm^{-1}, ($\nu_s PO_3$ vibration of Q^1), suggesting that all of the more soluble Q^2 species preferentially dissolve. A thorough absorption band attribution can be found in Table S1 in the Supplementary information. For the as prepared glass x20, the main transformations happen within the first 24 h, with the fundamental vibration at 1100 cm^{-1} of $\nu_s PO_3$ vibration of Q^1 being the dominating feature of the spectra regardless of time of immersion. The band at 718 cm^{-1} decreases in intensity and shifts towards higher wavenumbers upon immersion. With increased immersion time, the band at 887 cm^{-1} shifts to 910 cm^{-1} and decreases in intensity. More interesting is the band at ~960 cm^{-1} which is associated with ν_{ss}(P-O-P) Q^2 rings: this band disappears after 6 h of immersion whereas new bands appear at 988 and 1035 cm^{-1}. These new band can be associated with Q^0 and Q^1 phosphate vibrations respectively [62–64]. As seen in the spectra of the glass x0, the shoulder

Table 2
The glass compositions in mol%, the calculated network connectivity (NC), and Q distributions assuming that fluorine is present as F-Ca/Na(n) and P-F species.

Compositions			Assuming F is present as F-Ca/Na(n)			Assuming F is present as P-F				Calculated from ^{31}P NMR data		
$NaPO_3$	CaO	CaF_2	NC	Q^1	Q^2	NC	Q^0	Q^1	Q^2	NC	Q^1	Q^2
75	25	0	1.33	0.67	0.33	1.33	0.00	0.67	0.33	1.19	0.81	0.19
75	20	5	1.47	0.53	0.47	1.20	0.00	0.80	0.20	1.22	0.78	0.22
75	15	10	1.60	0.40	0.60	1.07	0.00	0.93	0.07	1.24	0.76	0.24
75	10	15	1.73	0.27	0.73	0.93	0.07	0.93	0.00	1.26	0.74	0.26
75	5	20	1.87	0.13	0.87	0.80	0.20	0.80	0.00	1.32	0.68	0.32

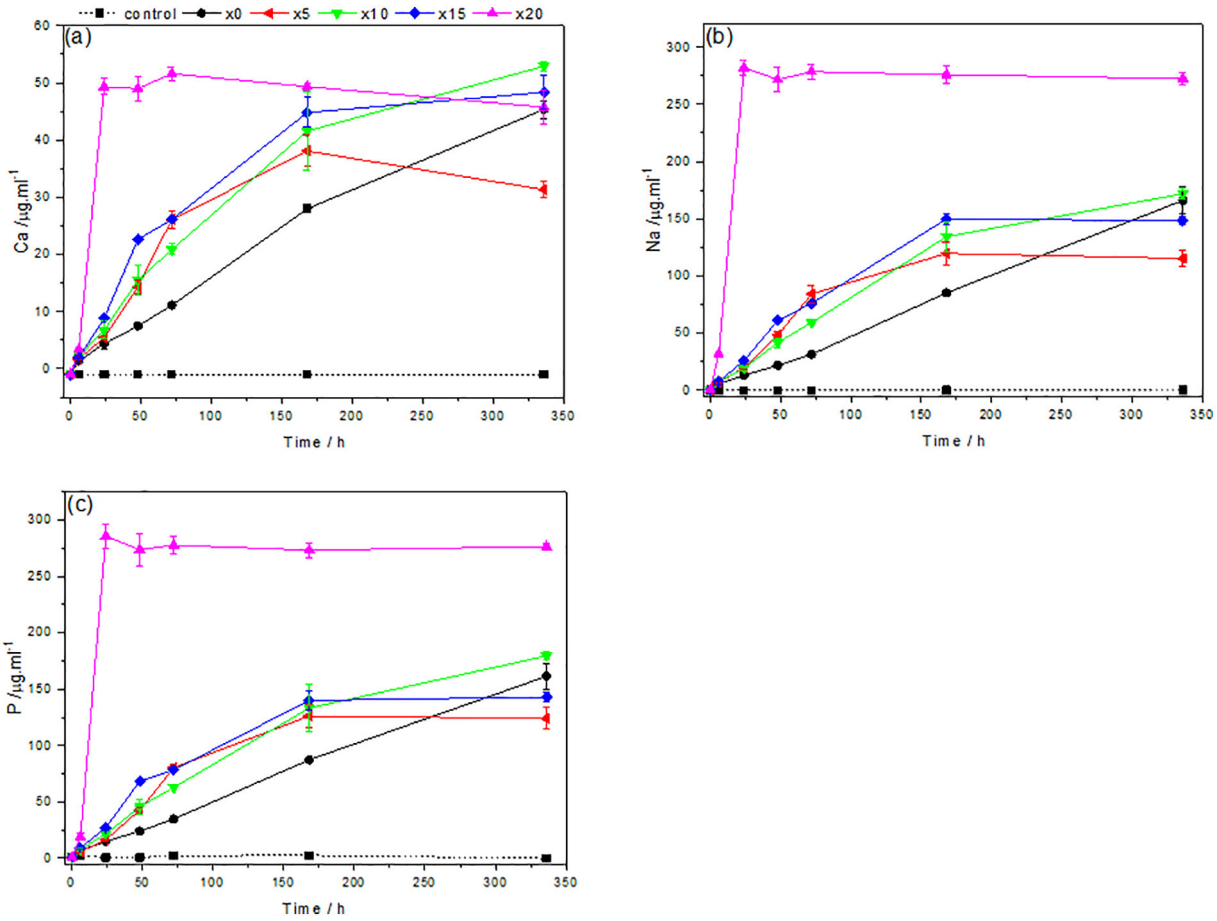

Fig. 2. Ca (a), Na (b), and P (c) ions concentration after immersion of the as prepared x0, x5, x15 and x20 glasses in TRIS buffer solution.

at 1240 cm^{-1} decreases in intensity between 24 h and 2 weeks while this decrease in intensity is already observed within 24 h in the spectrum of the x20 glass indicating a faster structural network hydrolysis for the later glass. For the x20 glass, the band at 1010 cm^{-1} that corresponds to the overlapping and stretching of P—F bonds disappears completely, and the bands associated with Q^2 also disband after 6 h in TRIS. This suggests that the P—F bonds are associated with the preferential dissolution of Q^2 units. Within this glass series, the quantity of Q^2 has increased with the progressive replacement of CaO by CaF_2 suggesting that in order to form P—F bonds in phosphate glasses a critical amount of Q^2 units must be available. This would explain the reason that no P—F bonds were reported to form in invert phosphate

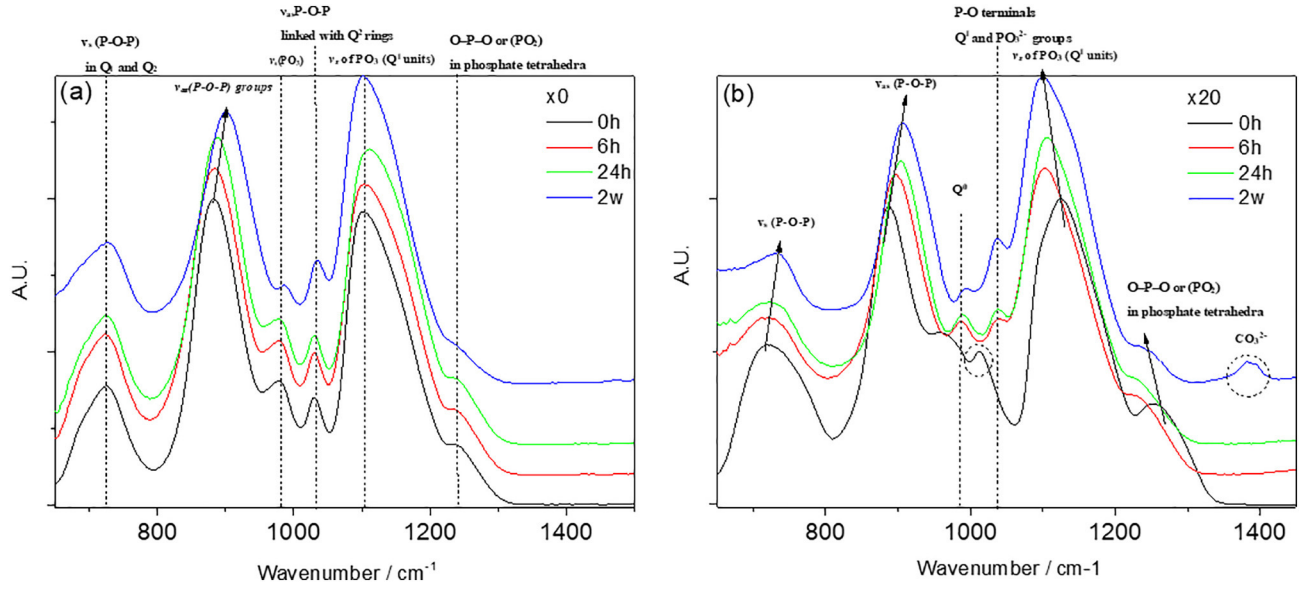

Fig. 3. FTIR spectra of the glass x0 a) and x20 b) at various immersion time.

glass [46], while they were reported to form in metaphosphate glasses [32]. Finally, a doublet in the 1360–1425 cm^{-1} region appears after immersion of the glass x20 for 2 weeks which can be assigned to carbonate groups.

As shown in Fig. 4, the x0 glass shows the formation of a thin reactive layer, in agreement with the ICP-OES and FTIR results, within the first 6 h of immersion. After two weeks of immersion, the glass particles dissolve to a greater extend with a thickening of the reactive layer. The EDS (Fig. S2) confirms that the unexposed regions of the glass remain at the same initial composition confirming that the dissolution of the glass is congruent. The surrounding areas, corresponding to the reactive layer deposited, become depleted in sodium and rich in calcium and phosphate (Ca (at.%)/P (at.%) = 1.17). In contrast, the SEM images of the x20 glass show significant degradation already after 6 h of immersion. The EDS results suggest a preferential leaching of the sodium ions. EDS results, combined to the ICP-OES data, seem to indicate that in the fluorine containing glasses the dissolution is no longer congruent, most likely due to a preferential attack of the P—F bonds over the P—O bonds. However, more in depth analysis should be performed to better understand the dissolution mechanisms. As for the glass x0, the reacted areas are depleted of sodium, but maintain a calcium phosphate ratio of 1.19. The Ca/P ratio lies between the ratio of dicalcium phosphate dihydrate (Ca/P = 1.0), found to precipitate on metaphosphate glasses [65] and octacalcium phosphate (Ca/P = 1.33) also found to precipitate at the surface of phosphate glass fibers upon immersion in simulated body fluids [66]. It is also interesting to point out that, from FTIR analysis, the reactive layer forming at the surface of the x20 glass contains carbonate and therefore can be considered a carbonated-CaP layer. Carbonate entering the CaP reactive layer has been reported in silicate bioactive glasses precipitating hydroxycarbonated apatite [67].

In conclusion, fluorine ions play a dual role in the glass formulation investigated: they form P—F bonds and they are also located around the Ca/Na modifying ions. The F speciation depends upon CaF_2 concentration. The dual role of fluorine leads to changes in the Q^2 to Q^1 ratio and thus in changes in the dissolution rate and dissolution mechanism. The dissolution of the glass depends on the hydration of bonds, in the phosphate network, with Q^2 dissolving preferentially to Q^1. Furthermore, the formation of P-O-F bonds is thought to control the dissolution mechanism of the glasses in this glass system: the glass x0 dissolves congruently while the CaF_2 containing glasses dissolves non-congruently and at a faster rate than the F-free glass.

3.2. Crystallization and its impact on dissolution properties

The thermal properties of the glasses are presented in [17] for a 10 K/min heating rate. Measurements were reproduced and extended to additional heating rates to study the crystallization mechanism and to account for any variability in fluorine content between this work and the [17]. The activation energy for crystallization was calculated using both the Kissinger and Friedman method. The Kissinger method (Fig. 5(a)) depends on the maximum crystallization peak temperature at the 4 heating rates. Using Eq. (1), a straight line is then plotted and fitted for each composition with the slope corresponding to E_c/R (Fig. 5(b)). The R^2 values calculated here were above 0.99 for all glass compositions.

The Friedman calculation (Eq. (2)) relies on no mathematical assumptions, and therefore, is expected to be a more accurate measure of the activation energy. This measure of activation energy depends on the areas of the crystallization peaks. The range 0.2–0.8 is chosen to negate issues surrounding the interpretation of the peak tails [69]. Fig. 5(c) presents the crystal fraction (α) as a function of temperature and Fig. 5(d) the activation energies calculated at specific glass transformation (α) into crystals. The standard deviation was calculated for each individual point and for the average activation energy. The values calculated for both methods are summarised in Table 3.

Both the Kissinger and Friedman calculations show that with increasing CaF_2 content, the activation energy for crystallization decreases. The values obtained from the Friedman calculation showed deviations less than 10% suggesting that only one crystallization mechanism governs the devitrification of these glasses [49] in agreement with our previous study [59]. The activation energies calculated using both methods are in good agreements, except for the x0 glass. This might indicate that the crystallization mechanism of this particular glass is more complex than for the fluorine containing glasses: multiple crystallization events may occur at the same time and/or mix of bulk and surface crystallization is expected to occur during the heat treatment.

The as prepared glasses, ground to 150–250 μm particle size, were heat treated for 180 min at T_x and T_x + 20 °C without any nucleation step, based on the study reported in [17]. The goal was to assess the crystallization tendency (surface vs bulk) of these glasses and the extent of the crystallization in view of testing the in-vitro dissolution and cytotoxicity of the glasses and glass-ceramics. Fig. 6(a), presents the SEM images of the particles' cross sections after heat treatment for 180 min at T_x, and T_x + 20 °C. The SEM images show that with increasing

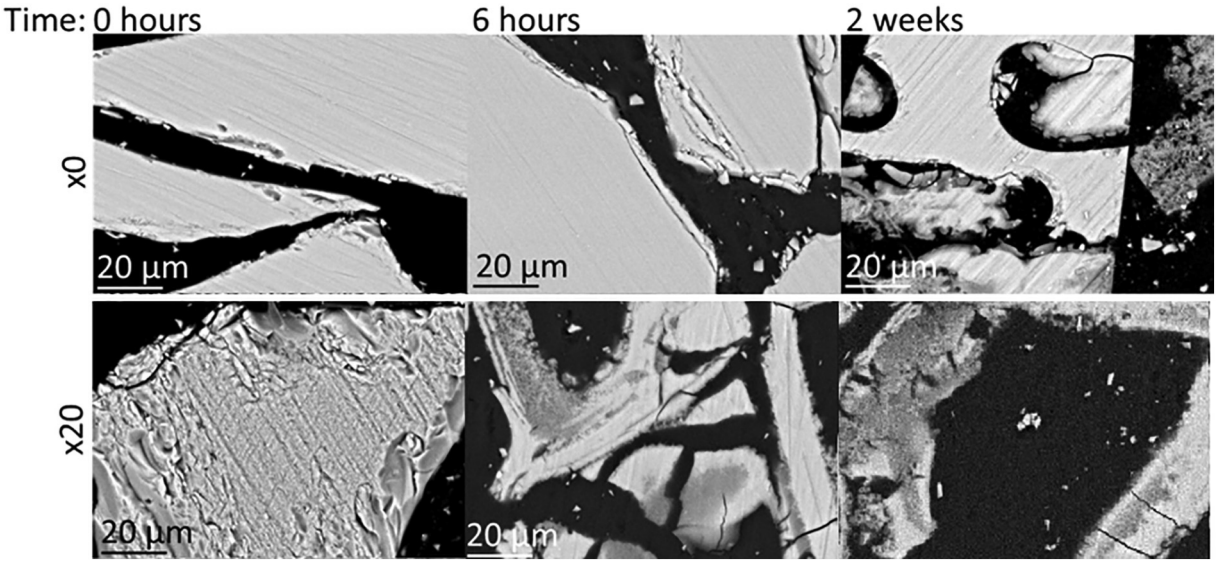

Fig. 4. SEM images of the glass particles at 0 h, 6 h, and 2 weeks after dissolution.

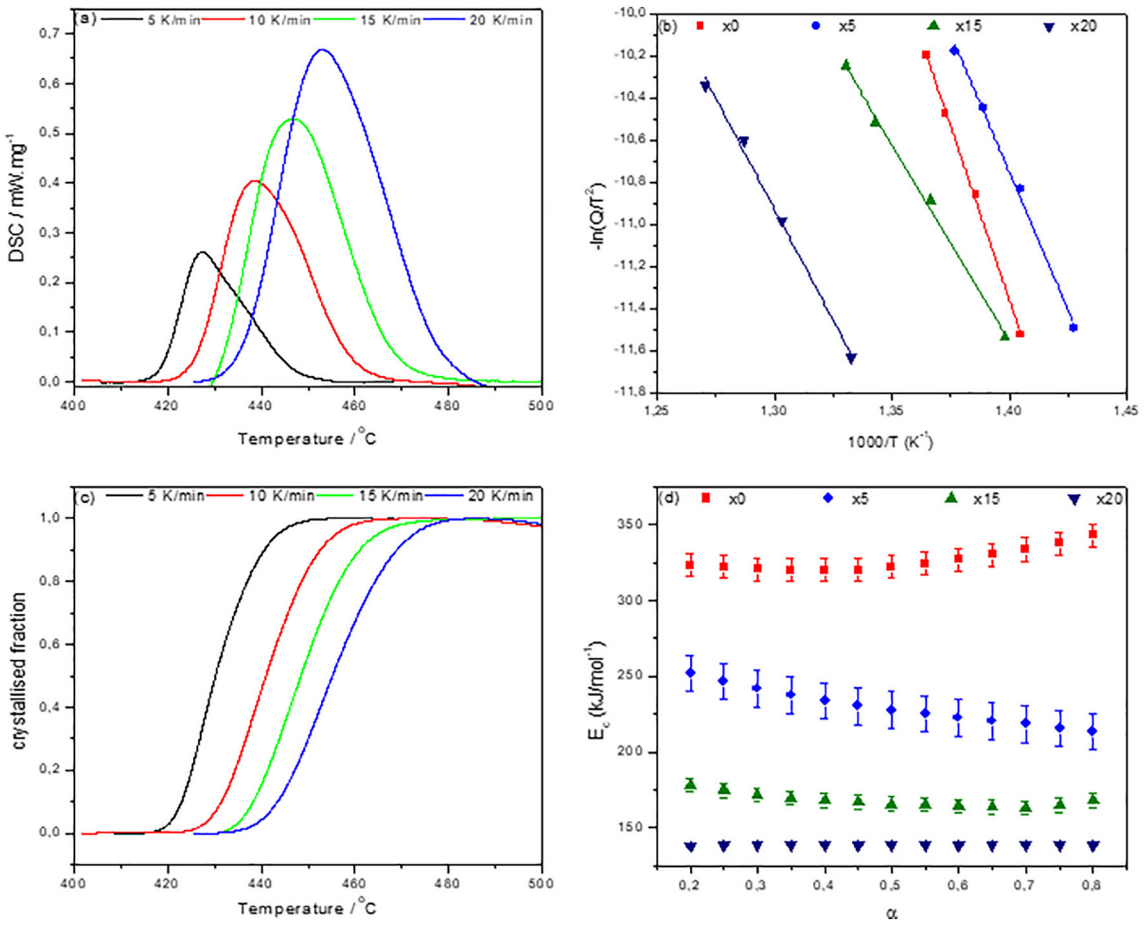

Fig. 5. (a) Non-isothermal DSC results obtained at 4 different heating rates for x0, (b) the application of the Kissinger equation (c) application of the Friedman equation, the normalized fraction transformed with heating rate, and (d) the fraction transformed against activation energy for x0, x5, x15 and x20.

Table 3
Calculated values for activation energy via the Friedman and Kissinger equation.

x	Kissinger	Friedman
	E_c ± 30 kJ/mol	E_c kJ/mol
0	274	326 ± 8
5	217	230 ± 12
15	156	168 ± 4
20	141	138 ± 1

substitution of CaF_2 the extent of the crystallization increases. The glass x0 heat treated at T_x exhibits limited surface crystallization after 180 min and complete crystallization was obtained as the temperature was increased to $T_x + 20$ °C. The x5 and x15 glasses crystallized more readily than the x0 glass after heat treatment at T_x, with flake like crystals growing across the surface. As the temperature was increased to $T_x + 20$ °C, clear plate like crystals grow across the surfaces of both glasses. The increased crystallization tendency of the F-containing samples is in line with the decrease of their activation energy for crystallization (Table 3). Indeed, a lower activation energy of crystallization is generally associated with crystallization occurring more readily at lower temperature. This only applies for glasses with similar structure and similar primary crystal field. It is also important to note that a low activation energy also indicates less of dependence of the crystallization process with small change in temperature. In contrast, the x20 glass undergoes bulk crystallization instead of surface crystallization as reported in [59]; nanometer sized crystals precipitate within the glass, at both T_x and $T_x + 20$ °C. The shape of the formed crystals is spherical suggesting that they are as a result of phase separation within the glass. Amorphous phase separation is a common phenomenon seen in the preparation of glass ceramics. The energy barrier to crystal nucleation decreases once phase separation occurs, due to the lower interfacial energy between the two glasses compared to that of a glass and ceramic phase [70]. In these glasses, this results in a homogenous precipitation of crystals across the bulk of the glass. This could be a result of the change in the speciation of the fluorine ions associating preferentially with the calcium over the sodium or bonded to P in the glass x20.

From XRD analysis (Fig. 6(b)), the diffraction peaks correspond to $Ca_2P_2O_7$ (00-009-0345) in the pattern of the glasses x0, x5 and x15 heat treated for 3 h at T_x. Some unassigned diffraction peaks might be attributable to $NaPO_3$ crystals as reported in Cui et al. [17]. The glass x20 exhibits a preferential crystallization of CaF_2 crystal phase (98-006-0370) suggesting that F-Ca(n) speciation is dominant compared to P—F bond vibrations. Upon heat treatment, limited structural rearrangement is required to then convert F-Ca(n), where n is 3 or 4, to the crystalline F-Ca(4) present in CaF_2. This was further confirmed by the ^{31}P NMR spectra of the heat treated x20 glass presented in Fig. 7. Indeed, upon heat treatment, clear chemical shifts at −131, −108 and −75 attributable to F-Ca(3)/Na(1), CaF_2 and P—F, respectively. With increasing heat treatment temperatures (red lines), the intensity of the peaks increases suggesting that a single crystallization process takes place in all glasses, except for x0, as predicted by the Friedman calculation. While there is no inclusion of fluorine into the precipitated crystal phase for glass x5 and x15, one should keep in mind that the peak position of the

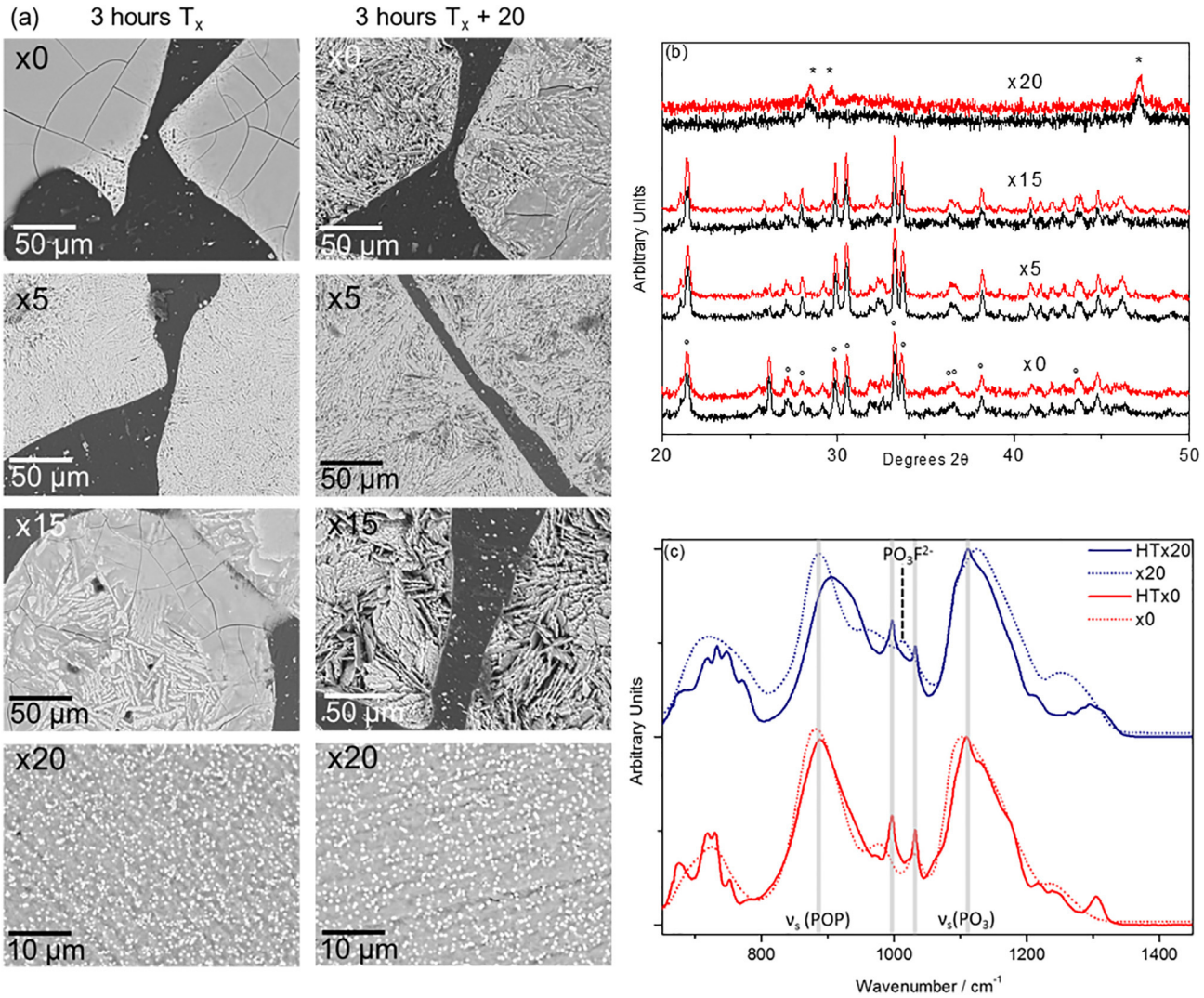

Fig. 6. (a) SEM images of glasses x0, x5, x15, and x20 heat-treated for 3 h at T_x and T_x + 20, (b) XRD patterns of the glasses heat treated for 3 h at T_x (black) and at Tx + 20 °C (red). The 'o' represents the peaks corresponding to $Ca_2P_2O_7$ (00-009-0345), and '*' denotes the peaks that correspond to Fluorite (CaF_2) (98-006-0370). (c) Normalized FTIR results of x0 and x20 pre and post heat treatment at T_x. (For interpretation of the references to colour in this figure legend, the reader is referred to the web version of this article.)

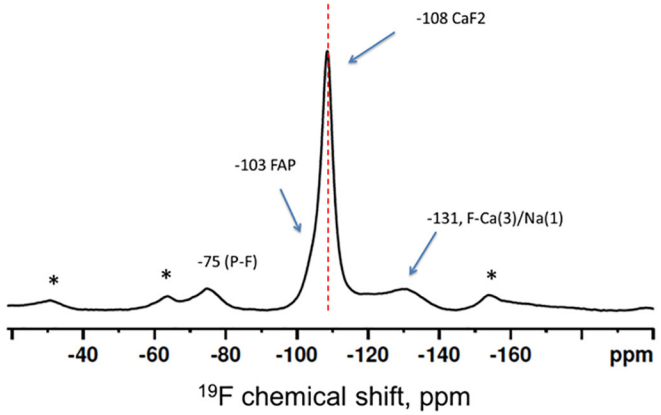

Fig. 7. ^{19}F NMR of the heat treated x20 glass.

$Na_2Ca_2P_2O_7F_2$, reported in [17] are fairly similar to the $Ca_2P_2O_7$ and therefore it is possible that a mix between fluorine-containing and fluoride free crystals coexist in these glasses.

Fig. 6(c) shows the IR spectra of the glasses x0 and x20 glasses prior to and after 3 h at T_x (heat treated glasses are labelled HTx0 and HTx20 respectively). The spectra of the heat-treated glasses exhibit sharp peaks due to the formation of a more regular crystal structure. The broad amorphous band between 650 and 800 cm^{-1} becomes discrete vibrations at 675, 718, 730, and 750 cm^{-1}. The band at 675 cm^{-1} can be associated with the vibration of the long v_s (P-O-P) chains of Q^2 [62]. The vibrations at 718 and 730 cm^{-1} can be equated to v_s (P-O-P) linkages in between Q^1 and Q^2, and the band at 750 cm^{-1} to v_s(P-O-P) in Q^1 units [62]. In addition, a change was seen in the region between 950 and 1050 cm^{-1}, where two distinct vibrations are formed at 998 and 1030 cm^{-1}. The vibration at 998 cm^{-1} can be attributed to the symmetric stretching mode of non-bridging oxygen's in Q^0 tetrahedral [62], while the band at 1030 cm^{-1} is assigned to ν_{as} P-O-P groups linked with metaphosphate rings of Q^2. Finally, the changes were also seen in the vibrations between 1200 and 1300 cm^{-1}, where instead of a broad shoulder, smaller peaks are formed at 1215, 1240, and 1305 cm^{-1}. The bands at 1215 and 1240 cm^{-1} are associated with two non-bridging oxygens as O-P-O in the phosphate tetrahedra (see Table S1 as Supplementary data). All structural changes observed after heat treating the glass x0 are a clear indication of the formation of calcium phosphate crystals in agreement with the XRD pattern. Interestingly, the heat treatment of x20 resulted in the disappearance of the vibration at

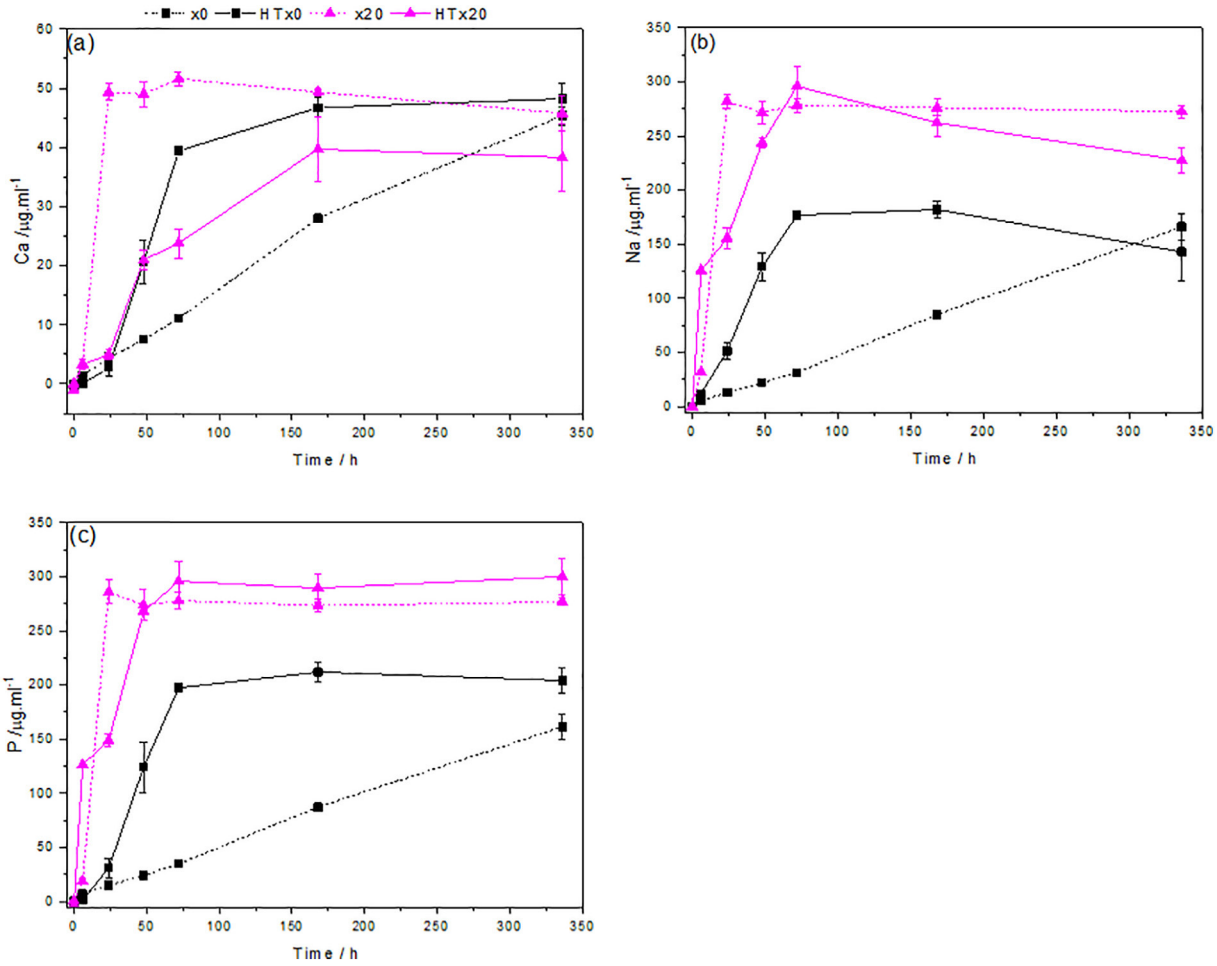

Fig. 8. Ca (a), Na (b), and P (c) ions concentration after immersion of the as prepared (x0 and x20 glasses, dashed line) and heat-treated (HTx0 and HTx20, solid lines) in TRIS buffer solution.

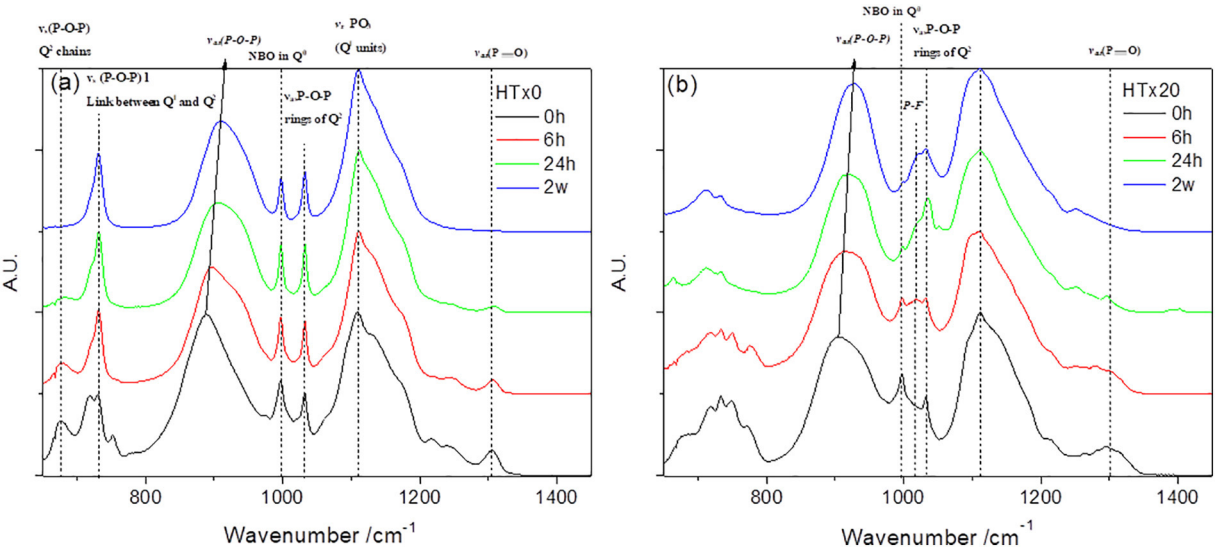

Fig. 9. FTIR spectra of the heat treated glass HTx0 a) and HTx20 b) at various immersion time.

1010 cm^{-1} attributed to PO_3F^{2-}. CaF_2 is transparent in FTIR, and therefore, conclusions can only be made regarding the remaining structure. However, ^{19}F NMR, presented in Fig. 7, reveals a clear chemical shift at −108 assigned to CaF_2, a shoulder at −103 attributable to fluorine in a calcium phosphate structure (most likely nanocrystals) and a peak at −131 ppm assigned to F-Ca(3)/Na(1). It is interesting to point out that despite the vibration of P—F bonds disappearing in the FTIR spectra, NMR still reveals some degree of P—F bonds present in the glass, as seen by the peak at −75 ppm.

The overall shape of the FTIR spectra has become much sharper

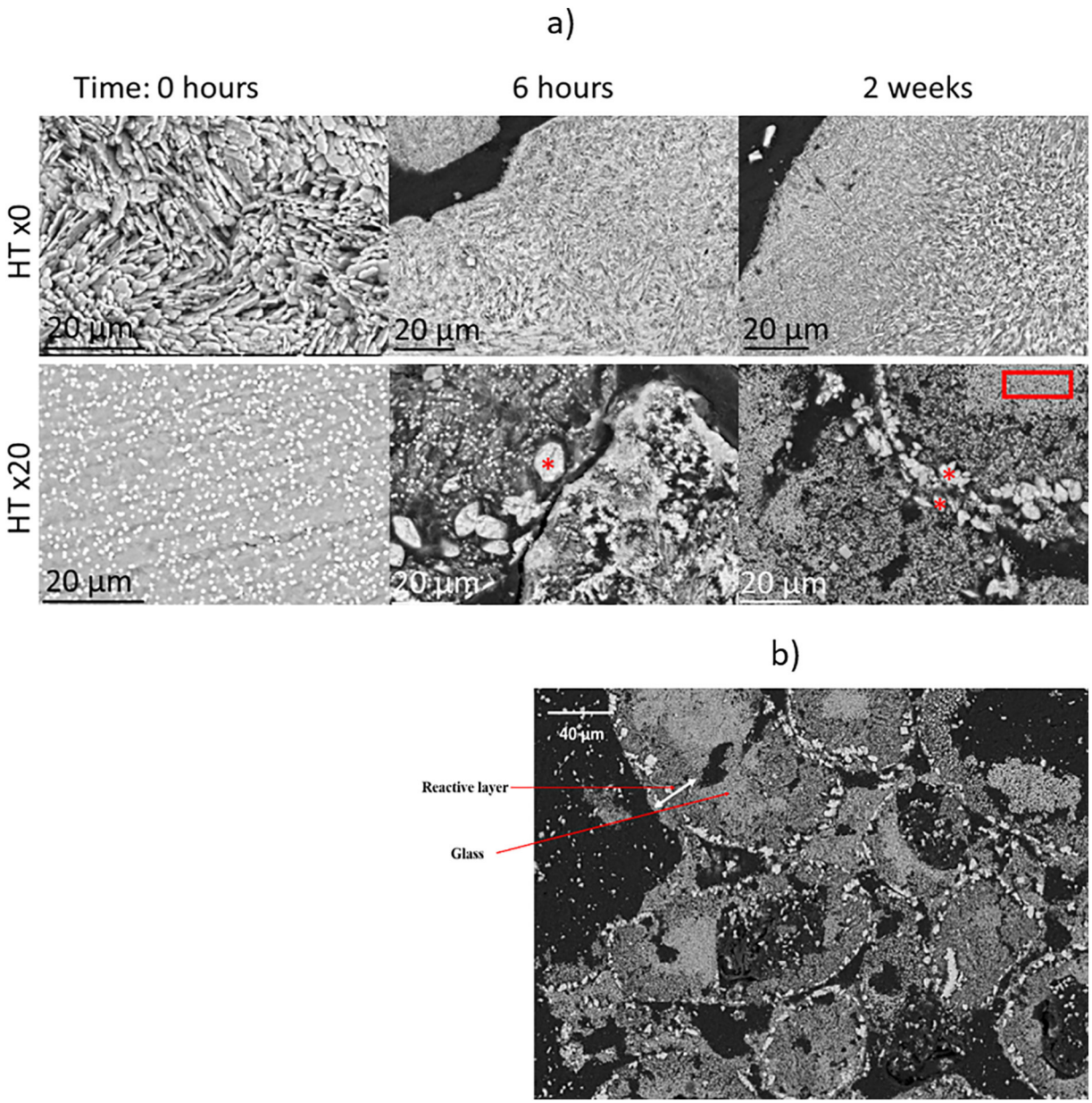

Fig. 10. (a) SEM images of particle cross sections of the heat treated HTx0 and HTx20 glasses, red * and highlight, draw the eye for points in this discussion. (b) SEM image of the cross section of the HTx20 glass-ceramics particle after immersion for 2 weeks in the TRIS buffer solution. (For interpretation of the references to colour in this figure legend, the reader is referred to the web version of this article.)

Table 4
Ca and P concentration in a-MEM and CM.

	[Ca] ppm	[P] ppm
α-MEM	50.8 ± 2.5	24.4 ± 1.2
x0 undiluted	210.2 ± 10.5	1919.4 ± 96.0
HTx0 undiluted	412.9 ± 20.6	4922.8 ± 246.1
x20 undiluted	606.9 ± 30.3	6558.3 ± 327.9
HTx20 undiluted	179.6 ± 9.0	6705.2 ± 335.3

than its amorphous counterpart suggesting that phase separation and some order exist within the remaining glass structure that is not detectable within the XRD results as supported by the MAS-NMR. Fluorine is known to alter crystallization processes in the glass network. Its incorporation can facilitate nano-crystallinity within the silicate and borosilicate structures [21–22,68]. This result suggests that the same is true for this series of phosphate glasses.

The impact of crystal formation on the material's dissolution was investigated. The glasses x0 and x20 were heat treated for 3 h at T_x + 20 °C to ensure crystallization and subjected to the same dissolution experiments as their amorphous counterparts. The ion concentrations in the dissolution medium are shown in Fig. 8. The dissolution rate of the heat treated glass x0 increases compared to the as prepared glass. The dissolution profiles become comparable to that of the glass x15. Instead of a linear dissolution, the dissolution is faster after heat treatment within the first 72 h and then plateaued, suggesting that either the crystallized phase or the remaining glassy phase is more prone to hydrolytic degradation than the as prepared amorphous x0 glass. $NaPO_3$ is known to be highly soluble (MSDS), while $Ca_2P_2O_7$ is insoluble. Therefore, the high initial release rate is attributable to the remaining glass phase and $NaPO_3$.

The heat-treated glass x20 (HTx20) had a subtle change across its dissolution behaviour. The total calcium released from the HTx20 glass-ceramic, after 2 weeks of immersion, is slightly lower than for the as

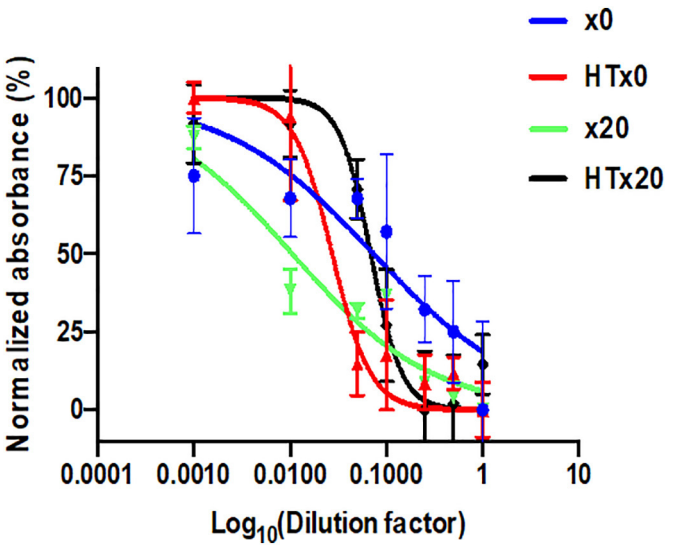

Fig. 11. Normalized absorbance as a function of glass concentration in the medium, for the four materials of investigation.

prepared glass x20. This could be due to the more chemically stable CaF_2 crystals not dissolving during dissolution. The sodium and phosphorous release from the heat-treated x20 glass after two weeks of immersion is comparable to that of the as prepared glass within the error of measurements. However, the heat-treated glass has a faster release rate during the first 6 h of immersion than the as prepared glass. Then during the following 72 h, the heat-treated glass reaches a similar plateau comparable to the one observed for the as prepared glass x20 after 24 h of immersion. The faster initial dissolution (up to 6 h of immersion) and slower dissolution rate (up to 72 of immersion) of the crystallized glass, compared to the amorphous equivalent, supports the suggestion that when the CaF_2 crystals precipitate within the glass-ceramic, the remaining glass may have become phase separated with the two phases promoting different dissolution profiles in aqueous solution.

Fig. 9 shows the changes in the FTIR spectra after dissolution in TRIS buffer solution over a 2 week time period of the heat treated glasses.

From Fig. 9, the structure of HTx0 changes during the degradation as evidenced by the multi peaked spectra at 0 h becoming only 5 dominant peaks after 2 weeks of immersion in the TRIS, with the fundamental vibration located at 1100 ($\nu_s PO_3$ vibration of Q^1). Within the first 6 h of immersion in the TRIS, the bands at 718, 730, 750 and 1215 cm^{-1} all associated with linkages between Q^1 and Q^2's fundamental vibrations disappear from the FTIR spectrum of HTx0 (Fig. 9(a)) [63]. The FTIR spectra of HTx20 show markedly different results when compared to the x20 glass. Without heat treatment, a clear vibration band at 1112 cm^{-1} (fundamental $\nu_s PO_3$ vibration of Q^1) appears with two shoulders at 1090 and 1140 cm^{-1} associated with the stretching vibrations of $P-O^-$ in Q^1 units [64] and the stretched symmetric connection between the P—O terminals of Q^1 and PO_3^{2-} groups [71], respectively. As the dissolution of the x20 glass takes place, the bands broaden into a rounder distribution with its peak remaining at 1112 cm^{-1}. The intensity of the peak at ~900 cm^{-1} associated with the $\nu_{as}(POP)$ slightly increases while the peak also shifted to a higher wavenumber. The FTIR spectra of HTx20 suggest preferential dissolution of the Q^2 phosphate structural units. While no new absorption peaks could be seen in the FTIR spectra of the immersed HTx0, the appearance a new peak at ~1018 cm^{-1} in the spectrum of HTx20 could indicate the precipitation of a reactive layer at its surface, that potentially contain P—F bonds.

Fig. 10a presents the SEM images of the heat-treated glasses x0 and x20 at various immersion times. EDX was conducted to gain insight into dissolution related compositional change. The initial composition of x0 in atomic percent was (42.8 ± 2.9), (39.9 ± 1.4) and (16.9 ± 1.2) of sodium, phosphorous and calcium, respectively. After two weeks of immersion the HTx0 has a composition of (43.9 ± 0.9), (38.3 ± 0.5) and (18.2 ± 1.1) of sodium, phosphorous, and calcium, respectively showing that the atomic percent composition across the sample does not vary with increasing the immersion time.

After the 6 h and two weeks immersion in the TRIS solution, the CaF_2 crystals are clearly visible in the HTx20 glass (highlighted in red box). After 6 h of immersion in the TRIS solution, a second phase becomes visible within the structure denoted by the asterisk (*) in Fig. 10. This phase is mainly present at the surface of the particles, and it is composed of all the constituents of the glass. This supports the prior evidence that the heat treatment not only leads to the formation of CaF_2 crystals, but also to the phase separation within the glass. One phase of the remaining glass preferentially degrades leaving this second phase and the CaF_2 crystals. The second phase was not observed in the XRD studies of the heat-treated glasses suggesting that this second phase is still amorphous.

Fig. 10b present the SEM image of the HTx20 glass-ceramics immersed for two weeks in the TRIS buffer solution. One can note the presence of a thick reactive layer at the surface of the particles as indicated in the image with some particles becoming hollow.

The HTx20 shows signs of reactive layer precipitation, as opposed to HTx0 that loses his ability to form a reactive layer after extended immersion. The Ca/P ratio of the reactive layer was 1.75. The Ca/P ratio is closer to the one of hydroxyapatite. This is a first indication that the glass-ceramics maintains its ability to precipitate a reactive layer beneficial to cells in potential applications.

3.3. In-vitro cell culture

The aim of the study was to assess the cell behaviour in conditioned culture medium (CM) at various dilution. ICP-OES was performed on the undiluted CM to assess the changes in Ca and P post glass dissolution (Table 4).

From the table the Ca and P concentration increases drastically upon immersion of all 4 glasses of interests, when compared to the original culture medium (α-MEM). With addition of F (x0 ➔ x20), the concentrations of Ca and P are significantly higher pertaining to the faster dissolution rate of the oxyfluorophosphate glass compared to corresponding phosphate glass as already discussed. Upon crystallization of the x0 glass, the Ca and P ions concentration increases. In the case of HTx20, the precipitation of the CaF_2 crystals leads to a lower Ca release in the medium compared to the untreated one while the P concentration remains sensibly similar within the accuracy of the measurements. All the results are in agreement with the in-vitro dissolution test conducted in TRIS buffer solution.

The cell activity was evaluated by the AlamarBlue test and is presented in Fig. 11. The figure presents the normalized absorbance (to the blank sample, i.e. cells population cultured in pure culture medium) for x0, x20, HTx0 and HTx20. All the graphs exhibit the characteristic sigmoidal curve where the percentage of normalized absorbance decreases with a decrease in the dilution factor and, therefore, with an increase in the dissolution by-products concentration.

The IC50 is taken as the dilution factor corresponding to 50% normalized absorbance. The IC50 was found to correspond to a dilution factor of be 1/13.5 ($R^2 = 0.7$) for the x0 glass and to increase to 1/95.1 ($R^2 = 0.93$) for the x20 glass. The increased cytotoxicity is most certainly assigned to the increased speed of degradation when adding fluorine to the based phosphate glass. The high ion release could lead to toxic amount of phosphorous and/or fluorine as well as low pH. Upon crystallization (HTx0) the IC50 was found to correspond to dilution factor of approximately 1/36.5 ($R^2 = 0.90$). The crystallization of the x0 glass was reported to increase the ion dissolution which, in turn, can

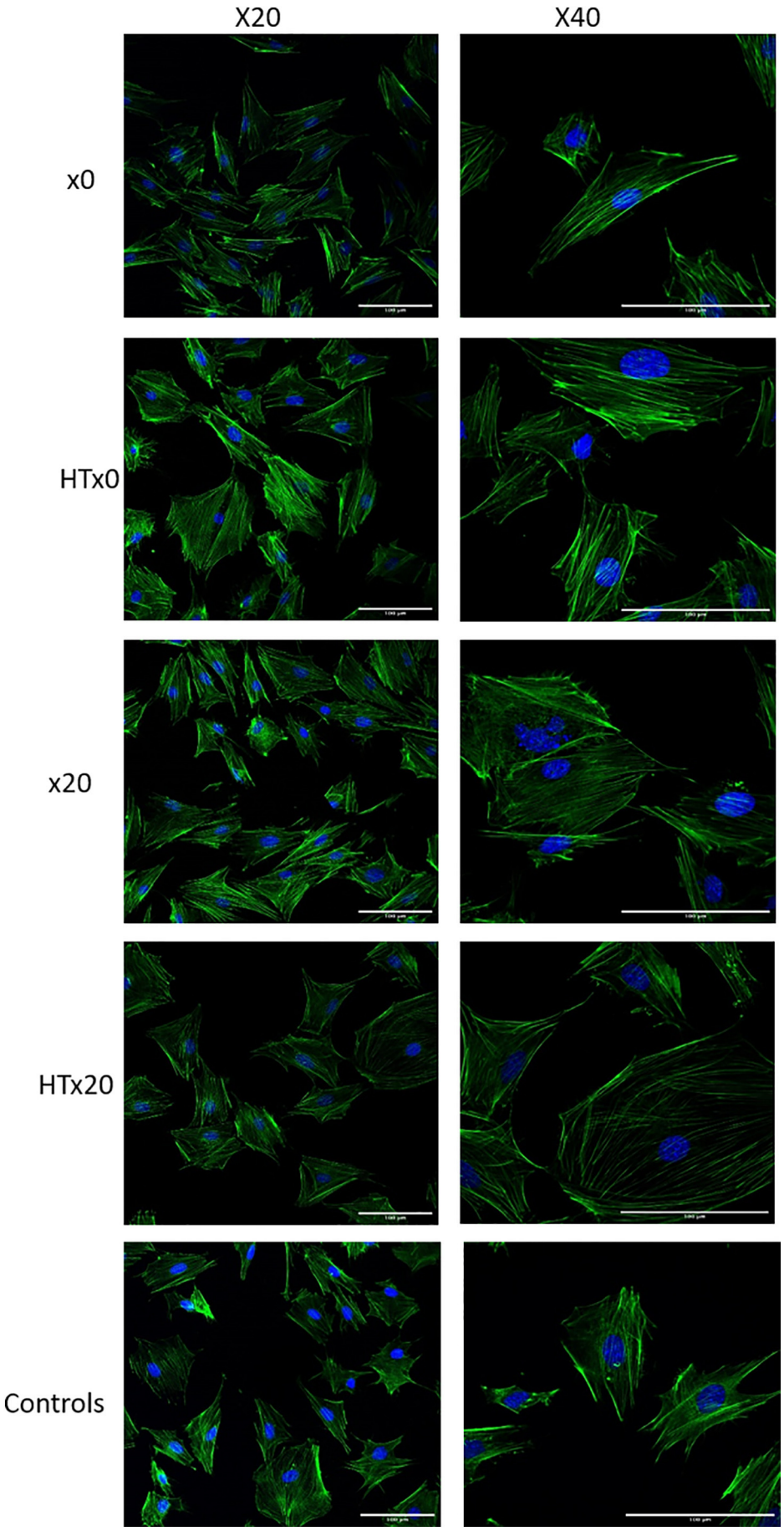

(caption on next page)

Fig. 12. Cells imaged at 20 and 40× magnification, after 2 days of incubation with medium supplemented with bioactive glass at a concentration 0.4375 mg/ml. Scale bar 100 µm.

lead to changes in ionic strength and osmotic pressure, thus increasing cytotoxicity. However, it was interesting to find out that, the HTx20 had a significantly lower cytotoxicity than its glass counterpart: its IC50 was measured at a dilution of 1/14.5 (R^2 = 0.90). As reported in the in-vitro dissolution test, the controlled crystallization of CaF_2 crystals reduced the initial dissolution rate, which leads to a reduction of ions released into solution. Furthermore, while the P concentration, in the medium, was similar in both as-prepared and heat-treated samples, the reason for the change in cytotoxicity can come from a lower Ca or F release in solution upon crystallization.

The morphology, spread and the cytoplasmic nuclear ratios (C:N) were analysed in conditioned culture medium diluted 100 times for 48 h (Fig. 12).

For each sample, ten random cells were chosen and the cytoplasmic and nuclear areas were calculated. When comparing the morphology and the spread of the cells, from Fig. 12, it can be seen that all samples exhibit cells with similar shape than in the control group. Indeed, the cells had multiple projections that protruded outwards allowing cell-to-cell contact. In addition, all the samples indicate similar spread across the well plates. When analysing the C:N, it was seen that HTx0 had the highest ratio of 19:1 and x20 had the lowest ratio of 10:1. Interestingly, HTx20 and the controlled group had the same C:N ratio of 13:1.

Overall, an increase in Q^2 units, in the phosphate glass, associated to an increase in fluoride, leads to an increased cytotoxicity, probably due to the high ion concentration in the culture medium. Similarly, surface crystallization of a F-free invert phosphate glass was linked to an increase in cytotoxicity, possibly due to the rapid dissolution of one of the crystalline phases and the remaining amorphous phase, thus leading to large P content in the medium. It is interesting to point out that bulk crystallization of the F-containing glass, led to a reduced cytotoxicity. When cultured in a conditioned medium diluted 100 times, all materials were found to support cell spreading. The morphology of the cells was typical of preosteoblastic cells. It should be noted that the spreading of the cells, in all condition were similar to the control group.

4. Conclusion

Oxyfluorophosphate glasses and glass ceramics, with potential in both dental and orthopaedics applications, have been developed. This work studies the effect of CaF_2 substitution on the structural and dissolution properties of $75NaPO_3$-(25-x) CaO-xCaF_2 (in mol%) glasses and glass ceramics. ^{19}F and ^{31}P MAS-NMR spectra reveal significant fluorine retention throughout the melting process, evidenced by the presence of both P−F bonds and F-M(n) species in the fluorophosphate glasses. The ratio of the P−F bonds and F-M(n) species depends on the glass composition. The addition of CaF_2 at the expense of CaO leads to an increase in the glass dissolution rate associated with an increase in the Q^2 phosphate species and F-Ca/Na bonding. This, in turns, leads to an increased cytotoxicity.

All glasses, at the exception of the x20, exhibit surface crystallization. As evidenced for x0, surface crystallization leads to an increased dissolution rate as well as to an increased in cytotoxicity. The glass x20 exhibits a bulk crystallization with preferential crystallization of CaF_2. The dissolution of the heat treated x20 glass was found to be faster when immersed for up to 6 h of immersion but then slower for longer immersion time in TRIS when compared to the amorphous glass. The differences in the dissolution behaviour can be explained by a phase separation occurring during the heat treatment of the glass x20. The formation of CaF_2 nanocrystal in the glass bulk does not inhibit the precipitation of a reactive layer and allows maintaining cell activity similar to the F-free glass.

The bulk crystallization of the glass prepared with high fluoride content opens the path to new glass-ceramics with tailored dissolution, mechanical properties and cell activity, with potential for hot forming into 3D scaffolds.

Supplementary data to this article can be found online at https://doi.org/10.1016/j.msec.2020.111269.

CRediT authorship contribution statement

A. Nommeots-Nomm: Conceptualization, Data curation, Formal analysis, Investigation, Methodology, Writing - original draft, Writing - review & editing. **A. Houaoui:** Conceptualization, Data curation, Formal analysis, Investigation, Methodology, Writing - original draft, Writing - review & editing. **A. Pradeepan Packiyanathar:** Investigation. **X. Chen:** Data curation, Formal analysis, Methodology. **M. Hokka:** Data curation, Formal analysis, Methodology. **R. Hill:** Data curation, Formal analysis, Methodology. **E. Pauthe:** Conceptualization, Data curation, Formal analysis, Funding acquisition, Investigation, Methodology, Writing - original draft, Writing - review & editing. **L. Petit:** Conceptualization, Data curation, Formal analysis, Funding acquisition, Investigation, Methodology, Writing - original draft, Writing - review & editing. **M. Boissière:** Conceptualization, Data curation, Formal analysis, Funding acquisition, Investigation, Methodology, Writing - original draft, Writing - review & editing. **J. Massera:** Conceptualization, Data curation, Formal analysis, Funding acquisition, Investigation, Methodology, Project administration, Resources, Software, Supervision, Validation, Visualization, Writing - original draft, Writing - review & editing.

Declaration of competing interest

The authors declare that they have no known competing financial interests or personal relationships that could have appeared to influence the work reported in this paper.

Acknowledgement

The authors would like to acknowledge The Academy of Finland (Academy Research Fellow #275427 and #284492) as well as TTY-Foundation for the financial support for A. N-N. IAS (Institute for Advanced Studies) is also acknowledged facilitating professor exchange between Tampere University and CY Cergy Paris University.

References

[1] G. Fernandez de Grado, L. Keller, Y. idoux-Gillet, Q. Wagner, A.-M. Musset, N. Benkirane-Jessel, F. Bornert, D. Offner, Bone substitutes: a review of their characteristics, clinical use, and perspectives for large bone defects management, Journal of Tissue Engineering 9 (2018) 1–18.
[2] T. Winkler, F.A. Sass, G.N. Duda, K. Schmidt-Bleek, A review of biomaterials in bone defect healing, remaining shortcomings and future opportunities for bone tissue engineering, Bone and Joint Research 7 (2018) 232–243.
[3] A. Hoppe, A. Boccaccini, Biological impact of bioactive glasses and their dissolution products, Frontiers of Oral Biology 17 (2015) 22–32.
[4] A.A. Gorustovich, J.A. Roehter, A.R. Boccaccini, Effect of bioactive glasses on angiogenesis: a review of in vitro and in vivo evidences, Tissue Engineering Part B 16 (2010) 199–207.
[5] R.M. Day, Bioactive glass stimulates the secretion of angiogenic growth factors and angiogenesis in vitro, Tissue Eng. 11 (2005) 768–777.
[6] L.L. Hench, Chronology of bioactive glass development and clinical applications, New Journal of Glass and Ceramics 3 (2013) 67–73.
[7] O.H. Andersson, I. Kangasniemi, Calcium phosphate formation at the surface of bioactive glass in vitro, J. Biomed. Mater. Res. 25 (1991) 1019–1030.
[8] L.L. Hench, O.H. Andersson, Bioactive glasses in an introduction to bioceramics, advanced series in ceramics: Volume 1, World Scientific, pp. 41–62.
[9] L.L. Hench, The story of bioglass, J. Mater. Sci. Mater. Med. 14 (2006) 967–978.
[10] N.A.P. van Geste, J. Geurts, D.J.W. Hulsen, B. van Rietbergen, S. Hofmann, J.J. Arts, Clinical applications of S53P4 bioactive glass in bone healing and osteomyelitic

treatment: a literature review, Biomed. Res. Int. 2015 (2015) 12, https://doi.org/10.1155/2015/684826 684826.
[11] Q. Yang, S. Chen, H. Shi, H. Xiao, Y. Ma, In vitro study of improved wound-healing effect of bioactive borate-based glass nano-/micro-fibers, Mater. Sci. Eng. C 55 (2015) 105–117.
[12] Q. Du Min, Z. Bian, H. Jiang, D.C. Greenspan, A.K. Burwell, J. Zhong, B.J. Tai, Clinical evaluation of a dentifrice containing calcium sodium phosphosilicate (novamin) for the treatment of dentin hypersensitivity, Am. J. Dent. 21 (2008) 210–214.
[13] A. Burwell, D. Jennings, D. Muscle, D.C. Greenspan, NovaMin and dentin hypersensitivity—in vitro evidence of efficacy, The Journal of Clinical Dentistry 21 (2010) 66–71.
[14] V. Gautam, H. Kumar, Comparison of clinical efficacy of four dentifrices in the management of dentinal hypersensitivity, International Journal of Scientific Research 6 (2017) 2277–8179.
[15] S.E. Stokowski, W.E. Martin, S.M. Yarema, Optical and lasing properties of fluorophosphate glass, J. Non-Cryst. Solids 40 (1980) 481–487.
[16] T. Suzuki, S. Masaki, K. Mizuno, Y. Ohishi, Preparation of novel transparent glass–ceramics containing fluoride crystals, Opt. Mater. 33 (2011) 1943–1947.
[17] S. Cui, J. Massera, M. Lastusaari, L. Hupa, L. Petit, Novel oxyfluorophosphate glasses and glass-ceramics, J. Non-Cryst. Solids 445–446 (2016) 40–44.
[18] D.S. Brauer, N. Karpukhina, M.D. Donnell, R.V. Law, R.G. Hill, Fluoride-containing bioactive glasses: effect of glass design and structure on degradation, pH and apatite formation in simulated body fluid, Acta Biomater. 6 (2010) 3275–3282.
[19] M. Poulain, Crystallization in fluoride glasses, Thermochim. Acta 280–281 (1996) 343–351.
[20] J.A. Griggs, K.J. Anusavice, J.J. Mlecholsky, Devitrification and microstructural coarsening of a fluoride-containing barium aluminosilicate glass, J. Mater. Sci. 37 (2002) 2017–2022.
[21] E.E. Assem, Effect of replacing calcium oxide with calcium fluoride on some physical properties of borosilicate glass ceramics, J. Phys. D. Appl. Phys. 38 (2005) 942.
[22] D.S. Brauer, M.N. Anjum, M. Mneimmer, R.M. Wilson, H. Doweidar, R.G. Hill, Fluoride-containing bioactive glass-ceramics, J. Non-Cryst. Solids 358 (2012) 1438–1442.
[23] P.A. Tick, K.E. Lu, S. Mitachi, T. Kanamori, S. Takahashi, Hot stage optical microscopy studies of crystallization in fluoride glass melts, J. Non-Cryst. Solids 140 (1992) 275–280.
[24] R.G. Hill, C. Goat, D. Wood, Thermal analysis of a SiO_2−Al_2O_3−CaO−CaF_2 glass, J. Am. Ceram. Soc. 75 (1992) 778–785.
[25] R.G. Hill, R.V. Law, M.D. O'Donnell, J. Hawes, N.L. Bubb, D.J. Wood, C.A. Miller, M. Mirsaneh, I. Reaney, Characterisation of fluorine containing glasses and glass-ceramics by 19F magic angle spinning nuclear magnetic resonance spectroscopy, J. Eur. Ceram. Soc. 29 (2009) 2185–2191.
[26] X. Chen, X. Chen, A. Pedone, D. Apperley, R.G. Hill, N. Karpukhina, New insight into mixing fluoride and chloride in bioactive silicate glasses, Sci. Rep. 8 (2018) 1316.
[27] F.A. Shah, D.S. Brauer, N. Desai, R.G. Hill, K.A. Hing, Fluoride-containing bioactive glasses and bioglass 45S5 form apatite in low pH cell culture medium, Mater. Lett. 119 (2014) 96–99.
[28] L.P. Gangarosa, Current strategies for dentist-applied treatment in the management of hypersensitive dentine, Arch. Oral Biol. 39 (1994) S101–S106.
[29] S. Overgaard, K. Søballe, M. Lind, C. Bünger, Resorption of hydroxyapatite and fluorapatite coatings in man. An experimental study in trabecular bone, J. Bone Joint Surg. 79 (1997) 654–659.
[30] C.O. Freeman, I.M. Brook, A. Johnson, P.V. Hatton, R.G. Hill, K.T. Stanton, Crystallization modifies osteoconductivity in an apatite-mullite glass-ceramic, J. Mater. Sci. Mater. Med. 14 (2003) 985–990.
[31] J. Liu, S.C.F. Rawlinson, R.G. Hill, F. Fortune, Fluoride incorporation in high phosphate containing bioactive glasses and in vitro osteogenic, angiogenic and antibacterial effects, Dent. Mater. 32 (2016) e221–e237.
[32] J.K. Christie, R.I. Ainsworth, N.H. de Leeuw, Ab initio molecular dynamics simulations of structural changes associated with the incorporation of fluorine in bioactive phosphate glasses, Biomaterials 35 (2014) 6164–6171.
[33] X. Chen, X. Chen, D.S. Brauer, R.M. Wilson, R.G. Hill, N. Karpukhina, Bioactivity of sodium free fluoride containing glasses and glass-ceramics, Materials 7 (8) (2014) 5470–5487.
[34] G. Lusvardi, G. Malavasi, F. Tarsitano, L. Menabue, M.C. Menziani, A. Pedone, Quantitative structure − property relationships of potentially bioactive fluoro phospho-silicate glasses, J. Phys. Chem. B 113 (2009) 10331–10338.
[35] F. Baino, G. Novajra, C. Vitale-Brovarone, Bioceramics and scaffolds: a winning combination for tissue engineering, Frontiers in Bioengineering and Biotechnology 3 (2015) 202.
[36] J. Massera, S. Fagerlund, L. Hupa, M. Hupa, Crystallization mechanism of the bioactive glasses, 45S5 and S53P4, J. Am. Ceram. Soc. 95 (2012) 607–613.
[37] O. Peitl Filho, G.P. LaTorre, L.L. Hench, Effect of crystallization on apatite-layer formation of bioactive glass 45S5, J. Biomed. Mater. Res. 30 (1996) 509–514.
[38] S. Fagerlund, J. Massera, N. Moritz, L. Hupa, M. Hupa, Phase composition and in vitro bioactivity of porous implants made of bioactive glass S53P4, Acta Biomater. 8 (2012) 2331–2339.
[39] J. Clément, J.M. Manero, J.A. Planell, G. Avila, S. Martínez, Analysis of the Structural Changes of a Phosphate Glass During Its Dissolution in Simulated Body Fluid, vol. 10, (1999), pp. 729–732.
[40] R. Colquhoun, K.E. Tanner, Mechanical behaviour of degradable phosphate glass fibres and composites—a review, Biomed. Mater. 11 (2015) 014105.
[41] J. Massera, Y. Shpotyuk, F. Sabatier, T. Jouan, C. Boussard-Pledel, C. Roiland, B. Bureau, L. Petit, N. Boetti, D. Milanese, L. Hupa, Processing and characterization of novel borophosphate glasses and fibers for medical applications, J. Non-Cryst. Solids 425 (2015) 52–60.
[42] D. De Silva Thompson, C. Peticone, I. Burova, R.J. Shipley, J.C. Knowles, H.W. Kim, M. Micheletti, I.B. Wall, Assessing behaviour of osteoblastic cells in dynamic culture conditions using titanium-doped phosphate glass microcarriers, Journal of Tissue Engineering 10 (2019) 1–13.
[43] E.A. Abou Neel, D.M. Pickup, S.P. Valappil, R.J. Newport, J.C. Knowles, Bioactive functional materials: a perspective on phosphate-based glasses, J. Mater. Chem. 19 (2009) 690–701.
[44] J. Massera, M. Mayran, J. Rocherullé, L. Hupa, Crystallization behavior of phosphate glasses and its impact on the glasses' bioactivity, 50 (2015) 3091–3102.
[45] T. Kasuga, Y. Hosoi, M. Nogami, M. Niinomi, Apatite formation on calcium phosphate invert glasses in simulated body fluid, J. Am. Ceram. Soc. 84 (2001) 450–452.
[46] Y. Shaharyar, E. Wein, J.-J. Kim, R.E. Youngman, F. Muñoz, H.-W. Kim, A. Tiloccah, A. Goel, Structure-solubility relationships in fluoride-containing phosphate based bioactive glasses, J. Mater. Chem. B 3 (2015) 9360–9373.
[47] E.K. Basdra, H. Huber, G. Komposch, Fluoride released from orthodontic bonding agents alters the enamel surface and inhibits enamel demineralization in vitro, Am. J. Orthod. Dentofac. Orthop. 109 (1996) 466–472.
[48] H.E. Kissinger, Reaction kinetics in differential thermal analysis, Anal. Chem. 29 (1957) 1702–1706.
[49] M.J. Starink, The determination of activation energy from linear heating rate experiments: a comparison of the accuracy of isoconversion methods, Thermochim. Acta 404 (2003) 163–176.
[50] H. Yinnon, D.R. Uhlmann, Applications of thermoanalytical techniques to the study of crystallization kinetics in glass-forming liquids, part I: theory, J. Non-Cryst. Solids 54 (1983) 253–275.
[51] H.L. Friedman, Kinetics of thermal degradation of char-forming plastics from thermogravimetry. Application to a phenolic plastic, Journal of Polymer Science 6C (1963) 183–195.
[52] A.L. Maçon, T.B. Kim, E.M. Valliant, K. Goetschius, R.K. Brow, D.E. Day, A. Hoppe, A.R. Boccaccini, I.Y. Kim, C. Ohtsuki, T. Kokubo, A. Osaka, M. Vallet-Regí, D. Arcos, L. Fraile, A.J. Salinas, A.V. Teixeira, Y. Vueva, R.M. Almeida, M. Miola, C. Vitale-Brovarone, E. Verné, W. Höland, J.R. Jones, A unified in vitro evaluation for apatite-forming ability of bioactive glasses and their variants, J. Mater. Sci. Mater. Med. 26 (2015) 115.
[53] D.S. Brauer, N. Karpukhina, R.V. Law, R.G. Hill, Structure of fluoride-containing bioactive glasses, J. Mater. Chem. 19 (2009) 5629–5636.
[54] M. Hayashi, T. Watanabe, H. Nakada, K. Nagata, Effect of Na2O on crystallization of mould fluxes for continuous casting of steel, The Iron and Steel Institute of Japan International 46 (2006) 1805–1809.
[55] R.J. Kirkpatrick, R.K. Brow, Nuclear magnetic resonance investigation of the structures of phosphate and phosphate-containing glasses: a review, Solid State Nucl. Magn. Reson. 5 (1995) 9–21.
[56] A. Pedone, T. Charpentier, M.C. Menziani, The structure of fluoride-containing bioactive glasses: new insights from first-principles calculations and solid state NMR spectroscopy, J. Mater. Chem. 22 (2012) 12599–12608.
[57] T. Kasuga, T. Kimata, A. Obata, Preparation of a calcium titanium phosphate glass–ceramic with improved chemical durability, J. Am. Ceram. Soc. 92 (2009) 1709–1712.
[58] N. Kanwal, D.S. Brauer, J. Earl, R.M. Wilson, N. Karpukhina, R.G. Hill, In-vitro apatite formation capacity of a bioactive glass – containing toothpaste, J. Dent. 68 (2018) 51–58.
[59] A. Nommeots-Nomm, N.G. Boetti, T. Salminen, J. Massera, M. Hokka, L. Petit, Luminescence of Er^{3+} doped oxyfluoride phosphate glasses and glass-ceramics, J. Alloys Compd. 751 (2018) 224–230.
[60] H. Fathi, A. Johnson, R. van Noort, J.M. Ward, I.M. Brook, The effect of calcium fluoride (CaF_2) on the chemical solubility of an apatite–mullite glass–ceramic material, Dent. Mater. 21 (2005) 551–556.
[61] N. Sharmin, F. Gu, I. Ahmed, A.J. Parsons, Compositional dependency on dissolution rate and cytocompatibility of phosphate-based glasses: effect of B_2O_3 and Fe_2O_3 addition, Journal of Tissue Engineering 8 (2017) 1–10.
[62] P.K. Jha, O.P. Pandey, K. Singh, FTIR spectral analysis and mechanical properties of sodium phosphate glass–ceramics, J. Mol. Struct. 1083 (2015) 278–285.
[63] J. Yifen, J. Dehua, C. Xiangsheng, B. Beiya, H. Xihuai, Raman spectrum studies of the glasses in the system Na_2O Al_2O_3 P_2O_5, J. Non-Cryst. Solids 80 (1986) 147–151.
[64] C.I. Andronache, D. Racolta, Structural investigation of MO·P_2O_5·Li_2O (MO = Fe_2O_3 or V_2O_5) glass systems by FTIR spectroscopy, AIP Conference Proceeding 1634 (2014) 115–119.
[65] J. Massera, I. Ahmed, L. Petit, V. Aallos, L. Hupa, Phosphate-based glass fiber vs. bulk in vitro bioactivity in SBF and TRIS: change in fiber optical response to probe in vitro glass reaction, Mater. Sci. Eng. C 37 (2014) 251–257.
[66] P. Lopez-Iscoa, N. Ojha, D. Pugliese, A. Mishra, R. Gumenyuk, N.G. Boetti, D. Janner, J. Troles, B. Bureau, C. Boussard-Plédel, J. Massera, D. Milanese, L. Petit, Design, processing and characterization of an optical core - bioactive clad phosphate fiber for biomedical applications, J. Am. Ceram. Soc. 102 (2019) 6882–6892.
[67] J. Massera, L. Hupa, Influence of SrO substitution for CaO on the properties of bioactive glass S53P4, J. Mater. Sci. Mater. Med. 25 (2014) 657–668.
[68] C. Rüssel, Nanocrystallization of CaF_2 from Na_2O/K_2O/CaO/CaF_2/Al_2O_3/SiO_2 glasses, Chem. Mater. 17 (2005) 5843–5847.
[69] J. Málek, T. Mitsuhashi, Testing method for the Johnson–Mehl–Avrami equation in kinetic analysis of crystallization processes, J. Am. Ceram. Soc. 83 (2000) 2103–2105.
[70] D. Wood, R. Hill, Structure-property relationships in ionomer glasses, Clin. Mater. 7 (1991) 301–312.
[71] T. Djouama, M. Poulain, B. Bureau, R. Lebullenger, Structural investigation of fluorophosphate glasses by ^{19}F, ^{31}P MAS-NMR and IR spectroscopy, J. Non-Cryst. Solids 414 (2015) 16–20.

Development of composite and hybrid materials based on bioactive glass for bone bioengineering

Bone fractures are common traumas usually compensated by the natural repair process called osteogenesis. In the case of complex and critical size defects, due to a traumatic or pathophysiological context, the repair must be assisted by substitutes that can serve as a support and mechanical replacement and/or as bone filling. The interest of bioactive glasses (BAG) as a bone substitute lies in their bioactivity. They have the particularity of releasing calcium and phosphate ions which will be able to form a reactive layer of hydroxyapatite. However, BAG are difficult to shape. Combining them with organic matrices would provide innovative materials for bone bioengineering.
In this project, two paths are explored: i) a composite material based on Poly (Lactic Acid) (PLA) and bioactive glass and ii) a hybrid material based on gelatin and bioactive glass. The first system is more dedicated to assist the functions of mechanical support, whereas the second will be more pertinent to address the need of filling bone defects. In this study, the BAG 13-93 was used directly and compared to the 13-93B20, its boron-doped form known to influence its dissolution properties. The combined materials, composites or hybrids, were compared after immersion in aqueous medium, and boron increased the rate of BAG dissolution and its bioactivity *in vitro*. Using myoblastic cells, composite materials have been shown to exhibit osteo-stimulating properties. The biocompatibility of the hybrids has been demonstrated using pre-osteoblastic cells. These tailor-made materials have real potential for physical support, resorbability properties, and bone regeneration capacities via the induction of suitable cellular behaviors favored by bioactive glasses, bringing an osteo-competent and osteo-stimulating dimension to the implant.

Développement de matériaux composites et hybrides à base de verre bioactif pour la bio-ingénierie osseuse

Les fractures des os sont des traumatismes courants généralement compensés par un processus naturel de réparation appelé ostéogénèse. Lorsqu'il s'agit de défauts complexes et de taille critique, dus à un contexte traumatique ou physiopathologique, la réparation doit être guidée par le biais de matériaux qui puissent servir de support et suppléance mécanique et/ou de comblement osseux. Les verres bioactifs (BAG) présentent la particularité de relarguer au cours de leur dissolution des ions calcium et phosphate capables de former une couche réactive d'hydroxyapatite. Exploiter leur bioactivité en tant que substitut osseux est une réelle opportunité. Cependant, les BAG sont difficiles à mettre en forme. Les combiner à des matrices organiques permettrait d'obtenir des matériaux innovants pour la bio-ingénierie de l'os. Dans ce projet, deux voies sont explorées : i) une association composite à base de Poly (Acide Lactique) (PLA) et de verre bioactif pour répondre aux besoins mécaniques et ii) des matériaux hybrides à base de gélatine et de verre bioactif pouvant servir de matériaux de comblement. Dans cette étude, le BAG 13-93 a été utilisé tel quel et dans sa forme dopée au bore 13-93 B20 ; le bore étant connu pour avoir une influence sur les propriétés de dissolution. Après études en milieux hydratés, il a été démontré que le bore permet en effet d'augmenter la vitesse de dissolution et la bioactivité du BAG dans les matériaux combinés, tant les composites que les hybrides. A l'aide de cellules myoblastiques, il a été montré que les matériaux composites présentaient des propriétés ostéo-stimulantes. La biocompatibilité des hybrides a été démontrée à l'aide de cellules pré-ostéoblastiques. Ces matériaux sur-mesure présentent de vrais potentiels de support physique, des propriétés de résorbabilité, et des capacités de régénération osseuse, via l'induction de comportements cellulaires idoines favorisés par les verres bioactifs, apportant une dimension ostéo-compétente et ostéo-stimulante à l'implant.

Amel HOUAOUI